AN INVESTIGATION OF CHF FLUID-TO-FLUID SCALING AND MULTI-FLUID PREDICTION TECHNIQUES

by

RA-MIN TAIN

A dissertation submitted to the School of Graduate Studies and Research of the Ottawa-Carleton Institute for Mechanical and Aeronautical Engineering at the University of Ottawa in partial fulfilment of the requirements for the degree of Doctor of Philosophy in Mechanical Engineering.

Ottawa-Carleton Institute for Mechanical and Aeronautical Engineering

University of Ottawa, Ottawa, Ontario, Canada K1N 6N5

1994 December

ISBN 0-612-04885-3

Canada

UNIVERSITÉ D'OTTAWA
UNIVERSITY OF OTTAWA

ABSTRACT

More than 800 points of critical heat flux (CHF) data were measured from three test rigs (UO, MR-7A and MR-1A loops). The UO loop is a multi-fluid boiling loop located at the University of Ottawa, in which HFC-134a, HCFC-123, HCFC-22, CFC-12 and CFC-11 have been tested. The CHF data of HFC-134a and HCFC-123 are the first ever published for these fluids. HFC-134a and HCFC-123 are non-ozone and low-ozone depletion fluids. The CHF data from the UO loop cover the range of mass flux from 1 to 4 Mg m^{-2} s^{-1}, pressure from 7 to 10 MPa of water-equivalent (water-equivalent is defined as the same dimensionless parameters, e.g. ρ_f/ρ_g and ψ_k, of flow condition for non-aqueous fluids as those for water) and heated length from 0.5 to 1 meter. The inner diameter of the test section is 4.2 mm. The MR-7A and MR-1A loops are the refrigerant and boiling water loops, respectively, located at the Chalk River Laboratories of AECL. In the MR-7A loop, CHF data were measured using HCFC-22 as a coolant for the following conditions: mass flux: 1—8 Mg m^{-2} s^{-1}, pressure: 7 and 10 MPa (water-equiv.), heated length: 0.67—1.61 m, and inner diameter: 4.38 and 8 mm. The CHF data for water from the MR-1A loop cover mass flux: 2.5—8 Mg m^{-2} s^{-1}, pressure: 7 and 10 MPa, heated length: 1.75 m, and inner diameter: 8 mm. HFC-134a, HCFC-123 and HCFC-22 are found suitable to replace the CFC's in the CHF experiment for water CHF simulation.

The CHF fluid-to-fluid and multi-fluid prediction techniques were examined based on the CHF data of various fluids measured in the present work. Two analytical CHF models were assessed and compared to data from the 5 fluids tested in this investigation. The CHF similarity between water and refrigerants was also examined via the analysis of geometric, thermodynamic and hydrodynamic similarities. A new methodology has been established to investigate the limitations of the CHF fluid-to-fluid scaling technique. The analysis of CHF similarity through the thermodynamic relationship leads to the conclusion that, not only the local thermodynamic quality, but also the upstream history (e.g. heating, flashing, friction, changes of kinetic energy and potential energy, etc.) are important factors in determining the CHF scaling accuracy. Finally, the limitations of the CHF fluid-to-fluid scaling technique were determined in terms of the scaling accuracy.

ACKNOWLEDGEMENT

I would like to thank Professor S.C. Cheng for his advice on this thesis work and for always being available to discuss the latest results with helpful scepticism, guidance and encouragement.

I am greatly indebted to Dr. D.C. Groeneveld, adjunct professor, for his assistance and technical advice.

I have enjoyed the four years Ph.D. study of the University of Ottawa and wish to thank my friends, especially N. Hammouda, Ph.D. student, with whom I had many valuable and enjoyable discussions on science, technology and social values. My appreciation also is addressed to Drs. L. Leung and S. Doerffer for their assistance during the experimental investigation at Chalk River Laboratories, AECL. Dr. X.C. Huang, post-doctoral fellow, provided valuable suggestions on the last draft of my thesis. I shall never forget his assistance.

I also thank my wife, Chiu-chin, for putting aside her own ambitions and taking care of our two lovely boys so that I could, with less stress, concentrate in the pursuit of what she felt was important to me.

The financial support provided by AECL and by the Natural Science and Engineering Research Council of Canada is also greatly appreciated.

TABLE OF CONTENTS

LIST OF TABLES

LIST OF FIGURES

NOMENCLATURE

a_1	Empirical constant from Lee and Mudawwar	
a_2	Empirical constant from Lee and Mudawwar	
a_3	Empirical constant from Lee and Mudawwar	
a_4	Empirical constant used in Eq. (2-107) by Weisman and Pei	
A_F	Flow cross-sectional area	m^2
A_H	Heated area	m^2
B	Parameter used in Green and Lawther's empirical correlation	
B_1	Dimensionless group as defined in Eq. (5-4)	
B_2	Dimensionless group as defined in Eq. (5-5)	
B_3	Dimensionless group as defined in Eq. (5-6)	
Bo	Boiling number as defined in Eq. (2-6)	
c	Mass concentration of liquid droplets in vapour core used in Eq. (2-118)	$kg\ m^{-2}\ s^{-1}$
c_1	A constant defined in Eq. (6-51)	
c_2	A constant defined in Eq. (6-52)	
c_3	A constant defined in Eq. (6-53)	
c_4	A constant defined in Eq. (6-54)	
c_5	A constant defined in Eq. (6-55)	
c_6	A constant defined in Eq. (6-56)	
c_7	A constant defined in Eq. (6-57)	
c_8	A constant defined in Eq. (6-58)	
c_9	A constant defined in Eq. (6-59)	

c_{10}	A constant defined in Eq. (6-60)	
c_{11}	A constant defined in Eq. (6-61)	
C	Constant used in Katto's correlation as defined in Eq. (2-58)	
C_D	Drag coefficient	
C_{EQ}	Local equilibrium concentration (Whalley et al.)	kg m^{-3}
C_H	Constant used in Eq. (6-65)	
CHF_n	CHF number as defined in Eq. (5-2)	
Cp_f	Specific heat of saturated liquid	J kg^{-1} $°C^{-1}$
Cp_g	Specific heat of saturated vapour	J kg^{-1} $°C^{-1}$
Cp_L	Specific heat of subcooled liquid	J kg^{-1} $°C^{-1}$
C_T	Dix's scaling constant as shown in Eq. (2-39)	
dP/dz	Total pressure gradient	N m^{-3}
dP	Total pressure drop in differential form	N m^{-2}
dP_a	Accelerational pressure drop in differential form	N m^{-2}
dP_f	Frictional pressure drop in differential form	N m^{-2}
dP_g	Gravitational pressure drop in differential form	N m^{-2}
$(dP/dz)_{LF}$	Liquid film frictional pressure gradient (Whalley et al.)	N m^{-3}
ds	Entropy change per unit mass	J kg^{-1} $°C^{-1}$
D	Tube diameter	m
D_b	Equivalent diameter of vapour blanket (Lee and Mudawwar)	m
D_D	Droplet deposition rate (Whalley et al.)	kg m^{-2} s^{-1}
D_{eb}	Equivalent diameter of the bubble (Lee and Mudawwar)	m

D_h	Hydraulic diameter	m
D_{he}	Equivalent heated diameter	m
DNB	Departure from nucleate boiling	
D_p	Average bubble diameter (Weisman and Pei)	m
E	Defined in Eq. (2-55)	
E_E	Entrainment mass flux (Whalley et al.)	kg m^{-2} s^{-1}
E^+	Defined in Eq. (2-54)	
f'	Friction factor	
f_{fo}	Friction factor defined in Eq. (V-29)	
f_G	Modified gas friction factor (Whalley et al.)	
f_{GC}	Interfacial friction factor (Whalley et al.)	
f_L	Liquid film friction factor (Whalley et al.)	
F_D	Scaling factor for diameter	
F_G	Scaling factor for mass flux	
F_L	Scaling factor for length	
F_{LE}	Entrained liquid flashing rate	kg m^{-2} s^{-1}
F_{LF}	Liquid film flashing rate	kg m^{-2} s^{-1}
F_{LFC}	Critical film flow rate defined in Eq. (5-24)	kg m^{-2} s^{-1}
Fr	Froude number as defined in Eq. (2-69)	
F_R	Lateral force caused by the rotation of vapour blanket (Lee and Mudawwar)	N
f_{TP}	Friction factor defined in Eq. (V-31)	

$F_{\Delta h_i}$	Scaling factor for inlet subcooling enthalpy	
F_ϕ	Scaling factor for critical heat flux	
g	Constant of gravitational acceleration	$m\ s^{-2}$
G	Mass flux	$kg\ m^{-2}\ s^{-1}$
G^*	Dimensionless mass flux	
G_3	Lateral mass flux from core to bubbly layer due to turbulence (Weisman and Pei)	$kg\ m^{-2}\ s^{-1}$
G_c	Critical mass flux at choking	$kg\ m^{-2}\ s^{-1}$
G_F	Mass flux for CFC as illustrated in Eq. (2-26)	$kg\ m^{-2}\ s^{-1}$
G_G	Mass flux of vapour (Whalley et al.)	$kg\ m^{-2}\ s^{-1}$
G_{LE}	Mass flux of entrained liquid (Whalley et al.)	$kg\ m^{-2}\ s^{-1}$
G_{LF}	Mass flux of liquid film (Whalley et al.)	$kg\ m^{-2}\ s^{-1}$
G_m	Relative mass velocity for liquid entering the sublayer (Lee and Mudawwar)	$kg\ m^{-2}\ s^{-1}$
G_W	Mass flux for water or water-equivalent	$kg\ m^{-2}\ s^{-1}$
h_{exit}	Enthalpy at the exit of test section	$J\ kg^{-1}$
h_f	Saturated liquid enthalpy	$J\ kg^{-1}$
h_{in}	Enthalpy at the inlet of test section	$J\ kg^{-1}$
h_L	Enthalpy of liquid (Weisman and Pei)	$J\ kg^{-1}$
h_{Ld}	Enthalpy at the point of bubble detachment (Weisman and Pei)	$J\ kg^{-1}$
h_{sc}	Subcooled heat transfer coefficient from Shah (Lee and Mudawwar)	$W\ m^{-2}\ °C^{-1}$

i_b	Turbulent intensity at the bubbly-layer-core interface (Weisman and Pei)	
I.D.	Inner diameter	m
k	Vapour velocity coefficient as defined in Eq. (2-102) by Katto	
k_1	Mass transfer coefficient defined in Eq. (2-122) by Whalley et al.	
k_f	Thermal conductivity of saturated liquid	W m^{-1} $°C^{-1}$
k_g	Thermal conductivity of saturated vapour	W m^{-1} $°C^{-1}$
K	Stevens and Kirby's scaling factor as shown in Eq. (2-22)	
K_1	Dix's scaling factor as shown in Eq. (2-38)	
K_2	Constant used in Ahmad's empirical correlation in Eq. (2-52)	
K_3	Katto's inlet subcooling parameter as shown in Eq. (2-57)	
K_4	Empirical constant used in Eq. (2-103) by Katto	
K_5	Empirical constant used in Eq. (2-103) by Katto	
K_6	Empirical constant used in Eq. (2-107) by Weisman and Pei	
K.E.	Kinetic energy per unit mass	J kg^{-1}
L	Heated length of the test section	m
L_b	Boiling length	m
L_B	Length of vapour blanket (Katto)	m
L_m	Length of the liquid sublayer or vapour blanket (Lee and Mudawwar)	m
LW	Loss of work	J kg^{-1}
m	Liquid film thickness (Whalley et al.)	m
$\dot{m}$	Mass flow rate	kg s^{-1}
$\dot{m}_1$	Axial mass flow rate in core (Weisman and Pei)	kg s^{-1}

$\dot{m}_2$	Mass flow rate difference between the axial flow in and out of the bubbly-layer control volume (Weisman and Pei)	kg s^{-1}
$\dot{m}_3$	Mass flow rate from core to bubbly layer (Weisman and Pei)	kg s^{-1}
$\dot{m}_4$	Mass flow rate from bubbly layer to core (Weisman and Pei)	kg s^{-1}
M	Molecular weight	g mol^{-1}
M_l	Rate of momentum (Lee and Mudawwar)	N
O.D.	Outer diameter	m
P	Pressure	
P_c	Critical pressure	Pa
Pe	Peclet number as defined in Eq. (2-68)	
P.E.	Potential energy per unit mass	J kg^{-1}
P_i	Inlet pressure	Pa
P_o	The outlet pressure used in Eq. (2-14) or the stagnation pressure used in Eq. (6-65)	Pa
P_r	Reduced pressure (i.e. P/P_c)	
Pr_f	Saturated liquid Prandtl Number	
Pr_g	Saturated Vapour Prandtl Number	
P_t	Pressure at choking plane	Pa
q	Heat input per unit mass	J kg^{-1}
$\dot{q}$	Power	W
Q'	Total power input	W
r	Radial position from centre to the wall of the tube (Weisman and Pei)	m

R	Tube radius	m
$\overline{R}$	Universal gas constant	
Re	Reynolds number	
Re_f	Saturated liquid Reynolds number as defined in Table 5-2	
Re_g	Saturated vapour Reynolds number	
Re_v	Vapour Reynolds number as defined in Table 5-2	
Re_{GC}	Reynolds number in gas core (Whalley et al.)	
Re_{LF}	Liquid film Reynolds number (Whalley et al.)	
RMS	Root mean square	
s	Bubbly layer thickness (Weisman and Pei)	m
s_f	Saturated liquid entropy	$J\ kg^{-1}\ °C^{-1}$
s_g	Saturated vapour entropy	$J\ kg^{-1}\ °C^{-1}$
s_o	Entropy at stagnation pressure condition	$J\ kg^{-1}\ °C^{-1}$
s_p	Perimeter	m
S	Dimensionless group defined in Eq. (2-125) by Whalley et al.	
t	Time	s
T_c	Critical temperature	°C
T_f	Liquid temperature	°C
T_g	Vapour temperature	°C
T_i	Inlet temperature	°C
T_L	Local mean bulk temperature (Lee and Mudawwar)	°C
T_m	Temperature for liquid entering the sublayer (Lee and Mudawwar)	°C

T_r	Reduced temperature	
T_{sat}	Saturation temperature	°C
T_w	Wall temperature	°C
u	Internal energy	J kg^{-1}
u_f	Internal energy of saturated liquid	J kg^{-1}
u_{fg}	$u_g - u_f$	J kg^{-1}
u_g	Internal energy of saturated vapour	J kg^{-1}
U_b	Vapour blanket velocity (Lee and Mudawwar)	m s^{-1}
U_B	Vapour blanket velocity (Katto)	m s^{-1}
$U_{bL}(=U_m)$	Mean liquid velocity at the radial position of the vapour blanket (Lee and Mudawwar)	m s^{-1}
U_f	Velocity in liquid phase used in Eq. (V-8)	m s^{-1}
U_g	Velocity in vapour phase used in Eq. (V-8)	m s^{-1}
U_G	Vapour velocity (Whalley et al.)	m s^{-1}
U_L	Liquid velocity (Lee and Mudawwar)	m s^{-1}
U_L^+	Dimensionless velocity profile defined in Eqs. (2-90a)—(2-90c)	
U_{LF}	Liquid film velocity (Whalley et al.)	m s^{-1}
U_∞	Global (or mean) velocity	m s^{-1}
U_δ	Local velocity at the distance of δ_m from the tube wall (Katto)	m
v	Specific volume	m^3 kg^{-1}
v_f	Specific volume of saturated liquid	m^3 kg^{-1}
v_{fg}	$v_g - v_f$	m^3 kg^{-1}

v_{fo}	Specific volume of saturated liquid under stagnation pressure condition	$m^3\ kg^{-1}$
v_g	Specific volume of saturated vapour	$m^3\ kg^{-1}$
v_{gt}	Specific volume of saturated vapour at choking plane	$m^3\ kg^{-1}$
v_H	Specific volume of two-phase homogeneous mixture	$m^3\ kg^{-1}$
V'	Volumetric flow rate	$m^3\ s^{-1}$
V_b	Vapour velocity due to evaporation of the sublayer (Lee and Mudawwar)	$m\ s^{-1}$
V_c	Critical volume	m^3
V_{GC}	Vapour velocity in the gas core (Whalley et al.)	$m\ s^{-1}$
W_f	Loss of work per unit mass due to friction	$J\ kg^{-1}$
W^+	Dimensionless power number defined in Eq. (2-48)	
W.T.	Wall thickness	m
x	Thermodynamic quality	
x_1	Average quality in core region (Weisman and Pei)	
$x_{1,eff}$	Average quality in core region corresponding α_{eff} (Ying and Weisman)	
x_2	Average quality in bubbly layer (Weisman and Pei)	
x_{avg}	Global quality (Weisman and Pei)	
X_c	Critical quality or dryout quality	
X_i	Inlet subcooling quality as defined in Eq. (2-7)	
x_t	Quality at the choking plane	
y^+	Dimensionless distance away from the tube wall used in Eqs. (2-90a)—(2-90c)	
Y^+	Defined in Eq. (2-52)	
Y	Shah's correlating parameter as defined in Eq. (2-67)	

z	Axial location or elevation	m
Z_c	Critical compressibility factor defined by Hauptmann and Lee	

Greek Letters

α	Void fraction	
$\overline{\alpha}$	Average void fraction in core (Ying and Weisman)	
α'	Void fraction in the core cross section (Whalley et al.)	
α_2	Average void fraction in bubbly layer (Weisman and Pei)	
α_{CHF}	Void fraction of bubbly layer at CHF (Weisman and Pei)	
α_D	Fraction of tube cross section occupied by the droplets and vapour (Whalley et al.)	
α_{eff}	Void fraction in core at edge of bubbly layer (Ying and Weisman)	
α_G	Fraction of core cross section occupied by gas (Whalley et al.)	
β	Defined in Eq. (2-16)	°C Pa^{-1}
β^*	Dimensionless mixing parameter as defined in Eq. (6-69)	
γ	Defined in Eq. (2-17)	Pa^{-1}
γ^*	Slip ratio of vapour to liquid	
δ_1	Parameter used in Green and Lawther's empirical correlation	
δ_2	Parameter used in Green and Lawther's empirical correlation	
δ_m	Thickness of liquid sublayer (Lee and Mudawwar) and (Katto)	m
Δh	Enthalpy increase	J kg^{-1}
ΔH_i	Inlet subcooling enthalpy	J kg^{-1}

ΔX	Total quality change for total effects	
ΔX_F	Quality change due to flashing	
ΔX_H	Quality change due to enthalpy increase	
$\Delta X_{K.E.}$	Quality change due to kinetic energy change	
$\Delta X_{P.E.}$	Quality change due to potential energy change	
ΔX_q	Quality change due to heat input	
ΔX_{Wf}	Quality change due to friction	
$\Delta\rho$	Density difference (ρ_f-ρ_g)	kg m^{-3}
ε_o	Fraction of liquid entrainment at the onset of annular flow	
θ^*	Ratio of transit time as defined in Eq. (6-70)	
λ	Heat of vaporization	J kg^{-1}
λ_c	Critical wavelength of Taylor's instability	m
μ	Viscosity	kg m^{-1} s^{-1}
$\overline{\mu}$	Mean two-phase viscosity used in Eq. (V-31)	kg m^{-1} s^{-1}
μ_{avg}	Average viscosity (Weisman and Pei)	kg m^{-1} s^{-1}
μ_f	Saturated liquid viscosity	kg m^{-1} s^{-1}
μ_g	Saturated vapour viscosity	kg m^{-1} s^{-1}
μ_L	Subcooled liquid viscosity	kg m^{-1} s^{-1}
v'	Radial fluctuating velocity (Weisman and Pei)	m s^{-1}
v_{11}	Radial velocity created by vapour generation (Weisman and Pei)	m s^{-1}
ν_L	Kinematic viscosity of subcooled liquid	m^2 s^{-1}
Π	Dimensionless group used for dimensional analysis, or Pi theorem	

ρ	Density	kg $m_{.3}$
ρ_{avg}	Average density (Weisman and Pei)	kg $m_{.3}$
ρ_f	Saturated liquid density	kg m^{-3}
ρ_g	Saturated vapour density	kg m^{-3}
ρ_H	Density of two-phase homogeneous mixture	kg m^{-3}
ρ_L	Subcooled liquid density	kg m^{-3}
σ	Surface tension	N m^{-1}
σ_{vf}	Defined in Eq. (2-112) (Weisman and Pei)	
τ	Vapour blanket passage time (Katto)	s
τ_i	Interfacial shear stress (Whalley et al.)	N m^{-2}
τ_w	Wall shear stress	N m^{-2}
ϕ	Heat flux	W m^{-2}
ϕ_b	Portion of heat flux used by vaporization (Lee and Mudawwar) and (Weisman and Pei)	W m^{-2}
ϕ_c	Critical heat flux	W m^{-2}
ϕ_c^*	Dimensionless critical heat flux as defined in Eq. (2-78)	
ϕ_o	CHF at zero inlet subcooling as defined in Eq. (2-56)	W m^{-2}
ψ	A function defined by Weisman and Pei	
ψ_B	Scaling parameter as defined in Eq. (5-8)	
ψ_{CHF}	Ahmad's scaling parameter resulted from the compensated distortion technique	
ψ_K	Katto's scaling parameter as defined in Eq. (2-81)	
ψ_L	Katto's scaling parameter as defined in Table 5-2	

ψ_λ Scaling parameter as defined in Eq. (5-18)

ψ_γ Ahmad's scaling parameter as a function of γ

ψ_σ Ahmad's scaling parameter as a function of σ

Chapter 1

INTRODUCTION

Boiling heat transfer is a very efficient convection process where the fluid is involved in a phase change (from liquid to vapour). This process has been applied in many industrial systems such as boilers (steam generators), refrigeration equipment, air-conditioning systems and nuclear reactors. Two fundamental areas of the boiling process, pool boiling and flow boiling, have received considerable attention for years. Pool boiling is boiling in which a heated surface is submerged in a static liquid pool. Flow boiling is boiling in which the heated surface is a channel wall confining the flow or is surrounded by a flow stream. In the present study, an aspect of flow boiling has been investigated which is particularly relevant to nuclear reactor equipment.

An important power-limiting criterion for a water-cooled nuclear reactor is the phenomenon called "dryout", which results in a sudden and dramatic decrease or deterioration of the heat transfer rate on the heated surface, due to the creation of a low conductivity vapour film. For a heat flux controlled surface, the surface temperature will rise rapidly when "dryout" occurs. This phenomenon is also referred to as "burnout" although a physical burnout does not necessarily occur. However, a more general term, "boiling crisis", is widely accepted in the literature, and the term "critical heat flux" is used to represent the heat flux at boiling crisis.

Many other terms have also been used to depict the boiling crisis phenomenon with a particular sense of mechanism, e.g. the flow patterns shown in Fig. 1-1. There are two distinct

mechanisms. The first mechanism is characterized by a transition from nucleate boiling to film boiling (see Fig. 1-1b). The terms "fast burnout", "departure from nucleate boiling (DNB)" and "burnout of the first kind" are thus used in the literature (Bergles, 1979). These terms normally refer to the subcooled or low-quality flow condition. The second mechanism occurs in the annular flow regime at low heat flux, where the liquid film on the wall becomes depleted or consumed by evaporation (see Fig. 1-1a). Here, the terms "slow burnout", "dry-out" and "burnout of the second kind" are used, and denote the high-quality flow condition (Bergles, 1979). In general, the term "critical heat flux (CHF)" is used for either case.

Full-scale experiments for boiling crises in nuclear reactors are very costly and sometimes are risky. Instead of using the fuel elements in the reactor, CHF measurements are usually undertaken in out-reactor loops using a similar test-section geometry. The reactor fuel is simulated by electrically heated bundles. Because of the high heat of vaporization and high critical pressure of water, equipment for measuring CHF, especially for complex geometries (e.g. rod bundles), is very expensive. Therefore, CHF fluid-to-fluid scaling theories have been developed which permit the use of scaling fluids (also called "modelling fluids") such as refrigerants (chlorofluorocarbons or CFC's). The advantages of scaling fluids include a lower CHF experimentation cost and less severe test conditions such as lower pressure, lower temperature and lower heat flux. For example, to scale the CHF requires an equal density ratio of liquid to vapour. CHF in water at 7 MPa would correspond to CHF in CFC-12 (trade name Freon-12 or R-12) at 1 MPa; at these pressures the heat of vaporization of CFC-12 is only 5% of water. This reduces the CHF power to 6% of the water CHF value. Lawther and Miles (1973) have also concluded other important advantages from using the scaling fluids:

1. The lower heat flux and lower temperature result in much lower temperature excursions at boiling crisis conditions. Thus, the possibility of physical burnout is extremely remote;
2. The accuracy and reproducibility of CHF data are much better than with water, so that parametric effects can be more fully investigated;
3. Instrumentation is less complex and experimental testing is safer, easier and quicker.

A review of the relevant literature shows that refrigerants are used extensively as the working fluids in most CHF simulation tests. However, CFC-12 (R-12), CFC-11 (R-11) and some other types of refrigerants have recently been considered harmful to the environment by depleting the ozone layer in the atmosphere. Therefore, new fluids to substitute for the above refrigerants are required, and CHF tests using these new fluids are also needed. Some fluids such as HCFC-123 (R-123) and HFC-134a (R-134a) have been found to be friendly to the environment (with a zero or very low ozone depletion index); and the thermophysical properties of HCFC-123 and HFC-134a are close to CFC-11 and CFC-12, respectively. Table 1-1 summarizes the basic properties of HCFC-123, CFC-11, HFC-134a, CFC-12 and HCFC-22; and Table 1-2 is the summary of the environmental characteristics of some refrigerants and several promising alternatives.

For refrigeration, air-conditioning and heat pump applications, it has been concluded that HFC-134a and HCFC-123 are the most likely substitutes for CFC-12 and CFC-11, respectively. HCFC-22 also is considered to be a temporary replacement fluid for CFC-12 during a transition period. The CHF test results for both HCFC-123 and HFC-134a have not yet been reported in the literature.

If the fluid-to-fluid scaling technique is proven to be suitable for CHF conversion from one fluid to another, this technique can also be used as a CHF prediction method for one fluid, for which no data are available, based on another fluid, for which either data or prediction methods are available. The experimental part of this investigation has provided systematic CHF measurements with HFC-134a, HCFC-123 and HCFC-22. CHF measurements for CFC-12 and CFC-11 were also performed to compare the CHF results with those from the CFC substitutes. The analytical part of this study examined the validity of the fluid-to-fluid scaling technique as well as the multi-fluid CHF prediction methods such as non-dimensional CHF equations and theoretical models. Also, the limitation of the fluid-to-fluid scaling technique was studied so that its range of application can be determined.

Chapter 2 will be devoted to a brief description of CHF mechanisms at various flow conditions, CHF scaling theories and a survey of various CHF scaling techniques and prediction methods. Chapter 3 will describe the details of CHF test equipment including the test procedure and the measurement uncertainties as well as the test matrix. In Chapter 4, the CHF test data will be summarized from the data reduction procedure and the observation of the parametric trends as well as the comparison against the CHF data from the literature. Chapter 5 then is devoted to the examination of the CHF scaling techniques and other CHF prediction methods based on the present CHF test data. In Chapter 6, the limitations of CHF fluid-to-fluid scaling technique will be investigated and its application range is determined. Finally, in Chapter 7, the conclusion of the CHF experiments using the CFC replacements, the validity of CHF scaling techniques and other CHF prediction methods as well as the recommendations for the future work will be presented.

Several appendices will also be appended to this thesis including a list of publications generated during the course of this study (in Appendix I), measurement uncertainties (in appendix II), equations of property prediction for new refrigerants (in Appendix III), tabulated CHF data measured from the present work (in Appendix IV) and the pressure drop derivations required for the analysis in Chapter 6 (in Appendix V).

Table 1-1 Physical properties of HCFC-123, CFC-11, HFC-134a, CFC-12 and HCFC-22 (DU PONT data).

Properties	HCFC-123	CFC-11	HFC-134a	CFC-12	HCFC-22
Chemical formula	$CHCl_2CF_3$	CCl_3F	CH_2FCF_3	CCl_2F_2	$CHClF_2$
Molecular weight	152.9	137.4	102.0	120.9	96.47
Boiling point at 1 atm (°C)	27.6	23.8	-25.5	-29.8	-40.8
Freezing point (°C)	-107	-111	-101	-158	-160
Critical temperature (°C)	185	198.1	100.6	112.0	96.15
Critical pressure (MPa)	3.61	4.41	3.95	4.12	4.97
Critical density (kg m^{-3})	583.4	554.2	488.5	557.4	513.0
Liquid density at 25°C (kg m^{-3})	1461	1476	1203	1311	1190
Vapour pressure at 25°C (kPa)	91.7	105.6	661.9	651.6	1040
Evaporation heat at boiling point of 1 atm (J g^{-1})	169.9	180.4	219.8	165.3	182.5

Table 1-2 Environmental characteristics of regulated CFC's and several promising alternatives (Watanabe, 1990).

Refrigerant	Atmospheric lifetime (year)[1]	ODP[2]	GWP[3]
CFC-11	65	1.0	1.0
CFC-12	120	0.9 -1.0	2.8 - 3.4
CFC-113	90	0.8 - 0.9	1.3 - 1.4
CFC-114	180	0.6 - 0.8	3.7 - 4.1
CFC-115	380	0.3 - 0.5	7.4 - 7.6
HCFC-123	1 - 4	0.013 - 0.022	0.017 - 0.02
HCFC-124	-	0.016 - 0.024	0.092 - 0.1
HFC-125	-	0	0.51 - 0.65
HFC-134a	6	0	0.24 - 0.29
HCFC-22	20	0.04 - 0.06	0.32 - 0.37

[1] Time required for a chemical compound to reduce the concentration to 1/e (37%) of its original value.

[2] Ozone depletion potential (relative to CFC-11, which is assigned the value 1).

[3] Global warming potential (relative to CFC-11, which is assigned the value 1).

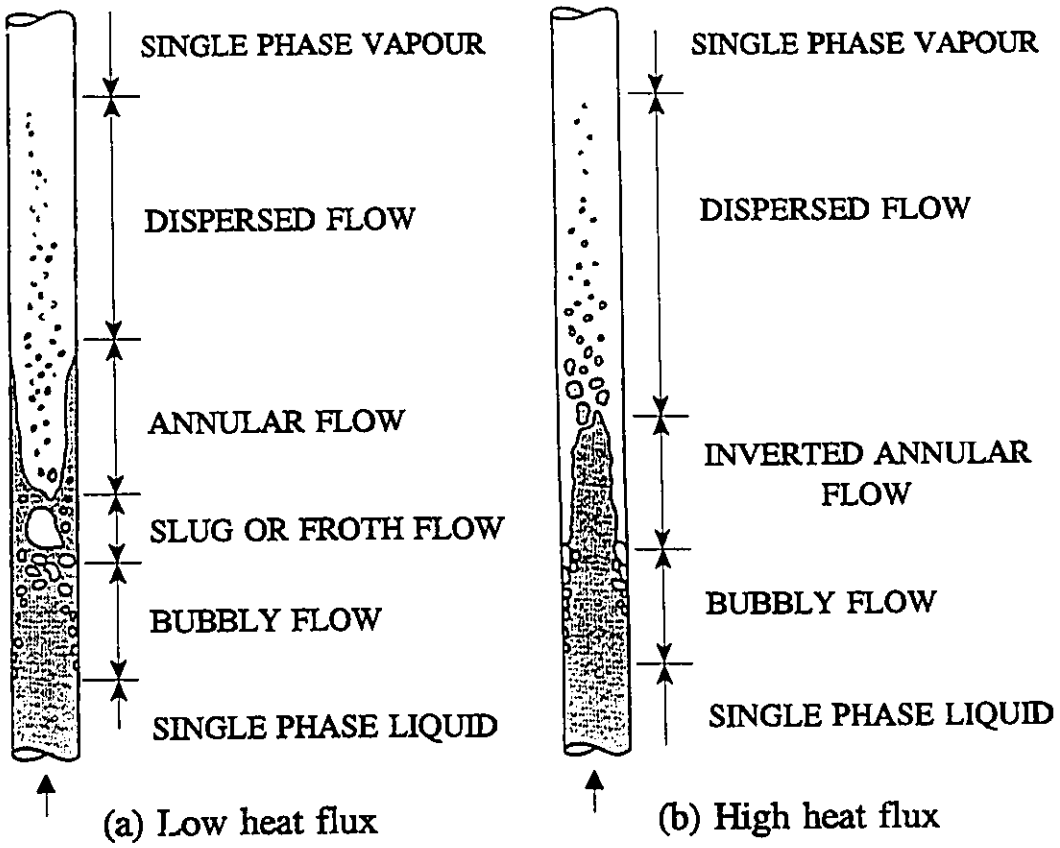

Figure 1-1 Flow regimes in directly heated tubes.

Chapter 2

LITERATURE SURVEY

2.1 Two-phase Flow Regimes

As illustrated in Fig. 1-1, two types of flow regimes may occur in a heated channel. For low heat flux conditions (Fig. 1-1a), a single phase liquid enters a heated tube and the evolution of the flow patterns at the downstream of the entrance may be bubbly flow, slug or froth flow, annular flow, dispersed flow and single phase vapour. The boiling crisis occurs at the dryout location at downstream end of the annular flow regime. For high heat flux conditions (Fig. 1-1b), the evolution of the flow patterns inside the heated tube may be single phase liquid, bubbly flow, inverted annular flow, dispersed flow and single phase vapour. The boiling crisis in this case occurs between the bubbly flow and inverted annular flow regimes. A detailed description of two-phase flow regimes can be found in Hewitt and Hall-Taylor (1970) and Collier (1981).

2.2 CHF Mechanisms

2.2.1 Subcooled and Low Quality CHF

Based on Tong and Hewitt's (1972) and Bergles's (1977) reviews, Hewitt (1978) concluded that there are three common postulated mechanisms for CHF in subcooled and low quality region. They are:

(1) Near-Wall Bubble-Crowding and Vapour Blanketing

As shown in Fig. 2-1, bubbles generated from the heated surface will form a "bubble boundary layer" along the flow and such a layer is thick enough to prevent enthalpy transport between the heated surface and the subcooled liquid core. Several hypotheses have been made to precisely describe the phenomenon occurring in the vicinity of a heated surface:

(a) Kutateladze and Leont'ev (1966) observed a "blowoff" or "breakaway" of the "bubble boundary layer", which indicates the evaporation of a stagnant liquid layer that leads to the overheating of the heated surface.

(b) Tong et al. (1965) suggested that there is a critical superheat in the liquid wall layer which is formed by separation of the "bubble boundary layer".

(c) The vapour accumulating at the heated surface leads to an overheating of the surface because of the limitation of vapour removal by condensation and by axial transport of bubbles (Hebel and Defavernier, 1977).

(d) Film boiling is formed at the heated surface when the rate of vapour removal from the nucleation centre reaches its maximum (Maroti, 1976).

(2) Local Overheating Following Bubble Growth from a Nucleation Centre

When the bubble grows at a nucleation centre, a dry patch is formed on the heated surface. Then, the surface is rewetted following the bubble departure. Kirby et al. (1967) suggested that, when the heat flux is sufficiently high, the dry patch spreads rapidly and cannot be rewetted after the bubble removal. Therefore, the temperature on the surface will continue to rise and leads to boiling crisis. For this type of boiling crisis, Kirby et

al. concluded that CHF depends on local bulk enthalpy and there is no upstream effect. Figure 2-2 illustrates the heat transfer around the area of the dry patch.

(3) Critical Phenomenon Associated with Vapour Clot or Slug Formation

In slug flow, a micro-layer may form underneath a large volume of vapour which blocks the access of subcooled liquid to the heat surface as illustrated in Figs. 2-3a and 2-3b. The boiling crisis can thus occur (Fiori and Bergles, 1970). Molen and Galijee (1977) commented that the vapour slug is not sufficient to cause the boiling crisis, but it results from the separation of vapour slug and heated wall by bubble overcrowding in the layer. This can be seen in Fig. 2-3c.

Semeria and Hewitt (1974) made a qualitative chart in which all the mechanisms described above can be applied in different regions as shown in Fig. 2-4. Hewitt (1978) concluded that since so many different mechanisms exist, the detail of the phenomenon is not fully understood.

2.2.2 High Quality CHF

Hewitt (1978) defined the boiling crisis in an annular type of two-phase flow as follows: *"to a reasonable approximation, the boiling crisis in annular flow occurs when the film flow rate falls locally, and smoothly, to zero. This condition arises as a result of a combination of liquid evaporation and liquid entrainment over the whole annular flow region preceding the critical point. Counteracting these film denudation processes, there is the process of droplet deposition*

which tends to replenish the film". To describe the mechanism of separation between the liquid and the wall, the measurement of the film flow rate at the end of the channel has been employed. A number of experiments have been performed in different laboratories and they were reported by Hewitt (1970), Mayinger and Langner (1977), Subbotin et al. (1978) and Semeria and Hewitt (1974). Generally, the film flow rate is expressed in terms of local quality along the channel. As a result, the CHF curve is also frequently demonstrated as a function of local quality. Figure 2-5 is a typical CHF curve observed by USSR researchers in which the region I is associated with the flow regime in Fig. 1-1b, the region II corresponds to the so called "limiting quality" effect, and the region III occurs at very low heat fluxes. However, Hewitt (1978) has made some points to discuss this curve:

(1). *"The form of curve is by no means universally obtained in practice, particularly if a subcooled inlet condition is used."*

(2). *"In most of the USSR experiments in this area, mixed inlet conditions are employed and one would certainly expect to see an effect of inlet mixing pattern and length-to-diameter ratio for such tests: the generality of the curve is therefore doubtful."*

In summary, the CHF for high quality (regions II and III) flow can be represented in the following form

$$\phi_c = f(T_i, P_o, G, L, D) \tag{2-1}$$

and the CHF for low quality (region I) flow can be expressed as

$$\phi_c = f(X_c,\ P_o,\ G,\ D) \tag{2-2}$$

where the symbols are defined in the nomenclature.

2.3 CHF Scaling Theories and Scaling Techniques

2.3.1 General Theory

Strictly speaking, in fluid-to-fluid scaling, geometric and dynamic similarities must be matched. Usually, by using the same L/D ratio in model and prototype, geometric similarity is achieved, i.e.,

$$\left(\frac{L}{D}\right)_M = \left(\frac{L}{D}\right)_W \tag{2-3}$$

where subscript "M" denotes the modelling (or scaling) fluid and subscript "W" indicates the equivalent value for the water or prototype system. The dynamic similarities include thermodynamic and hydrodynamic similarities. Thermodynamic similarity can be achieved when the thermodynamic qualities in both systems are the same at any axial location (z/D) along the length, i.e.,

$$x(z)_M = x(z)_W \tag{2-4}$$

From the heat balance equation,

$$x(z) = 4\left(\frac{\phi_c}{\lambda G}\right)\left(\frac{z}{D}\right) - \left(\frac{\Delta H_i}{\lambda}\right) \tag{2-5}$$

where the ΔH_i is the inlet subcooling enthalpy. It follows that the dimensionless groups also must be equal:

$$Bo = \left(\frac{\phi_c}{\lambda G}\right)_M = \left(\frac{\phi_c}{\lambda G}\right)_W \tag{2-6}$$

and

$$X_i = \left(\frac{\Delta H_i}{\lambda}\right)_M = \left(\frac{\Delta H_i}{\lambda}\right)_W \tag{2-7}$$

where Bo is the so-called boiling number and X_i is the inlet subcooling quality. For hydrodynamic similarity, a similar density ratio in both systems is needed, i.e.,

$$\left(\frac{\rho_f}{\rho_g}\right)_M = \left(\frac{\rho_f}{\rho_g}\right)_W \tag{2-8}$$

as well as the dimensionless mass flux in both systems

$$G_M^* = G_W^* \tag{2-9}$$

where G^* is derived based on the classical dimensional analysis associated with experimental evidence and can be expressed in various ways depending on the investigators (e.g. Steven and Kirby (1964), Dix (1970) and Ahmad (1973)).

To convert the scaling fluid parameters into water-equivalent system parameters, requires the introduction of the scaling factors:

$$F_D = D_W / D_M \tag{2-10}$$

$$F_G = G_W / G_M \tag{2-11}$$

$$F_{\Delta H_i} = (\Delta H_i)_W / (\Delta H_i)_M = \lambda_W / \lambda_M \tag{2-12}$$

$$F_\phi = (\phi_c)_W / (\phi_c)_M = F_G \cdot F_{\Delta H_i} \tag{2-13}$$

2.3.2 Scaling Laws and Scaling Factors

2.3.2.1 Barnett's CHF Scaling Laws

Barnett (1963) employed classical dimensional analysis to find the most likely scaling laws which describe the boiling heat transfer for forced convection of a vertical up-flow in a uniformly heated tube. He found that there are six quantities of system parameters representing the occurrence of a burnout situation at particular combinations. These parameters are tube diameter (D), tube length (L), inlet pressure (P_i), outlet pressure (P_o), inlet temperature (T_i), and heat flux (ϕ). The relation of these parameters can be written as

$$\phi_c = f(L, D, P_i, P_o, T_i) \tag{2-14}$$

where ϕ_c represents the critical heat flux and is treated as a dependent variable. Then, the mass velocity (G) is used instead of P_o (there is a unique relationship between P_i-P_o and G), ρ_f/ρ_g is used to replace P_i to ensure that the voidage is scaled under steady conditions, and the inlet subcooling of enthalpy (ΔH_i) is used to substitute (T_i). Thus, Eq. (2-14) becomes

$$\phi_c = f(L, D, \rho_f/\rho_g, G, \Delta H_i) \tag{2-15}$$

Barnett (1963) considered P_i and the corresponding saturation temperature to be the significant conditions from which to select the properties required in non-dimensionalized Eq. (2-15). Therefore, the liquid density (ρ_f), vapour density (ρ_g), thermal conductivity of liquid phase (k_f), specific heat of liquid phase (Cp_f) and heat of vaporization (λ) are evaluated at the conditions of P_i and its corresponding saturation temperature. In addition to these properties, two other properties may be used if the analysis shows that they are required. They are the surface tension (σ) and the slope of the saturation temperature vs. pressure, which is expressed as

$$\beta = \frac{dT_{sat}}{dP} \tag{2-16}$$

where the subscript "sat" indicates the saturation condition.

Barnett (1964) suggested that the properties of ρ_f, ρ_g and λ are obviously important in the case of forced-convection boiling heat transfer because their presence ensures that the mean conditions of voidage and quality are correctly scaled. Also, ρ_f and ρ_g could be combined as the density ratio of liquid to vapour (ρ_f/ρ_g) which is a significant parameter for evaluating void fraction and slip ratio and is a unique function of pressure: it is always possible to find pressures for which any two fluids have the same value of ρ_f/ρ_g. Therefore, Barnett (1964) constructed 14 possible sets of scaling laws with the help of examining the experimental data for water and CFC-12, and based on the consideration that those possible sets of scaling laws contain only one dimensionless group, ρ_f/ρ_g, which involves only properties. These 14 possible sets of scaling laws are illustrated in Table 2-1. The scaling laws contain various fluid properties, including γ, which has not been introduced before and is defined as

$$\gamma = \frac{-d(\rho_f/\rho_g)_{sat}}{dP} \tag{2-17}$$

After testing the 14 sets of scaling laws by comparing the water-equivalent CHF of CFC-12 with actual water data, Barnett (1964) concluded that the scaling law 4 shown in Table 2-1 gives the best comparison between the actual and equivalent water CHF data (within ±6%). Scaling law 4 is written as

$$\frac{\phi_c \gamma^{1/2}}{\lambda \rho_f^{1/2}} = f\left(\frac{L}{D}, \frac{DCp_f \rho_f^{1/2}}{k_f \gamma^{1/2}}, \frac{G\gamma^{1/2}}{\rho_f^{1/2}}, \frac{\rho_f}{\rho_g}, \frac{\Delta H_i}{\lambda}\right) \tag{2-18}$$

To use Eq. (2-18), each dimensionless group at the right hand side (RHS) should be equal in both fluid systems. Then the values of the dimensionless CHF at the left hand side (LHS) in Eq. (2-18) will be the same in both fluid systems.

Barnett (1964) concluded that scaling law 4 scales the water CHF reasonable well by using CFC-12 CHF data. However, scaling law 4 may not contain all the information which is required to model the water CHF data. For example, scaling law 4 assumes the Cp_f, k_f and γ are the important properties in addition to ρ_f, ρ_g and λ. Barnett suggested that the property β may improve the scaling law 4 if β is included to form another dimensionless group. Barnett and Wood (1965) continued the investigation of the validity of scaling law 4 by testing a third fluid system, CFC-21. They also examined whether β is an important physical property by adding β in scaling law 4. A dimensionless group of properties, $\lambda\gamma/\beta Cp_f$, thus is formed and is included in scaling law 4. The addition of β to scaling law 4 yields

$$\frac{\phi_c \gamma^{1/2}}{\lambda \rho_f^{1/2}} = f\left(\frac{L}{D}, \frac{D C p_f \rho_f^{1/2}}{k_f \gamma^{1/2}}, \frac{G \gamma^{1/2}}{\rho_f^{1/2}}, \frac{\rho_f}{\rho_g}, \frac{\Delta H_i}{\lambda}, \frac{\lambda \gamma}{\beta C p_f}\right) \tag{2-19}$$

The investigation by Barnett and Wood (1965) showed that

1. The scaling law 4 containing λ, ρ_f, ρ_g, Cp_f, k_f and γ was successful in scaling the CHF data for water by using CFC-12 and CFC-21 within ±7%.
2. The CHF data of CFC-12 and CFC-21 are related within ±3% whether β is included in scaling law 4 or not. This implies that β may not be an important property.
3. The above finding suggest that the properties involved in scaling flow boiling CHF can be categorized as follows:

   The primary properties: λ, ρ_f, ρ_g and γ.

   The secondary properties: Cp_f, k_f and β.

   Not important properties: All others, with a possible exception of μ_f.

2.3.2.2 Stevens and Kirby's Mass Flux Scaling Factor

Stevens and Kirby (1964) presented a graphical correlation to scale the CHF data of CFC-12 at 1 MPa (155 psia) to those of water at 7 MPa (1000 psia) for vertical up-flow in uniformly heated round tubes. For the same values of ρ_f/ρ_g in water at 7 MPa and in CFC-12 at 1 MPa, Stevens and Kirby (1964) proposed that if

$$\left(\frac{L}{D}\right)_F = \left(\frac{L}{D}\right)_W \tag{2-20}$$

$$\left(\frac{\Delta H_i}{\lambda}\right)_F = \left(\frac{\Delta H_i}{\lambda}\right)_W \tag{2-21}$$

and

$$(GD^{\frac{1}{4}})_F = (KGD^{\frac{1}{4}})_W \quad where\ K = 0.658 \tag{2-22}$$

then

$$\left(\frac{\phi_c}{\lambda G}\right)_F = \left(\frac{\phi_c}{\lambda G}\right)_W \tag{2-23}$$

where the subscript "F" indicates the CFC system and the subscript "W" refers to the water system. Note that in Eq. (2-22), $GD^{1/4}$ is not a dimensionless group and it does not seem to have any physical meaning related to CHF occurrence. However, this empirical function, Eq. (2-22), did improve the CHF prediction. Figure 2-6 shows the thermodynamic quality of water at CHF conditions vs. the function $KGD^{1/4}(D/L)^{0.59}$ as well as the best fit of CFC-12 data. Both the CFC-12 and water data correspond to a subcooling ratio ($\Delta H_i/\lambda$) equal to 0.2. Figure 2-7 illustrates the comparison between the water-equivalent CHF of CFC-12 data and the actual water CHF data as a function of mass velocity for various L/D conditions. The shaded area indicates the regions of uncertainty given by three different experimental sources. Stevens and Kirby (1964) claimed that the accuracy of their scaling technique is within the range of experimental uncertainty.

To obtain the water-equivalent CHF from a CFC-12 system, requires the use of several scaling factors for various system parameters, e.g.

$$\phi_{c,w} = F_{\phi}\phi_{c,F} \tag{2-24}$$

$$\Delta H_{i,W} = F_{\Delta H_i}\Delta H_{i,F} \tag{2-25}$$

$$G_W = F_G G_F \tag{2-26}$$

$$D_W = F_D D_F \tag{2-27}$$

and

$$L_W = F_L L_F \tag{2-28}$$

Substituting Eqs. (2-24)—(2-28) into Eqs. (2-20)—(2-23), yields

$$F_L = F_D \tag{2-29}$$

$$F_{\Delta H_i} = \frac{\lambda_W}{\lambda_F} \tag{2-30}$$

$$F_{\phi} = \frac{\lambda_W}{\lambda_F} F_G \tag{2-31}$$

and

$$F_G = \frac{1}{K} \times F_D^{-1/4} \tag{2-32}$$

Note that for ρ_f/ρ_g=20.63, K=0.658.

If F_D is chosen, F_G and F_ϕ can be obtained accordingly. Since $F_{\Delta H_i}$ is fixed to 11.72 when ρ_f/ρ_g=20.63 and since F_L=F_D, the corresponding water-equivalent values and parameters can be calculated.

2.3.2.3 Staub's Scaling Study

Staub (1969) suggested a modification of Stevens and Kirby's scaling technique in which the equilibrium boiling length (L_b) is used in Stevens and Kirby's scaling relation instead of the total heated length (L) without changing the scaling constant (K=0.658). Figure 2-8 shows that Staub's HCFC-22 data agree with the best fit of Stevens and Kirby's correlation where the L in the abscissa is replaced by L_b. Because of this modification, Staub concluded that a change in heated length (L) has a negligible effect on the CHF occurrence. In Fig. 2-8, the HCFC-22 data for inlet subcooling from 0.04 to 0.26 fall on the same curve. Therefore, the effect of inlet subcooling becomes unimportant because of the use of the equilibrium boiling length (L_b). This reduces the system parameter approach (Eq. (2-1)) to the local condition approach (Eq. (2-2)). Staub also concluded that the scaling constant (K=0.658) does not dramatically respond to a change of pressure. However, this correlation can still be improved by adjusting the scaling constant as a function of pressure.

2.3.2.4 Coffield et al.'s Subcooled DNB Investigation of CFC-113

Coffield et al. (1969) measured the DNB (defined in Chapter 1 and in the Nomenclature) type of dryout for CFC-113 flowing vertically through a uniformly heated round tube. These subcooled CHF data were used to examine Barnett's (1963) and Stevens and Kirby's (1964) scaling techniques, which were developed for the low- and high-quality CHF conditions. Coffield et al. found that both the Barnett's and Stevens and Kirby's methods simulate the subcooled CFC-113 CHF data to the equivalent subcooled water CHF data within ±15%, that is, the methods of Barnett (1963) and Steven and Kirby (1964) can be extended to the subcooled region.

However, Stevens and Kirby's scaling technique was recommended by Coffield et al. because of the convenience of selecting a diameter scaling factor. Coffield et al. concluded that the value of constant K in Stevens and Kirby's scaling function varies with the density ratio (ρ_f/ρ_g). They found that

$$K = 0.684 \quad for \ \frac{\rho_f}{\rho_g} = 20.6 \quad (7\ MPa\ \ water\text{-}equiv.) \tag{2-33}$$

$$K = 0.690 \quad for \ \frac{\rho_f}{\rho_g} = 11.8 \quad (10.3\ MPa\ water\text{-}equiv.) \tag{2-34}$$

and

$$K = 0.715 \quad for \ \frac{\rho_f}{\rho_g} = 7.2 \quad (14\ MPa\ water\text{-}equiv.) \tag{2-35}$$

The inlet subcooling may also affect the value of K.

2.3.2.5 Dix's Technique for CFC — Water Scaling of CHF in a Round Tube

Dix (1970) modeled the water CHF in round tubes by using CHF data obtained in CFC-114. The parameter ranges of the CFC-114 tests are listed in Table 2-2. For a uniformly heated test section, the energy balance at thermal equilibrium is given by

$$Q' = \dot{m}x\lambda + \dot{m}\Delta H_i \tag{2-36}$$

where Q' is the power added to the test section, $\dot{m}$ the mass flow rate, x the flow thermodynamic quality. It can be expressed in terms of dimensionless groups if the heat flux ϕ and mass flux G are introduced, i.e.,

$$\frac{\phi_c}{G\lambda} = \frac{A_F}{A_H}\left(x + \frac{\Delta H_i}{\lambda}\right) \tag{2-37}$$

where A_F is the flow cross-section area and A_H is the heated-surface area. For the case of both fluids having identical geometries (A_F/A_H) with equal thermodynamic quality (x) and dimensionless subcooling values ($\Delta H_i/\lambda$), these two fluids would have the same value of dimensionless heat flux ($\phi_c/G\lambda$) in the above equation. Then Dix (1970) added a mass velocity relation between the CFC-114 (G_F) and water (G_W), where this relation completely defines the scaling of the two fluids for CHF and is written as

$$G_F = K_1 \cdot G_W \tag{2-38}$$

where K_1 is a factor, not necessarily a constant. The factor K_1 is determined by a graphical technique, where the dimensionless heat flux (Boiling number) for both fluids is plotted against the flow quality. The K_1 value is then determined based on various parameter values. The scaling factor K_1 obtained from the above method was found to be a function of density ratio, length to diameter ratio and mass velocity. It is expressed as

$$K_1 = \frac{G_F}{G_W} = C_T\left(1.0 - \frac{0.09G_W}{10^6}\right)\left(1.04 - \frac{0.05}{100}\frac{L}{D}\right)\left(1.41 - 0.02\frac{\rho_f}{\rho_g}\right) \tag{2-39}$$

where C_T is a scaling constant depending on the type of fluid. Table 2-3 illustrates the C_T values for various fluids and the range of K_1 predicted by Eq. (2-39). Note that the C_T values shown in Table 2-3 were determined from the data for pressure at 7 MPa (1000 psia) water-equivalent only; and the water data used in the above scaling relation were calculated by using Biasi et al.'s (1967) water correlation. Dix claimed that the RMS error for the CHF prediction from his scaling

technique against his experimental data was found to be 4.2%, which is also shown in Table 2-3.

2.3.2.6 Ahmad's Scaling Technique

Ahmad (1973) applied Buckingham's Pi theorem to the dimensional analysis for CHF scaling. Similar to Barnett's (1963) CHF scaling law, he found 13 dimensionless groups from the Pi theorem for CHF scaling where these dimensionless groups can be expressed as

$$\Pi_1 = f(\Pi_2, \Pi_3, \cdots, \Pi_{13}) \tag{2-40}$$

Because the parameters from Π_8 to Π_{13} have a weak influence on CHF, Equation (2-40) becomes

$$\Pi_1 = f(\Pi_2, \Pi_3, \cdots, \Pi_7) \tag{2-41}$$

where Π_1—Π_7 are defined in Table 2-4.

Ideally, if

$$(\Pi_2)_{prototype} = (\Pi_2)_{model}$$

$$(\Pi_3)_{prototype} = (\Pi_3)_{model}$$

$$\vdots \qquad \vdots$$

$$(\Pi_7)_{prototype} = (\Pi_7)_{model}$$

then

$$(\Pi_1)_{prototype} = (\Pi_1)_{model}$$

In fact, for many cases the above condition is difficult to satisfy. For example, when

$$(\Pi_6)_{prototype} = (\Pi_6)_{model}$$

but

$$(\Pi_4)_{prototype} \neq (\Pi_4)_{model}$$

then

$$(\Pi_1)_{prototype} \neq (\Pi_1)_{model}$$

Ahmad called this case the distorted model. Therefore he used the so-called compensated distortion technique to create a parameter (ψ_{CHF}) for CHF scaling, i.e.

$$\psi_{CHF} = f(\Pi_2, \Pi_3, \Pi_4) \tag{2-42}$$

The functional relationship between dimensionless groups in Eq. (2-42) can be expressed by a product of power functions, that is,

$$\psi_{CHF} = \Pi_2 \times \Pi_3^{n_1} \times \Pi_4^{n_2} \tag{2-43}$$

The n_1 and n_2 are empirical constants. If values of n_1 and n_2 are known then the CHF prediction equation can be written as

$$\Pi_1 = f(\psi_{CHF}, \Pi_5, \Pi_6, \Pi_7) \tag{2-44}$$

Therefore, if

$$(\psi_{CHF})_{prototype} = (\psi_{CHF})_{model}$$

$$(\Delta H_i/\lambda)_{prototype} = (\Delta H_i/\lambda)_{model} = \Pi_5$$

$$(\rho_L/\rho_g)_{prototype} = (\rho_L/\rho_g)_{model} = \Pi_6$$

and

$$(L/D)_{prototype} = (L/D)_{model} = \Pi_7$$

then

$$(\phi_c/G\lambda)_{prototype} = (\phi_c/G\lambda)_{model} = \Pi_1$$

An optimization program has obtained values of n_1 and n_2 as 2/3 and -1/5, respectively. Therefore, Equation (2-43) becomes

$$\psi_{CHF} = \psi_\sigma = \left[\left(\frac{GD}{\mu_f}\right) \times \left(\frac{\mu_f^2}{\sigma D \rho_f}\right)^{\frac{2}{3}} \times \left(\frac{\mu_g}{\mu_f}\right)^{\frac{1}{5}}\right] \tag{2-45}$$

Note that n_1 and n_2 were based on CFC-12 and water CHF data at ρ_f/ρ_g=20 obtained in tubes. However, Ahmad claimed that Eq. (2-45) is general in nature and is applicable to different fluids, density ratios and geometries.

For some fluids, the property of surface tension may not be predicted accurately. To avoid the difficulty for obtaining a reliable scaling parameter ψ_σ, Ahmad suggested an alternative form of scaling parameter

$$\psi_{CHF} = \psi_\gamma = \left[\left(\frac{GD}{\mu_f}\right) \times \left(\frac{\gamma^{\frac{1}{2}}\mu_f}{D\rho_f^{1/2}}\right)^{\frac{2}{3}} \times \left(\frac{\mu_f}{\mu_g}\right)^{\frac{1}{8}}\right] \tag{2-46}$$

where γ is defined in Eq. (2-17). Ahmad concluded that Eq. (2-46) can be recommended for practical application and for this reason only. In fundamental investigations, Equation (2-45) should be used for the scaling parameter.

According to Eq. (2-44), the Boiling number ($\phi_c/G\lambda$) vs. ψ_γ relationship for the model and prototype should be identical if ρ_f/ρ_g, $\Delta H_i/\lambda$ and L/D are the same for both cases. Ahmad compared this relationship for water, CO_2 and CFC-12 based on data obtained from uniformly heated tubes at ρ_f/ρ_g=20. Figure 2-9 shows that the results fall along the same curve.

2.4 CHF Prediction Methods

2.4.1 Non-Dimensional CHF Equations

2.4.1.1 Ahmad's Empirical Dimensionless Correlation

Ahmad (1973) employed his fluid-to-fluid scaling technique, which has been discussed in previous section, to develop an empirical dimensionless correlation for CHF including the effect of complex geometries. To incorporate the effect of the complex geometries, the equivalent heated diameter (D_{he}) is used as a parameter in the CHF equation. The dimensionless CHF (Boiling number) is rewritten as the following function:

$$\frac{\phi_c}{G\lambda} = f\left(\psi_{CHF}, \frac{\Delta H_i}{\lambda}, \frac{\rho_f}{\rho_g}, \frac{L}{D}, \frac{D_{he}}{D}\right) \tag{2-47}$$

Ahmad introduced a dimensionless power number (W^+) defined as

$$W^+ = \frac{\dfrac{4\phi_c L}{G\lambda D_{he}}}{1+\dfrac{\Delta H_i}{\lambda}} = \frac{X_c + \dfrac{\Delta H_i}{\lambda}}{1 + \dfrac{\Delta H_i}{\lambda}} \tag{2-48}$$

where the top represents the quality increase during a channel experiencing CHF and the bottom represents the maximum possible quality rise. Equation (2-48) can also be arranged in the same form as Eq. (2-47), i.e.,

$$W^+ = f\left(\psi_{CHF}, \frac{\Delta H_i}{\lambda}, \frac{\rho_f}{\rho_g}, \frac{L}{D}, \frac{D_{he}}{D}\right) \tag{2-49}$$

Note that the range of W^+ is

$$0 \le W^+ \le 1$$

Ahmad then proposed a functional form for Eq. (2-49), i.e.,

$$W^+ = 1 - e^{(-Y^+)} \tag{2-50}$$

where

$$Y^+ = f\left(\psi_{CHF}, \frac{\Delta H_i}{\lambda}, \frac{\rho_f}{\rho_g}, \frac{L}{D}, \frac{D_{he}}{D}\right) \tag{2-51}$$

Then, Ahmad derived Y^+ as a product of power function, i.e.,

$$Y^+ = K_2 \psi_{CHF}^a \left(1 + \frac{\Delta H_i}{\lambda}\right)^b \left(\frac{\rho_f}{\rho_g} - 1\right)^c \left(\frac{L}{D}\right)^d \left(\frac{D_{he}}{D}\right)^e \tag{2-52}$$

K_2 and a—e are constants to be determined empirically.

For a circular geometry, Ahmad used the CFC-12 data of a round tube at ρ_f/ρ_g=20 to optimize these constants. These constants result in another form of Eq. (2-50), i.e.

$$W^+ = 1 - e^{\left(\frac{-0.522}{E^+}\right)} \tag{2-53}$$

where

$$E^+ = \frac{E}{\left(1 + \Delta H_i / \lambda\right)^{E/2}} \tag{2-54}$$

and

$$E = \frac{\Psi_{CHF}}{(L/D)^{3/5}} \tag{2-55}$$

Figure 2-10 shows the plot of W^+ vs. E^+ from the CHF data for various fluids. Note that Eq. (2-53) also agrees with water and HCFC-22 data.

For an annular geometry, Ahmad compared 233 published water CHF data with his empirical dimensionless correlation and obtained 8% of overall RMS error. This correlation also compared with Barnett's (1966) correlation and obtained 5.9% of RMS error.

2.4.1.2 Katto's Generalized Correlation for CHF in Vertical and Uniformly Heated Round Tubes

Katto (1978) presented a generalized correlation for CHF in vertical and uniformly heated round tubes. The work of this generalized CHF correlation has been continued by Katto (1979(a), 1979(b), 1980(a), 1980(b), 1980(c), 1982) and Katto and Ohno (1984). Katto and Ohno's version will be mainly discussed in this survey.

Katto (1978) applied dimensional analysis to find the important dimensionless parameters controlling the CHF, that is,

$$\frac{\phi_o}{G\lambda} = f\left(\frac{\rho_g}{\rho_f}, \frac{\sigma\rho_f}{G^2 L}, \frac{L}{D}\right) \tag{2-56}$$

where ϕ_o is the CHF at the zero inlet subcooling condition. Katto then proposed a linear relationship between the CHF and inlet subcooling enthalpy (ΔH_i), i.e.,

$$\phi_c = \phi_o\left(1+K_3\frac{\Delta H_i}{\lambda}\right) \tag{2-57}$$

where K_3 is the inlet subcooling parameter. In Katto and Ohno's version, the CHF is divided into the regimes of $\rho_g/\rho_f<0.15$ and $\rho_g/\rho_f>0.15$. CHF can be calculated by one of the following correlations:

$$\frac{\phi_o}{G\lambda} = C\left(\frac{\sigma\rho_f}{G^2L}\right)^{0.043}\frac{1}{L/D} \tag{2-58}$$

where

C = 0.25 for L/D<50

C=0.25+0.0009[(L/D)-50] for 50≤L/D≤150

C=0.34 for 150>L/D

$$\frac{\phi_o}{G\lambda} = 0.1\left(\frac{\rho_g}{\rho_f}\right)^{0.133}\left(\frac{\sigma\rho_f}{G^2L}\right)^{1/3}\frac{1}{1+0.0031(L/D)} \tag{2-59}$$

$$\frac{\phi_o}{G\lambda} = 0.098\left(\frac{\rho_g}{\rho_f}\right)^{0.133}\left(\frac{\sigma\rho_f}{G^2L}\right)^{0.433}\frac{(L/D)^{0.27}}{1+0.0031(L/D)} \tag{2-60}$$

$$\frac{\phi_o}{G\lambda} = 0.0384\left(\frac{\rho_g}{\rho_f}\right)^{0.6}\left(\frac{\sigma\rho_f}{G^2L}\right)^{0.173}\frac{1}{1+0.28\left(\frac{\sigma\rho_f}{G^2L}\right)^{0.233}\left(\frac{L}{D}\right)} \tag{2-61}$$

and

$$\frac{\phi_o}{G\lambda} = 0.234\left(\frac{\rho_g}{\rho_f}\right)^{0.513}\left(\frac{\sigma\rho_f}{G^2L}\right)^{0.433}\frac{(L/D)^{0.27}}{1+0.0031(L/D)} \tag{2-62}$$

The inlet subcooling parameter K_3 can be calculated by one of the following equations:

$$K_3 = \frac{1.043}{4C\left(\frac{\sigma\rho_f}{G^2L}\right)^{0.043}} \tag{2-63}$$

$$K_3 = \frac{5}{6}\frac{0.0124+(D/L)}{\left(\frac{\rho_g}{\rho_f}\right)^{0.133}\left(\frac{\sigma\rho_f}{G^2L}\right)^{1/3}} \tag{2-64}$$

and

$$K_3 = 1.12\frac{1.52\left(\frac{\sigma\rho_f}{G^2L}\right)^{0.233}+\frac{D}{L}}{\left(\frac{\rho_g}{\rho_f}\right)^{0.6}\left(\frac{\sigma\rho_f}{G^2L}\right)^{0.173}} \tag{2-65}$$

For CHF in the regime of $\rho_g/\rho_f<0.15$, the ϕ_o is determined as

if ϕ_o(2-58)<ϕ_o(2-59), $\phi_o=\phi_o$(2-58)

if ϕ_o(2-58)>ϕ_o(2-59), then

if ϕ_o(2-59)<ϕ_o(2-60), $\phi_o=\phi_o$(2-59)

if ϕ_o(2-59)>ϕ_o(2-60), $\phi_o=\phi_o$(2-60)

In this case, K_3 is calculated as

if K_3(2-63)>K_3(2-64), $K_3=K_3$(2-63)

if K_3(2-63)<K_3(2-64), $K_3=K_3$(2-64)

For CHF in the regime of $\rho_g/\rho_f>0.15$, ϕ_o is determined as

if $\phi_o(2\text{-}58)<\phi_o(2\text{-}62)$, $\phi_o=\phi_o(2\text{-}58)$

if $\phi_o(2\text{-}58)>\phi_o(2\text{-}62)$, then

if $\phi_o(2\text{-}62)>\phi_o(2\text{-}61)$, $\phi_o=\phi_o(2\text{-}62)$

if $\phi_o(2\text{-}62)<\phi_o(2\text{-}61)$, $\phi_o=\phi_o(2\text{-}61)$

also, K_3 is calculated as

if $K_3(2\text{-}63)>K_3(2\text{-}64)$, $K_3=K_3(2\text{-}63)$

if $K_3(2\text{-}63)<K_3(2\text{-}64)$, then

if $K_3(2\text{-}64)>K_3(2\text{-}65)$, $K_3=K_3(2\text{-}64)$

if $K_3(2\text{-}64)<K_3(2\text{-}65)$, $K_3=K_3(2\text{-}65)$

(Numbers in parentheses correspond to equation numbers)

The numerical accuracy of this correlation was not reported by Katto and Ohno. However, it was compared graphically with their own CFC-12 CHF data. Figures 2-11 and 2-12 show the comparison between the correlation and CHF data for the dimensionless CHF vs. $\sigma\rho_f/G^2L$. Katto and Ohno concluded that there is an intermediate regime in the region near $\rho_g/\rho_f=0.15$, and ϕ_o and K_3 also exhibit transitional characteristics between the two regimes. Katto and Ohno (1984) did not state clearly the application range of their generalized CHF correlations.

2.4.1.3 Shah's Generalized Correlation for CHF in Uniformly Heated Vertical Tubes

Shah (1979) presented a generalized graphical method to predict CHF in uniformly heated vertical tubes. Later, in 1987, Shah derived an improved version of this generalized correlation, permitting a computerized calculation from the graphical method and extending its use to more

fluids. In both versions, the Boiling number is expressed as

$$\frac{\phi_c}{G\lambda} = f\left(Y, \frac{L}{D}, P_r, X_i, X_c\right) \tag{2-66}$$

where P_r is the reduced pressure and Y is Shah's correlating parameter, which is written as

$$Y = Pe\ Fr^{0.4}\left(\frac{\mu_f}{\mu_g}\right)^{0.6} \tag{2-67}$$

where

$$Pe = \frac{GDCp_f}{k_f} \qquad (Peclet\ number) \tag{2-68}$$

and

$$Fr = \frac{G^2}{\rho_f^2 g D} \qquad (Froude\ number) \tag{2-69}$$

In Shah's correlation, CHF is divided into the upstream condition correlation (UCC) and the local condition correlation (LCC). In UCC, CHF is determined mainly by the effect of inlet subcooling. However, in the LCC, CHF depends on the local thermodynamic quality. For details of the CHF calculation, see Shah (1987).

Shah (1979) compared his correlating parameter (Y) with Ahmad's scaling parameter (ψ_y), which is shown below:

$$Y = G^{1.8}D^{0.6}\left(\frac{Cp_f}{k_f\rho_f^{0.8}g^{0.4}}\right)\left(\frac{\mu_f}{\mu_g}\right)^{0.6} \tag{2-70}$$

and

$$\psi_{\gamma}^{1.8} = G^{1.8} D^{0.6} \left(\frac{\gamma^{0.6}}{\rho_f^{0.6} \mu_g^{0.225} \mu_f^{0.375}} \right) \qquad (2\text{-}71)$$

Shah (1979) concluded that both parameters are identical in G and D but are different in property function. Shah also concluded that the use of P_r appears to be no different from the use of ρ_f/ρ_g to determine CHF for $P_r \leq 0.9$. Shah's correlation chose P_r because P_r is easier to calculate. The improved Shah's correlation has been tested for the CHF data from 23 fluids instead of the 11 fluids tested on the earlier work. The mean deviation of the improved version against 62 independent sources is about 16%. The parameter ranges of this new version are shown in Table 2-5.

2.4.1.4 Green and Lawther's Dimensionless Empirical Correlation of CHF for CFC-12 and Water

Based on dimensional analysis, Green and Lawther (1981) proposed an empirical dimensionless correlation for CHF in uniformly heated vertical tubes. Their empirical correlation was developed based on the experimental data obtained from CFC-12 and water, and their correlation is not recommended for use at the following parameter conditions:

(1). Mass flux < 300 kg m^{-2} s^{-1}

(2). Dryout quality < 10%

(3). Water-equivalent pressure < 3.5 MPa or > 12 MPa

The dimensionless groups resulting from the dimensional analysis and the relation of CHF with these dimensionless parameters are as follows:

$$\frac{\phi_c D}{\mu_g \lambda} = f\left(\left(\frac{\rho U_\infty D}{\mu}\right)_g, \left(\frac{\mu Cp}{k}\right)_g, \frac{\sigma}{\rho_g D\lambda}, \frac{\rho_f}{\rho_g}, \frac{\mu_f}{\mu_g}, \frac{k_f}{k_g}, \frac{Cp_f}{Cp_g}, \frac{L_b}{D}\right) \qquad (2\text{-}72)$$

where $\phi_c D/\mu_g\lambda$ is the critical-heat-flux number, $(\rho U_\infty D/\mu)_g$ the vapour Reynolds number, $(\mu C_p/k)_g$ the vapour Prandtl number, $\sigma/\rho_g D\lambda$ the surface tension number and L_b/D the dimensionless saturation length (boiling length). After examining the relation of CHF with these dimensionless groups, e.g. the trends for CHF vs. $(\rho U_\infty D/\mu)_g$ and L_b/D etc., Green and Lawther derived a dimensionless correlation for CHF at moderate and high flow rates (for flow $\leq$ 300 kg m^{-2} s^{-1} use Green (1982)). The final form of this correlation is expressed as

$$\frac{\phi_c D}{\mu_g \lambda} = \frac{1}{17000}\left(\frac{\rho_g U_\infty D}{\mu_g}\right)^n \left(\frac{\rho_f}{\rho_g}\right)^m \left(\frac{\sigma}{\rho_g D\lambda}\right)^p f\left(\frac{L_b}{D}\right) Pr_g^q (1+\delta_1)(1-\delta_2) \qquad (2\text{-}73)$$

where

n = 1-exp[-0.0067L_b/D]

m = 0.1+exp[-0.007L_b/D]

p = -0.5(0.15+exp[-0.007L_b/D])

q = -(0.22+0.6exp[-0.011L_b/D])

$f(L_b/D)$ = exp[4.25exp[-0.00366L_b/D]]

δ_1 = exp[-0.14×10^8($\sigma/\rho_g D\lambda$)-0.02(L/D)Pr_g]

δ_2 = 0.75exp[-B(L/D)($G\sigma/\rho_f\mu_f\lambda$)]

and

B = 130.5exp[5.0exp[-0.02L/D]]

Note that δ_1 is a modifier for short tubes, i.e. when the aspect ratio (L/D) is less than 120, and

δ_2 is a modifier for the flow at the lower region of the parameter range, i.e. $300 \leq G \leq 1000$ kg m^{-2} s^{-1}. For CFC-12 CHF data, Green and Lawther claimed that the mean ratio of calculated to experimental CHF is 0.992 and the RMS error is 3.3% for 1760 CHF data. For water CHF data, they claimed that the mean ratio of calculated to experimental CHF is 0.982 and the RMS error is 5.8% for 2063 CHF data.

2.4.1.5 Hauptmann and Lee's Thermodynamic Similarity Correlation for CHF in Tubes and Bundles

Hauptmann and Lee (1983) developed a general correlation for CHF in tubes and bundles based on the assumption that fluid-to-fluid scaling involves the simultaneous similarities of thermodynamics, hydrodynamics and geometry. In their study, CHF experiments were also conducted by using CO_2 in vertical upflow channels, with test conditions corresponding to that of benchmark test in water and CFC-12.

For thermodynamic similarity, the prototype and scaling fluids should have similar heat transfer mechanisms and equivalent thermophysical properties. According to Reid and Sherwood (1987), the properties of various fluids can be written as functions of T_r, P_r and Z_c. For example, the liquid viscosity and thermal conductivity can be expressed as

$$\mu_f = \frac{M^{1/2} P_c^{2/3}}{T_c^{1/6}} f(P_r, Z_c) \tag{2-74}$$

and

$$k_f = \frac{P_c^{2/3}}{T_c^{1/6} M^{1/2}} f(P_r, Z_c) \tag{2-75}$$

where

$P_r = P/P_c$

$Z_c = P_c V_c M/(\bar{R} T_c)$ (critical compressibility factor)

P_c critical pressure

M molecular weight

T_c critical temperature

and

V_c critical volume

For CHF in flow boiling, Hauptmann and Lee proposed a relation including hydrodynamic and geometric similarities, i.e.,

$$\phi_c = a f_1(P_r Z_c) f_2\left(\frac{GD}{\mu_f}\right) f_3\left(\frac{L_b}{D}\right) \tag{2-76}$$

where f_1 is the thermodynamic similarity function, f_2 the hydrodynamic similarity function and f_3 the geometric similarity function. Therefore, the CHF is written as

$$\phi_c = a \left(\frac{\bar{R} T_c P_c^2}{M}\right)^{1/2} P_r^b \left(\frac{GD}{\mu_f}\right)^c \left(\frac{L_b}{D}\right)^d (Z_c)^e \tag{2-77}$$

where $\bar{R}$ is the universal gas constant and L_b is the equilibrium boiling length. In a dimensionless form, Equation (2-77) becomes

$$\phi_c^* = \frac{\phi_c}{\left(\frac{\bar{R}T_c P_c^2}{M}\right)^{1/2}} = a\, P_r^b \left(\frac{GD}{\mu_f}\right)^c \left(\frac{L_b}{D}\right)^d (Z_c)^e \qquad (2\text{-}78)$$

The constants a, b, c, d and e were optimized from experimental CHF data. The optimized constants for both single tubes and bundles are given in Table 2-6. For single tubes, the optimized constants were obtained by using the CO_2 data (Hauptmann et al., 1973) and water data (Lee and Obertelli, 1963). The RMS error for the correlation compared with experimental data are 11.2% and 12.7% for CO_2 and water, respectively. Also, these constants yields 10.3% of RMS error when compared with Stevens et al.'s (1964) CFC-12 CHF data. The parameter ranges for the three fluids correlated are shown in Table 2-7. For the bundle case, the optimized constants were obtained from the water and CFC-12 data (McPherson and Ahmad, 1971). The RMS error between the predicted and measured CHFs for water and CFC-12 are 6.96% and 7.4%, respectively. No CO_2 data are reported for the above comparison. The parameter ranges for the two fluids are shown in Table 2-8.

2.4.2 Tabular Approach

The USSR Academy of Sciences (1977) produced a series of standard tables for CHF. The CHF values are tabulated as a function of the local G, x and P for a tube of 8 mm inside diameter. The CHF for the tube diameter other than 8 mm can be approximated by

$$\phi_{c,D\neq 8mm} = \phi_{c,D=8mm} \times \left(\frac{8}{D}\right)^{1/2} \qquad (2\text{-}79)$$

where $4 \leq D \leq 16$ mm. Note that the standard CHF table from USSR Academy of Sciences has

shown a parametric trend of a so-called "limiting quality" phenomenon (Doroshchuk et al. 1970) as illustrated by region II of Fig. 2-5. Several reviewers (Hewitt, 1978; Bergles, 1979 etc.) have concluded that this is cause by a mixed inlet condition (vapour and liquid). Therefore, the generality of the parametric curve (in Fig. 2-5) is doubtful.

Groeneveld et al. (1986a) also presented a standard CHF table, which is considered accurate and reliable (based on 15000 CHF data), for water in round tubes covering a very wide range of quality, mass flux and pressure. By using the correction factors, this standard table can predict CHF in various flow geometries, e.g. rod bundle, etc., for different flow orientations, and in flow channels with a non-uniform distribution of heat flux. Employing the scaling parameters from the fluid-to-fluid scaling technique (e.g. Ahmad (1973) and Katto and Ohno (1984)), Groeneveld et al. (1986b) converted their standard CHF table for water into a dimensionless form and obtained satisfactory predictions when compared with Weisman and Pei's (1983) and Katto and Ohno's (1984) predicting methods and with CHF data for various fluids.

The CHF table presented by Groeneveld et al. (1986a) is based on local conditions. It presents the CHF for water in tabular form for discrete values of pressure (P), mass flux (G) and critical quality (X_e). The table was derived for an 8 mm tube with vertical upflow of water by statistically averaging the experimental CHF values within each P, G and X_e interval. CHF values for a tube of D≠8 mm are obtained from

$$\phi_{c,D\neq 8mm} = \phi_{c,D=8mm} \times \left(\frac{8}{D}\right)^{1/3} \qquad (2\text{-}80)$$

for $2 \leq D \leq 16$ mm. Linear interpolation is required for non-table P, G and X_e values. CHF values for fluids other than water also can be predicted from this table method. It requires the

use of the fluid-to-fluid scaling technique (Groeneveld et al., 1986b).

Employing the thermodynamic and hydrodynamic similarities, Eqs. (2-4) and (2-8), the Boiling number, Eq. (2-6), is assumed to be equal in both fluids if the G^* values are the same in both fluids. For G^*, Ahmad's scaling parameters (ψ_σ and ψ_γ) and Katto's (derived by Groeneveld et al., 1986b) scaling parameter (ψ_k) can be applied, where Katto's scaling parameter is written as

$$\psi_k = \sqrt{\frac{G^2 D}{\sigma \rho_f}} \tag{2-81}$$

Groeneveld et al. (1986b) concluded that the prediction errors by using the three scaling parameters are approximately equal. Hence, the use of ψ_k is recommended because of its simpler form. Once the similarities of all the scaling parameters are achieved, the CHF for non-aqueous fluid can be calculated by using Eq. (2-6), i.e.,

$$\phi_{c,M} = \left(\frac{\phi_c}{G\lambda}\right)_W \times (G\lambda)_M \tag{2-82}$$

However, CHF prediction error based on the local critical quality (X_c) may be questionable because X_c is an experimentally obtained value and is therefore not known prior to the experiment. As illustrated in Fig. 2-13, the prediction error should be evaluated based on a constant inlet condition and by satisfying the heat balance equation, Eq. (2-5).

2.4.3 CHF Theoretical Models

2.4.3.1 Lee and Mudawwar's Subcooled Flow Model

Lee and Mudawwar (1988) presented the first model based on liquid sublayer dryout (similar to Figs. 2-3b and 2-3c) for CHF in subcooled flow, especially for the flow conditions in pressurized water reactors (PWRs). They showed schematically the phase distribution of subcooled flow immediately before and just after CHF as shown in Fig. 2-14. Their model is based on the following assumptions (which, in turn, are based on observations reported earlier):

(1). Bubble layers (called "Vapour blankets") are formed as a result of small bubbles piling up to form vertically distorted vapour cylinders. The development of each blanket is strongly influenced by neighbouring blankets, which tend to confine its circumferential growth and to prevent liquid from entering the sublayer from the sides of the blanket. Therefore, the equivalent diameter of each blanket is assumed to be approximately equal to the bubble diameter at departure from the heated surface. The departing bubbles are assumed to merge into a distorted blanket, which maintains a constant equivalent diameter while stretching in the direction of flow due to the generation of more vapour by sublayer evaporation. Neighbouring blankets may coalesce circumferentially to form a continuous blanket on the inner wall of the tube.

(2). The velocity of the vapour blanket in the turbulent flow stream is assumed to be the sum of the local liquid velocity and the relative vapour-blanket velocity, determined by a balance between the buoyancy and drag forces exerted on the blanket.

(3). The thin liquid sublayer beneath the blanket is interrupted by the formation of a dry patch after a Helmholtz instability at the sublayer-blanket interface (see Fig. 2-15). The

length of the blanket is assumed to be equal to the critical Helmholtz wavelength.

(4). CHF occurs when the rate of sublayer mass loss by evaporation exceeds that of the liquid entering the sublayer from the core region.

Figure 2-15 shows the control volume surrounding the sublayer and moving at the same velocity as that of the vapour blanket. The CHF occurs when the dry patch persists and spreads quickly, preventing the subcooled liquid from entering the sublayer. Thus, the enthalpy balance cannot be continued between the subcooled liquid and the heated surface. At the onset of CHF, the energy equation is written as

$$\pi D \phi_c L_m = \pi D G_m \delta_m [\lambda + Cp_L (T_{sat} - T_m)] \tag{2-83}$$

where L_m is the length of the sublayer or vapour blanket, δ_m the sublayer thickness, G_m the relative mass velocity of liquid entering the sublayer, Cp_L the specific heat of the liquid and T_m the temperature of the liquid entering the sublayer. The term $(T_{sat}-T_m)$ is correlated as

$$T_{sat} - T_m = a_1(T_{sat} - T_L) \tag{2-84}$$

where a_1 is an empirical constant and T_L is the local mean bulk temperature of the subcooled liquid. Combining Eqs. (2-83) and (2-84), gives

$$\phi_c = \frac{G_m \delta_m [\lambda + a_1 Cp_L (T_{sat} - T_L)]}{L_m} \tag{2-85}$$

To determine the CHF, parametric relations for the relative sublayer mass velocity (G_m), the length of the sublayer or vapour blanket (L_m) and the sublayer thickness (δ_m) are required.

(1). Sublayer mass velocity (G_m) and vapour blanket length (L_m)

The velocity of the vapour blanket in vertical turbulent flow is determined by a balance between buoyancy force and drag force:

$$\frac{\pi}{4}D_b^2 L_m \Delta\rho \cdot g - \frac{1}{2}\rho_L C_D (U_b - U_{bL})\frac{\pi D_b^2}{4} = 0 \qquad (2\text{-}86)$$

where D_b is the equivalent diameter of the vapour blanket, $\Delta\rho=\rho_f-\rho_g$, (U_b-U_{bL}) the relative velocity of the bubble with respect to the liquid at a position corresponding to the centre line of the bubble and C_D the drag coefficient which has been correlated by different investigators. The drag coefficient used in Lee and Mudawwar's model is based on two references:

Harmathy (1960),

$$C_D = \frac{2}{3}D_{eb}\sqrt{\frac{g\Delta\rho}{\sigma}} \qquad (2\text{-}87a)$$

and Chan and Prince (1965),

$$C_D = \frac{48\mu_L}{\rho_L D_{eb}(U_b - U_{bL})} \qquad (2\text{-}87b)$$

where D_{eb} is the equivalent diameter of the bubble. It is postulated that D_{eb} is approximately equal to the departure diameter, D_b, of the coalescing vapour blanket.

To determine the D_b, three references are employed:

Levy (1967),

$$D_b = 0.015\sqrt{\frac{\sigma D}{\tau_w}} \qquad (2\text{-}88a)$$

Cole and Rohsenow (1968),

$$D_b = 1.5\times10^{-4}\sqrt{\frac{\sigma}{g\Delta\rho}}\left(\frac{\rho_L Cp_L T_{sat}}{\rho_g \lambda}\right)^{1.25} \qquad (2\text{-}88b)$$

and Smogalev (1981),

$$D_b = 0.0208\sqrt{\frac{\sigma}{g\Delta\rho}}\left[1 - 0.65(P_c - P)^3\frac{\rho_g \nu_L G}{\rho_L \sigma g}\right]^2 \qquad (2\text{-}88c)$$

where $\tau_w(=f'G^2/2\rho_L)$ is the wall shear stress based on $f'=0.046Re^{-0.2}$ for a pure liquid flowing at Reynolds number (Re) in a tube of diameter D, G the liquid mass velocity, ν_L the liquid kinematic viscosity, P the local static pressure and P_c the critical pressure. Combining Eqs. (2-86) and (2-87) yields the velocity of the vapour blanket:

$$U_b = \sqrt{\frac{2L_m g\Delta\rho}{\rho_L C_D}} + U_{bL} \qquad (2\text{-}89)$$

The velocity profile for a turbulent flow in a tube is represented by the three-layer distribution of liquid velocity, U_L, as a function of distance y from the wall correlated by Arpaci and Larsen (1984):

$$U_L^+ = y^+, \quad 0\le y^+\le 5 \qquad (2\text{-}90a)$$

$$U_L^+ = 5\ln(y^+) - 3.05, \quad 5\le y^+\le 30 \qquad (2\text{-}90b)$$

$$U_L^+ = 2.5\ln(y^+) + 5.5, \quad y^+\ge 30 \qquad (2\text{-}90c)$$

where U_L^+ and y^+ are the dimensionless parameters commonly defined in turbulence text books. Lee and Mudawwar found that the liquid velocity profile around the vapour blanket is within the

buffer region, Eq. (2-90b), for the PWR condition of their interest. Thus, the mean velocity of the liquid at the distance of $y=\delta_m + D_b/2$ from the wall is given by

$$U_{bL} = 0.758 Re^{-0.1} \frac{G}{\rho_L} \left\{ ln \left[\frac{0.152 Re^{-0.1} G(\delta_m + \frac{D_b}{2})}{\mu_L} \right] - 0.61 \right\} \tag{2-91}$$

From Eq. (2-89), the vapour velocity is obtained as

$$U_b = \sqrt{\frac{2L_m \Delta\rho}{\rho_L C_D}} + 0.758 Re^{-0.1} \frac{G}{\rho_L} \left\{ ln \left[\frac{0.152 Re^{-0.1} G(\delta_m + \frac{D_b}{2})}{\mu_L} \right] - 0.61 \right\} \tag{2-92}$$

Also from Eq. (2-89), the length of the sublayer or vapour blanket can be deduced as

$$L_m = \frac{2\pi\sigma(\rho_L + \rho_g)}{\rho_L \rho_g (U_b - U_m)^2} \tag{2-93}$$

where $U_m(=U_{bL})$ is negligible compared to U_b. Therefore, the final forms of the relative microlayer mass velocity and the length of the vapour blanket become

$$G_m = \rho_L U_b \tag{2-94}$$

and

$$L_m \cong \frac{2\pi\sigma(\rho_L + \rho_g)}{\rho_L \rho_g U_b^2} \tag{2-95}$$

Lee and Mudawwar postulated that the CHF occurs as a result of the Helmholtz instability; that is, L_m is assumed to be equal to the critical Helmholtz wavelength.

(2). Sublayer thickness (δ_m)

The liquid sublayer thickness is determined by a force balance on the vapour blanket in the radial direction as illustrated in Fig. 2-16. The rate of momentum flow, M_1 is created by the vapour generated from the sublayer, pushing the vapour blanket away from the wall. The lateral force, F_R, is caused by the rotation of the vapour blanket due to U_L-U_b and δU_{bL}. Just before CHF, the rate of momentum flow is derived as

$$\dot{M}_1 = \rho_g V_b^2 D_b L_m \tag{2-96}$$

where

$$V_b = \frac{\phi_b}{\rho_g \lambda} \tag{2-97}$$

and

$$\phi_b = h_{sc}(T_w - T_{sat}) = \phi - h_{sc}(T_{sat} - T_m) \tag{2-98}$$

where ϕ_b is the portion of the heat flux used by vaporization and h_{sc} the subcooled heat transfer coefficient correlated by Shah (1977). Combining Eqs. (2-84) and (2-96)—(2-98), the rate of momentum due to sublayer evaporation reduces to

$$\dot{M}_1 = \frac{[\phi - a_1 h_{sc}(T_{sat} - T_L)]^2 D_b L_m}{\rho_g \lambda^2} \tag{2-99}$$

Employing Beyerlein et al.'s (1985) derivation for the lateral force on a bubble in turbulent two-phase flow in a vertical tube, a final form of the lateral force is obtained as

$$F_R = \frac{0.421 a_2 Re^{(a_3-0.1)} G D_b^2 L_m}{\delta_m}\left(1+\frac{\delta_m}{\delta_m+D_b}\right)\sqrt{\frac{L_m g \Delta\rho}{\rho_L C_D}} \qquad (2\text{-}100)$$

where a_2 and a_3 are empirical constants. Balancing the rate of momentum, Eq. (2-99), to the lateral force, Eq. (2-100), the sublayer thickness at CHF is given by

$$\delta_m = \frac{0.421 a_2 Re^{(a_3-0.1)} G \rho_g \lambda^2 D_b}{[\phi_c - a_1 h_{sc}(T_{sat}-T_L)]^2}\left(1+\frac{\delta_m}{\delta_m+D_b}\right)\sqrt{\frac{L_m g \Delta\rho}{\rho_L C_D}} \qquad (2\text{-}101)$$

Then, CHF (i.e. ϕ_c) can be predicted by substituting Eqs. (2-94), (2-95) and (2-101) into Eq. (2-85). However, iterative calculation is required to obtain the final value of the CHF prediction.

Lee and Mudawwar evaluated the empirical constants a_1, a_2 and a_3 based on CHF values recommended by the USSR Academy of Sciences (1977). Table 2-9 shows the empirical values of a_1, a_2 and a_3 evaluated based on various correlations for subcooled heat-transfer coefficient (Mole and Shaw, 1972; Shah, 1977; Gungor and Winterton, 1986), the bubble drag coefficient (Harmathy, 1960; Chan and Prince, 1965) and the bubble departure diameter (Levy, 1967; Cole and Rohsenow, 1968; Smogalev, 1981). The accuracy of their model was also tested against 89 experimental CHF data points from sources other than the USSR Academy of Sciences. Their model obtained the least mean deviation of 11.94% against USSR's data base and 13.37% against other data bases when a_1, a_2 and a_3 are equal to 0.35, 240 and -0.8, respectively. However, the latter data base yields 13.4% of mean deviation against the W-3 correlation (Tong, 1972). Lee and Mudawwar claimed that the W-3 correlation requires 17 empirical constants and their model only includes three constants.

The validity of Lee and Mudawwar's CHF model to fluids other than water remains unknown. They also emphasized that the development of the model requires the use of available correlations to describe the dynamics of bubbles in the wall region. Therefore, the accuracy of their model strongly depends on the reliability of these individual correlations. However, this model can be adjusted by using more suitable correlations for specific ranges of conditions.

2.4.3.2 Katto's Subcooled Flow Model

Following the same principle of Lee and Mudawwar's model, i.e. similar flow configuration of liquid sublayer underneath the vapour blanket, Katto (1990a) also presented a physical model with a somewhat different type of analysis. In Katto's model, the boiling crisis is assumed to occur when a liquid sublayer of initial thickness δ_m is depleted during the passage time (τ) of a vapour blanket of length L_B and velocity U_B sliding on the liquid sublayer, where L_B and U_B correspond to L_m and U_b in Lee and Mudawwar's model. The evaluation of the initial sublayer thickness (δ_m) was modified from Haramura and Katto's (1983) model used for pool boiling CHF. The length of the vapour blanket (L_B) is obtained by essentially the same procedure as that employed by Lee and Mudawwar, i.e. Eq. (2-95). The velocity of the vapour blanket (U_B) is evaluated by relating it to the local velocity (U_δ) of the homogeneous two-phase flow at the distance of δ_m from the tube wall, i.e.

$$U_B = kU_\delta \tag{2-102}$$

where U_δ is determined from Eq. (2-90) with U_L^+ being replaced by U_δ^+ and k is the only empirical constant required in this model to predict the subcooled CHF. It is obtained by correlating the CHF data of subcooled flow boiling of water in 8-mm-diameter tubes, presented

by the USSR Academy of Sciences (1977).

The vapour velocity coefficient (k) evaluated in Katto's model is not continuous in magnitude at the boundary between two adjacent void fraction regimes, which causes some degree of discontinuity in CHF prediction and gives rise to a dramatic increase of computational time if an averaging procedure for the CHF value near the boundary between two adjacent void fraction regimes is needed. Therefore, Katto (1990b) presented a modified version not only to improve the evaluation of the vapour velocity coefficient but also to investigate the nature of this empirical coefficient so that a better prediction of CHF for non-aqueous fluid can be obtained. The improved version of the vapour velocity coefficient was obtained as

$$k = \frac{242[1+K_4(0.355-\alpha)][1+K_5(0.1-\alpha)]}{[0.0197+(\rho_g/\rho_f)^{0.733}][1+90.3(\rho_g/\rho_f)^{3.68}]} Re^{-0.8} \qquad (2\text{-}103)$$

where

α	void fraction
$K_4=0$	for $\alpha > 0.355$
$K_4=3.76$	for $\alpha < 0.355$
$K_5=0$	for $\alpha > 0.1$
$K_5=2.62$	for $\alpha < 0.1$

Further, Katto (1992) modified his models (1990a and 1990b) to be capable of predicting the subcooled water CHF for a very wide range of pressure (0.1—20 MPa). Since reliable data for subcooled water CHF at low pressure conditions (about 0.1 MPa) are scarce, Katto's (1992) improved model can facilitate the study of CHF in a low pressure condition. Detailed procedures of CHF prediction can be found in Katto (1990a, 1990b and 1992). The prediction accuracy of

CHF of Katto's (1990b) model for various fluids is illustrated in Table 2-10.

Since there are no existing experimental data to be compared with the predicted values of δ_m, L_B, U_B and τ. Katto (1990a) compared these quantities predicted from his model with those predicted from Lee and Mudawwar's (1988) model by using water table CHF values from the USSR Academy of Sciences (1977). These predicted quantities from Katto's and Lee and Mudawwar's models are shown in Table 2-11 and Table 2-12, respectively. From these tables, magnitudes of δ_m, L_B and τ from Lee and Mudawwar's prediction are much smaller than Katto's prediction. Because of the large discrepancies in the prediction of δ_m, L_B and τ between these two models, it is recommended that more experimental and analytical work is needed to permit a better estimate of these quantities.

2.4.3.3 Weisman and Pei's Bubbly Flow Model

Based on a similar flow pattern as shown in Figure 2-1, Weisman and Pei (1983) developed a CHF model for flow at low quality conditions. Here, a "bubble boundary layer" is formed along the flow; at high heat fluxes, this layer can become thick enough to prevent enthalpy transport between the heated surface and the liquid core, leading to the occurrence of CHF. The development of the model is based on the following assumptions:

(1). CHF is a local phenomenon in subcooled and low-quality flow conditions.

(2). The turbulent eddy size in the bubbly layer is insufficient to transport the bubbles radially when the bubbly layer is thick enough to fill the region close to the wall. Then, the bubbly layer is assumed to be at maximum thickness at the location of CHF.

(3). CHF occurs when the volume fraction of vapour in the bubbly layer exceeds the critical

void fraction. The critical void fraction is the void fraction obtained when an array of ellipsoidal bubbles can be maintained without significant contact between the bubbles.

(4). The volume fraction of vapour in the bubbly layer is determined by a balance between the outward flow of vapour and the inward flow of liquid at the bubbly-layer-core interface.

Figure 2-17 shows the control volume segment of two-phase mass transfer at the location of CHF. The quality in the bubbly layer is assumed as a constant average value, x_2. The total mass balance in the bubbly layer is

$$\dot{m}_3 = \Delta\dot{m}_2 + \dot{m}_4 \tag{2-104}$$

where $\dot{m}_3$ is the total flow rate from the core to the bubbly layer, $\dot{m}_4$ the total flow rate from the bubbly layer to the core and $\Delta\dot{m}_2$ the difference between the axial flow in and out of the bubbly-layer control volume. Then, a mass balance of the liquid in the bubbly layer gives

$$\dot{m}_3(1-x_1)=\frac{\phi_b(2\pi r)\Delta z}{\lambda}-\dot{m}_2(\Delta x_2)+\Delta\dot{m}_2(1-x_2)+\dot{m}_4(1-x_2) \tag{2-105}$$

where ϕ_b is the portion of total heat flux effective in generating vapour, r the radial position from centre to the wall of the tube and x_1 and x_2 the qualities at the core and bubbly layer, respectively. Omitting the second order term, Equation (2-105) can be further simplified to a dimensionless form:

$$\frac{\phi}{\lambda G_3}\frac{h_L-h_{Ld}}{h_f-h_{Ld}} = (x_2-x_1) \tag{2-106}$$

where

G_3 = $\dot{m}_3/[2\pi\Delta L(R-s)]$

s = bubbly layer thickness

h_L = enthalpy of liquid

h_f = saturated liquid enthalpy

h_{Ld} = enthalpy at the point of bubble detachment

Weisman and Pei postulated that the heat flux ϕ in the above equation becomes the CHF when x_2 corresponds to the critical void fraction. The critical void fraction was determined based on the investigations of Tong (1965) and Cumo et al. (1975) that bubbles are approximately ellipsoidal with the ratio of major to minor ellipse axes being about 3:1. Then it is assumed that the maximum void fraction can be obtained when the bubbles inside the bubbly layer are just touching, or $\alpha_2=\alpha_{CHF}=0.82$. The x_2 is thus calculated from α_2 based on the assumption that vapour slip is negligible, and it is believed that this assumption is reasonable at high mass flow rate (for water, G≥875 kg m^{-2} s^{-1}).

To evaluate the mass transfer between the core and the bubbly layer, the magnitude of turbulent interchange at the bubbly-layer-core interface is required. Pei (1981) derived an equation for the turbulent intensity at the bubbly-layer-core interface as

$$i_b=0.462\left(\frac{GD}{\mu_{avg}}\right)^{-0.1} K_6^{0.6}\left(\frac{D_p}{D}\right)^{0.6}\left[1+a_4\left(\frac{\rho_f-\rho_g}{\rho_g}\right)\right] \qquad (2\text{-}107)$$

where K_6 and a_4 were obtained by an empirical fit of experimental CHF data and were found to be

K_6 = 0.24

a_4 = 0.135, $G \le 9.7\times10^6$ kg h^{-1} m^{-2}

$$a_4 = 0.135\times(G/9.7\times10^6)^{-0.3}$$

D_p is the average bubble diameter and is determined using Levy's (1966) model, which balances buoyancy and drag forces against surface tension. For subcooled and low-quality flow conditions, the flow velocity usually is high enough to neglect the effect of buoyancy force. Therefore,

$$D_p = 0.015\left(\frac{\delta\rho_{avg}\sigma D_h}{f' G^2}\right) \tag{2-108}$$

where f' is the friction factor. The range of bubble diameters is found to be from 0.001 to 0.005 cm.

The G_3 in Eq. (2-106) can be derived as

$$G_3 = G\psi i_b \tag{2-109}$$

and

$$\psi = \frac{1}{\sqrt{2\pi}}e^{-\frac{1}{2}\left(\frac{v_{11}}{\sigma_{v'}}\right)} - \frac{1}{2}\left(\frac{v_{11}}{\sigma_{v'}}\right)erfc\left(\frac{1}{\sqrt{2}}\frac{v_{11}}{\sigma_{v'}}\right) \tag{2-110}$$

where

$$v_{11} = \frac{\dot{\phi}_b}{\rho_g\lambda} \tag{2-111}$$

and

$$\sigma_{v'} = \frac{i_b G}{\rho_{avg}} = i_b\left[\frac{G}{\rho_L}+\left(\frac{G}{\rho_g}-\frac{G}{\rho_L}\right)x_{avg}\right] \tag{2-112}$$

Finally, Equation (2-106) becomes

$$\phi = \phi_c = \lambda G(x_2 - x_1) i_b \psi \left(\frac{h_f - h_{Ld}}{h_L - h_{Ld}} \right) \qquad (2\text{-}113)$$

For details of the calculations for x_1, x_2, h_L and h_{Ld}, see Weisman and Pei (1983). An iterative calculation is required to compute ϕ_c. The ranges of parameters for water considered by the model are:

Pressure (MPa):	2—20.5
Mass flux (kg m^{-2} s^{-1}):	972—13600
Heated length (m):	0.36—3.6
Diameter (cm):	0.115—3.75
α_{CHF}:	≤ 0.6

Weisman and Pei set a upper limit of α_{CHF} to 0.6 rather than 0.82 to ensure the flow is in bubbly flow condition. Weisman and Pei also extended the application of their model to fluids other than water without a change of empirical constants. Based on a comparison of their model with various fluids, their model underpredicts the CHF for water and overpredicts the CHF for non-aqueous fluids. However, the comparison of their predicted CHF against the experimental CHF showed reasonable agreement. Compared with other prediction methods for water CHF, e.g. W-3 (Tong, 1967) and CISE (Bertoletti et al., 1964a), Weisman and Pei's model obtained a better prediction.

An independent assessment of Weisman and Pei's model was conducted by Kiameh (1986). The results of this assessment are summarized as follows:

(1). This model underpredicts the water CHF and overpredicts the CHF for non-aqueous fluids.

(2). The prediction error was reasonable and decreases with increasing pressure.

(3). For pressures lower than 2 MPa, the model has a convergence problem.

(4). The model is applicable for void fractions less than 60% and qualities less than 20%.

(5). The model also performs adequately at highly subcooled conditions: as low as -55% dryout quality.

(6). The model is limited to the bubbly flow pattern in which the slip between liquid and vapour is negligible.

2.4.3.4 Ying and Weisman's Bubbly Flow Model for Intermediate Quality Condition

Since the upper limit of α_{CHF} in Weisman and Pei's model is 0.6, at low pressure conditions (e.g. water at 35 bar) the dryout quality in the model is limited to about 3% only. Even for water at 140 bar, the dryout quality cannot exceed 18%. Therefore, Ying and Weisman (1986) extended this model for void fraction in the bubbly region near the wall up to 0.8, which corresponds to the intermediate dryout quality (e.g. dryout quality≤24% for water at 100 bar).

At low average void fraction conditions, Weisman and Pei used a flat void profile across the central core in tubes and it is reasonable to use average core quality (x_1) in Eq. (2-106). However, as the average void fraction increases, the radial void profile is no longer flat and begins to take on a parabolic shape. It means that the fluid interchanging with the bubbly layer is at a quality whose value is smaller than x_1. Therefore, the Eq. (2-106) is modified to

$$\frac{\phi}{\lambda G_3}\frac{h_L - h_{Ld}}{h_f - h_{Ld}} = (x_2 - x_{1,eff}) \qquad (2\text{-}114)$$

where $x_{1,eff}$ is the quality corresponding to α_{eff} and the α_{eff} in round tubes is correlated as

$$\alpha_{eff} = \overline{\alpha} \quad for \quad \overline{\alpha} \le 0.642 \tag{2-115}$$

$$\alpha_{eff} = 0.642 + 0.37\,(\overline{\alpha} - 0.642) \quad for \quad 0.642 \le \overline{\alpha} \le 0.788 \tag{2-116}$$

and

$$\alpha_{eff} = 0.696 + 0.2\,(\overline{\alpha} - 0.788) \quad for \quad 0.788 \le \overline{\alpha} \le 0.81 \tag{2-117}$$

where α_{eff} is the void fraction in the core at edge of bubbly layer and $\overline{\alpha}$ is the average void fraction in the core. The expansion of void fraction range also allows the range of mass flux to be reduced to 1.8×10^{6} kg m^{-2} h^{-1}.

Ying and Weisman claimed that reasonable agreement has been obtained between the test data and the model although their model results in underpredictions when compared with water and Freon-11 data. They also concluded that the new application range of $\alpha \le 0.8$ is close to the upper limit of the DNB mechanism and they therefore suggested that, at higher void fractions, their model would be inapplicable.

2.4.3.5 Whalley et al.'s Annular Flow Model

Following the mechanism observed in high-quality flow conditions as discussed in Section 2.2.2, Whalley et al. (1974 and 1978) presented a model to predict CHF in the annular type of flow condition. Their model analyzes the evolution of the liquid distribution associated with processes of droplet mass transfer between the vapour core and liquid film along the heated length in uniformly heated vertical tubes. From the mass balance and upstream information, liquid-film flow rate, vapour flow rate, liquid film thickness, pressure gradient, droplet entrainment rate and droplet deposition rate can be determined. The effects of flashing of liquid

flow, variation of inlet quality, inlet flow transients and flow in complex geometries have also been investigated.

The governing equations for this model are derived based on the assumptions that the liquid film does not contain vapour and the average vapour-liquid interface is cylindrical. A control volume is shown in Fig. 2-18 to describe the mass balances for the different phases. During the time δt, the mass fluxes entering the control volume are denoted by liquid film (G_{LF}), entrained liquid (G_{LE}) and vapour (G_G); and the mass fluxes leaving the control volume are expressed as $(G_{LF}+(\partial G_{LF}/\partial z)\delta z)$, $(G_{LE}+(\partial G_{LE}/\partial z)\delta z)$ and $(G_G+(\partial G_G/\partial z)\delta z)$. At the same time, the heat flux through the wall evaporates the liquid film with the flux of ϕ/λ. Other mass flux exchanges such as the entrainment of droplets from large amplitude waves, the deposition of droplets onto the liquid film and the evaporation of droplets due to the pressure gradient are also considered.

From the mass balance, the continuity equations for each flux (i.e. G_{LF}, G_{LE} and G_G) are written as below for the limit of δz approaching zero.

$$\frac{\partial(1-\alpha_D)\rho_f}{\partial t}+\frac{\partial G_{LF}}{\partial z} = \frac{4}{D}\left(D_D-E_E-\frac{\phi}{\lambda}-F_{LF}\right) \qquad (2\text{-}118)$$

$$\frac{\partial[\alpha_D(1-\alpha_D)]\rho_f}{\partial t}+\frac{\partial G_{LE}}{\partial z} = \frac{4}{D}(E_E-D_D-F_{LE}) \qquad (2\text{-}119)$$

and

$$\frac{\partial \alpha_D \alpha_G \rho_f}{\partial t}+\frac{\partial G_G}{\partial z} = \frac{4}{D}\left(\frac{\phi}{\lambda}+F_{LF}+F_{LE}\right) \qquad (2\text{-}120)$$

where α_D is the fraction of the tube cross-section occupied by the droplets and vapour, α_G the

fraction of core cross-section occupied by vapour, z the axial location in the channel, D_D the droplet deposition rate, E_E the entrainment mass flux, F the flashing rate and ϕ the heat flux. The equation for the overall heat balance is required to form a complete set. Therefore,

$$\frac{\partial}{\partial t}(h_f G_{LF} + h_f G_{LE} + h_g G_G) + \frac{\partial}{\partial t}[(1-\alpha_D)\rho_f U_{LF} + \alpha_D(1-\alpha_G)\rho_f U_{LF} + \alpha\alpha'\rho_g U_G] = \frac{4\phi}{D} \qquad (2\text{-}121)$$

where D is the tube diameter, α' the void fraction in the core cross-section, and U_{LF} and U_G the velocities of liquid film and the vapour, respectively.

Equations (2-118)—(2-121) can be simplified for various special cases, e.g. steady state, thermodynamic equilibrium and non-flashing effect etc., associated with their initial and boundary conditions. In this section, only the relationships between the variables and some assumptions common to all special cases are described, permitting the solution for the above set of equations. Firstly, from the process of classical chemical engineering mass transfer, the relation between deposition and mass fluxes can be modelled as

$$D_D = k_1 \cdot c \qquad (2\text{-}122)$$

where k_1 is the mass transfer coefficient which has been correlated as a function of surface tension as shown in Fig. 2-19 and c is the mass concentration of liquid droplets in the vapour core. The velocity of the droplets in the vapour core is assumed to be the same as that of vapour, V_{GC}, and this leads to the relationships

$$V_{GC} = \frac{G_{LE}}{\rho_f} + \frac{G_G}{\rho_g}, \qquad c = \frac{G_{LE}}{V_{GC}} \qquad (2\text{-}123)$$

Secondly, the entrainment process is described by an approximate equilibrium situation

in adiabatic flow, in which D_D=E_E. From Eq. (2-122), it is written as

$$E_E = k_1 \cdot C_{EQ} \tag{2-124}$$

where C_{EQ} is the local equilibrium concentration. The value of C_{EQ} is calculated from a curve-fit correlation (Fig. 2-20) by Hutchinson and Whalley (1972) using a dimensionless group

$$S = \frac{\tau_i \cdot m}{\sigma} \tag{2-125}$$

where τ_i is the interfacial shear stress, m the liquid film thickness and σ the surface tension. In order to determine S, two relationships are used as follows:

(1) Geometrical similarity relationship

The interfacial shear stress (τ_i) is expressed in terms of the core velocity

$$\tau_i = \frac{1}{2}\rho_g f_{GC} V_{GC}^2 \tag{2-126}$$

where f_{GC} is an interfacial friction factor given by Wallis (1970)

$$f_{GC} = f_G \left(1+\frac{360\, m}{D}\right) \tag{2-127}$$

where f_G is a modified gas friction factor expressed as

$$f_G = 0.079\, Re_{GC}^{-1/4}, \qquad Re_{GC} = (G_G+G_{LE})\frac{D}{\mu_g} \tag{2-128}$$

(2) Triangular relationship

The liquid film flow, liquid film thickness and pressure drop are related to each other by a suitable turbulent velocity profile for the liquid film. Any one of the

parameters can be determined if the other two are known. From Armand (1946) and Turner and Wallis (1965), the relation between the liquid film thickness and the pressure drop is given as

$$\frac{4m}{D} = \left[\frac{(dP/dz)_{LF}}{(dP/dz)}\right]^{1/2} \tag{2-129}$$

where dP/dz is the total frictional pressure drop approximated by

$$\frac{dP}{dz} = -\frac{4\tau_i}{D} \tag{2-130}$$

and $(dP/dz)_{LF}$, the liquid film frictional pressure drop, is calculated as

$$\left(\frac{dP}{dz}\right)_{LF} = \frac{2\,G_{LF}^2 f_L}{\rho_f D} \tag{2-131}$$

where f_L is the liquid-film friction factor depending on the liquid-film Reynolds number and is calculated as

$$f_L = 0.079\,Re_{LF}^{-1/4}, \qquad Re_{LF} = G_{LF}\frac{D}{\mu_f} \tag{2-132}$$

An independent computerized program procedure for using this model to predict the CHF in annular flow has been developed by Chin (1985), in which Hewitt and Roberts's (1969) flow pattern map is used to determine the CHF data for annular flow. The CHF predictions are compared with an experimental data base (15,000 data points) with 44.9% of RMS error. Chin concluded that such a large error is due to the incapability of determining the existence of annular flow from the flow pattern map. Detail of his assessment can be found in Chin's thesis

(1985).

2.5 Experimental Data Base

CHF experiments have been conducted in many laboratories using various fluids. Most of the CHF data were obtained for water because of the importance of CHF in the design and safety analysis of nuclear reactors. Groeneveld et al.'s (1968a) water CHF Look-up Table was based on a large data base (15000 points). Compared to this water CHF data bank, the non-aqueous CHF data base is very limited. Since a full-scale experiment of CHF for a nuclear reactor core is usually impossible, smaller scale CHF tests on electrically-heated fuel-bundle simulators are usually performed in experimental rigs using fluids other than water. The water CHF then can be scaled through the fluid-to-fluid scaling techniques using the non-aqueous fluids CHF tests. From the literature, the working fluids in most CHF scaling tests are refrigerants (CFC's) because of their lower latent heat and lower critical pressure compared with water. Table 2-13 summarizes the non-aqueous CHF data base.

2.6 Summary

The generalized CHF prediction methods can be categorized into (1) non-dimensional CHF equations (2) theoretically based models, and (3) data based CHF tables. The non-dimensional CHF equations can provide accurate predictions, however, only for a limited range. The application for these CHF equations is thus restricted. The analytical methods can be applied to more general flow conditions with less accuracy due to their generality. Most

analytical methods contain some empirical constants. To apply the analytical methods for various fluids, those empirical constants also need to be generalized. The table method usually is based on water CHF data due to the large water-CHF data base. Using fluid-to-fluid scaling techniques, the water-based CHF table can be applied to various fluids. The application range of flow conditions (e.g. pressure, mass flux, dryout quality etc.) are wider than the non-dimensional CHF equations and analytical methods. Among these various methods, the table method has become popular because of its simplicity and the well developed fluid-to-fluid scaling techniques. All these methods employ various dimensionless groups associated with the fluid-to-fluid scaling theories. CHF experiments for non-aqueous fluids are needed to verify the validity of the scaling techniques, especially for the particular flow conditions or for complex geometries. A summary of the CHF scaling techniques and various prediction methods discussed in this survey is given in Table 2-14.

Table 2-1 Possible sets of scaling laws (Barnett 1964). (Reproduced from Stevens and Kirby, 1964)

Set No.	Physical properties assumed important in addition to λ, ρ_f and ρ_g	Resulting dimensionless equation assuming $\phi_c = f(L, D, G, P, \Delta H_l)$	Implied ratio of variables in water at 1000 psi and CFC-12 at 155 psi (abs.), i.e. the scaling factor F			
			$F_1=F_D$	F_G	$F_{\Delta H}$	F_ϕ
1	Cp_f, k_f, β	$\frac{\phi_c \beta^{1/2} Cp_f^{1/2}}{\lambda^{3/2}\rho_f^{1/2}} = f\left(\frac{L}{D}, \frac{DCp_f^{1/2}\lambda^{1/2}\rho_f^{1/2}}{k_f \beta^{1/2}}, \frac{G\beta^{1/2}Cp_f^{1/2}}{\lambda^{1/2}\rho_f^{1/2}}, \frac{\rho_f}{\rho_g}, \frac{\Delta H_l}{\lambda}\right)$	0.588	2.33	11.72	27.32
2	Cp_f, k_f	$\frac{\phi_C}{\rho_f \lambda^{3/2}} = f\left(\frac{L}{D}, \frac{DCp_f\rho_f\lambda^{1/2}}{k_f}, \frac{G}{\rho_f\lambda^{1/2}}, \frac{\rho_f}{\rho_g}, \frac{\Delta H_l}{\lambda}\right)$	0.669	2.053	11.72	24.03
3	Cp_f, k_f, σ	$\frac{\phi_c k_f}{\lambda\sigma\rho_f Cp_f} = f\left(\frac{L}{D}, \frac{D\sigma\rho_f Cp_f^2}{k_f^2}, \frac{Gk_f}{\sigma\rho_f Cp_f}, \frac{\rho_f}{\rho_g}, \frac{\Delta H_l}{\lambda}\right)$	1.155	1.189	11.72	13.92
4	Cp_f, k_f, γ	$\frac{\phi_c \gamma^{1/2}}{\lambda\rho_f^{1/2}} = f\left(\frac{L}{D}, \frac{DCp_f\rho_f^{1/2}}{k_f\gamma^{1/2}}, \frac{G\gamma^{1/2}}{\rho_f^{1/2}}, \frac{\rho_f}{\rho_g}, \frac{\Delta H_l}{\lambda}\right)$	0.717	1.914	11.72	22.43
5	β, k_f, γ	$\frac{\phi_c \gamma^{1/2}}{\lambda\rho_f^{1/2}} = f\left(\frac{L}{D}, \frac{D\lambda\gamma^{1/2}\rho_f^{1/2}}{\beta k_f}, \frac{G\gamma^{1/2}}{\rho_f^{1/2}}, \frac{\rho_f}{\rho_g}, \frac{\Delta H_l}{\lambda}\right)$	0.482	1.914	11.72	22.43
6	σ, μ_f	$\frac{\phi_c \mu_f}{\lambda\sigma\rho_f} = f\left(\frac{L}{D}, \frac{D\sigma\rho_f}{\mu_f^2}, \frac{G\mu_f}{\sigma\rho_f}, \frac{\rho_f}{\rho_g}, \frac{\Delta H_l}{\lambda}\right)$	0.1016	4.007	11.72	46.95
7	σ, μ_g	$\frac{\phi_c \mu_g}{\lambda\sigma\rho_f} = f\left(\frac{L}{D}, \frac{D\sigma\rho_f}{\mu_g^2}, \frac{G\mu_g}{\sigma\rho_f}, \frac{\rho_f}{\rho_g}, \frac{\Delta H_l}{\lambda}\right)$	1.488	1.407	11.72	12.27
8	μ_f, γ	$\frac{\phi_c \gamma^{1/2}}{\lambda\rho_f^{1/2}} = f\left(\frac{L}{D}, \frac{D\rho_f^{1/2}}{\mu_f\gamma^{1/2}}, \frac{G\gamma^{1/2}}{\rho_f^{1/2}}, \frac{\rho_f}{\rho_g}, \frac{\Delta H_l}{\lambda}\right)$	0.2128	1.914	11.72	22.43
9	μ_f, k_f, β	$\frac{\phi_c \beta^{1/2} k_f^{1/2}}{\lambda^{3/2}\rho_f^{1/2}\mu_f^{1/2}} = f\left(\frac{L}{D}, \frac{D\lambda^{1/2}\rho_f^{1/2}}{k_f^{1/2}\beta^{1/2}\mu_f^{1/2}}, \frac{G\beta^{1/2}k_f^{1/2}}{\lambda^{1/2}\rho_f^{1/2}\mu_f^{1/2}}, \frac{\rho_f}{\rho_g}, \frac{\Delta H_l}{\lambda}\right)$	0.3204	1.27	11.72	14.87

Table 2-1 (Continued)

Set No.	Physical properties assumed important in addition to λ, ρ_f and ρ_g	Resulting dimensionless equation assuming $\phi_c = f(L, D, G, P, \Delta H_l)$	Implied ratio of variables in water at 1000 psi and CFC-12 at 155 psi (abs.), i.e. the scaling factor F			
			$F_L=F_D$	F_G	$F_{\Delta H}$	F_ϕ
10	μ_g, γ	$\frac{\phi_c \gamma^{1/2}}{\lambda \rho_f^{1/2}} = f\left(\frac{L}{D}, \frac{D\rho_f^{1/2}}{\mu_g \gamma^{1/2}}, \frac{G\gamma^{1/2}}{\rho_f^{1/2}}, \frac{\rho_f}{\rho_g}, \frac{\Delta H_l}{\lambda}\right)$	0.8144	1.914	11.72	22.43
11	σ, γ	$\frac{\phi_c \gamma^{1/2}}{\lambda \rho_f^{1/2}} = f\left(\frac{L}{D}, \frac{D}{\sigma \gamma}, \frac{G\gamma^{1/2}}{\rho_f^{1/2}}, \frac{\rho_f}{\rho_g}, \frac{\Delta H_l}{\lambda}\right)$	0.4455	1.914	11.72	22.43
12	Cp_g, k_g, β	$\frac{\phi_c \beta^{1/2} Cp_g^{1/2}}{\lambda^{3/2} \rho_f^{1/2}} = f\left(\frac{L}{D}, \frac{DCp_g^{1/2}\lambda^{1/2}\rho_f^{1/2}}{k_g \beta^{1/2}}, \frac{G\beta^{1/2}Cp_g^{1/2}}{\lambda^{1/2}\rho_f^{1/2}}, \frac{\rho_f}{\rho_g}, \frac{\Delta H_l}{\lambda}\right)$	0.371	1.968	11.72	23.06
13	Cp_g, k_g, γ	$\frac{\phi_c \gamma^{1/2}}{\lambda \rho_f^{1/2}} = f\left(\frac{L}{D}, \frac{DCp_g\rho_f^{1/2}}{k_g \gamma^{1/2}}, \frac{G\gamma^{1/2}}{\rho_f^{1/2}}, \frac{\rho_f}{\rho_g}, \frac{\Delta H_l}{\lambda}\right)$	0.3814	1.914	11.72	22.43
14	Cp_g, k_g, σ	$\frac{\phi_c k_g}{\lambda \sigma \rho_f Cp_g} = f\left(\frac{L}{D}, \frac{D\sigma\rho_f Cp_g^2}{k_g^2}, \frac{Gk_g}{\sigma\rho_f Cp_g}, \frac{\rho_f}{\rho_g}, \frac{\Delta H_l}{\lambda}\right)$	0.6269	2.487	11.72	29.13

Table 2-2 Parameter range of Dix's (1970) CFC-114 CHF test.

Parameter	Minimum	Maximum	Unit
ρ_f/ρ_g	10.7	20.6	—
Pressure	123	200	psia
Pressure (water-equiv.)	1000	1600	psia
Mass velocity	0.3×10^6	1.5×10^6	lb hr^{-1} ft^{-2}
$\Delta H_i/\lambda$	0.03	0.54	—
Diameter	0.393	0.555	inch
Length	25	76	inch

Table 2-3 CFC scaling constant and heat flux prediction error from Dix (1970).

CFC or HCFC	Scaling constant C_T	K_t range	No. of points	RMS error (%)
CFC-114	0.740	0.54–0.87	424	4.2
CFC-12	0.800	0.51–0.80	973	6.3
HCFC-22	0.807	0.65–0.72	11	3.6
CFC-21	0.920	0.61–0.90	557	8.5

Table 2-4 Scaling parameters derived by Ahmad (1973).

Parameter	Formula	Definition
Π_1	$\phi/(G\lambda)$	Boiling number
Π_2	$(GD)/\mu_f$	Reynolds number
Π_3	$\mu_f^2/(\sigma D\rho_f)$	Weber-Reynolds number
Π_4	μ_f/μ_g	Liquid/vapour viscosity ratio
Π_5	$\Delta H_i/\lambda$	Subcooling number
Π_6	ρ_f/ρ_g	Liquid/vapour density ratio
Π_7	L/D	Specified geometric similarity

Table 2-5 Parameter range of Shah's correlation.

Parameter	Range	Unit
Diameter	0.315 – 37.5	mm
L/D	1.3 – 940	–
Mass flux	4 – 29051	kg m^{-2} s^{-1}
Reduced pressure (P_r)	0.0014 – 0.96	–
Inlet quality (x_{in})	-4 – 0.85	–
Critical quality (x_c)	-2.6 – 1	–

Table 2-6 Optimized constants for single tubes and bundles of Hauptmann and Lee's (1983) correlation.

Geometry	a	b	c	d	e
Single tube	0.0001505	-0.6138644	0.2172085	-0.4894932	0.361891
Bundles	0.0001342	-0.228348	0.480077	-0.40322	3.23069

Table 2-7 Parameter ranges in single tube of Hauptmann and Lee's (1983) correlation.

	CO_2	water	CFC-12
$\phi_c^* \times 10^{-4}$	0.8 – 4.1	1.2 – 8.1	0.9 – 3.1
P/P_c	0.23 – 0.74	0.16 – 0.5	0.26
$(GD/\mu_l) \times 10^3$	30 – 353	79 – 393	24 – 147
L_h/D	35 – 166	35 – 337	35 – 328
No. of data Points	1140	293	248

Table 2-8 Parameter ranges in bundles of Hauptmann and Lee's (1983) correlation.

	water	CFC-12
$\phi_c^* \times 10^{-4}$	0.34 – 1.3	0.63 – 2.15
P/P_c	-0.16 – 0.37	0.19 – 0.31
$(GD/\mu_f) \times 10^3$	47 – 596	36 – 453
No. of data points	76	119

Table 2-9 Empirical values of a_1, a_2 and a_3 evaluated from Lee and Mudawwar's (1988) model.

Parameter	Reference	a_1	a_2	a_3
Subcooled heat transfer coefficient	Moles & Shaw (1972)	0.6	240	-0.8
	Shah (1977)	0.35	240	-0.8
	Gungor & Winterton (1986)	0.5	240	-0.8
Bubble drag coefficient	Harmathy (1960)	0.35	8	-0.8
	Chan & Prince (1965)	0.35	240	-0.8
Bubble departure diameter	Levy (1967)	0.35	10	-0.8
	Cole & Rohsenow (1968)	0.35	240	-0.8
	Smogalev (1981)	0.35	56	-0.8

Table 2-10 Prediction accuracy of Katto's (1990b) model for CHF of various fluids.

Data source	Fluid	Data of $\alpha < 0.7$	$\mu(R)$	$\sigma(R)$
USSR (1977)	Water	307	0.978	0.144
Thompson and Macbeth (1964)	Water	270	1.021	0.120
Katto and Yokoya (1982); Katto and Ashida (1982)	CFC-12	53	1.064	0.291
Purcupile et al. (1973)	CFC-11	37	1.039	0.271
Pappell et al. (1966)	Nitrogen	51	1.165	0.145
Katto and Yokoya (1984)	Helium	11	1.038	0.179
Ogata and Sato (1976)	Helium	4	1.147	0.260
Coffield et al. (1969)	CFC-113	35	1.494	0.387
	Total	768	1.040	0.210

R = (predicted CHF) / (measured CHF)

$\mu(R)$ = mean value of R

$\sigma(R)$ = standard deviation of R

Table 2-11 Magnitudes of δ, L_B, U_B and τ predicted by Katto (1990a) based on the table CHF values of USSR Academy of Sciences (1977).

	No. of data	δ (μm)		L_B (mm)		U_B (m s^{-1})		τ (ms)	
		range	mean	range	mean	range	mean	range	mean
$0.25<\alpha<0.7$	94	23 – 661	192	3.88 – 20.2	10.3	0.0625 – 1.60	0.447	3.24 – 261	44.6
$0<\alpha<0.25$	65	50.9 – 662	214	3.53 – 11.0	6.59	0.0813 – 0.942	0.260	5.62 – 119	36.5
$\alpha=0$	61	49.5 – 953	341	2.35 – 13.3	5.78	0.0756 – 0.999	0.242	3.86 – 147	47.3

Table 2-12 Magnitudes of δ, L_B, U_B and τ predicted by Lee and Mudawwar (1988) based on the table CHF values of USSR Academy of Sciences (1977).

	No. of data	δ (μm)		L_B (mm)		U_B (m s^{-1})		τ (ms)	
		range	mean	range	mean	range	mean	range	mean
$0.25<\alpha<0.7$	94	0.294 – 40.8	10.9	0.141 – 4.31	1.61	0.328 – 3.52	1.19	0.307 – 9.28	2.36
$0<\alpha<0.25$	65	0.008 – 18.7	3.59	0.003 – 1.3	0.409	0.346 – 4.60	1.41	0.0007 – 3.32	0.557
$\alpha=0$	61	0.01 – 6.02	0.962	0.003 – 1.06	0.127	0.467 – 4.60	2.08	0.0007 – 0.927	0.109

Table 2-13 Summary of non-aqueous CHF data in tubes

Reference	Fluid	No. of data	Ranges				
			D (m)	L (m)	G (kg m^{-2} s^{-1})	P (kPa)	Quality (%)
Barnett and Wood (1965)	CFC-21	504	0.0067 – 0.0161	0.53 – 3.3	470 – 2370	731 – 1380	-3 – 96
Pappel et al. (1966)	N_2	49	0.0128	0.3048	1442 – 2532	345 – 1655	-40 – 1
Coffield et al. (1969)	CFC-113	40	0.0102	0.762	1292 – 5617	910 – 2186	-54 – 2.5
Groeneveld (1974)	CFC-12	268	0.0078 – 0.0161	0.6 – 1.83	509 – 3264	1062 – 1089	-6.2 – 80
Staub (1969)	HCFC-22	32	0.01	1.524	490 – 1316	620 – 2037	23 – 79
Dix (1970)	CFC-114	441	0.01 – 0.0141	0.635 – 1.93	449 – 3944	841 – 1434	2 – 75
Rotem and Hauptmann (1969)	CO_2	172	0.006	1.056	680 – 5848	1923 – 5219	0 – 74
Leung (1980)	CFC-11	20	0.0117	2.74	1396 – 2802	1988 – 2897	8 – 18
Lazarek and Black (1982)	CFC-113	32	0.0031	0.126	230 – 740	114 – 272	30 – 90
Boltienko (1991)	CFC-12	59	0.008 – 0.020	0.5 – 4	1000	1080	0 – 60

Table 2-14 Summary of CHF scaling techniques and prediction methods

CHF scaling techniques and prediction methods		
Reference	Description	Comment
Scaling techniques		
Barnett's 14 scaling laws (1964)	shown in Table 2-1	Dimensionless groups were developed based on classical dimensional analysis. No empirical constant is required.
Stevens and Kirby's K factor (1964)	Eq. (2-22)	$KGD^{1/4}(D/L)^{0.59}\times10^{-4}$ used in Fig. 2-6 is not a dimensionless factor. K is a fixed value within their test range.
Coffield et al.'s K factor for subcooled flow (1969)	Eqs. (2-33)—(2-35)	K value changes with ρ_f/ρ_g and may be affected by inlet subcooling.
Dix's K_1 factor (1970)	Eqs. (2-38)—(2-39)	C_T in Eq. (2-39) is fluid dependent and is shown in Table (2-3).
Ahmad's scaling factor (1973)	Eqs. (2-45)—(2-46)	ψ_γ and ψ_σ were developed based on classical dimensional analysis and the so-called compensated distortion technique, and are fluid independent.
Non-dimensional CHF equations		
Ahmad's equations (1973)	Eqs. (2-48)—(2-55)	Only applicable to 7 MPa water-equiv. pressure with satisfactory comparison against data.
Katto and Ohno's equation (1984)	Eqs. (2-57)—(2-65)	Neither the numerical comparison nor the statement of their application range is reported. Only the graphical comparisons were presented.
Shah's equations (1987)	Eqs. (2-66)—(2-71)	23 fluids with a very wide range of flow conditions were tested. The application range is shown in Table 2-5.
Green and Lawther's equations (1981)	Eqs. (2-72)—(2-73)	Water and CFC-12 data were used. Equations are not applicable to $G<300$ kg m^{-2} s^{-1}, $X_e<0.1$, $P<3.5$ and $P>12$ MPa water-equiv.

Table 2-14 (continued)

Reference	Description	Comment
Hauptmann and Lee's equations (1983)	Eqs. (2-74)–(2-78). Tables 2-6 and 2-7 contain the empirical constants.	Fluid properties at critical points are needed. Water, CO_2 and CFC-12 data were used. Equations also are applicable to the bundle case.
Table approaches		
USSR Academy of Science (1977)	Water CHF table for an 8 mm inner diameter tube. CHF is presented as a function of P, G and X_e.	For data whose I.D. is not 8 mm, use Eq. (2-79).
Groeneveld et al.'s CHF table (1986a)	Water CHF table for an 8 mm inner diameter tube. CHF is presented as a function of P, G and X_e.	For data whose I.D. is not 8 mm, used Eq. (2-80). The table can be used to predict the CHF for non-aqueous fluids via the scaling technique.
Analytical CHF models		
Lee and Mudawwar's subcooled flow model (1988)	Assumes a liquid sublayer dryout in a subcooled flow. Information for sublayer mass velocity, vapour blanket length and sublayer thickness is needed.	Three empirical constants were correlated as shown in Table 2-9. Only water CHF data are compared. The model is used for PWR application.
Katto's subcooled flow model (1990a, 1990b)	Assumes a similar dryout mechanism as in Lee and Mudawwar's model.	Only one empirical constant was correlated as shown in Table 2-10. The difference in magnitudes of δ_l, L_B and τ compared with those in Lee and Mudawwar's model are large.

Table 2-14 (continued)

Reference	Description	Comment
Weisman and Pei's bubbly flow model (1983)	Based on the near-wall bubble-crowding assumption for preventing the enthalpy transport between the heated surface and subcooled liquid core.	The model can be used for subcooled and low quality flows. Empirical constants were correlated based on water data. However, the model can be used for other fluids.
Whalley et al.'s annular flow model (1974, 1978)	Based on the liquid film flow dryout on the heated channel wall assumption. The information of the rates for liquid entrainment and deposition is needed.	The model is used for a high quality flow condition and is independent of fluid type.

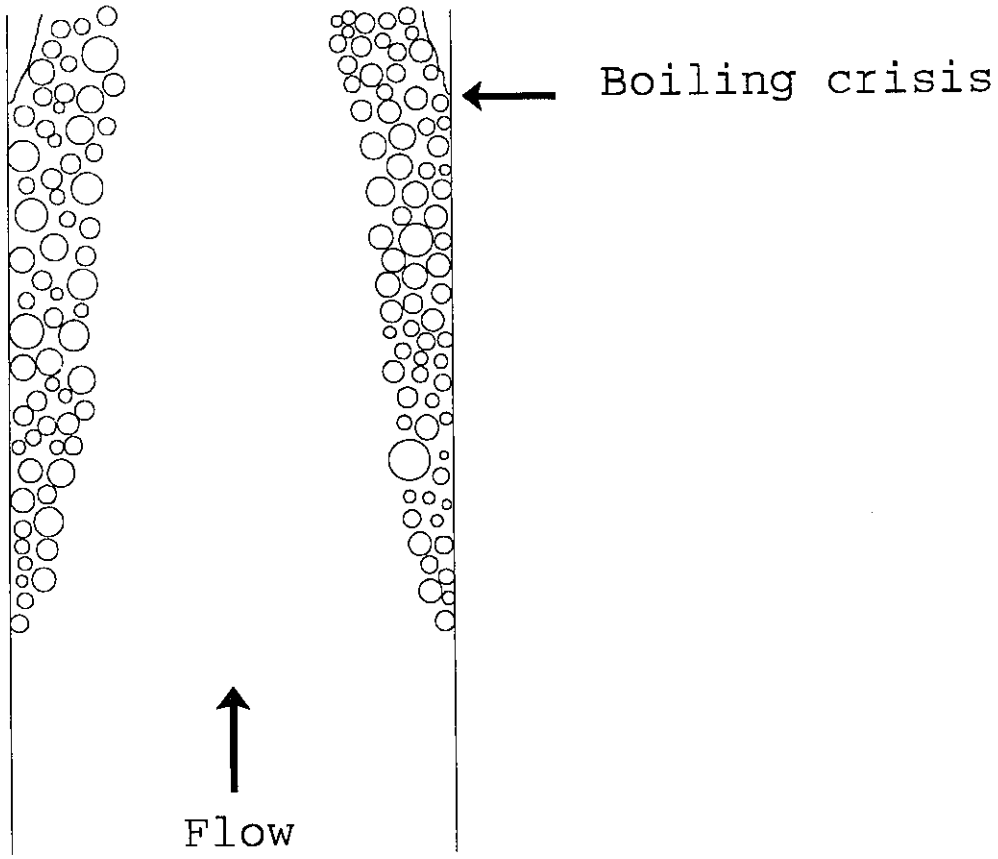

Figure 2-1 Near-wall bubble crowding and vapour blanketing mechanism for critical heat flux in subcooled and low quality flow (Hewitt, 1978).

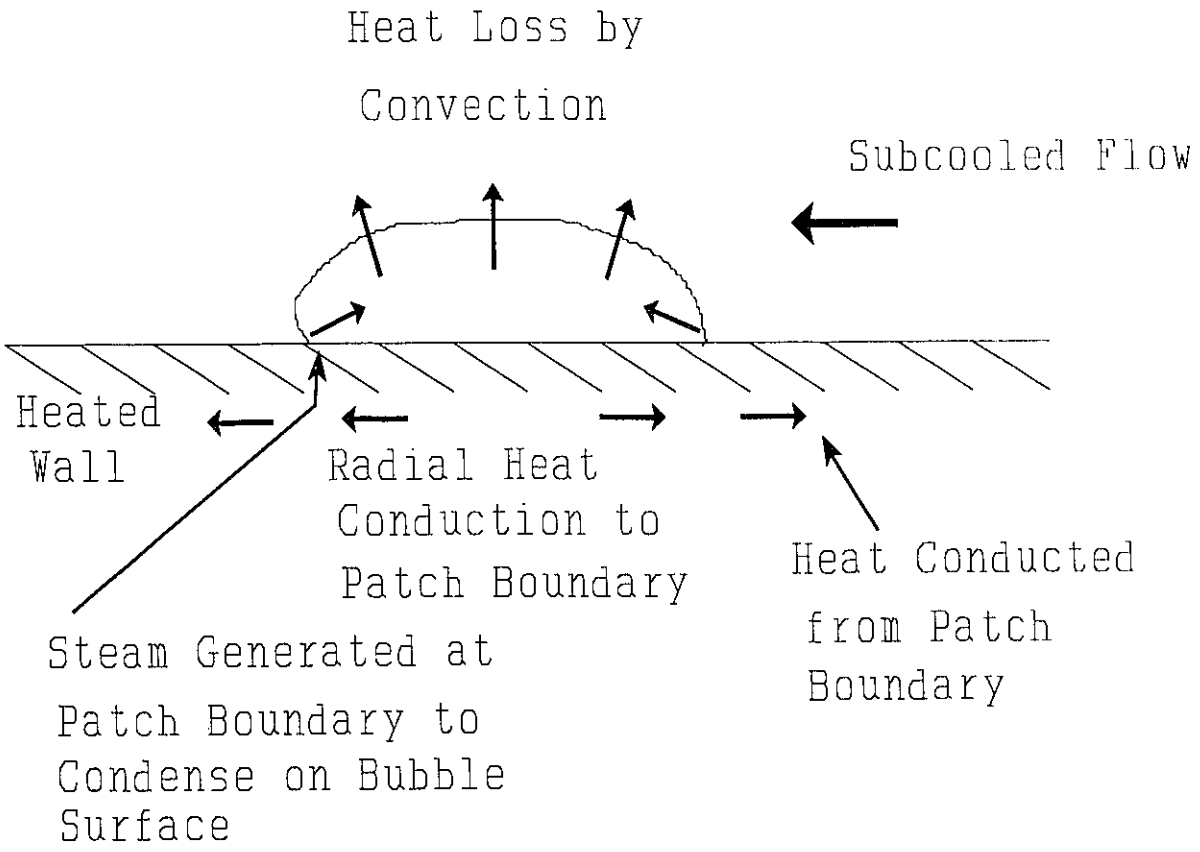

Figure 2-2 Heat flows in around bubble with a dry base (Kirby et al., 1967). (Reproduced from Hewitt, 1978)

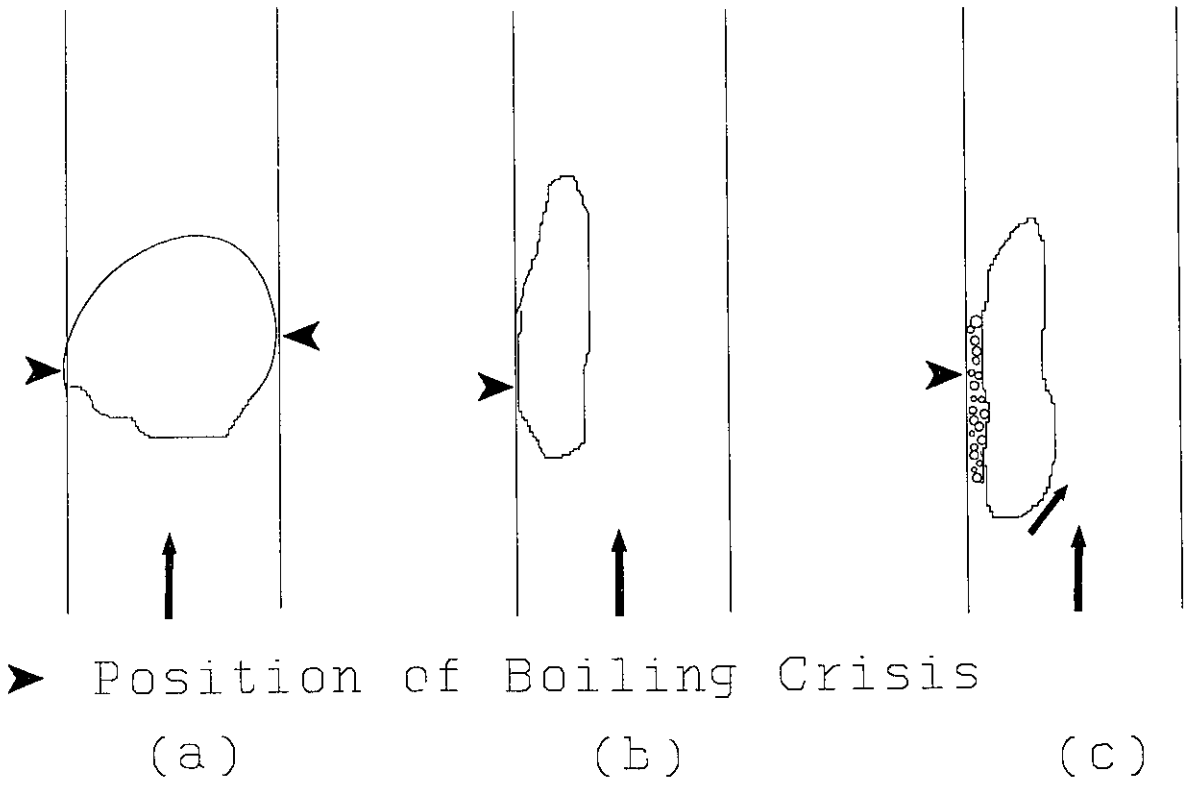

Figure 2-3 Boiling crisis arising from vapour slug or dot formation in subcooled or low quality flows (Hewitt, 1978).

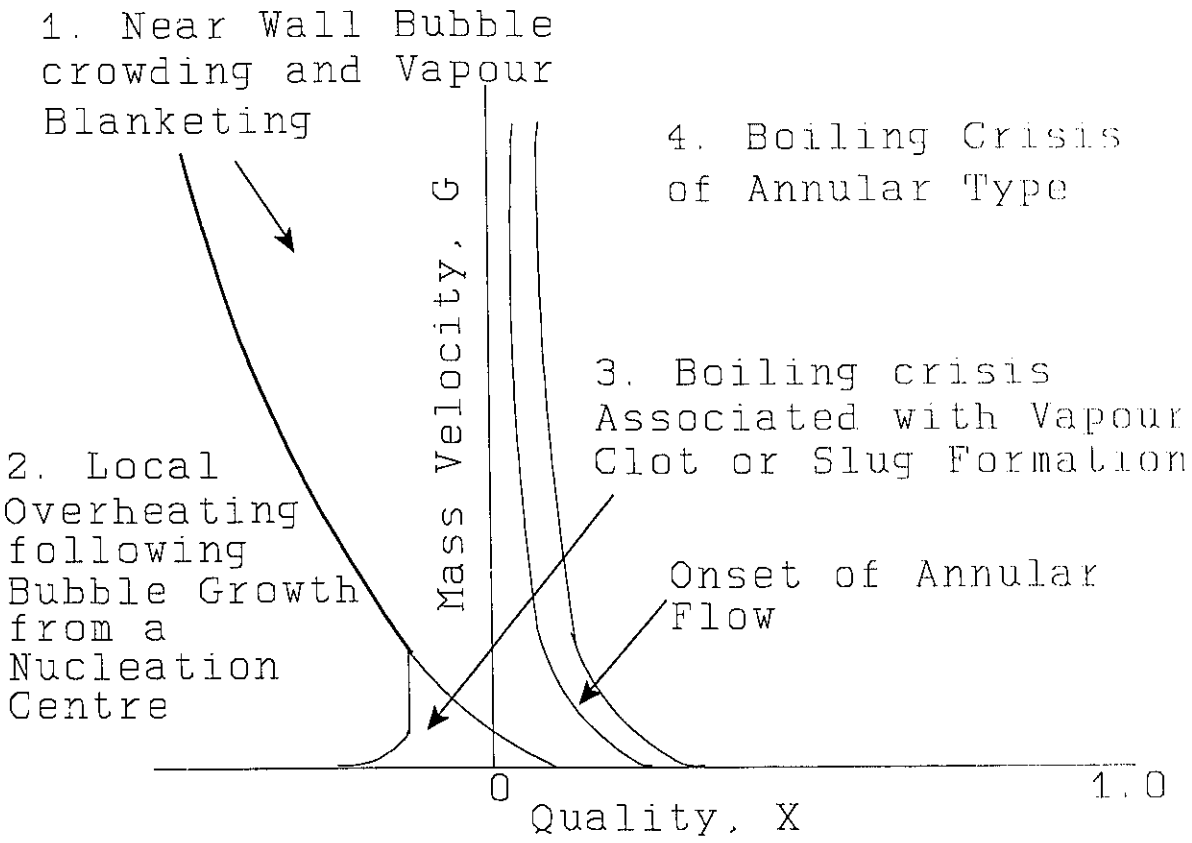

Figure 2-4 Tentative map of regions of operation of various critical heat flux mechanisms (Semeria and Hewitt, 1974). (Reproduced from Hewitt, 1978)

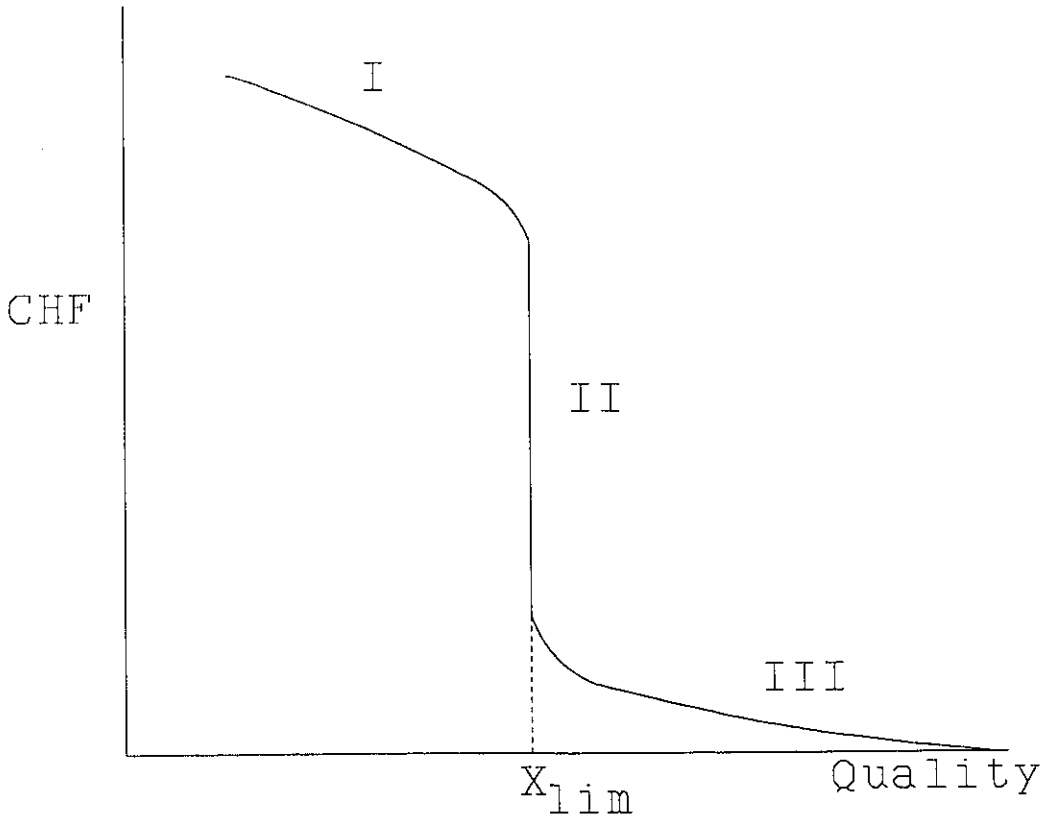

Figure 2-5 Critical heat flux curve with a limiting heat flux (Hewitt, 1978).

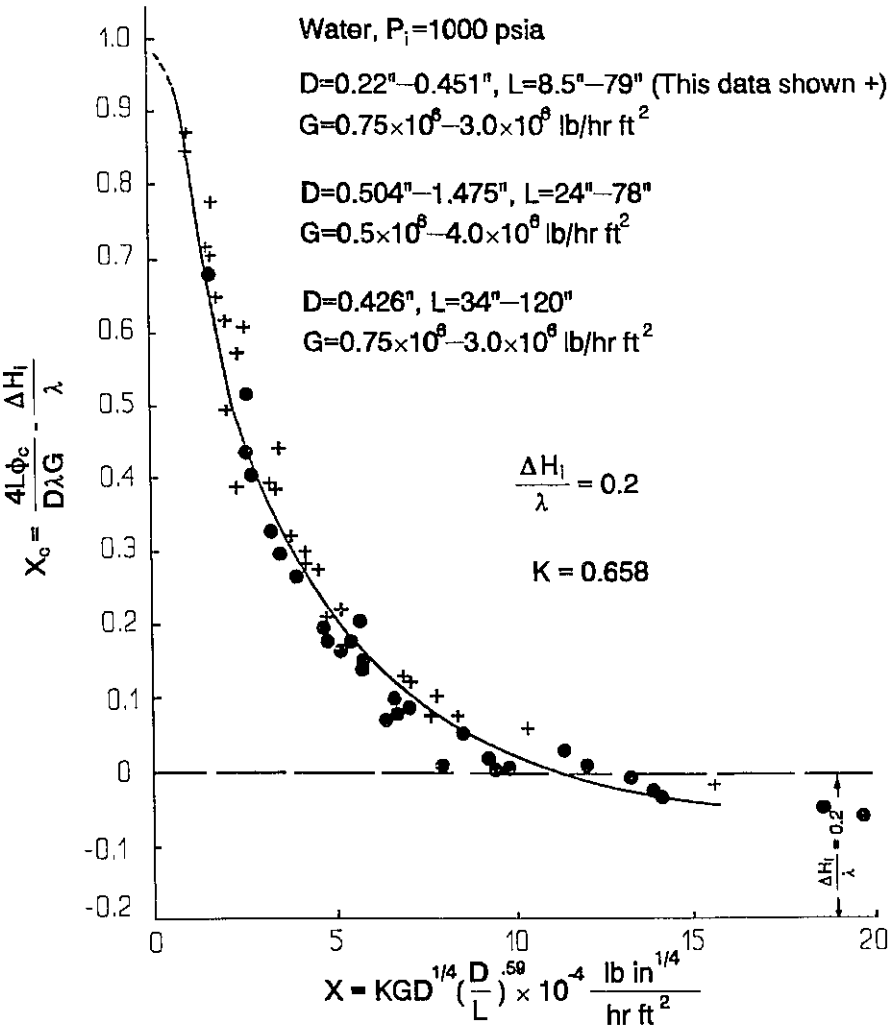

Figure 2-6 Correlation of water data superimposed on the best curve for CFC-12 data (Stevens and Kirby, 1964).

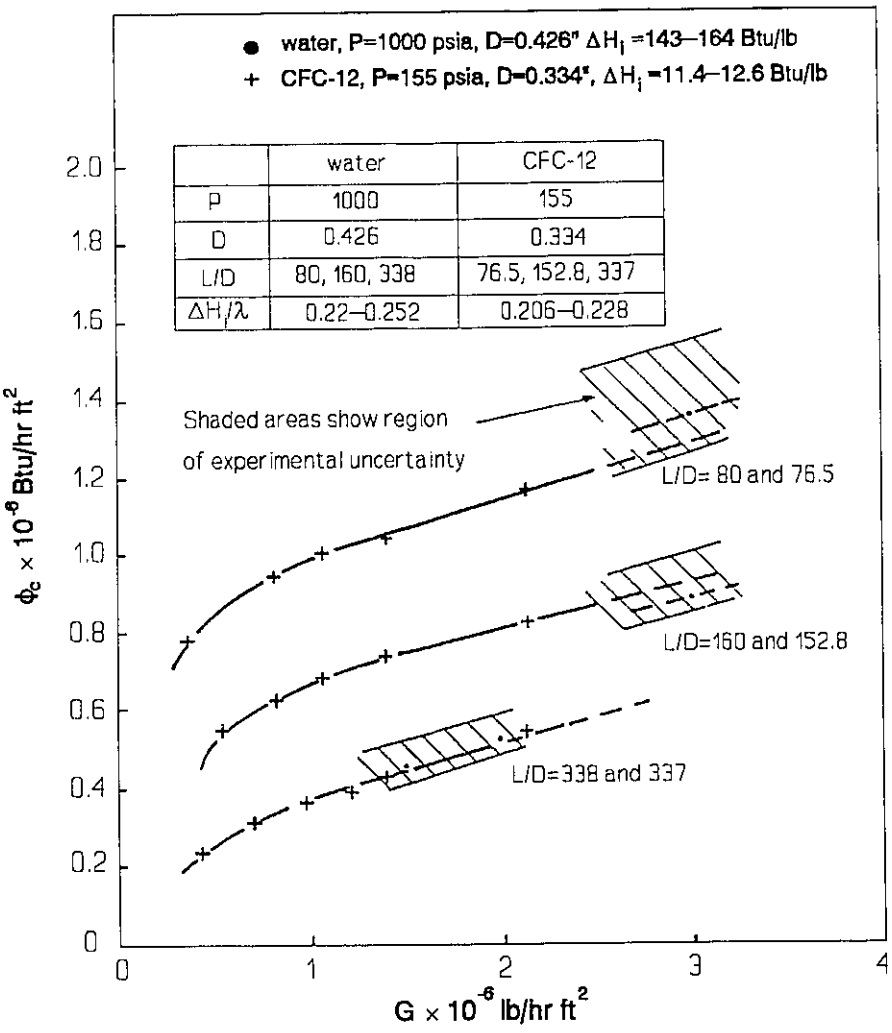

Figure 2-7 Comparison between CHF data for water and water-equivalent CFC-12 data (Stevens and Kirby, 1964).

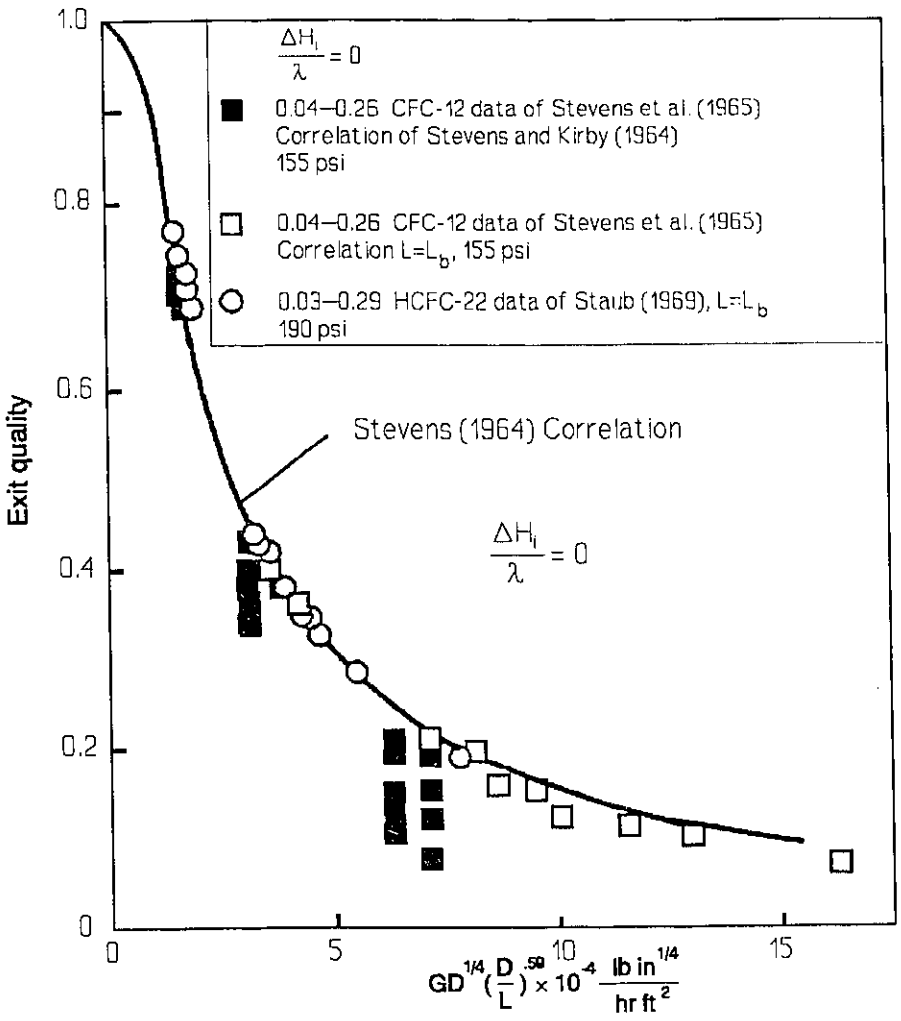

Figure 2-8 CHF data for CFC and HCFC at various inlet subcooling using the correlation of Stevens and Kirby (1964) as well as the modified of Staub (1964) (Staub, 1969).

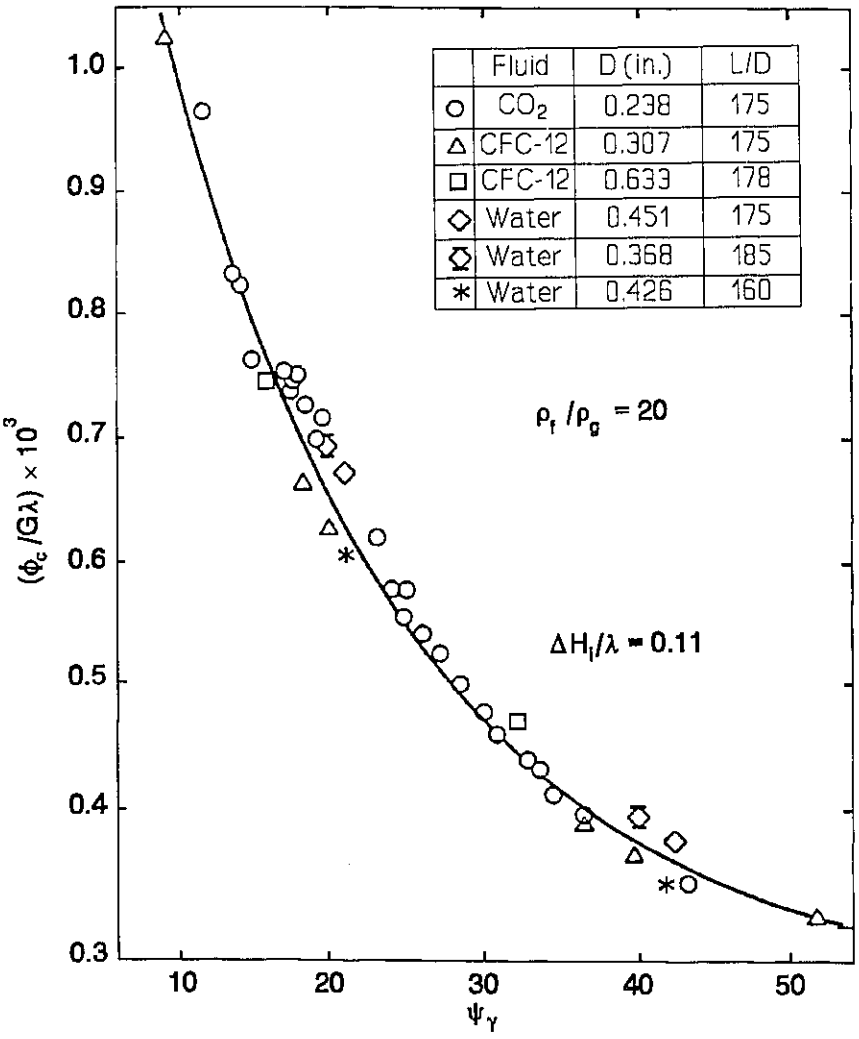

Figure 2-9 Comparison of water, CO_2 and CFC-12 data (in tubes) at water-equivalent pressure 1000 psia, i.e., ρ_f/ρ_g=20 (Ahmad, 1973).

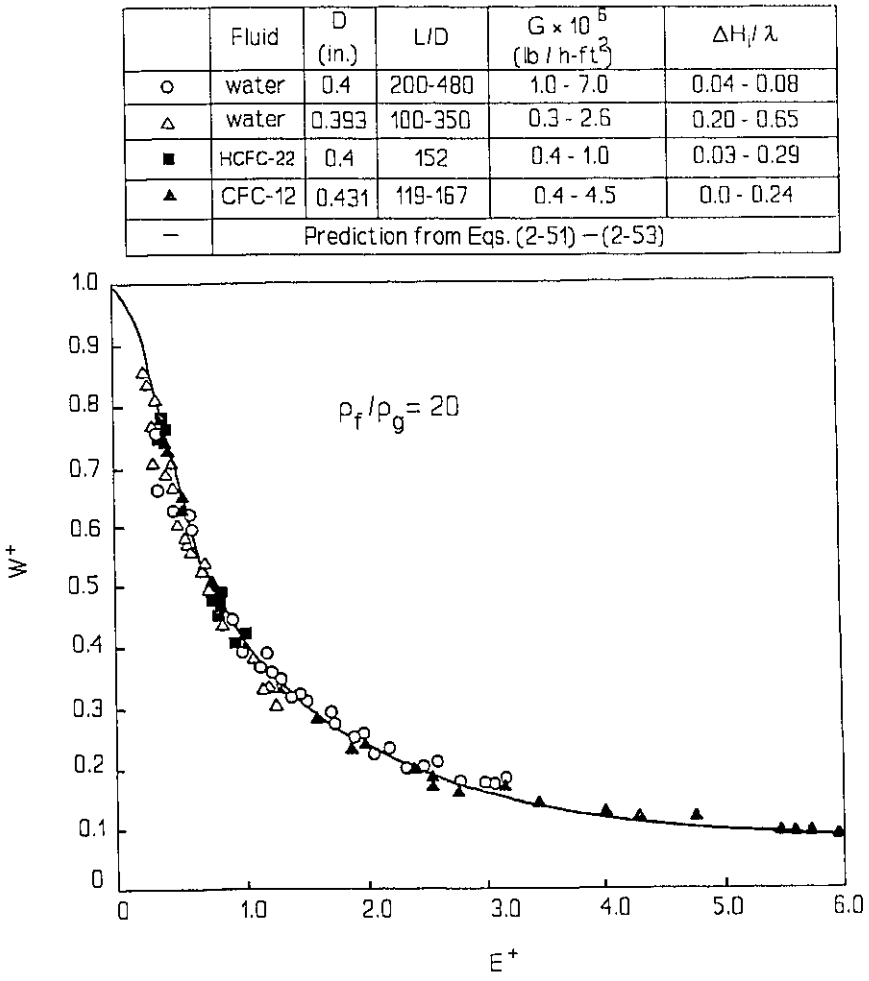

Figure 2-10 Comparison of water, HCFC-22 and CFC-12 data (in tubes) with prediction from dimensionless correlation based on CFC-12 data, at water-equivalent pressure 1000 psia, i.e. ρ_f/ρ_g=20 (Ahmad, 1973).

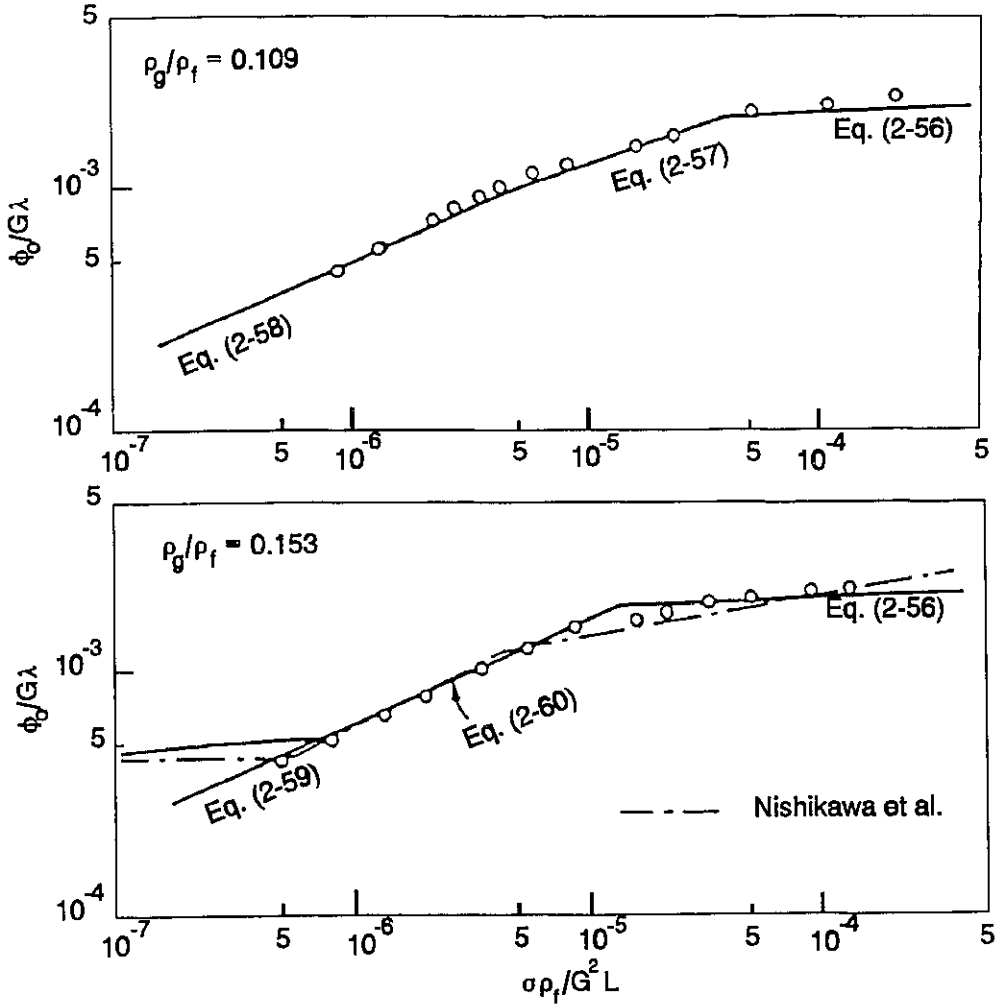

Figure 2-11 Comparison between the experimental and the predicted ϕ_o for CFC-12 at D=0.01 m and L/D=100 (Katto and Ohno, 1984).

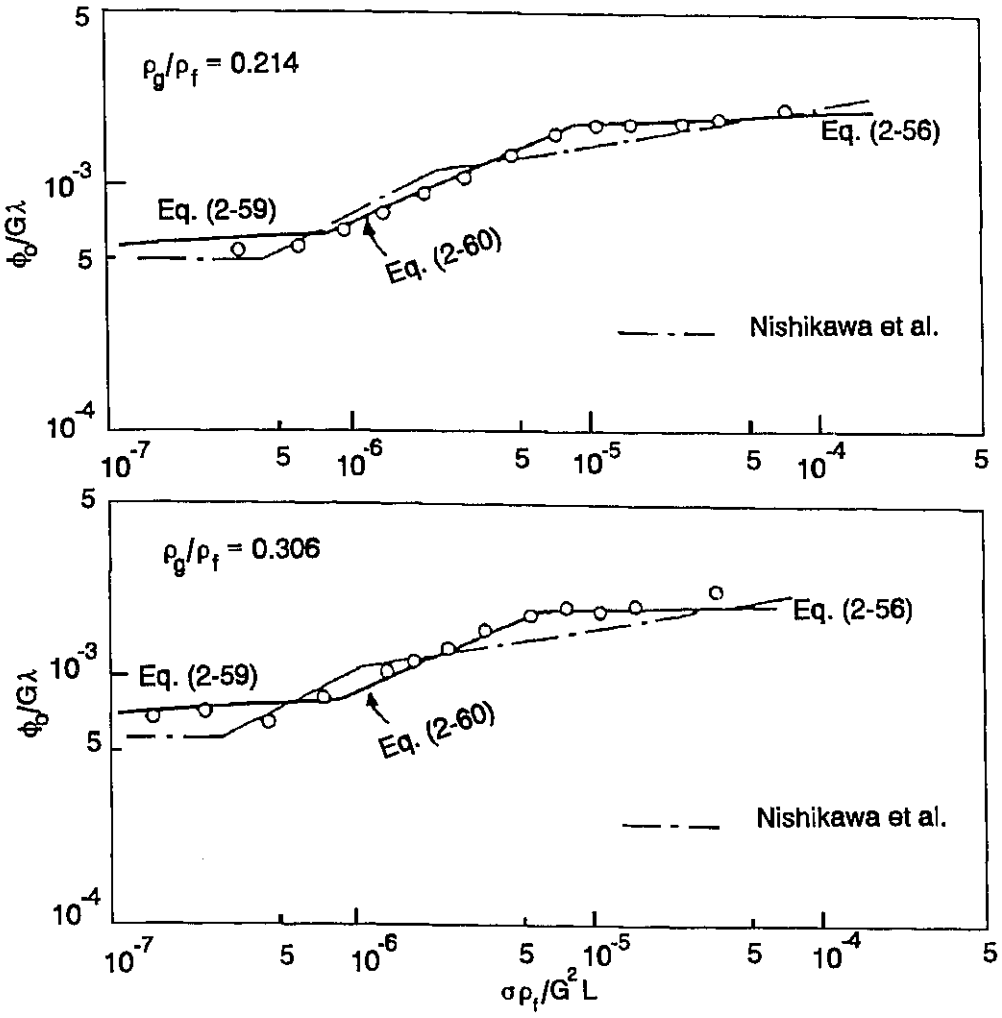

Figure 2-12 Comparison between the experimental and the predicted ϕ_0 for CFC-12 at D=0.01 m and L/D=100 (Katto and Ohno, 1984).

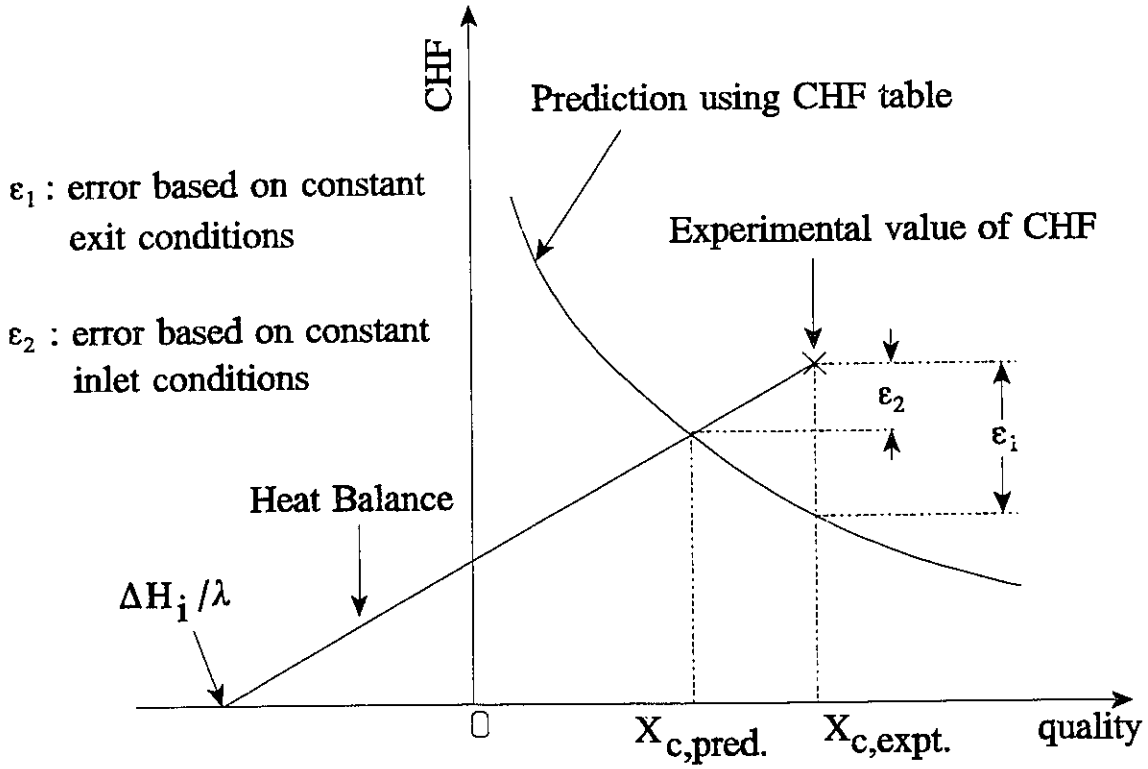

Figure 2-13 Errors based on constant exit and inlet conditions.

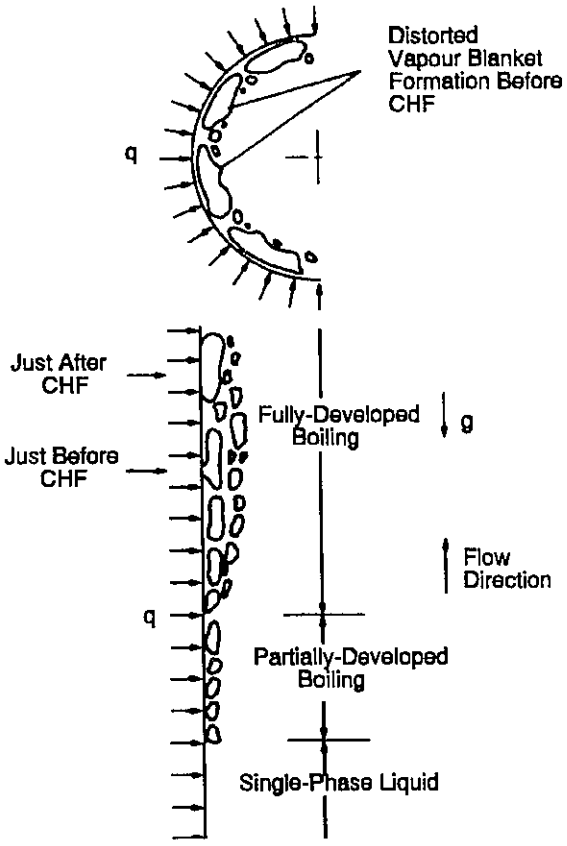

Figure 2-14 Subcooled flow CHF at high pressure and high mass velocity (Lee and Mudawwar, 1988).

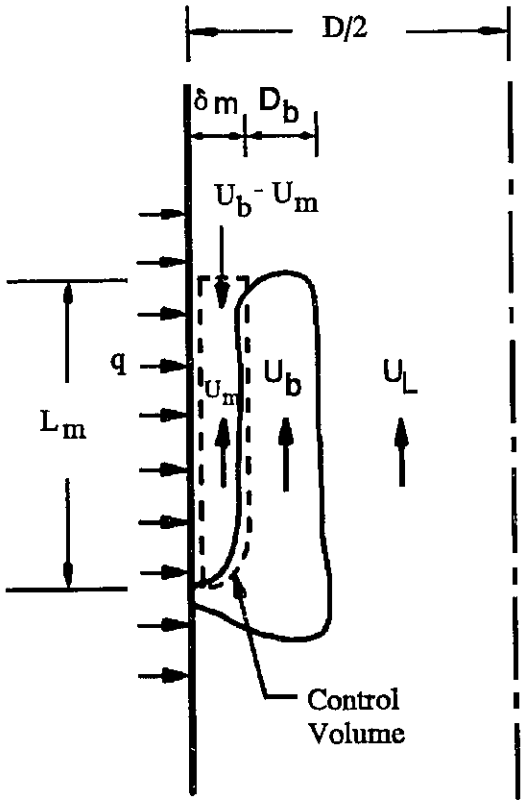

Figure 2-15 Schematic representation of the onset of sublayer dryout (Lee and Mudawwar, 1988)

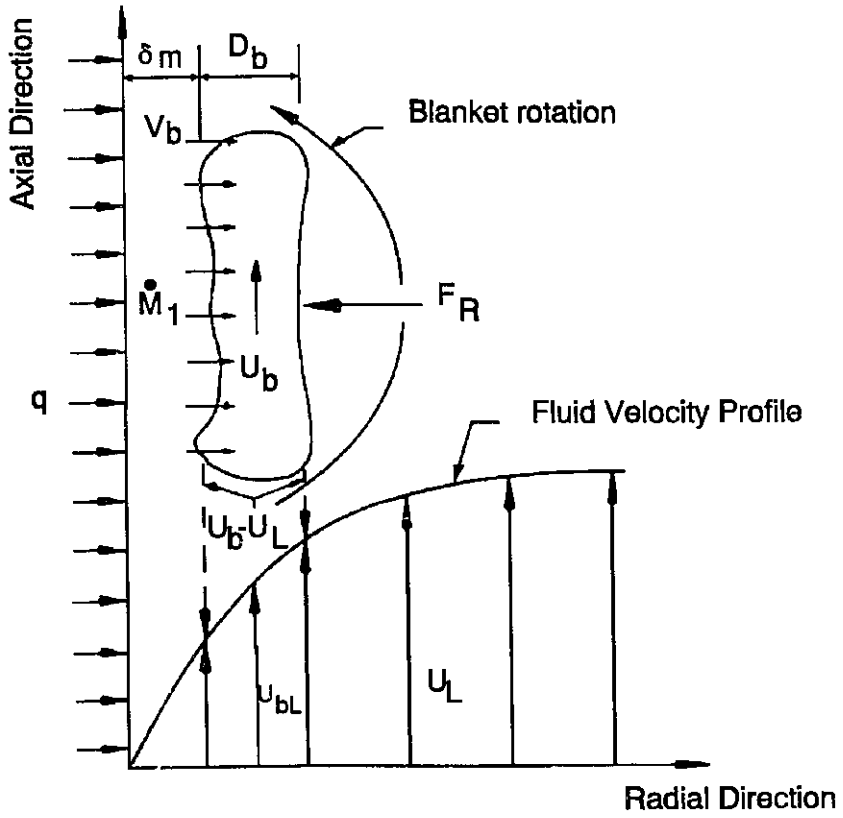

Figure 2-16 Schematic diagram of a vapour blanket moving in vertical turbulent flow before the onset of CHF (Lee and Mudawwar, 1988).

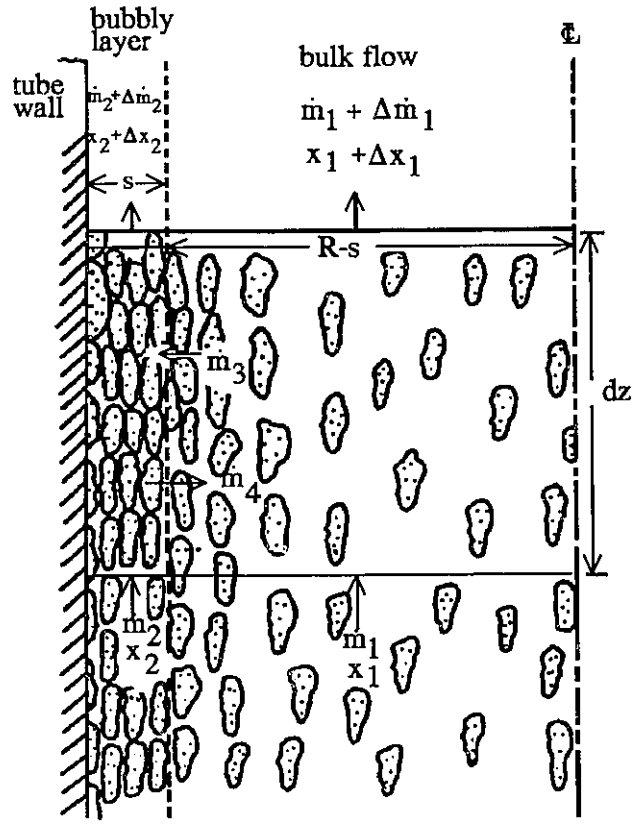

Figure 2-17 Schematic diagram of transport between core and bubbly layer (Weisman and Pei, 1983).

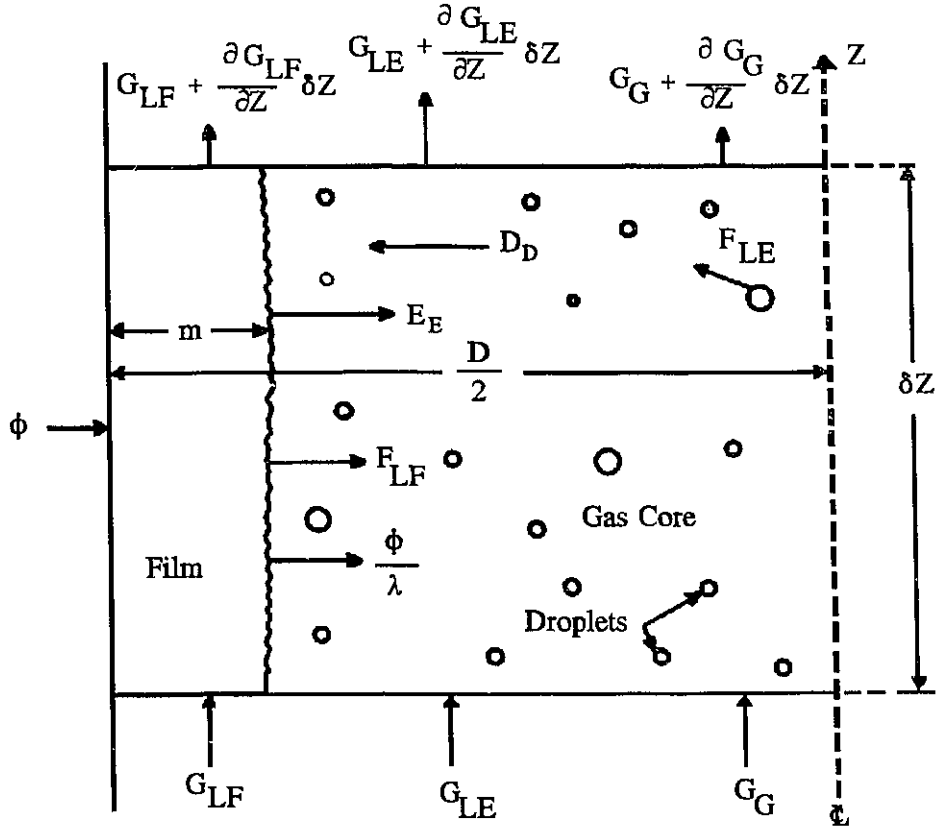

Figure 2-18 Mass balance on an incremental control volume (Whalley et al., 1978).

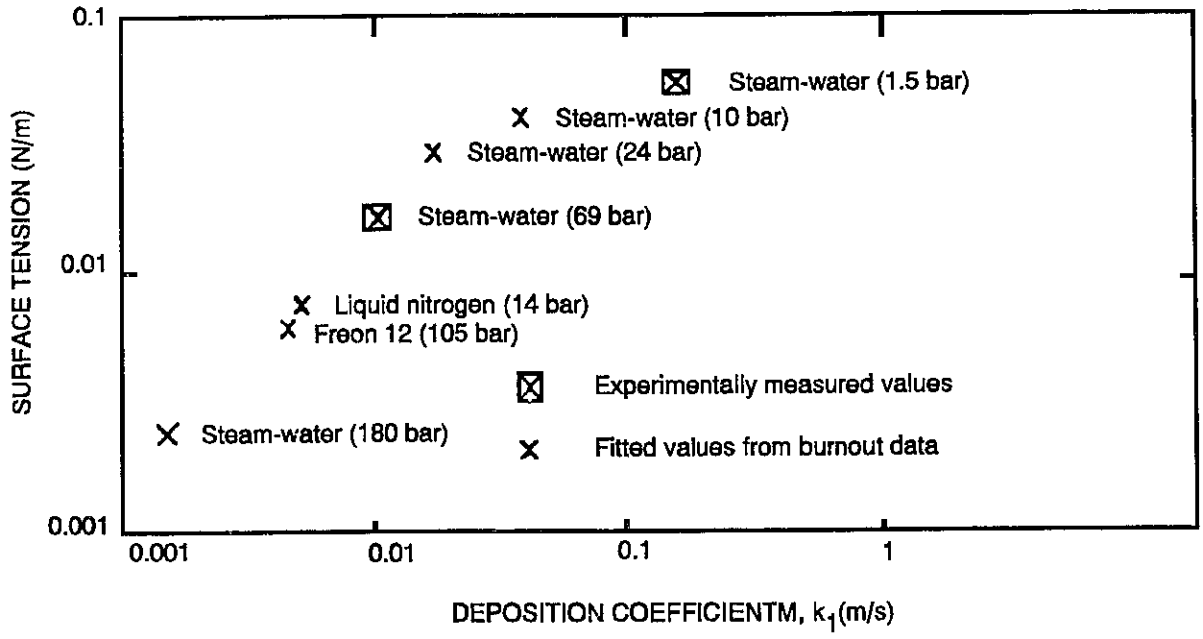

Figure 2-19 Variation of deposition coefficient with surface tension (Whalley et al., 1974)

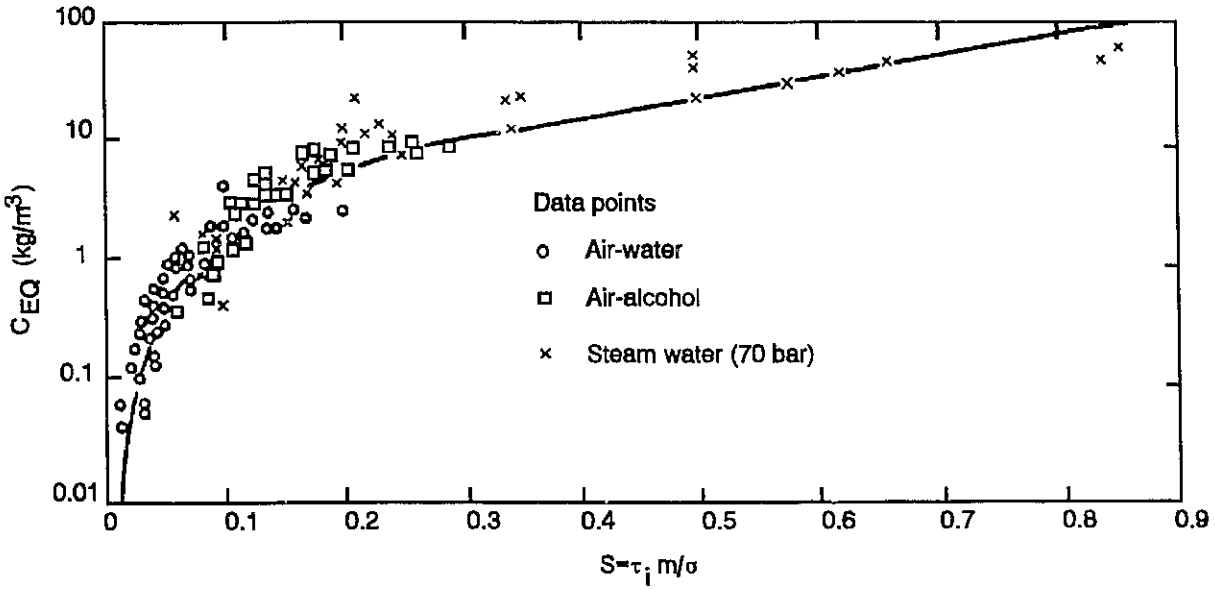

Figure 2-20 Variation of equilibrium concentration of entrained droplets with S (Whalley et al., 1978).

Chapter 3

EXPERIMENTAL EQUIPMENT

3.1 General

The CHF measurements were conducted in three test rigs. The University of Ottawa Multi-fluid Boiling Loop (UO loop) has been tested for the fluids of CFC-11, CFC-12, HCFC-123, HCFC-22 and HFC-134a with single geometry (i.e. a 4.2 mm inner diameter (I.D.) tube). The other two test rigs, MR-7A and MR-1A loops, are located at the Chalk River Laboratories of Atomic Energy Canada Limited. The MR-7A loop is also a multi-fluid boiling loop, but only HCFC-22 was used in this loop for this investigation, with tests performed on 4.38 and 8 mm I.D. tubes. The MR-1A loop is a water loop and only an 8 mm I.D. tube is used.

3.2 Loop Description

3.2.1 UO Loop

This multi-fluid boiling loop was designed by this author and was constructed with the assistance of a University of Ottawa technologist during construction. The loop was designed specifically to perform CHF tests for non-aqueous fluids such as CFC-11, CFC-12, HFC-134a, HCFC-123 and HCFC-22. Due to their low latent heat, about 12 times less than that of water, the power required for the test is less than 5 kW, and the mass flux can reach 4000 kg m^{-2} s^{-1} or more, depending on the pump capacity. The volume of this loop is limited to between 2 and 3 litres. Therefore, the size of the loop is only 80 cm deep, 100 cm wide and 170 cm high

(without including the height of the pressurizer). The maximum pressure of the CHF test for all fluids is 2 MPa. This provides a generous safety factor as the loop has been designed to sustain pressures up to 3.45 MPa. Most of the material used for building up the loop is stainless steel except for the heat exchanger and some minor connections, which are made of brass. Figure 3-1 is a schematic of the UO loop and illustrates all major components. The loop consists of gear pumps, turbine flow meter, preheater, test section, heat exchanger and pressurizer. The vertical test section as shown in Fig. 3-2 is made of Inconel 718 alloy tube of 4.2 mm I.D. (inner diameter) × 4.6 mm O.D. (outer diameter) × 1.3 m length; the maximum heated length is 1 meter. The wall temperature of the test section in the vicinity of the flow exit is measured by K-type thermocouples, also shown in Fig. 3-2. These thermocouples are fixed on the tube wall by wood clips. Inside the pressurizer, a tubular heater with 500 W of maximum power is located at the bottom to boil the liquid and a cooling coil is mounted at the top to condense the vapour so that the pressure can be controlled by adjusting the heater power and the water flow rate in the cooling coil. A detailed design analysis of all major components can be seen in the author's design report, which is included in Cheng et al. (1991).

3.2.2 MR-7A Loop

Due to the limitation of the test conditions of the UO loop (e.g. mass flux capacity less than 4 Mg m^{-2} s^{-1} and power capacity less than 5 kW), the CHF measurements for non-aqueous fluids in larger test sections and higher power consumption were conducted at the MR-7A loop. The design of the MR-7A loop is similar to that of the UO loop. However, the major components such as pump, power supply and heat exchanger have a higher flow capacity (mass flux up to

10 Mg m^{-2} s^{-1}) and consumption rate (power up to 30 kW) compared with those in the UO loop. The schematic of the MR-7A loop is shown in Fig. 3-3. The pressure in MR-7A can be controlled in the pressurizer (a steel tank containing a bladder) by varying the nitrogen pressure on the bladder side. The flow rate is controlled by a throttle valve (V2 as shown in Fig. 3-3) and measured by a turbine flow meter. The flow temperature at the inlet of the test section is adjusted by two preheaters (#1 and #2) and by the flow in a sub-cooler. Two vertical test sections with different I.D.'s but the same length were used in the loop. Their I.D.'s are 4.38 mm and 8 mm, respectively. Both test sections are made of Inconel 600 and are directly heated by DC current, and differ only in diameter; they are schematically shown by the same sketch (i.e. Fig. 3-4). The wall temperature of the test sections are measured by thermocouples (K-type, ungrounded) and their axial locations are given in Fig. 3-4. The flow temperature at the inlet and outlet of the test section is also measured by K-type thermocouples. The absolute pressures, as well as the pressure difference, at the inlet and outlet of the test section are measured by the absolute pressure (AP) and differential pressure (DP) transducers. The heated length can be changed simply by switching the connection of the test section to either one of the two lower power clamps.

3.2.3 MR-1A Loop

To complete the study of CHF fluid-to-fluid scaling techniques, CHF data for water are required. Therefore, the water CHF measurements for this work were conducted in Chalk River's MR-1A loop. The MR-1A loop is specifically designed for water CHF tests and the power and pressure limitations of this loop are thus much higher than those of the UO and MR-7A loops. Figure 3-5 shows the schematic of MR-1A loop, which includes a centrifugal pump (≤50

USGPM), an AC preheater (100 kW), a venturi flow meter, a pressurizer, a DC power supply (350 kW), a condenser and a cooler. The loop main body is composed of stainless steel tubing with the dimension of 19.05 mm (3/4") O.D. × 2.413 mm (0.095") W.T. (wall thickness) while the instrument lines are composed of 6.35 mm (1/4") O.D. × 0.889 mm (0.035") W.T. stainless steel tubing. The dimensions of the vertical test section are 8 mm I.D. × 1 mm W.T., and is made of Inconel 718. The I.D. of the test section is the same as that used in MR-7A loop for the HCFC-22 CHF test. K-type thermocouples are used to measure the fluid and test section wall temperatures. The locations of the thermocouple on the test section wall are shown in Fig. 3-6. Only one heated length (1.75 m) is used for the water CHF test as can be seen in Fig. 3-6. The absolute pressure and pressure difference at the inlet and outlet of the test section are measured by AP and DP cells. Similar to MR-7A loop, the pressure is controlled in the bladder-type pressurizer by varying the nitrogen pressure.

3.3 Test Procedure

Although the detailed operating procedures are different for each of the three test rigs because of their different component arrangement and instrument installation, the general test procedures are similar and are described as follows: While the flow is circulating in the loop, the power supply to the preheater, the test section and the heater inside the pressurizer (for the UO loop) are turned on to adjust the system temperature and pressure. The test section power is raised rapidly to about 80% of the CHF power, beyond which the power is slowly increased until CHF occurs. Meanwhile, the mass flow rate and system pressure are monitored carefully so that the flow rate and pressure are maintained steady. When CHF is observed, the wall temperature

at the exit of the test section increases rapidly as seen from a recorder trace. The test section power is subsequently reduced to 80-95% of the CHF power and the flow conditions are adjusted for the next CHF test.

3.4 Instrument Calibration and Measurement Uncertainties

3.4.1 UO Loop

The estimates for the measurement uncertainties were based on the manufacturers' specifications and the calibration procedures. Using a so-called electrical-equivalent ice bath, the errors of the thermocouple measurement at the inlet and outlet of the test section were calibrated to be ±0.2°C. The pressure transducer was calibrated to have 0.6% of RMS error for the full range (0.1—4.8 MPa) by the manufacturer. The flow meter was calibrated to have 1.06% of RMS error between 1.325 and 13.25 l/m by using water. According to the manufacturer, no correction factor is needed for different fluids. The stability of the DC power supply is 0.04 volts for the voltage mode and 0.63 amperes for the current mode. The heat loss test has shown that the heat loss from the test section through the insulation increases with increasing wall temperature. The heat balance test for the test section indicated a 1.9% of RMS deviation with respect to the power, flow rate and temperature measurements. Details of the heat loss and heat balance tests for the test section are given in Appendix II.

3.4.2 MR-7A Loop

All instruments were calibrated prior to the CHF experiments. The read-outs from thermocouples, absolute pressure (AP) transducer, differential pressure (DP) transducer and flow

meter are compared with those from an external reference device. All thermocouples were calibrated over a range from 30°C to 150°C using a JOFRA Temperature Calibrator Model 650 SE and a Thermo Electric Instruments Micromite II. The errors of the thermocouple measurement at the inlet and outlet of the test section were found to be ±0.5°C. The flow meter was calibrated by measuring the volumetric flow rate of water and was found to have a 2.5% RMS error between 0 to 0.45 *l*/m. The pressure transducers for AP and DP are calibrated to be ±3% for 95% of the test range. A correction equation is used for all the above instruments based on the results of the calibration procedures. Different values of coefficients were applied in the correction equation for specific instrument. A series of heat balances was performed. The heat loss from the test section is calibrated to be 2.95% by using CFC-12 in a heat balance test and is due to the inaccuracies of flow meter, voltage and current measurements as well as the inlet and outlet temperature measurements and enthalpy evaluation in CFC-12. More detailed information can be found in Blumenröhr et al. (1991).

3.4.3 MR-1A Loop

The thermocouples were calibrated in the same manner as for the MR-7A loop. The errors in temperature measurement at the inlet and outlet of test section were found to be ±0.5°C. The venturi flow meter was calibrated within ±0.5% of the flow measurement uncertainty and this calibration is traceable to the National Institute of Standard and Technology of the U.S.A. The AP and DP pressure transducers are calibrated within ±0.4% and ±0.2% of error, respectively. The DC power is calculated by measuring the voltages across the test section and the current shunt. A series of heat balances was also performed. The heat loss from the test section is

calibrated to be 3.12% by using water in a heat balance test and this is due to the inaccuracies of flow meter, voltage and current measurements as well as the inlet and outlet temperature measurements.

3.5 Test Matrix

3.5.1 UO Loop

HCFC-22 is the major test fluid in the present experimental investigation because HCFC-22 will temporarily be the replacement fluid of CFC-12 before HFC-134a is widely available in the market. Therefore, the mass fluxes for CHF experiments were first chosen for HCFC-22. Then, Katto's scaling parameter (ψ_k) is calculated in terms of the flow rate and properties for the corresponding pressures. The pressure of the CHF experiment for all fluids is chosen for the water-equivalent pressure at 7 and 10 MPa, that is ρ_f/ρ_g equals to 20.26 and 12.38, respectively. Once the values of ψ_k are determined for HCFC-22, the corresponding mass fluxes for the other fluids are calculated based on the same ψ_k values for HCFC-22. Table 3-1 shows the mass fluxes of HCFC-22, CFC-12, HCFC-123, HFC-134a and water with respect to the same ψ_k at the pressure of 7 and 10 MPa water-equivalent. The diameter of the test section is 4.2 mm I.D. and the heated length varies from 0.5 to 1 m.

3.5.2 MR-7A Loop

As mentioned in Section 3.2.2, for the higher flow rate condition (above 4000 kg m^{-2} s^{-1}), the CHF experiments are conducted at the MR-7A loop. Therefore, the CHF test for HCFC-22 is continued in MR-7A loop for the mass flux values from 4000 to 8000 kg m^{-2} s^{-1}. The diameter

of the test section is 4.38 mm I.D. and the heated lengths are 0.68 and 1.46 m, respectively. In addition, a tube with 8 mm I.D. is also used for CHF measurements in the MR-7A loop. The heated length varies from 0.67 to 1.61 m. The measured CHF data for this geometry will be compared with the water CHF data measured in MR-1A loop for the same diameter. Table 3-2 shows the test matrix for MR-7A for both the 4.38 and the 8 mm I.D. tubes.

3.5.3 MR-1A Loop

The main purpose of the water CHF test in the MR-1A loop is to generate the water CHF data using the same geometry (8 mm I.D.) as that used in the MR-7A loop for the HCFC-22 CHF test. Therefore, CHF data for water and refrigerant can be compared by examining the fluid-to-fluid scaling techniques. The mass flux is chosen to correspond to the same ψ_k values as in the MR-7A loop for the 8 mm I.D. and the pressures corresponds to the same density ratio of liquid to vapour. Only one heated length (1.75 m) is used for the water CHF test. Table 3-3 shows the test matrix for the MR-1A loop.

Table 3-1 Test matrix for HCFC-22, CFC-12, HCFC-123 and HFC-134a in the UO loop.

(a) for pressure at 7 MPa water-equivalent

Pressure=7 MPa water-equivalent; ρ_f/ρ_g=20.26				
ψ_k	Mass flux (kg m^{-2} s^{-1})			
	HCFC-22	CFC-12	HCFC-123	HFC-134a
35.15	1500	1531	1449	1383
46.87	2000	2041	1932	1845
58.59	2500	2552	2415	2306
70.31	3000	3062	2898	2767
82.02	3500	3572	3381	3228
93.74	4000	4083	3864	3689
Fluid pressure (MPa)	1.34	1.06	0.98	1.13

(b) for pressure at 10 MPa water-equivalent

Pressure=10 MPa water-equivalent; ρ_f/ρ_g=12.38				
ψ_k	Mass flux (kg m^{-2} s^{-1})			
	HCFC-22	CFC-12	HCFC-123	HFC-134a
43.73	1500	1535	1436	1371
58.31	2000	2047	1915	1828
72.89	2500	2559	2394	2286
87.47	3000	3071	2873	2743
102.05	3500	3583	3352	3200
116.63	4000	4095	3831	3657
Fluid pressure (MPa)	1.96	1.58	1.46	1.66

Table 3-2 Test matrix for HCFC-22 in the MR-7A loop.

(a) for pressure at 1.34 MPa (7 MPa water-equiv.)

I.D. (mm)	ψ_k	Mass flux (kg m^{-2} s^{-1})	Heated length (m)
4.38	95.73	4000	0.68 and 1.46
	119.6	5000	
	143.6	6000	
	167.5	7000	
	191.5	8000	
8	32.35	1000	0.67 – 1.61
	64.68	2000	
	97.04	3000	
	129.4	4000	
	194.1	6000	

(b) for pressure at 1.96 MPa (10 MPa water-equiv.)

I.D. (mm)	ψ_k	Mass flux (kg m^{-2} s^{-1})	Heated length (m)
4.38	119.0	4000	0.68 and 1.46
	148.7	5000	
	178.4	6000	
	208.2	7000	
	238.0	8000	
8	40.24	1000	0.67 – 1.61
	80.47	2000	
	120.7	3000	
	160.9	4000	
	241.4	6000	

Table 3-3 Test matrix for water in the MR-1A loop.

Pressure (MPa)	ψ_k	Mass flux (kg m^{-2} s^{-1})	D (mm)	L (m)
7	64.68	2618	8	1.75
	97.04	3928		
	129.4	5238		
	161.8	6550		
	194.1	7857		
10	80.47	2563	8	1.75
	120.7	3844		
	160.9	5124		
	201.2	6407		
	241.4	7687		

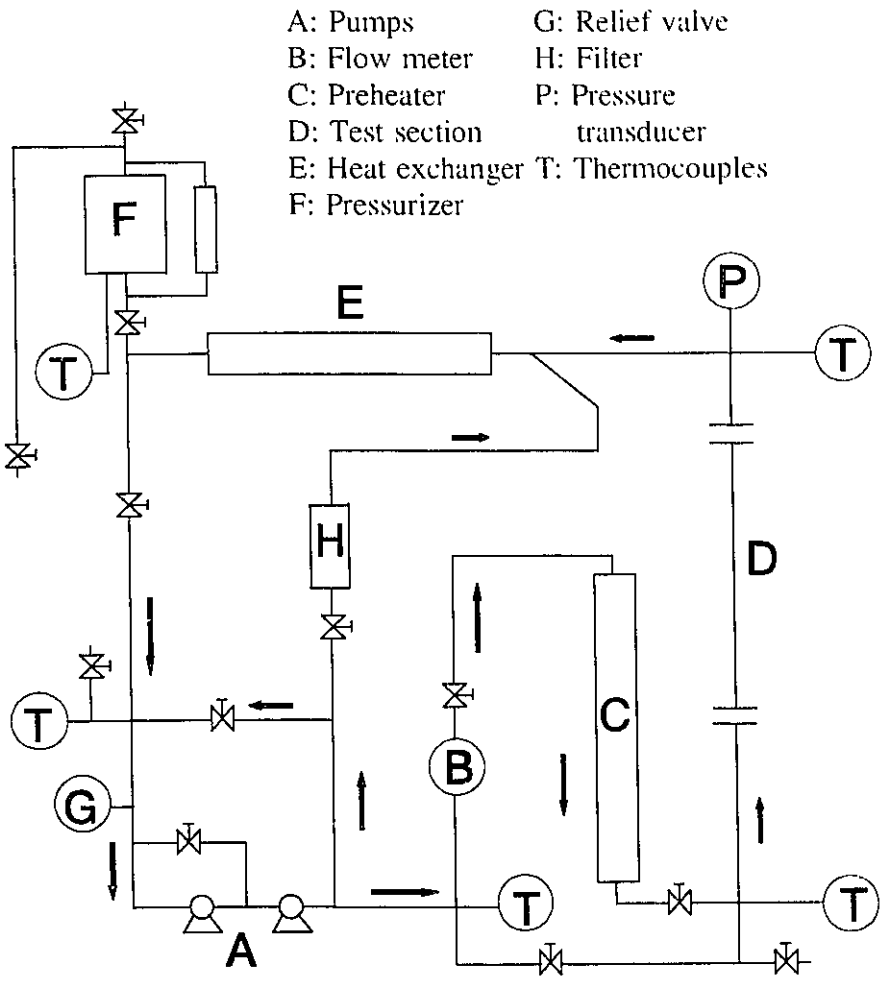

Figure 3-1 Outline sketch of the UO multi-fluid boiling loop.

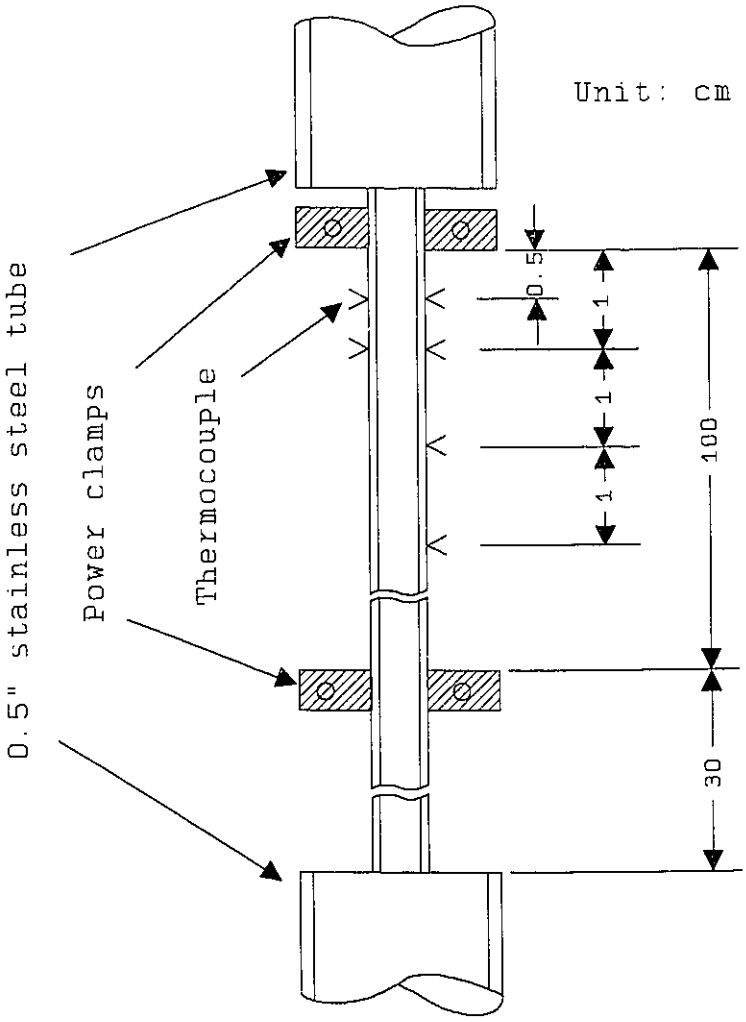

Figure 3-2 Sketch of the test section in the UO loop.

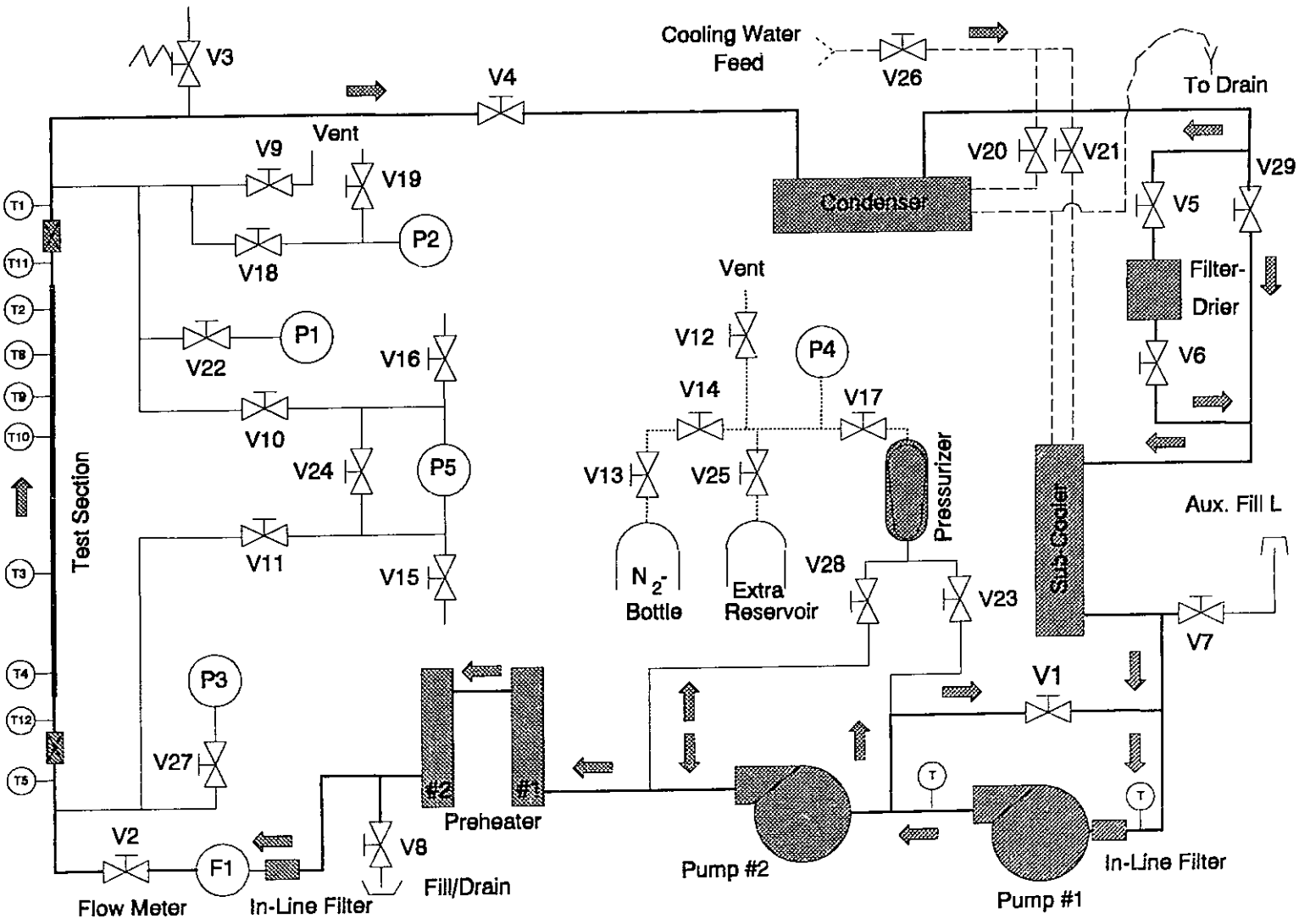

Figure 3-3 Schematic of the MR-7A loop (courtesy of AECL).

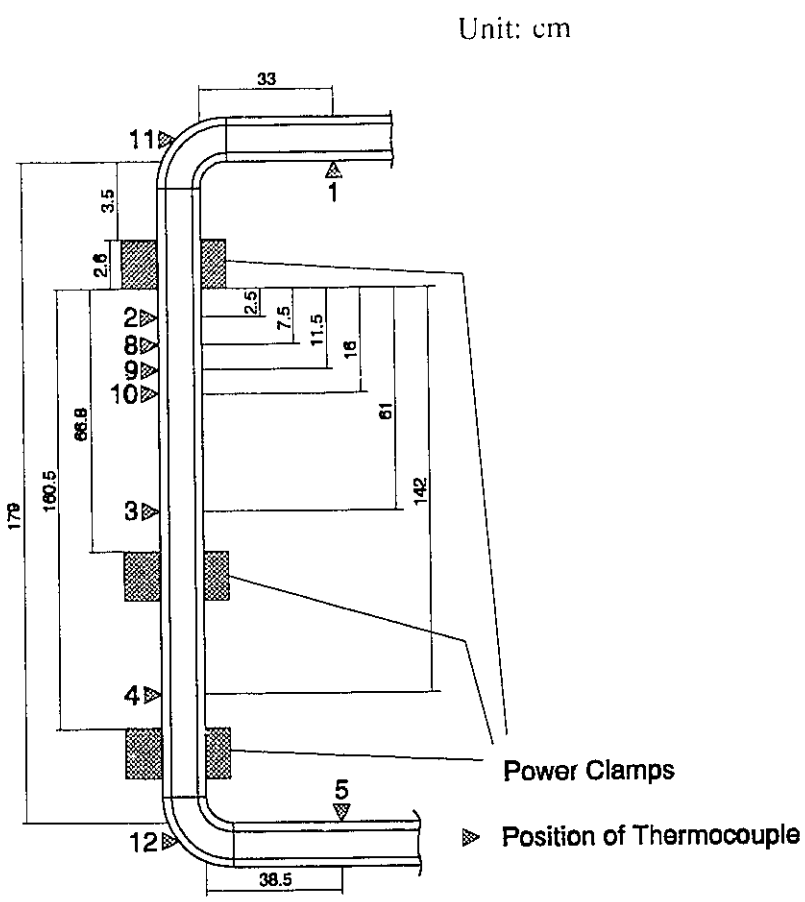

Figure 3-4 Sketch of the test section for 4.38 mm and 8 mm I.D. in the MR-7A loop (courtesy of AECL).

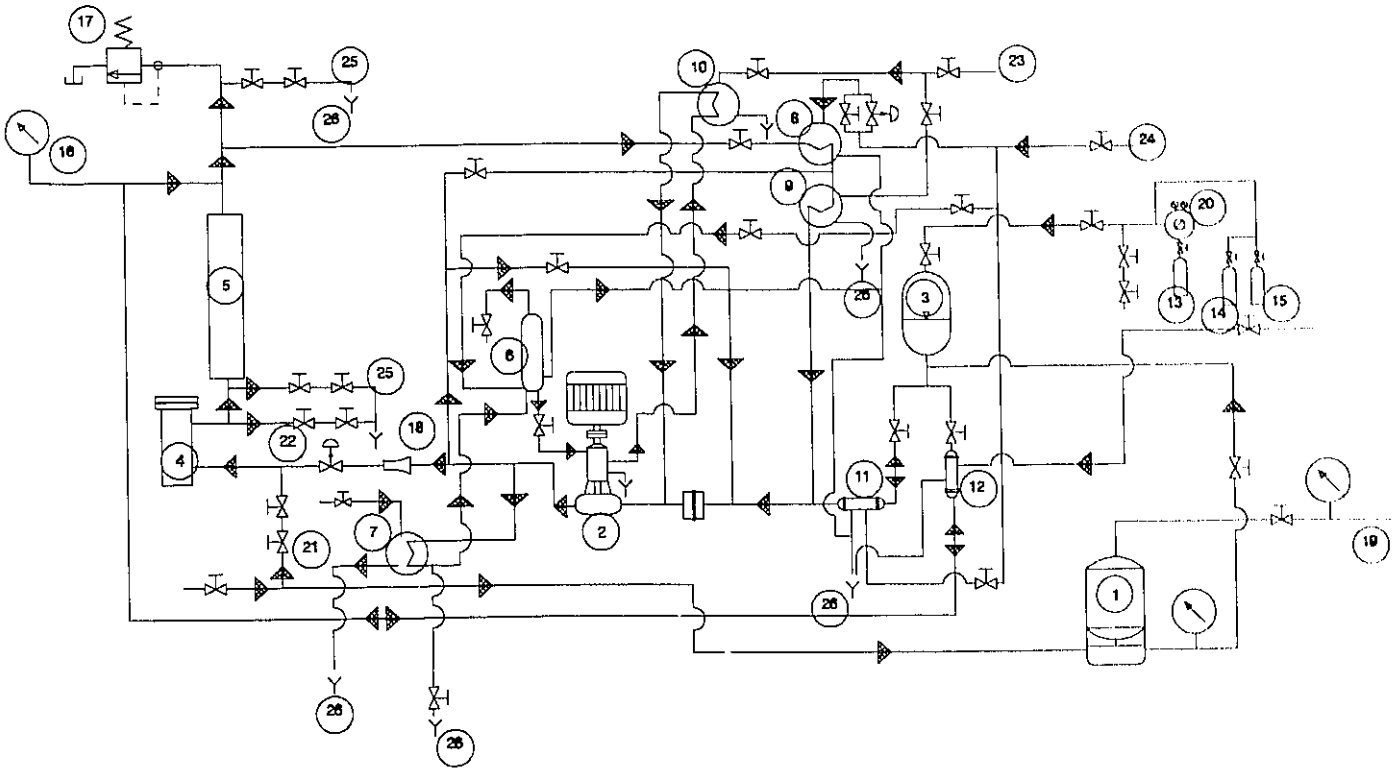

LEGEND

1 Make-up Pump
2 Main Pump
3 Pressurizer
4 Pre-heater
5 Test section
6 & 7 Pump-seal cooler
8 Condenser
9 [illegible]
10 Pump-seal water heater
11 & 12 Cooler loop water to pressurizer
13 Nitrogen bottle for maintaining loop pressure
14 Nitrogen bottle for high pressure expansion of pressurizer
15 Nitrogen bottle for low pressure expansion of pressurizer
16 Pressure gage indication test section outlet pressure
17 Pressure relief valve
18 Venturi flow meter
19 Plant air to run make-up pump
20 Pressure regulator
21 Loop fill
22 Loop drain
23 Plant steam to heat pump-seal water and loop cooler
24 Plant water for coolers
25 Vents
26 Drains

Figure 3-5 Schematic of the MR-1A loop (courtesy of AECL).

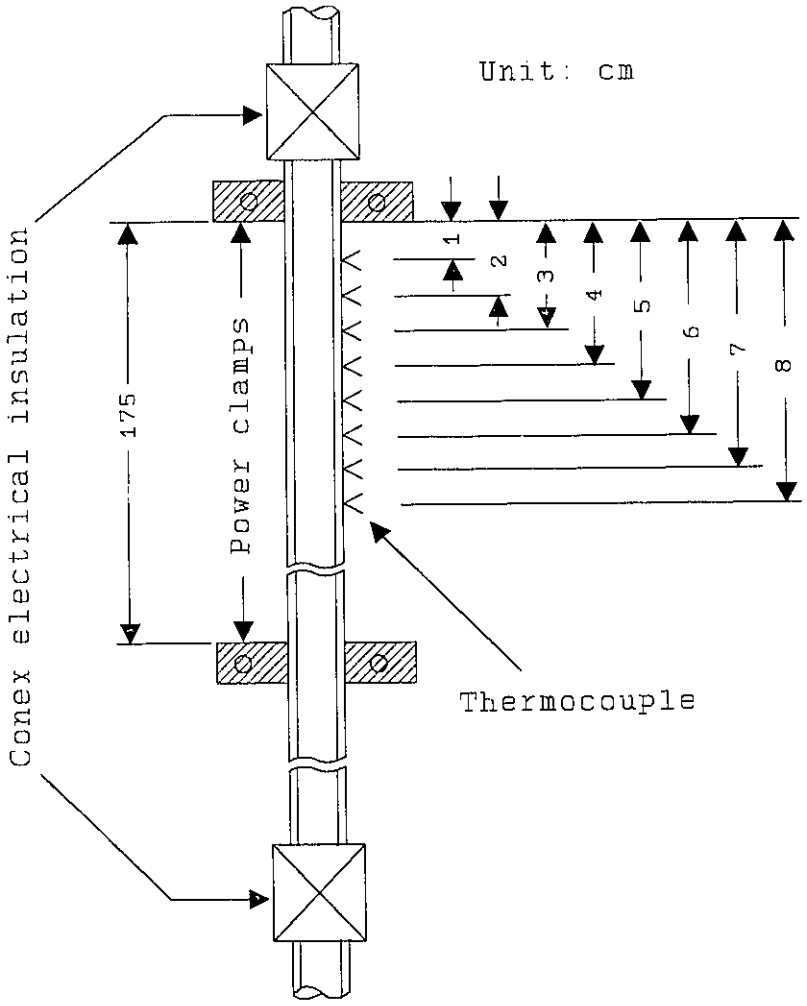

Figure 3-6 Sketch of the test section in the MR-1A loop.

Chapter 4

EXPERIMENTAL RESULTS

4.1 Data Reduction

The CHF is primarily a function of P (pressure), G (mass flux), D (diameter) and X_e (critical quality). P is measured directly, while G and X_e are calculated from other parameters (temperature, pressure etc.):

$$G = \frac{\dot{m}}{A_F} = \frac{4}{\pi}\frac{\rho V'}{D^2} \tag{4-1}$$

$$X_e = \frac{h_{exit} - h_f}{\lambda} \tag{4-2}$$

where

$$h_{exit} = h_{in} + \frac{Q'}{\dot{m}} \tag{4-3}$$

and enthalpy h_f and heat of vaporization λ are based on outlet pressure, the volumetric flow rate V' is measured from the turbine flow meter, the CHF power Q' is the product of the DC current and the voltage across the heated length and h_{in} is calculated based on the flow inlet temperature. The CHF is then calculated from

$$CHF = \phi_c = \frac{Q'}{\pi DL} \tag{4-4}$$

The symbols are also defined in the nomenclature. The thermophysical properties required for

the present work are based on Cheng et al. (1993). The details of the property subroutines can be seen in the Appendix III; all the test data of the present experiment are tabulated in Appendix IV.

4.2 Observed Parametric Trends

4.2.1 UO Loop

Table 4-1 is a summary of the test results from the UO loop. Note that the CHF data for HCFC-123 for the high pressure condition (10 MPa of water-equivalent pressure) were not reported because the high saturation temperature (130°C) created a cooling problem in the heat exchanger. CFC-11 was also found to have a similar problem. In addition, after a few tests for CFC-11, a deposit was found on the tube wall of the test section. This is probably due to the decomposition of CFC-11 at temperatures above 100°C. Therefore, very few data for CFC-11 were taken. The CHF data are plotted against the critical quality (X_e) as shown in Figs. 4-1—4-5 for various pressures, heated lengths and mass fluxes. Theses figures show that all fluids display a similar trend of increasing CHF with decreasing X_e. At high quality and high pressure conditions, a tendency towards the "limiting quality" phenomenon (Doroshchuk et al., 1970) was observed for all fluids except CFC-11. This phenomenon is in the region II as shown in Fig. 2-5 and has been discussed in Section 2.4.2. For high pressure and high mass flux values (3000 - 4000 kg m^{-2} s^{-1}), the effect of mass flux tends to be less significant. The pressure effect on CHF is shown in Figs. 4-6—4-8; the CHF decreases when pressure increases for constant X_e values. However, at high flow rates, the pressure effect on CHF decreases, especially at low qualities. At most pressures and flow conditions, the effect of the ratio of heated length to diameter (L/D)

is not significant for L/D between 119 and 238 as shown in Fig. 4-9.

4.2.2 MR-7A Loop

4.2.2.1 Results from the 4.38 mm I.D. Test Section

Table 4-2 summarizes the CHF test results from the MR-7A loop including the test sections with an I.D. of 4.38 mm and of 8 mm. For the results from the 4.38 mm I.D. tube, the CHF data again are plotted against the critical quality (X_c) as shown in Fig. 4-10 for 7 and 10 MPa water-equiv. pressures, respectively. Similar to the CHF test results from the UO loop, the effect of mass flux becomes less significant at high mass flux (4000 - 8000 kg m^{-2} s^{-1}) but an L/D effect has been observed, especially at low pressures (7 MPa water-equiv. pressure). Since the I.D. is very close to the one in the UO loop (I.D. difference less than 0.2 mm), we assume that the CHF data from both loops should agree with the same test conditions. Therefore, the CHF data for a mass flux at 4000 kg m^{-2} s^{-1} from both loops are compared by plotting them in the same graph as shown in Fig. 4-11 for 7 and 10 MPa water-equiv. pressures. At low pressure (7 MPa water-equiv. pressure), the L/D effect is not significant in the range from 185 to 333. When the L/D ratio decreases, the effect of L/D on CHF becomes noticeable (e.g. L/D from 185 to 155). However, at high pressure condition (10 MPa water-equiv.), the L/D effect is not significant for the whole test range ($155 \leq L/D \leq 333$). To obtain a wider range of parametric trends for CHF against critical quality, the CHF data from the UO and MR-7A loops are incorporated in the same graphs ($1.5 \leq G \leq 8$ Mg m^{-2} s^{-1}) as shown in Fig. 4-12. From both figures, we observed that the L/D effect on CHF tends to be more significant with increasing mass flux.

4.2.2.2 Results from the 8 mm I.D. Test Section

CHF experiments in 8 an mm I.D. tube has become a standard test in thermalhydraulic laboratories. As mentioned in Section 2.4.2, two standard CHF tables (by the USSR Academy of Science (1977) and by Groeneveld et al. (1986a)) have been established for water and both tables are based on 8 mm I.D. CHF data. The effort to improve the accuracy of the CHF table continues. One of the methods is to conduct the CHF experiments with the same I.D. test section but using fluids other than water. Then, the CHF data from the non-aqueous fluids will be converted to the water-equivalent values through fluid-to-fluid scaling techniques. Thereafter, CHF experiments using HCFC-22 in the 8 mm I.D. test section were performed in the MR-7A loop because this loop can provide enough capacities of flow rate and power.

As seen from Table 4-2, CHF data for the 8 mm I.D. were obtained at 1.34 MPa (7 MPa water-equiv.) and 1.96 MPa (10 MPa water-equiv.) and 1–6 Mg m^{-2} s^{-1}. The L/D varies from 84 to 199 and the critical quality from 0.02 to 0.6. The CHF data are also plotted against the critical quality for all mass fluxes and pressures as shown in Fig. 4-13. From this figure, the mass flux effect on CHF shows the same trend as those for the 4.2 and 4.38 mm I.D. test sections obtained from the UO and MR-7A loops. Generally the L/D effect for 8 mm I.D. is negligible for most mass fluxes and pressures. Only at high mass flux and high pressure conditions, does the L/D effect become noticeable. The pressure effect is illustrated in Fig. 4-14 which shows that the CHF decreases when the pressure increases from 1.34 to 1.96 MPa, similar to the trend in the 4.2 and 4.38 mm I.D. test sections. Note that the scattering in the data increases at low flow rate conditions (i.e. 1 Mg m^{-2} s^{-1}). This is probably because the flow rate and power are the lowest among all test conditions, and due to the occurrence of flow oscillations as well as the unstable

CHF condition. The relative measurement uncertainty is thus expected to be higher than at other flow conditions.

4.2.3 MR-1A Loop

Because the values of most properties for water are different by an order of magnitude compared to those for non-aqueous fluids used in the UO and MR-7A loops, the water CHF data obtained from MR-1A loop serve two purposes: (1) to examine the validity of CHF scaling techniques for a wide range of properties, and (2) to validate CHF prediction methods for water, used for the application in nuclear reactor safety. The CHF test results from the MR-1A loop are summarized in Table 4-3. Note that only one heated length (1.75 m) and one I.D. (8 mm) are used for the water CHF test. The mass fluxes are based on the same values of ψ_k for the HCFC-22 CHF test in the MR-7A loop. The CHF results are also schematically illustrated in Fig. 4-15 by plotting the CHF against the critical quality. The parametric trends are generally consistent with those observed from the UO and MR-7A loops for HCFC-22, that is, the effect of mass flux on CHF is significant at low mass flux and high quality and becomes less significant at high mass flux and low quality. Similar to the trend for HCFC-22, Figure 4-16 shows that the water CHF decreases with increasing pressure (from 7 to 10 MPa). However, at high mass flux and low quality conditions, the pressure effect becomes negligible. Since only one heated length is used for this water CHF test, the L/D effect on water CHF cannot be observed from the present work.

4.3 Comparison against Data Obtained from Elsewhere

To verify the accuracy of CHF experiments from the present results, the CHF data reported from the literature are used for comparison. However, the author has found it difficult to exactly match the data with those from the literature in terms of the same test conditions (e.g. diameter, pressure and mass flux etc.). In addition, the CHF data for HFC-134a and HCFC-123 are unique as so far no one else is known to ever have employed these fluids for CHF measurements. Therefore, only a portion of present data can be used for the comparison, and sometimes the data for similar but not exactly the same test conditions were used.

Firstly, the CFC-12 CHF data reported by Cheng et al. (1992) are compared with those from the present work. The comparison is illustrated in Figs. 4-17—4-19: the data show satisfactory agreement except for the mass flux condition at 2 Mg m^{-2} s^{-1}, where the data do not show good agreement. Cheng et al.'s data also demonstrate a noticeable L/D effect on CHF.

Secondly, the water CHF data from the present study have been compared with a number of data sources reported by different investigators. Generally, as shown from Fig. 4-20 to 4-24, the water CHF data from the present study are in satisfactory agreement with those from other sources. As discussed in Section 2.4.2, Groeneveld et al.'s (1986a) standard water CHF table was derived for an 8 mm tube by statistically averaging the experimental CHF values with each P, G and X_e interval. For the CHF values at non-table P, G and X_e values, linear interpolation within the intervals of P, G and X_e is used. Therefore, the water CHF data from the present study can also be compared with the table-CHF values for each test P, G and X_e. The results of the comparison are shown in Table 4-4, indicating satisfactory agreement. Table 4-4 also shows that the CHF table results in lower CHF values than the measurements at low mass flux (e.g. 2.5 Mg

m^{-2} s^{-1}) for both the 7 and 10 MPa of pressure. In addition, the CHF table underpredicts the CHF for all tested mass fluxes at 10 MPa of pressure. The experimental result from the UO loop and the comparisons against other prediction techniques can also be seen in the Section 5 of next chapter.

Table 4-i CHF test results for CFC's and CFC alternatives from the UO loop for I.D.=4.2 mm.

Fluid	P (MPa)	G (Mg m^{-2} s^{-1})	L/D	No. of data	X_e	CHF (kW m^{-2})
HFC-134a	1.13 (7)[†]	1.38-3.69	185-238	65	0.11-0.48	110-250
HFC-134a	1.65 (10)	1.37-3.66	185-238	73	0.09-0.40	85-254
HCFC-22	1.34 (7)	1.50-4.00	119-238	68	0.15-0.50	140-270
HCFC-22	1.96 (10)	1.50-4.00	185-238	61	0.12-0.40	100-250
CFC-12	1.06 (7)	1.53-4.08	185-238	58	0.13-0.49	104-215
CFC-12	1.58 (10)	1.53-4.09	185-238	69	0.12-0.40	74-200
HCFC-123	0.98 (7)	1.45-3.86	185-238	60	0.07-0.46	100-252
CFC-11	1.13 (7)	1.05	238	1	0.58	103
CFC-11	1.65 (10)	1.05-2.17	238	6	0.17-0.47	80-150

[†] The number inside the parentheses referred to water-equivalent pressure.

Table 4-2 CHF test results for HCFC-22 from the MR-7A loop.

I.D. (mm)	P (MPa)	G (Mg m^{-2} s^{-1})	L/D	No. of data	X_e	CHF (kW m^{-2})
4.38	1.34 (7)†	4 - 8	155	27	0.03 - 0.2	267 - 415
		4 - 8	333	29	0.1 - 0.28	130 - 270
	1.96 (10)	4 - 8	155	42	0 - 0.17	197 - 620
		4 - 8	333	35	0.05 - 0.26	140 - 335
8	1.34 (7)	1 - 6	199	22	0.14 - 0.6	125 - 200
		1 - 6	144	21	0.05 - 0.54	150 - 250
		1 - 2	110	10	0.18 - 0.46	200 - 245
		1 - 6	84	26	0.02 - 0.43	215 - 360
	1.96 (10)	1 - 6	199	30	0.06 - 0.45	85 - 250
		1 - 6	144	25	0.04 - 0.43	120 - 320
		1 - 6	84	22	0.02 - 0.37	170 - 400

† The number inside the parentheses referred to water-equivalent pressure.

Table 4-3 CHF test results for water from the MR-1A loop for heated length=1.75 m and I.D.=8 mm.

P (MPa)	G (kg m^{-2} s^{-1})	ψ_k	No. of data	X_c	CHF (MW m^{-2})
7	2540	64.68	6	0.28 - 0.39	1.8 - 2.5
	3800	90.03	6	0.17 - 0.3	2.0 - 2.7
	5200	129.4	6	0.1 - 0.24	2.3 - 3.2
	6400	161.8	5	0.06 - 0.2	2.5 - 3.6
	7700	194.1	8	0.04 - 0.18	2.6 - 4.5
10	2500	80.47	5	0.14 - 0.3	1.5 - 2.0
	3850	120.7	5	0.11 - 0.21	1.6 - 2.4
	5200	160.9	5	0.08 - 0.19	2.0 - 3.0
	6450	201.2	5	0.06 - 0.18	2.3 - 3.5
	7700	241.4	4	0.06 - 0.13	2.7 - 4.0

Table 4-4 CHF comparison for table prediction (Groeneveld et al. 1986a) against measured water data from the MR-1A loop based on constant X_e condition.

No. of data	Mass flux (kg m^{-2} s^{-1})	RMS error (%)[1]	Avg. error (%)[2]	Mean error (%)[3]
For pressure at 7 MPa				
6	2540	10.50	-8.63	9.65
6	3800	4.62	-1.11	3.41
6	5200	3.99	1.98	3.71
5	6400	8.11	7.45	7.45
8	7700	7.05	4.61	6.02
total=31	2540–7700	7.28	0.89	6.00
For pressure at 10 MPa				
5	2500	12.35	-12.04	12.04
5	3850	5.30	-4.20	4.79
5	5200	6.28	-5.88	5.88
5	6450	4.09	-3.83	3.83
4	7700	4.69	-4.12	4.12
total=24	2500–7700	7.21	-6.10	6.22

[1] R.M.S error = $\sqrt{\dfrac{\sum_{1}^{N}\left(\dfrac{CHF_{prdicted}-CHF_{measured}}{CHF_{measured}}\right)^2}{N}} \times 100\%$

[2] Avg. error = $\dfrac{\sum_{1}^{N}\dfrac{CHF_{prdicted}-CHF_{measured}}{CHF_{measured}}}{N} \times 100\%$

[3] Mean error = $\dfrac{\sum_{1}^{N}\left|\dfrac{CHF_{prdicted}-CHF_{measured}}{CHF_{measured}}\right|}{N} \times 100\%$

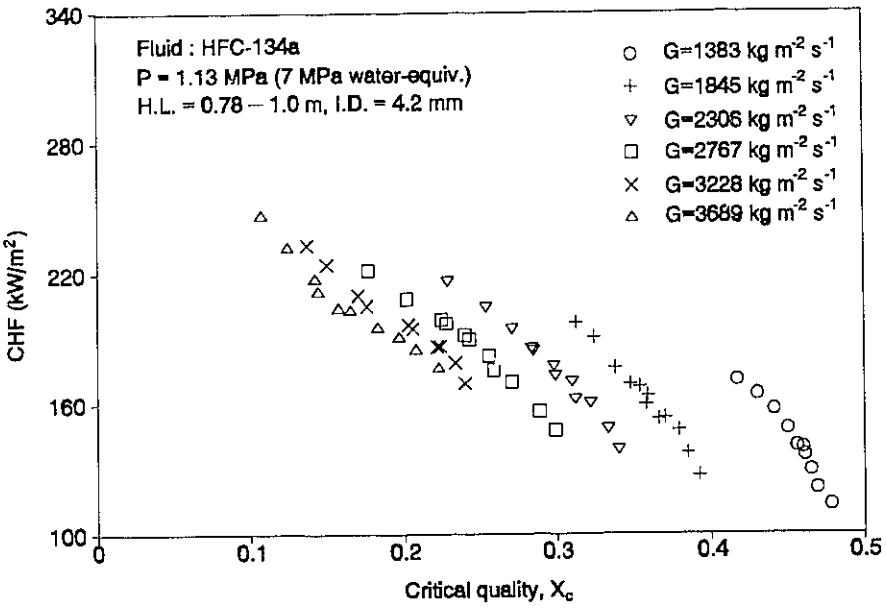

(a)

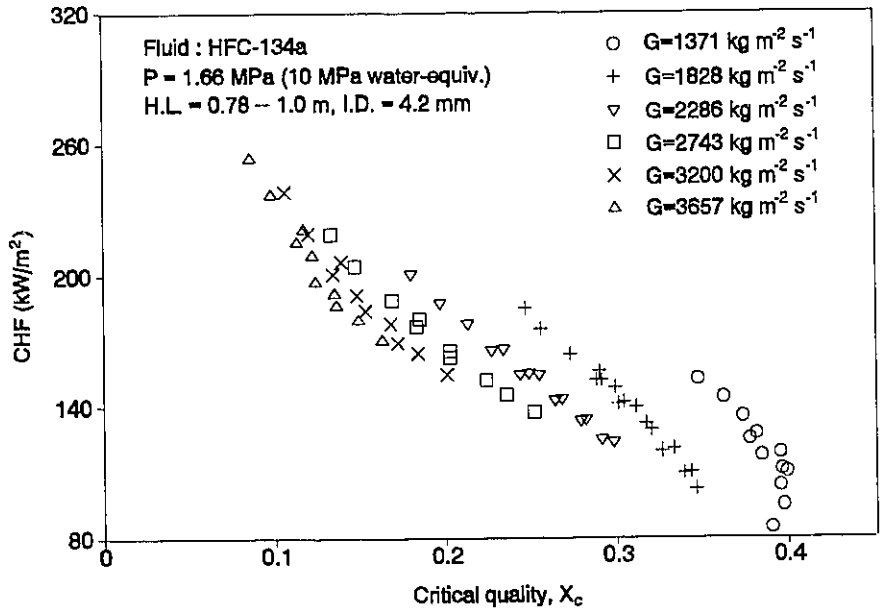

(b)

Figure 4-1 Effect of mass flux on CHF for HFC-134a from the UO loop at (a) 7 MPa and (b) 10 MPa water-equivalent pressure.

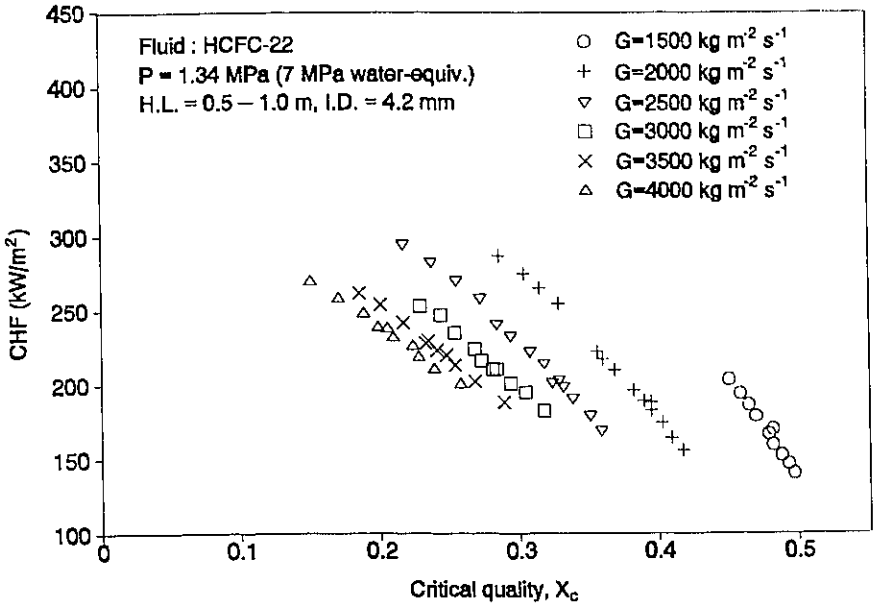

(a)

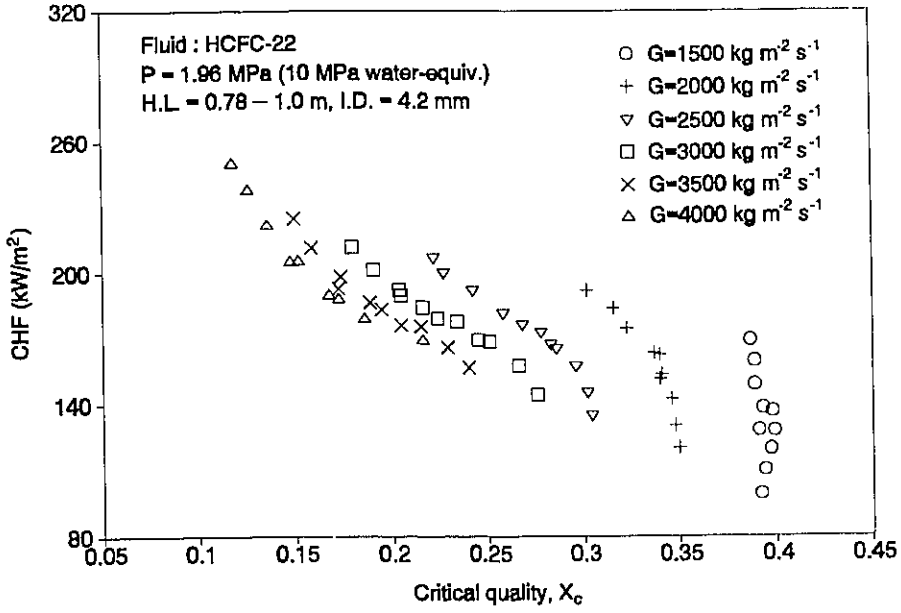

(b)

Figure 4-2 Effect of mass flux on CHF for HCFC-22 from the UO loop at (a) 7 MPa and (b) 10 MPa water-equivalent pressure.

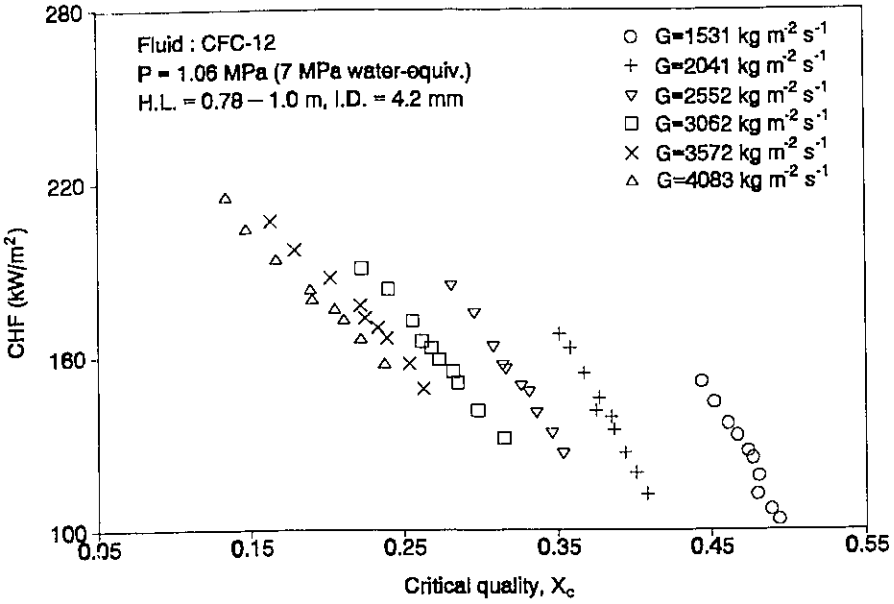

(a)

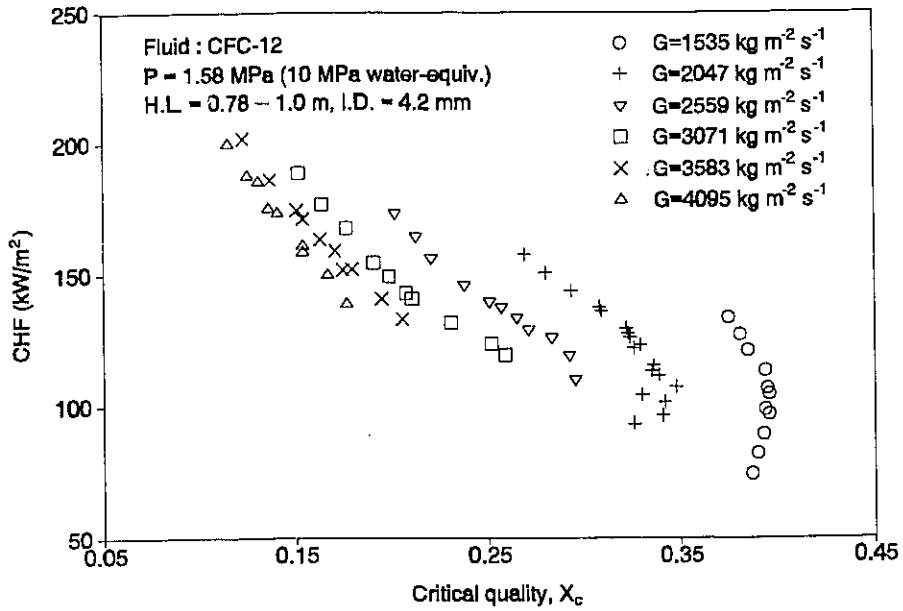

(b)

Figure 4-3 Effect of mass flux on CHF for CFC-12 from the UO loop at (a) 7 MPa and (b) 10 MPa water-equivalent pressure.

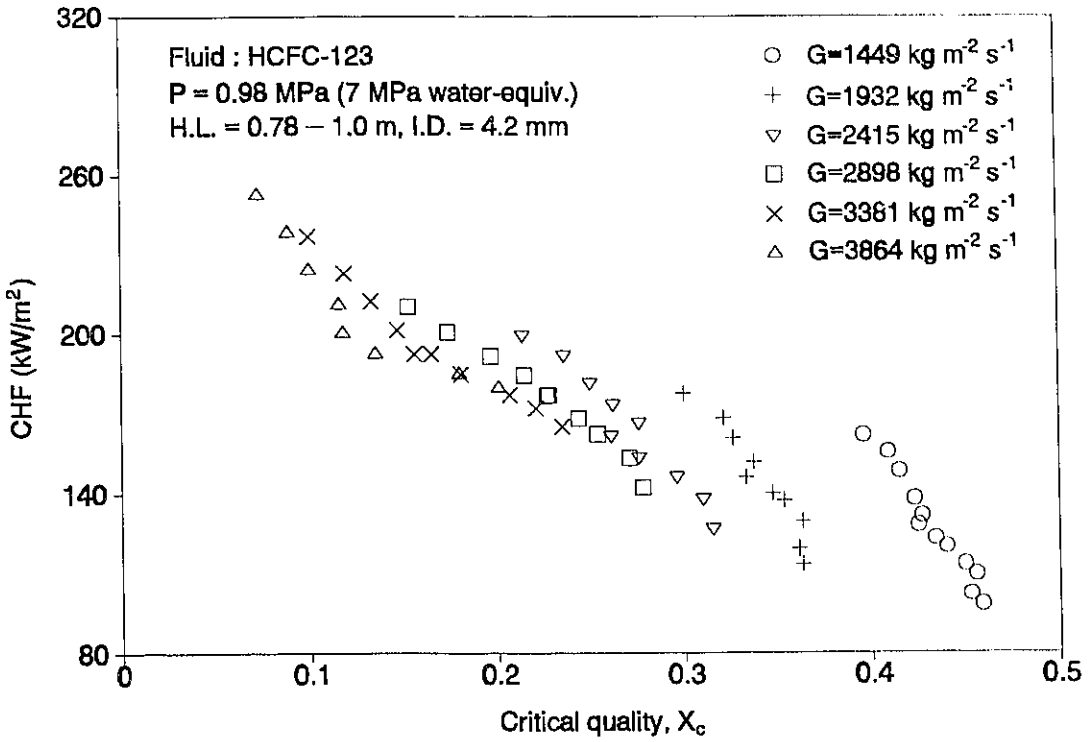

Figure 4-4 Effect of mass flux on CHF for HCFC-123 from the UO loop at 7 MPa water-equivalent pressure.

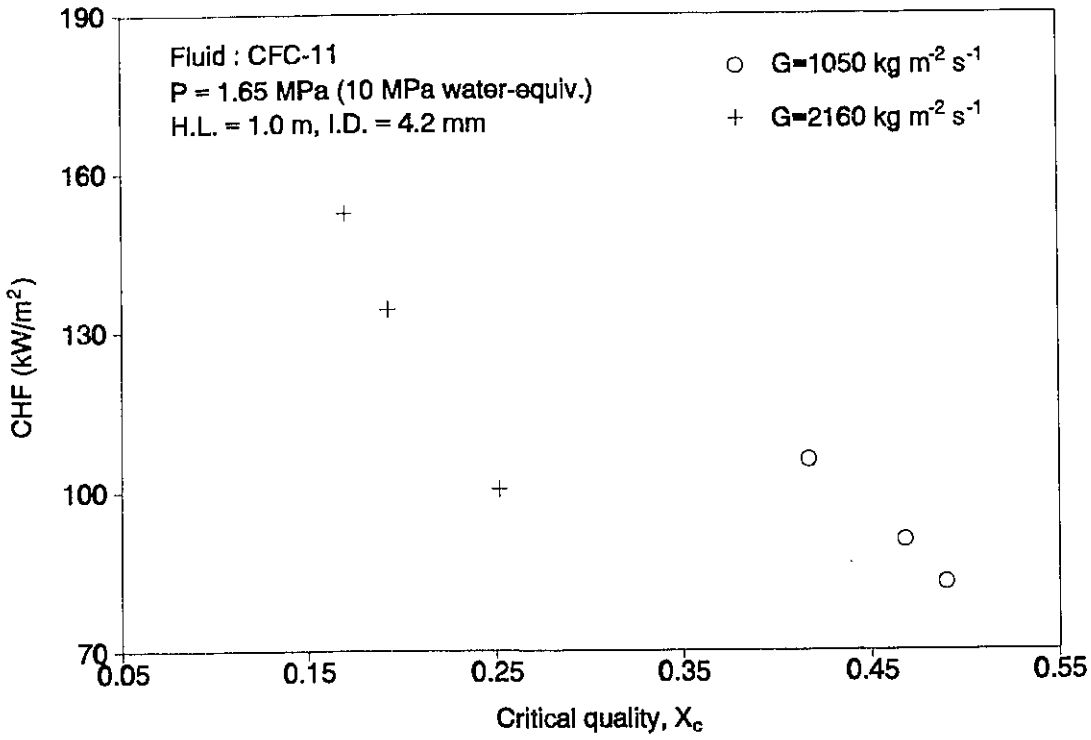

Figure 4-5 Effect of mass flux on CHF for CFC-11 from the UO loop at 10 MPa water-equivalent pressure.

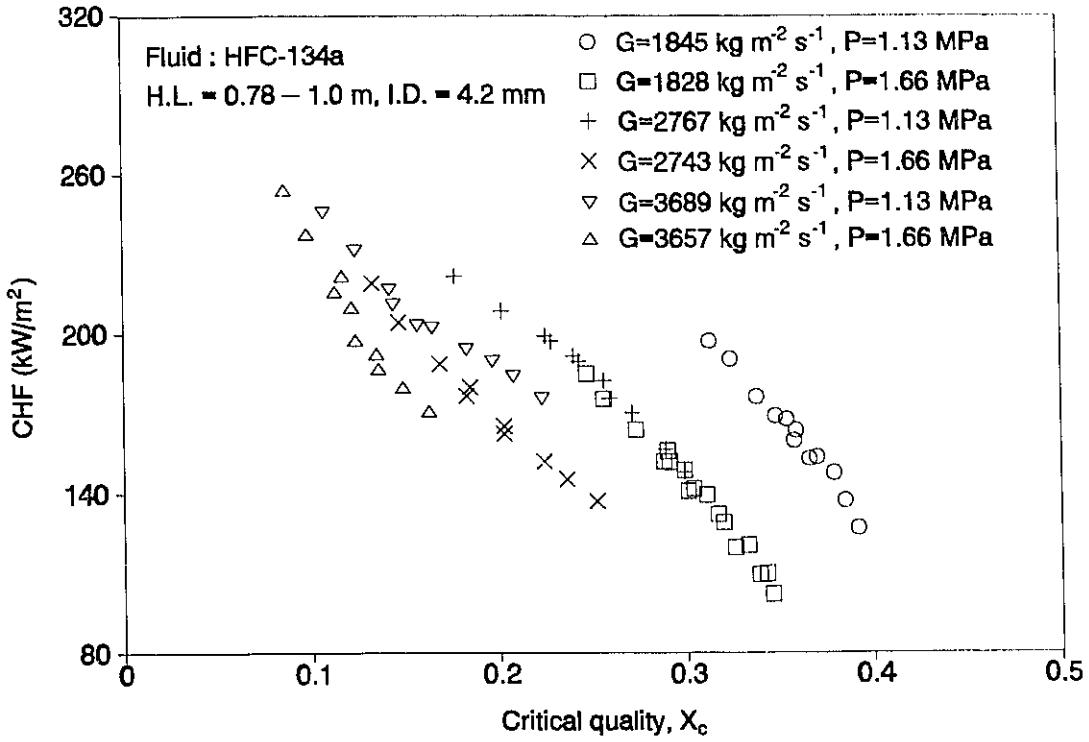

Figure 4-6 Effect of pressure on CHF for HFC-134a from the UO loop at fixed mass flux.

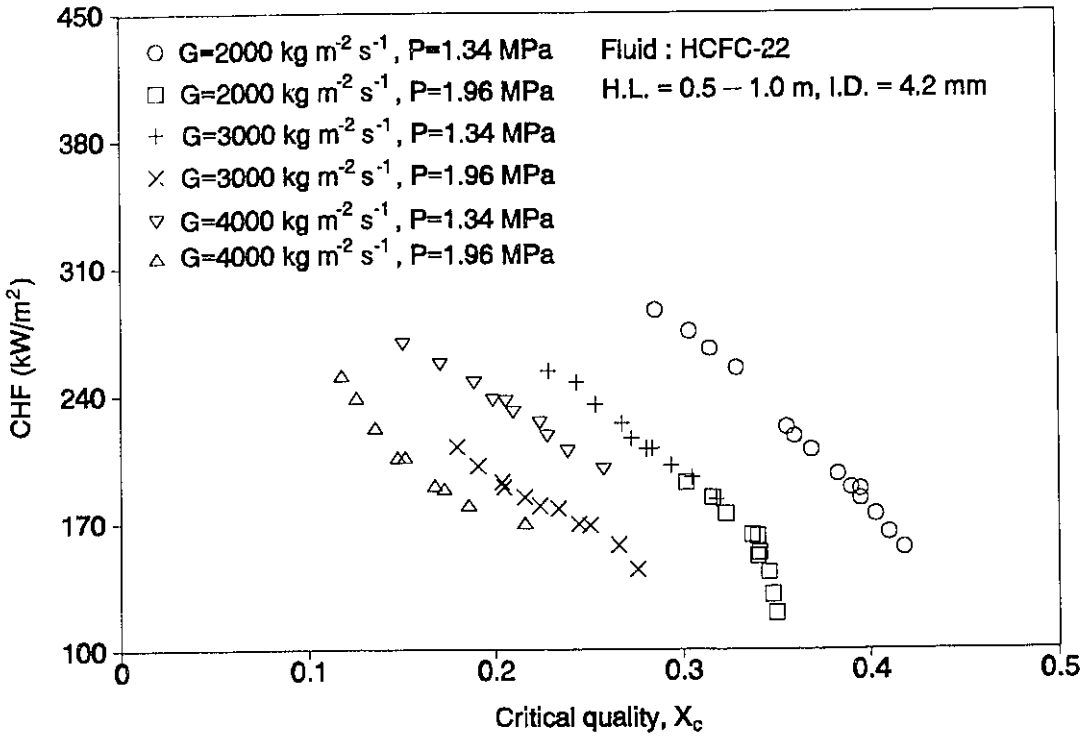

Figure 4-7 Effect of pressure on CHF for HCFC-22 from the UO loop at fixed mass flux.

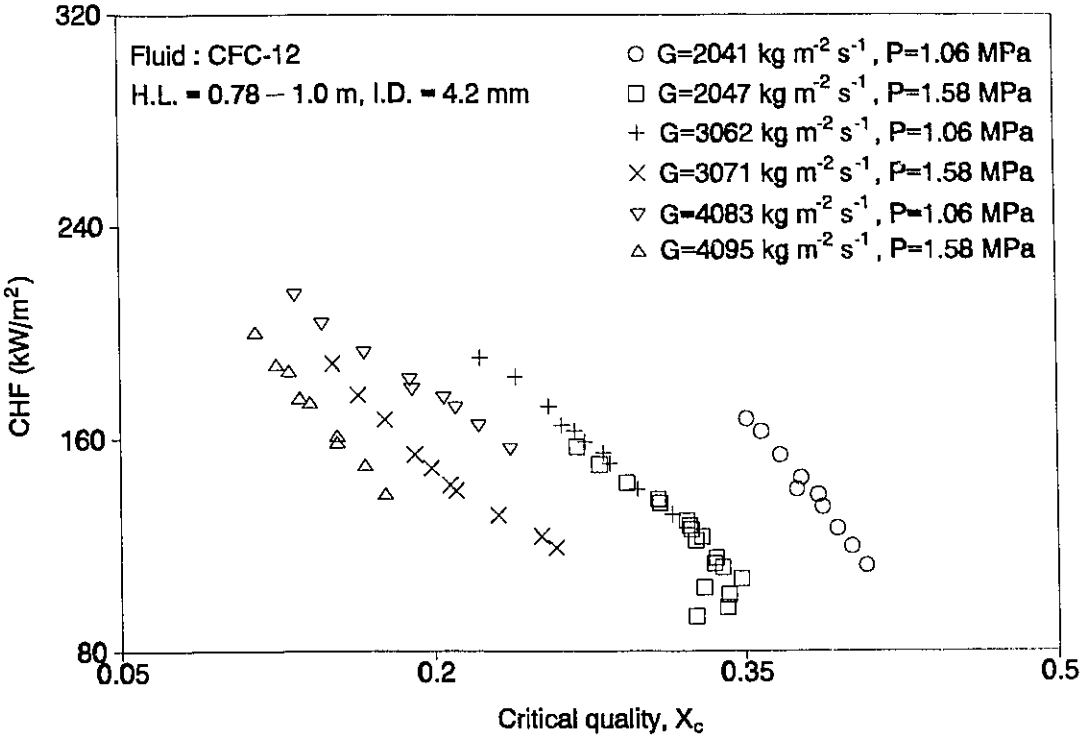

Figure 4-8 Effect of pressure on CHF for CFC-12 from the UO loop at fixed mass flux.

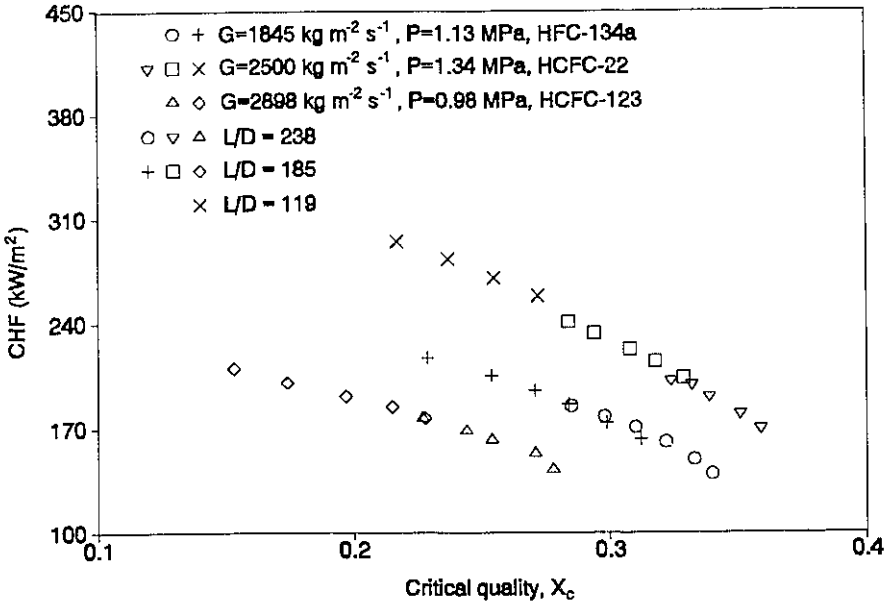

(a)

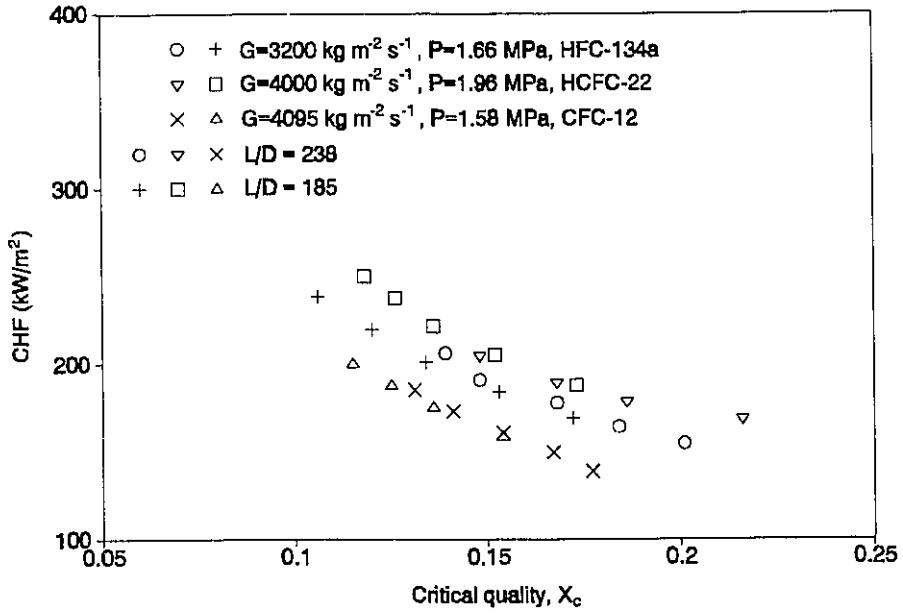

(b)

Figure 4-9 Effect of L/D on UO CHF data for (a) 119 ≤ L/D ≤ 238 at 7 MPa water-equiv. and (b) 185 ≤ L/D ≤ 238 at 10 MPa water-equivalent pressure for various fluids.

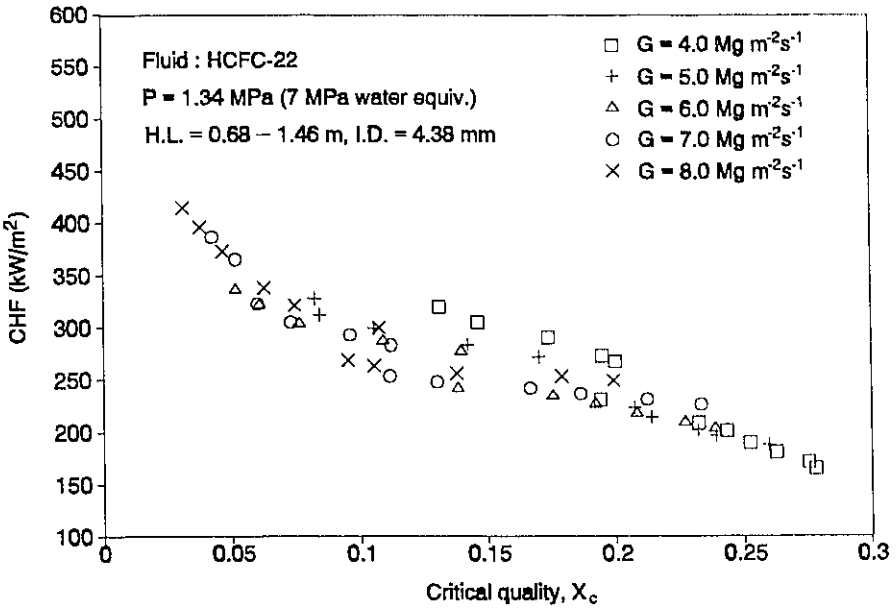

(a)

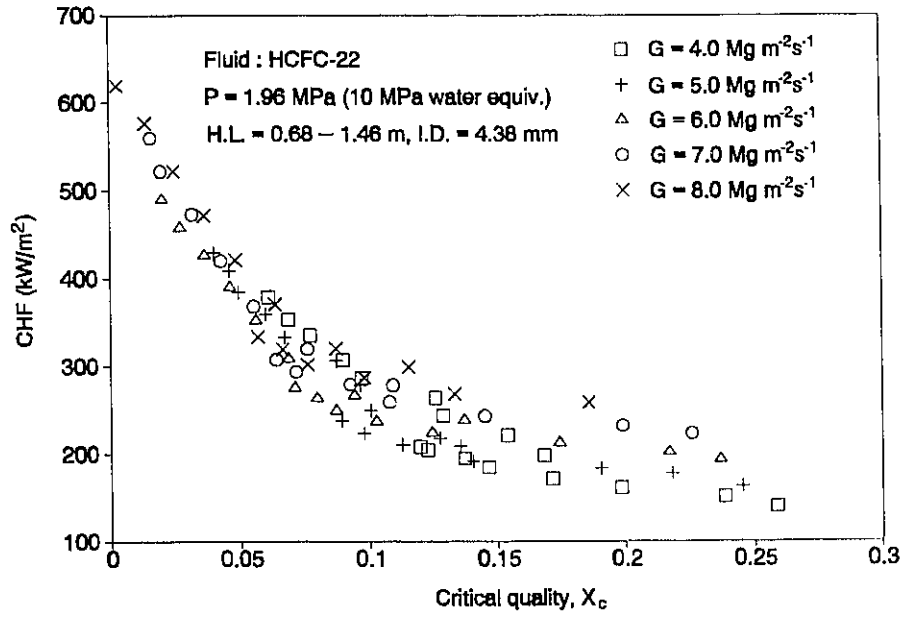

(b)

Figure 4-10 Effects of mass flux and L/D on CHF for HCFC-22 from the MR-7A loop at (a) 7 MPa and (b) 10 MPa water-equivalent pressure.

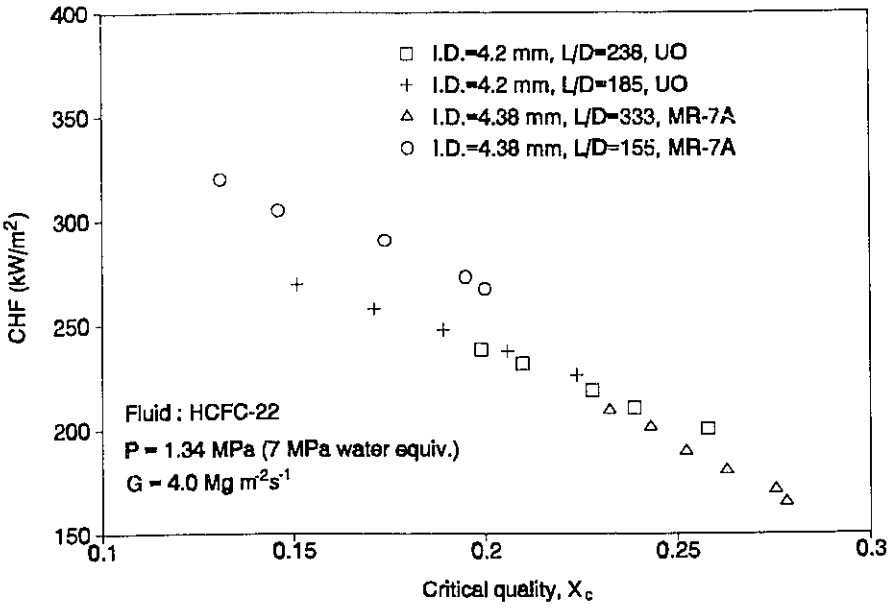

(a)

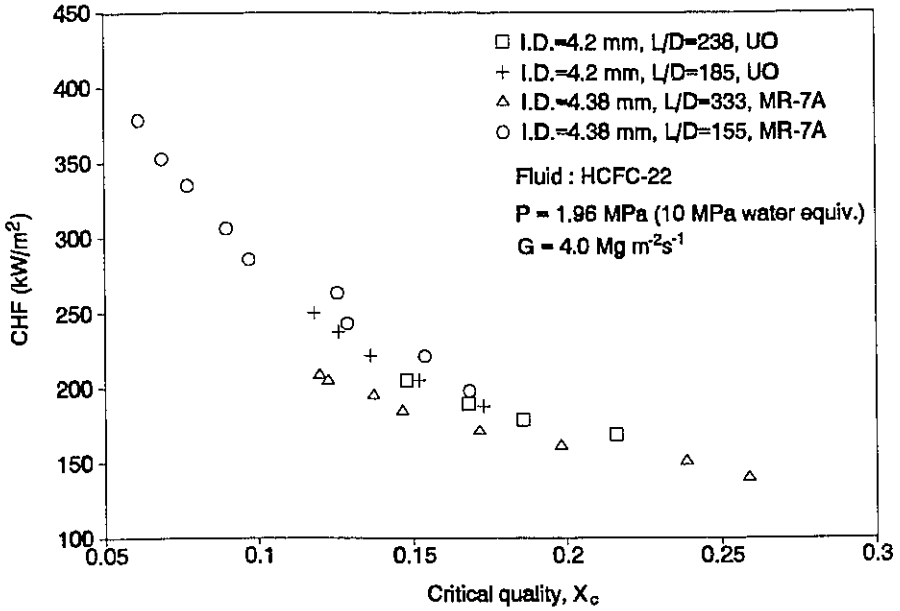

(b)

Figure 4-11 Effect of L/D on CHF for HCFC-22 data obtained from UO and MR-7A loops at (a) 7 MPa and (b) 10 MPa water-equivalent pressure.

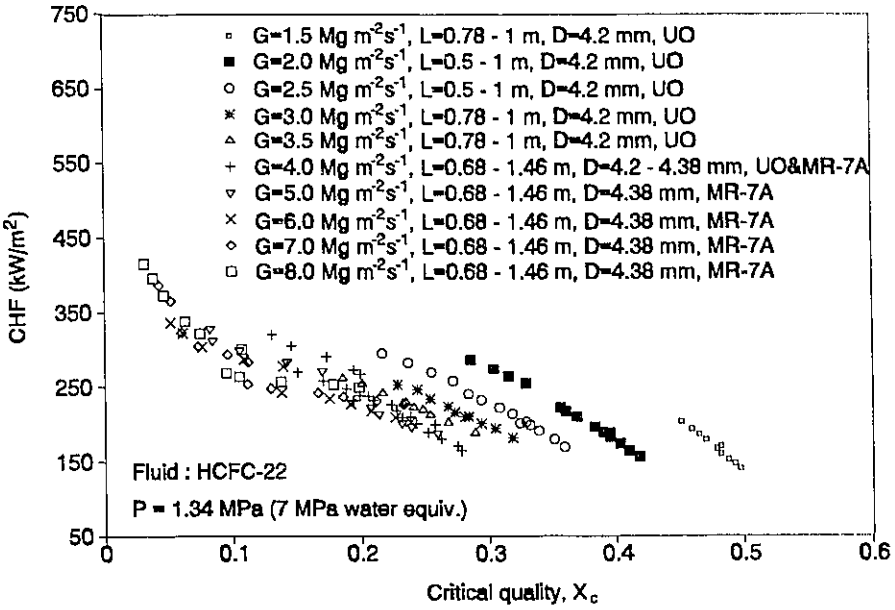

(a)

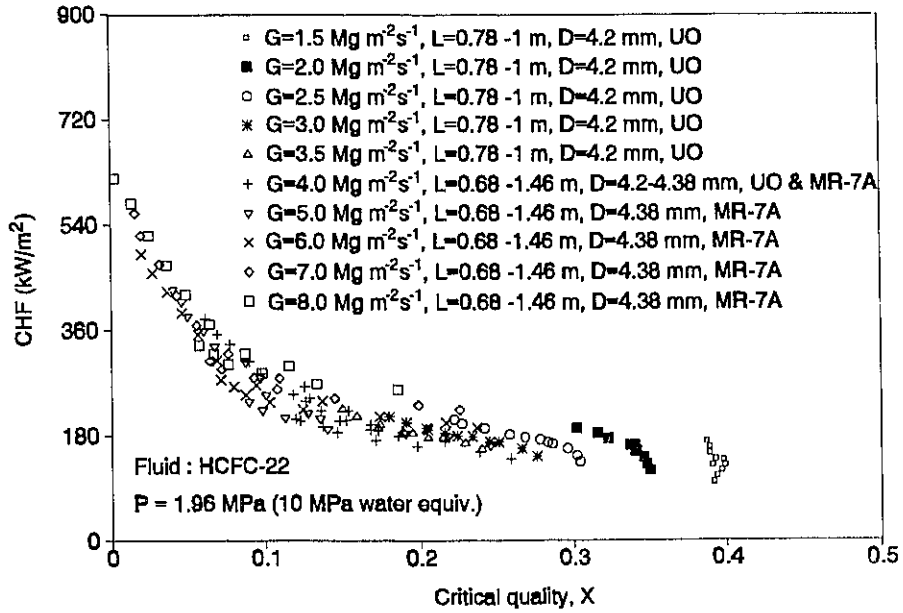

(b)

Figure 4-12 CHF vs X_c for HCFC-22 data obtained from UO and MR-7A loops at (a) 7 MPa and (b) 10 MPa water-equivalent pressure.

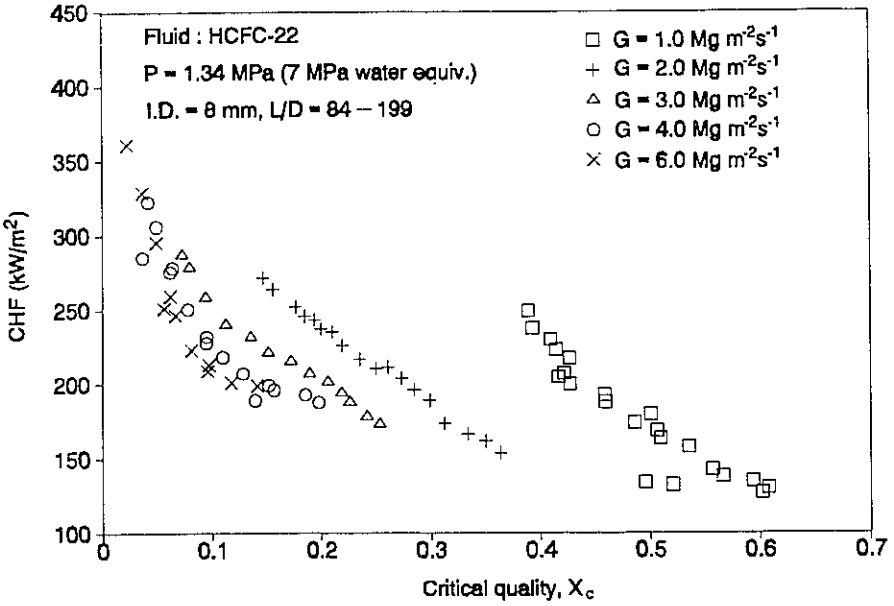

(a)

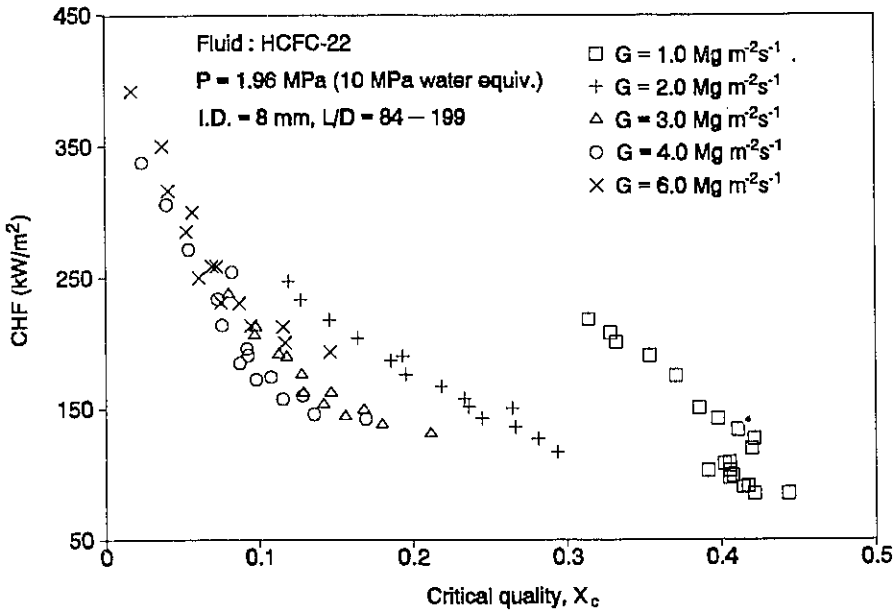

(b)

Figure 4-13 Effects of mass flux and L/D on CHF for HCFC-22 from the MR-7A loop at (a) 7 MPa and (b) 10 MPa water-equivalent pressure.

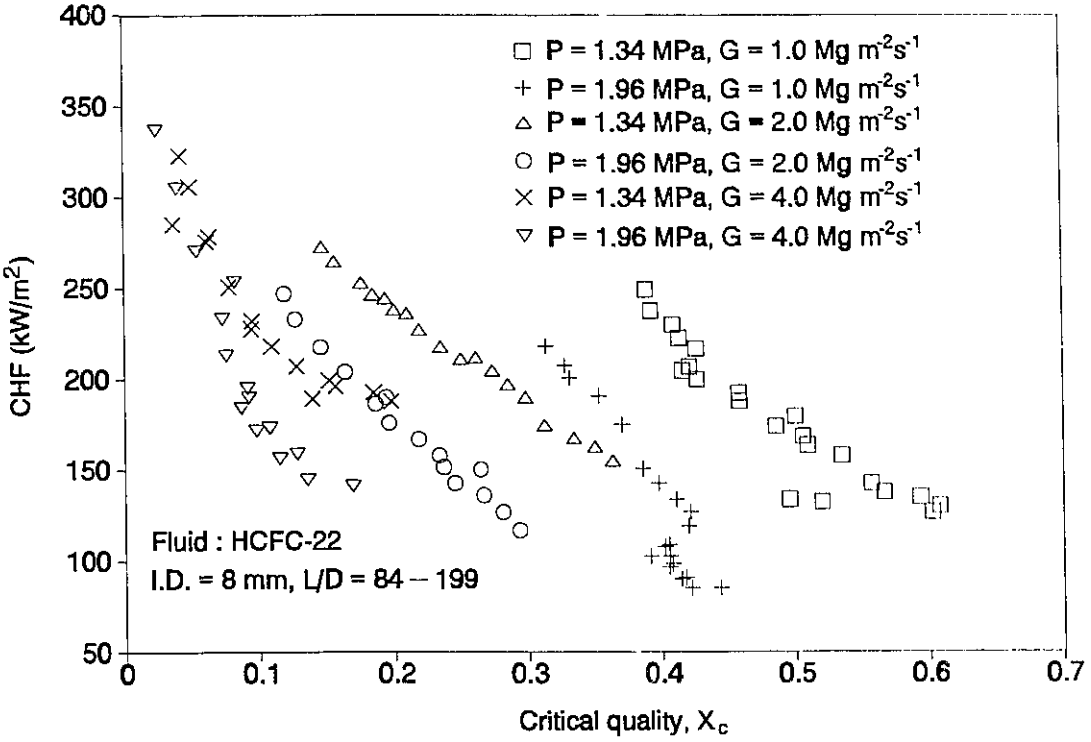

Figure 4-14 Effect of pressure on CHF for HCFC-22 from the MR-7A loop at fixed mass flux.

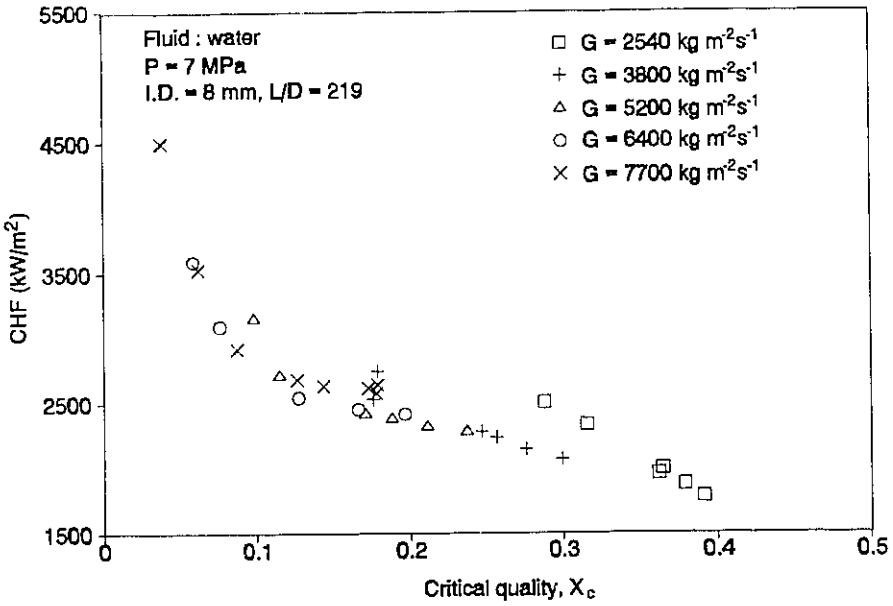

(a)

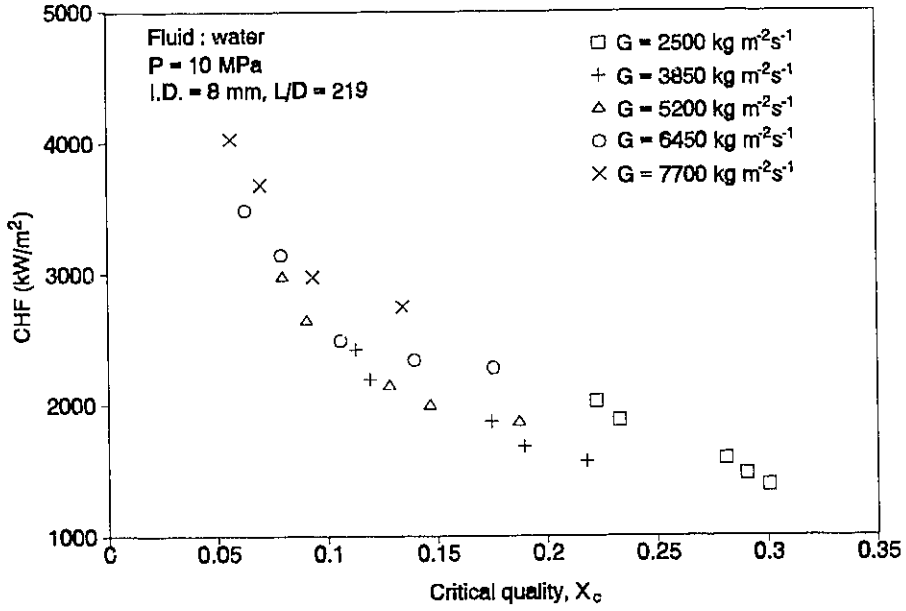

(b)

Figure 4-15 Effect of mass flux on CHF for water from the MR-1A loop at (a) 7 MPa and (b) 10 MPa pressure.

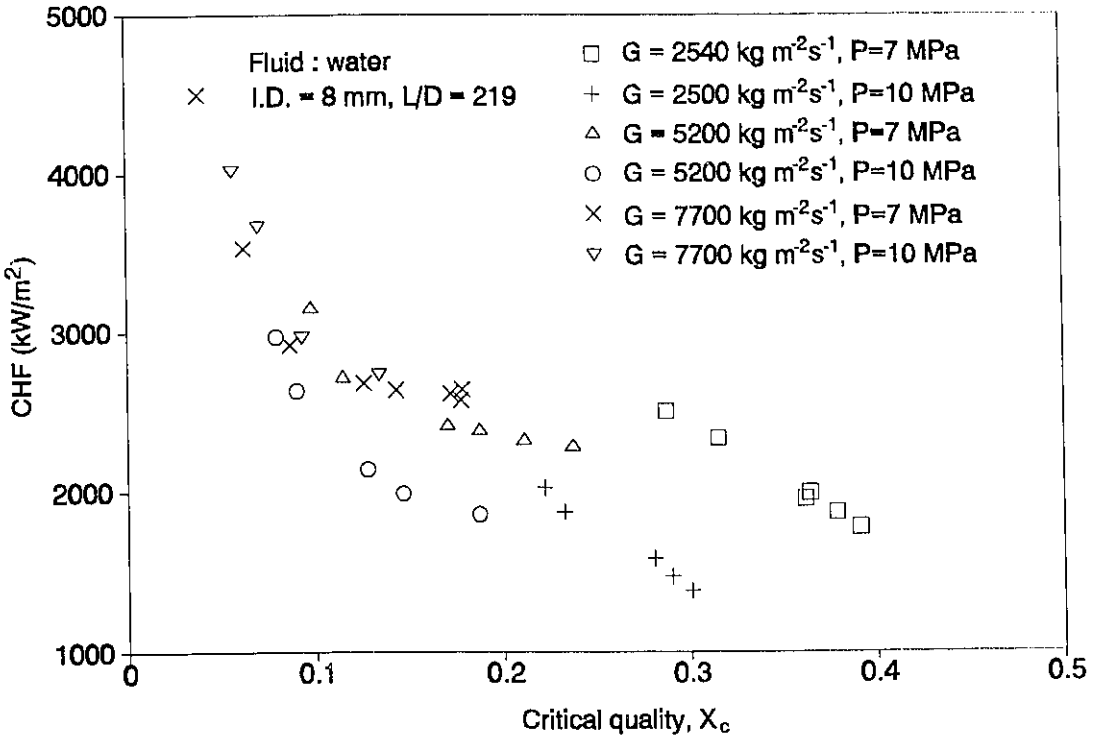

Figure 4-16 Effect of pressure on CHF for water from the MR-1A loop at fixed mass flux.

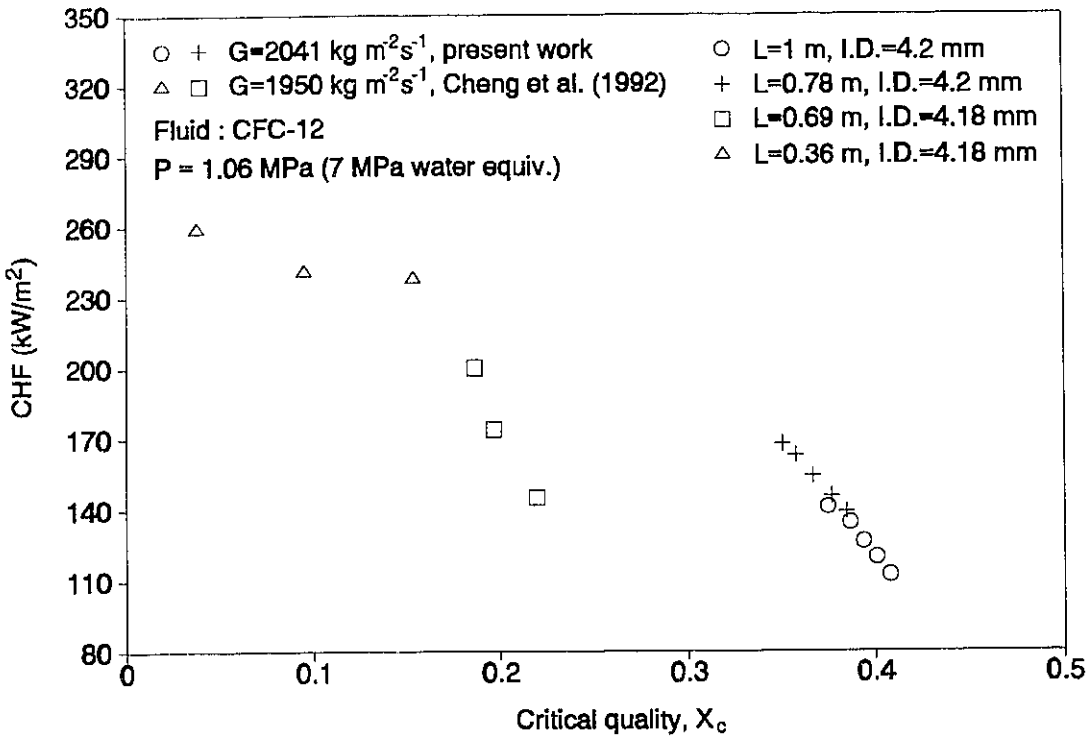

Figure 4-17 Comparison of CFC-12 CHF data from the UO loop against Cheng et al.'s (1992) measurements.

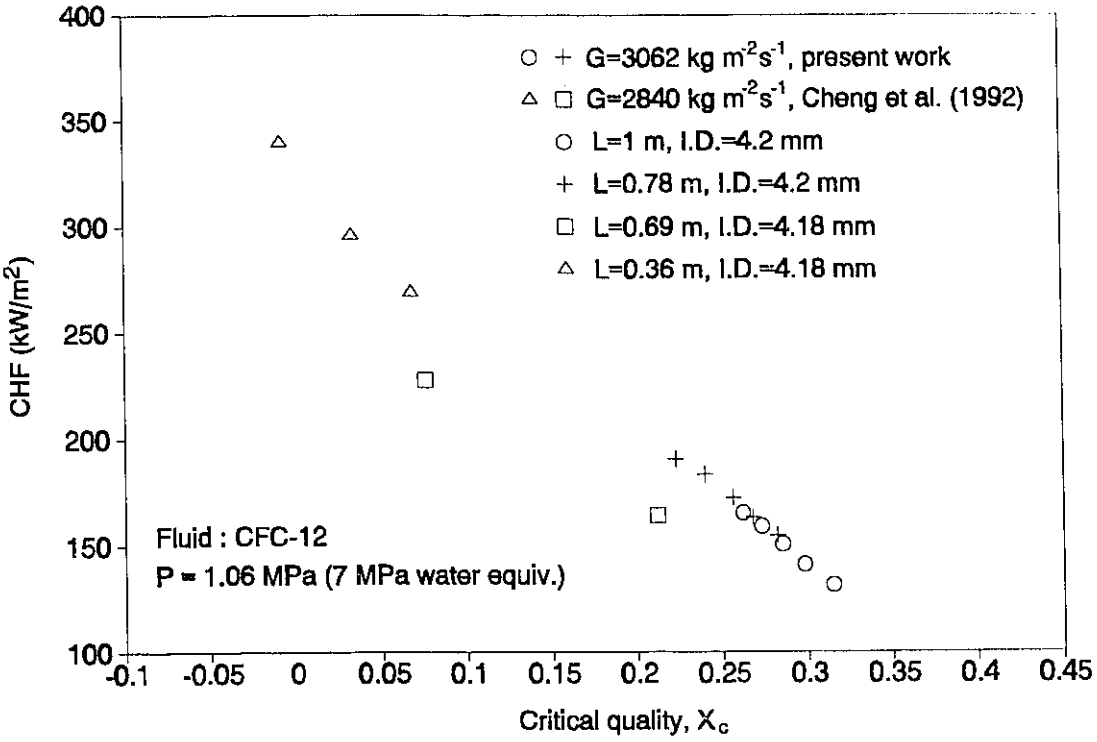

Figure 4-18 Comparison of CFC-12 CHF data from the UO loop against Cheng et al.'s (1992) measurements.

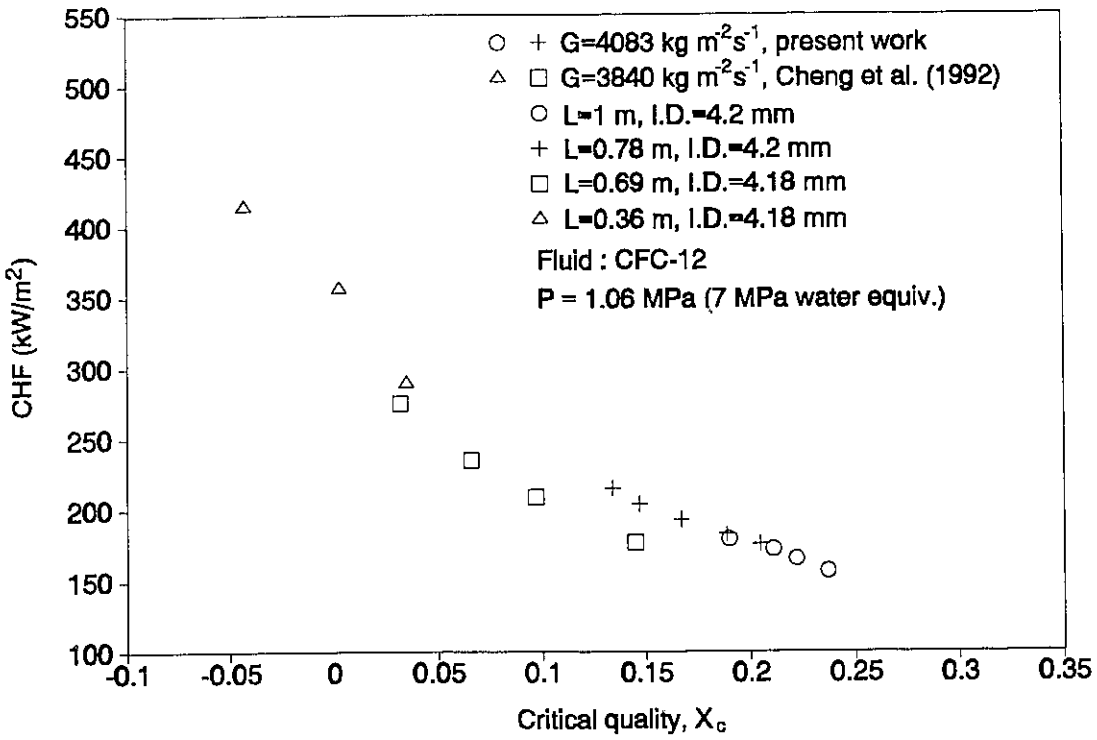

Figure 4-19 Comparison of CFC-12 CHF data from the UO loop against Cheng et al.'s (1992) measurements.

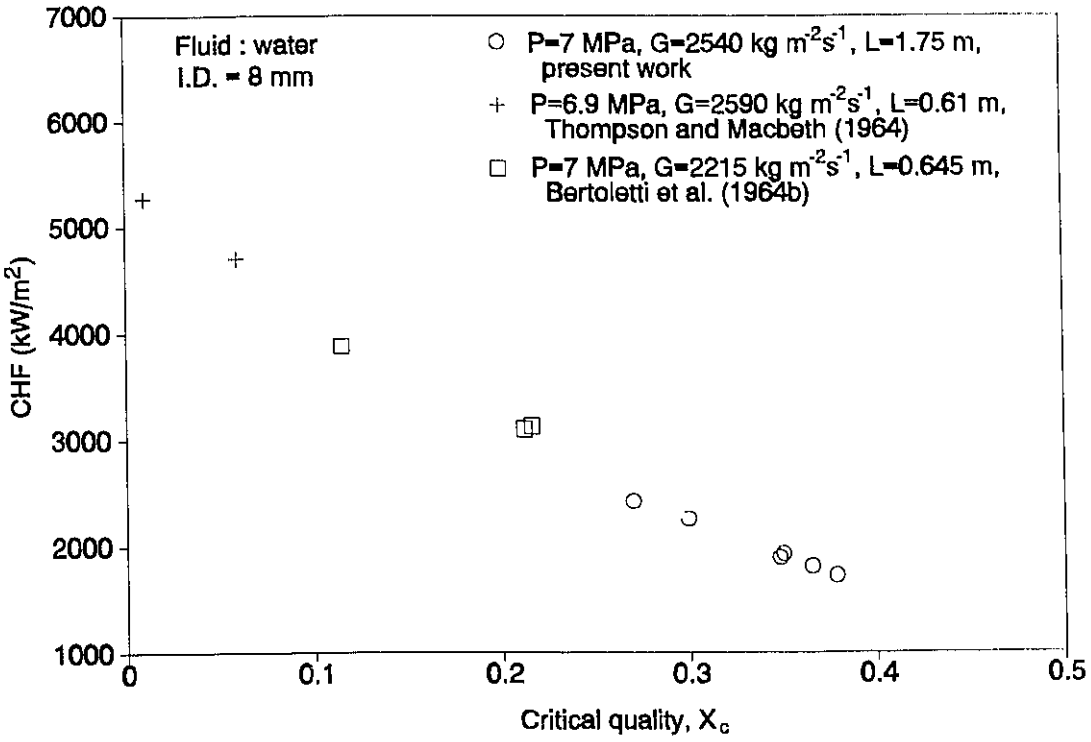

Figure 4-20 Comparison of water CHF data from the MR-1A loop against other data sources.

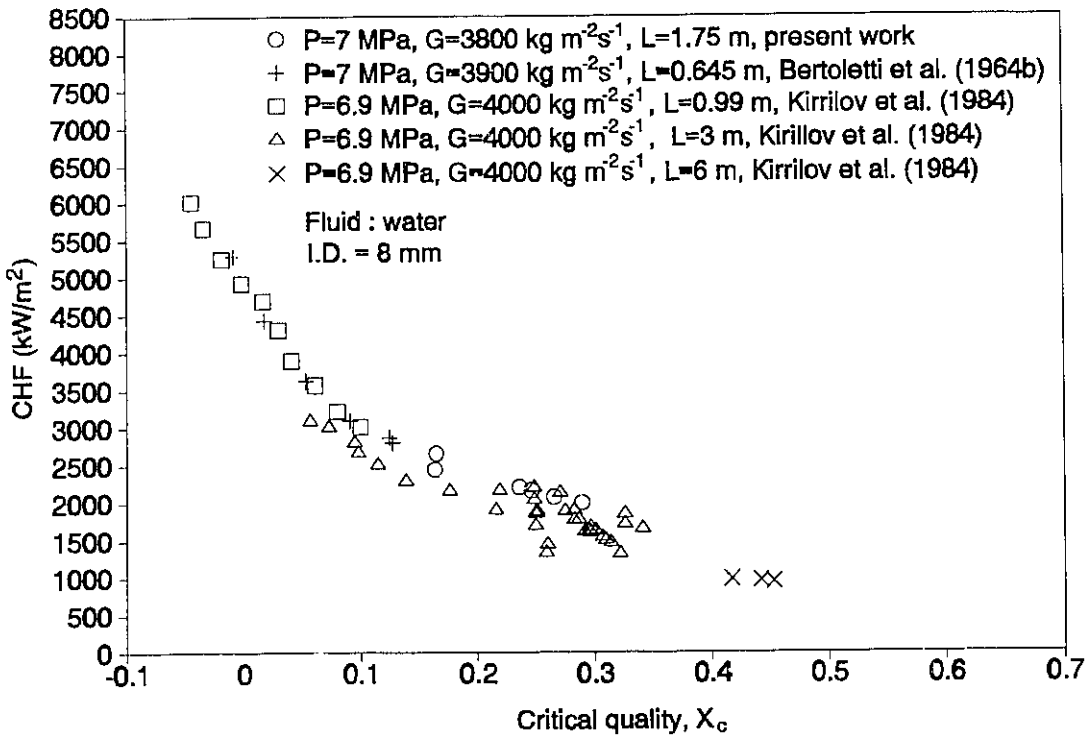

Figure 4-21 Comparison of water CHF data from the MR-1A loop against other data sources.

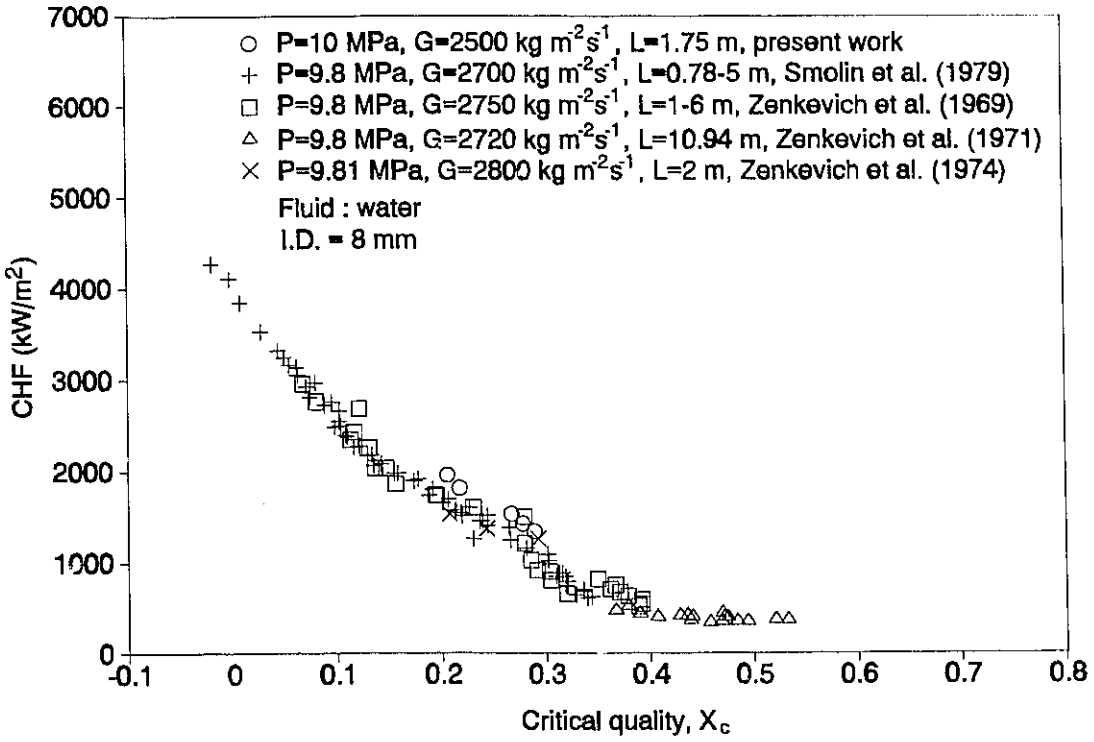

Figure 4-22 Comparison of water CHF data from the MR-1A loop against other data sources.

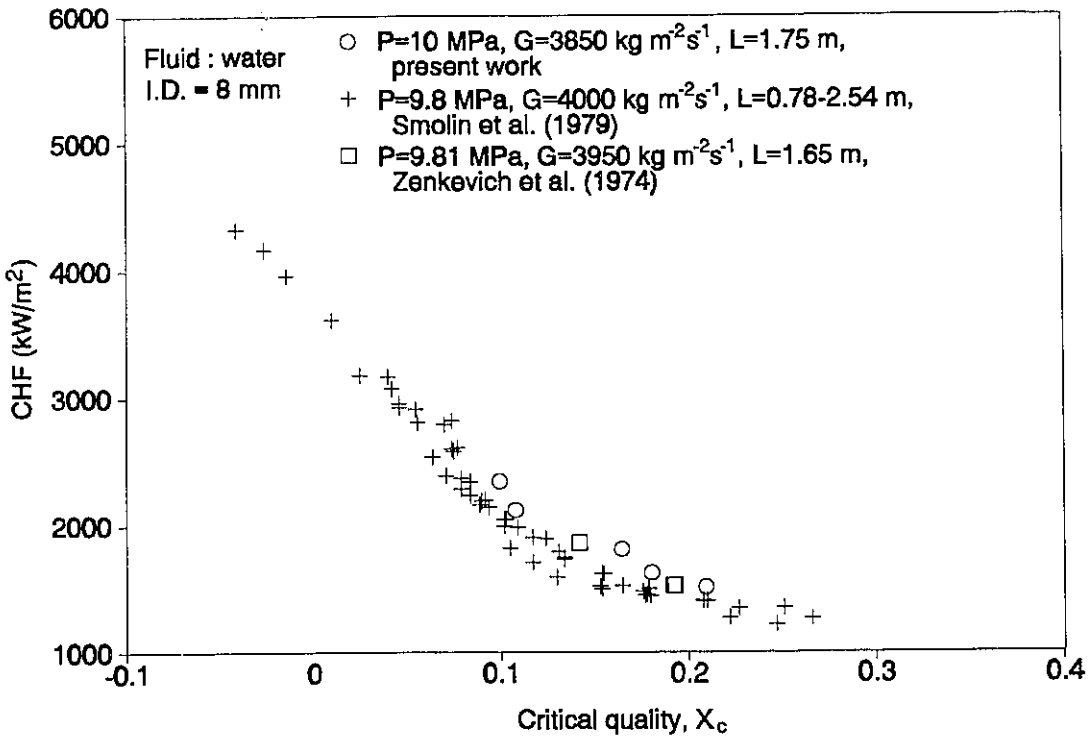

Figure 4-23 Comparison of water CHF data from the MR-1A loop against other data sources.

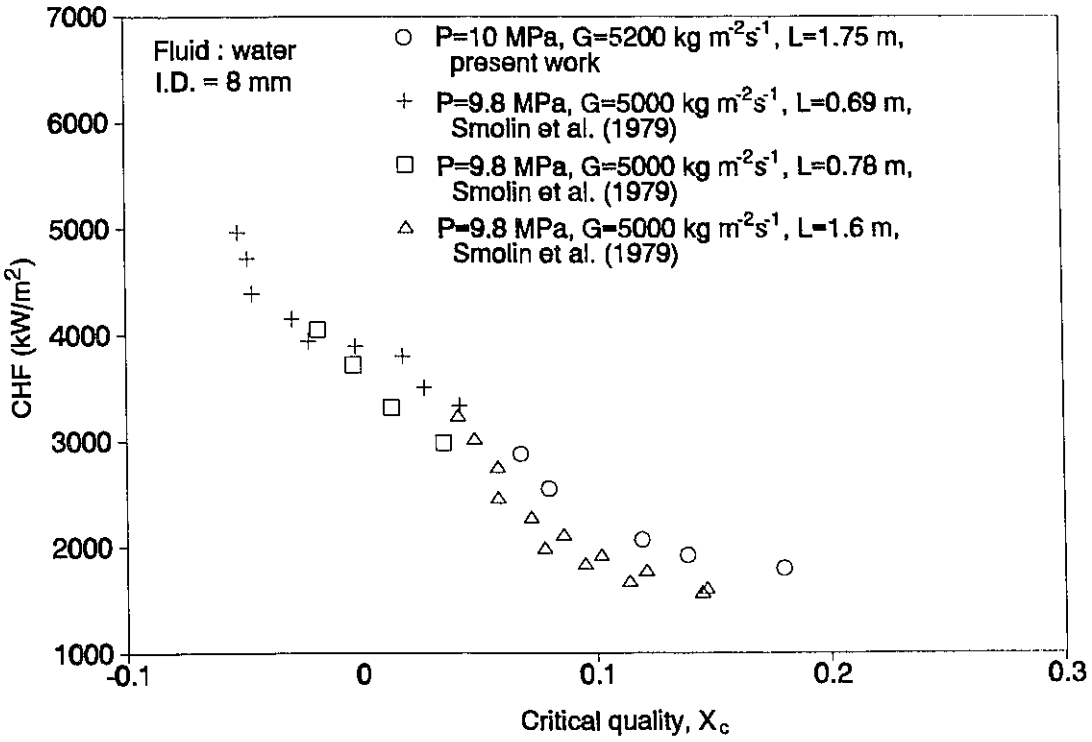

Figure 4-24 Comparison of water CHF data from the MR-1A loop against other data sources.

Chapter 5

EXAMINATION OF CHF SCALING TECHNIQUES AND OTHER PREDICTION METHODS

5.1 General

The CHF experimental data for non-aqueous fluids usually serve two purposes. Firstly, they provide the design data required for the thermal analysis of cooling or refrigeration systems. Secondly, CHF in non-aqueous fluids can be used to simulate the CHF in water-cooled systems via the CHF fluid-to-fluid scaling techniques. This is important because of the high cost for CHF experiments using steam-water. The simulation of the CHF in water using non-aqueous fluid data requires the techniques of fluid-to-fluid modelling (or scaling), that is, converting CHF from one fluid to another fluid using dimensionless groups. This technique thus can be categorized as a CHF prediction method. Other CHF prediction methods for multi-fluid use are: (1) non-dimensional CHF equations and (2) theoretical CHF models.

5.2 Assessment of Scaling Techniques

The dimensionless parameters (i.e. G^* in Eq. (2-9)) derived from the dimensional analysis are composed of fluid properties (σ, ρ_f, ρ_g μ_f, μ_g etc.), flow condition (G) and geometry (L or D).

These dimensionless groups will be examined with the objective of studying the importance of fluid properties and geometry with respect to the accuracy of scaling based on the measured data. A comparison of the sets of dimensionless groups used in CHF scaling could result in the selection of different dimensionless groups, which may have been neglected before. If such parameters can be found, they will be used to assess the accuracy of the scaling techniques. From Table 5-1, G^* derived from different prediction methods are ψ_{CHF} (ψ_σ and ψ_γ), ψ_k, Y, $\sigma\rho_f/G^2L$ (this is defined as ψ_L in Table 5-2), Re_v, and Re_f, where their functional forms are listed in Table 5-2. The several dimensionless CHF expressions are represented by

$$Bo = \frac{\phi_c}{G\lambda} \quad (Boiling\ number) \tag{5-1}$$

$$CHF_n = \frac{\phi_c D}{\mu_g \lambda} \quad (CHF\ number) \tag{5-2}$$

and

$$\phi_c^* = \frac{\phi_c}{\left(\frac{\bar{R}T_c P_c^2}{M}\right)} \quad (Reduced\ CHF) \tag{5-3}$$

The Bo calculated based on the test data of the present study are plotted against the ψ_σ, ψ_γ, Y and ψ_k, respectively, corresponding to the sub-figures from Figs. 5-1 to 5-8. These figures cover the following ranges:

ρ_f/ρ_g: 20.3 and 12.4 (7 and 10 MPa water-equiv. pressures)

L/D: 185 – 238

I.D.: 4.2 and 8 mm

G: 1.0 – 8.0 Mg m^{-2} s^{-1}

$\Delta H_f/\lambda$: 0.07 – 0.17

Note that ψ_k, which has been defined in Eq. (2-81), is termed Katto's dimensionless group by Groeneveld et al. (1986b). In fact, ψ_k is a modified dimensionless group based on ψ_L from Katto and Ohno (1984). ψ_k is used in this analysis because the test conditions for the study were based on ψ_k.

In Figs. 5-1–5-8, ψ_k generally results in larger discrepancies of Bo between water and non-aqueous fluids than ψ_σ, ψ_γ and Y. This is probably due to the diameter effect (I.D.= 8 mm for water and 4.2 mm for the other fluids) or due to the exclusion of μ_f and μ_g in ψ_k. However, in Figs. 5-3, 5-4, 5-7 and 5-8, ψ_k results in the least scattering in Bo for different diameters in the same fluid (HCFC-22). In general, Y and ψ_σ show a similar degree of scattering in Bo for different fluids. However, both dimensionless groups contain quite different properties except for μ_f and μ_g. Therefore, in addition to μ_f and μ_g, the primary properties for fluid-to-fluid scaling techniques could be ρ_f, σ, k_f and Cp_f. In Table 5-2, none of the dimensionless groups includes all the properties. If there were such a group, it would be interesting to study its parametric trend on Bo. Fortunately, the dimensionless group set No. 3 in Table 2-1 provides the information to form such a parameter. The second and third dimensionless groups in set No. 3 are termed B1 and B2 below, i.e.

$$B1 = \frac{D\,\sigma\,\rho_f Cp_f^2}{k_f^2} \tag{5-4}$$

and

$$B2 = \frac{G k_f}{\sigma \rho_f Cp_f} \tag{5-5}$$

The ratio of μ_f to μ_g is termed B3 below, i.e.

$$B3 = \frac{\mu_f}{\mu_g} \tag{5-6}$$

Combining these three terms with different exponents, a new scaling parameter is obtained

$$\psi_B = \left(\frac{D \sigma \rho_f Cp_f^2}{k_f^2}\right)^{n_1} \times \left(\frac{G k_f}{\sigma \rho_f Cp_f}\right)^{n_2} \times \left(\frac{\mu_f}{\mu_g}\right)^{n_3} \tag{5-7}$$

To decide the values of n_1, n_2 and n_3, ψ_B is compared with ψ_σ, ψ_γ and ψ_k where the exponent of G in these three parameters is set to unity. Therefore, n_2 is also designated as unity. If n_1=1/2 and n_3=0, k_f and Cp_f are cancelled and ψ_B becomes ψ_k, which we want to avoid. In ψ_γ, the exponential values of D, μ_f/μ_g are 1/3 and 1/8, respectively. Therefore, n_1 and n_3 are determined to be 1/3 and 1/8. Thus, the complete form of ψ_B becomes

$$\psi_B = \frac{G D^{\frac{1}{3}} k_f^{\frac{1}{3}} \mu_f^{\frac{1}{8}}}{\sigma^{\frac{2}{3}} \rho_f^{\frac{2}{3}} Cp_f^{\frac{1}{3}} \mu_g^{\frac{1}{8}}} \tag{5-8}$$

The parametric results for Bo vs. ψ_B are then illustrated in Figs. 5-9 and 5-10. From these figures, ψ_B resulted in a similar degree of scattering in Bo for different fluids as ψ_γ.

For Katto and Ohno's (ψ_L), Green and Lawther's (Re_v) and Hauptmann and Lee's (Re_l) dimensionless groups, their parametric trends of dimensionless CHF (Bo, CHF_n and ϕ_c^*) are illustrated in Figs. 5-11–5-12, Figs. 5-13—5-14 and Figs. 5-15—5-16, respectively. Figures 5-11—5-16 showed that none of these dimensionless groups resulted in a reduced

scattering in dimensionless CHFs at the tested flow conditions. Note that ψ_L showed a similar scattering in Bo as ψ_k although different geometries (L and D) are used in both dimensionless groups. This is because

$$\psi_L = \frac{1}{\psi_k^2} \times \frac{D}{L} \tag{5-9}$$

Since Eq. (2-5) is used to calculate x, the L/D will be the same if ρ_f/ρ_g, x, ΔH_i and Bo are the same for different fluids. Figures 5-1—5-16 showed that, for the same L and D at most flow conditions, the dimensionless CHFs of non-aqueous fluids (i.e. CFC-12, HFC-134a, HCFC-123 and HCFC-22) satisfactorily fell along the same curve when plotted against all the dimensionless groups except for Re_f. This implies that HFC-134a, HCFC-123 and HCFC-22 are the most promising fluids of CFC alternatives for CHF scaling and Re_f is not a suitable dimensionless group for CHF scaling. Figures 5-1—5-16 did not illustrate the accuracies of CHF scaling from these dimensionless groups. For ψ_σ, ψ_γ, ψ_k, ψ_B, Y and ψ_λ (defined in Eq. (5-18)), a water CHF table will be used to assess the quantitative accuracy in CHF scaling in next section. The dimensionless CHF equation resulted from the developments of ψ_γ, Y, ψ_L, Re_v and Re_f also will be assessed later in this chapter.

5.3 Comparison against Reference Water CHF Table

5.3.1 General

To compare the adequacy of using the ψ_B as a scaling parameter with ψ_σ, ψ_γ, ψ_k etc. Groeneveld et al.'s (1986a and 1986b) CHF look-up table is used since the table permits the use of a scaling parameter (e.g. ψ_σ, ψ_γ and ψ_k) as G^*. Similarly, the ψ_B and Y can also be used. The

methodology is to compare the table values with all the experimental data using different scaling parameters and calculate the Avg., Mean and RMS errors as defined in Table 4-4. Then, the overall effect of using ψ_B and other dimensionless mass flux scaling parameters on the scaling accuracy can be quantified.

5.3.2 Calculation Procedure in Table Method

As the geometric, thermodynamic and density ratio similarities are satisfied (Eqs. (2-3), (2-4) and (2-8)), Bo is assumed to be equal in both fluids if the G^* values are the same in both fluids. For G^*, the ψ_σ, ψ_γ, ψ_k, ψ_B or Y may be used. Since the table data are valid only for water in an 8 mm I.D. tube, Groeneveld et al. (1986a) suggest that hydrodynamic similarity (same G^*) for fluids with a different I.D. can be achieved using the following procedure (termed method A):

Method A: (using ψ_k as an example)

$$\left(\frac{G\,D^{1/2}}{\rho_f^{1/2}\,\sigma^{1/2}}\right)_W = \left(\frac{G\,D^{1/2}}{\rho_f^{1/2}\,\sigma^{1/2}}\right)_M \tag{5-10}$$

where the subscript "W" represents the water condition in the CHF table and subscript "M" represents the modelling fluid condition. Initially assume that D=8 mm for both fluids, then

$$G_W = \left(\frac{G}{\rho_f^{1/2}\,\sigma^{1/2}}\right)_M \times (\rho_f^{1/2}\,\sigma^{1/2})_W \tag{5-11}$$

and use G_W to find a CHF value (ϕ_e) from the table. Then, correct ϕ_e for a diameter other than 8 mm, i.e.

$$(\phi_{c,\ D*8\ mm})_W = (\phi_{c,\ table})_W \times \left(\frac{8}{D}\right)^{1/3} \tag{5-12}$$

Finally, the CHF for the modelling fluid is predicted via

$$\phi_{c,M} = \left(\frac{\phi_{c,D*8\,mm}}{G\lambda}\right)_W \times (G\lambda)_M \tag{5-13}$$

According to the scaling theories, there is no need for the diameter correction procedure such as in Eqs. (5-11)—(5-13). A second method thus is also used based on the classical scaling theory. The calculation procedure (termed method B) is illustrated below:

Method B: (using ψ_k as an example)

$$\left(\frac{G D^{1/2}}{\rho_f^{1/2}\,\sigma^{1/2}}\right)_W = \left(\frac{G D^{1/2}}{\rho_f^{1/2}\,\sigma^{1/2}}\right)_M \tag{5-14}$$

Let D=8 mm for water (table method) and D for the modelling fluid is kept as it is, thus,

$$G_W = \left(\frac{G D^{1/2}}{\rho_f^{1/2}\,\sigma^{1/2}}\right)_M \times \left(\frac{\rho_f^{1/2}\,\sigma^{1/2}}{0.008^{1/2}}\right)_W \tag{5-15}$$

Use G_W to find a CHF value (ϕ_c) from the table. Then, calculate ϕ_c for the modelling fluid via

$$\phi_{c,M} = \left(\frac{\phi_c}{G\lambda}\right)_W \times (G\lambda)_M \tag{5-16}$$

If the I.D. for the modelling fluid is also 8 mm, these two methods would have no difference.

The first method (method A) corrects ϕ_c from the table prediction indirectly at the end using

Eq. (5-12), while the second method (method B) corrects the ϕ_c prediction directly due to the change of G by varying the flow cross-section. In the method A, the D on both sides of Eq. (5-10) will be equal to 8 mm. This suggests that, if the use of D=8 mm in Eq. (5-10) for both fluids is replaced by another variable which also has the same unit of length, it may result in more accurate scaling. For example, the critical wavelength in a hydrodynamic instability model can be used. The critical wavelength for Taylor's instability is written as

$$\lambda_c = 2\pi\sqrt{\frac{\sigma}{g(\rho_f - \rho_g)}} \tag{5-17}$$

If D in ψ_k is replaced by λ_c, it results in a new scaling parameter (termed ψ_λ) as shown below:

$$\psi_\lambda = \left(\frac{2\pi}{\sqrt{g}}\right)^{1/2} \frac{G}{\rho_f^{1/2}\,\sigma^{1/4}\,(\rho_f-\rho_g)^{1/4}} \tag{5-18}$$

The use of λ_c in ψ_k converts the geometry effect into the property effect and thus the Eq. (5-10) becomes

$$\left[\frac{G}{\rho_f^{1/2}\,\sigma^{1/4}\,(\rho_f-\rho_g)^{1/4}}\right]_W = \left[\frac{G}{\rho_f^{1/2}\,\sigma^{1/4}\,(\rho_f-\rho_g)^{1/4}}\right]_M \tag{5-19}$$

Then,

$$G_W = \left[\frac{G}{\rho_f^{1/2}\,\sigma^{1/4}\,(\rho_f-\rho_g)^{1/4}}\right]_M \times \left[\rho_f^{1/2}\,\sigma^{1/4}\,(\rho_f-\rho_g)^{1/4}\right]_W \tag{5-20}$$

Therefore, the scaling parameter ψ_λ is added to G^* list of Table 5-2 and is used in method A.

5.3.3 Assessment of the Table Method for Predicting Water and Non-aqueous Fluid CHF

As discussed by Tain et al. (1993) as well as in Section 2.4.2, the CHF values from Groeneveld et al.'s table method are functions of X_e (critical quality or dryout quality) but the CHF should not be predicted based on an experimental value of X_e since X_e is not known prior to the experiment. Therefore, the independent parameters should be P, G, D, L and $\Delta H_i/\lambda$. The CHF and X_e are calculated simultaneously through the iterations as illustrated in Fig. 2-13; the prediction error should be evaluated based on constant inlet conditions, else the CHF will not satisfy the heat balance equation (Eq. (2-5)). The prediction accuracies from these two methods (method A and B) are illustrated in Tables 5-3 and 5-4. In both tables, the water CHF from table predictions constantly show an overprediction of CHF for the low pressure (7 MPa) condition and an underprediction of CHF for the high pressure (10 MPa) condition against the test data of water for all scaling parameters. Note that the water CHF predictions do not vary with scaling parameter. Comparing both methods (A and B) and all mass flux scaling parameters, the ψ_{fl} resulted in the best overall prediction accuracy; none of the remaining scaling parameters could obtain a more accurate prediction for both methods. The results show that ψ_{fl} is a promising dimensionless group to be used in CHF fluid-to-fluid scaling technique. In Table 5-3, ψ_λ gives unacceptably large errors; it results in overpredictions of CHF at all pressure conditions and in all fluids except water at 10 MPa. This is probably due to the replacement of geometry by properties, which results in a lower water-equivalent mass flux (G_w) compared with the use of ψ_k. For example, G_w calculated from ψ_λ is 70% of that from ψ_k (i.e. F_G from ψ_λ is 30% less than that from ψ_k). However, the water CHF prediction from table using ψ_λ is about 85% of that using ψ_k. Therefore, the CHF for non-aqueous fluids using Eq. (5-16) is larger when using ψ_λ than

when using ψ_k. Table 5-3 shows that ψ_k results in an overall underprediction of the experimental CHF and ψ_λ results in an overall overprediction of the data; or CHF prediction from ψ_λ is about 20% higher than those from ψ_k.

Finally, from Tables 5-3 and 5-4, method B constantly obtained a better CHF prediction against the test data than method A regardless of the use of scaling parameters. The classic scaling theory used in the method B is therefore considered to be superior to the modified scaling theory used in the method A.

5.4 Assessment of Non-Dimensional CHF Equations

Non-dimensional CHF equations (as discussed in Section 2.4.1) based on dimensionless groups derived from dimensional analysis can be derived by employing a regression method and based on experimental data. Their application ranges are thus limited to the data bases used and, sometimes, the type of fluid. The non-dimensional CHF equations were examined in Chapter 2 with the objective of selecting those dimensionless groups controlling the CHF. CHF test results from the present work are compared with the non-dimensional CHF equations discussed in Section 2.4.1. They were obtained by Ahmad (1973), Shah (1987), Katto and Ohno (1984), Green and Lawther (1981) and Hauptmann and Lee (1983). The results of the comparison are shown in Table 5-5, where the Avg. and RMS errors have been defined in Table 4-4. Note that the comparison is based on the constant inlet condition ($\Delta H_i/\lambda$) as discussed in Section 5.3.3.

Table 5-5 shows that Ahmad's equation does not predict the high pressure data condition (10 MPa water-equiv.) very well because the empirical constants for this equation are derived based on one pressure condition, i.e. 7 MPa. For 7 MPa, Ahmad's equation gives reasonable

agreement. Shah's and Katto and Ohno's equations show fair agreement against the test data for both 7 and 10 MPa pressure conditions. Green and Lawther's equation gives the best comparison against the test data although the empirical constants are derived based only on CFC-12 and water data base. Hauptmann and Lee's equation results in the largest error. The dimensionless parameters used in these equations have been listed in Table 5-1: ρ_f/ρ_g or ρ_g/ρ_f represents the hydrodynamic similarity, while the P_r is an index related to the value of ρ_f/ρ_g or ρ_g/ρ_f. Shah (1979) has concluded that the use of P_r appears to be no different from the use of ρ_f/ρ_g or ρ_g/ρ_f. However, if ρ_g/ρ_f is plotted against P_r as shown in Fig. 5-17, the trend of water deviates from those of non-aqueous fluids. In Table 5-5, Shah's equation results in the worst comparison for water data vs. modelling fluids. This is probably due to the use of P_r.

Hauptmann and Lee incorporated Z_c (critical compressibility) with P_r to avoid the deviation of ρ_g/ρ_f between water and non-aqueous fluids. As illustrated in Fig. 5-18, the use of P_rZ_c does improve the trend not only between water and non-aqueous fluids but also among the non-aqueous fluids themselves. However, Hauptmann and Lee's empirical equation results in different exponents (*b* and *e* as shown in Table 2-6) for P_r and Z_c. As illustrated in Fig. 5-19, the use of *b* and *e* as P_r's and Z_c's exponents yields a different parametric trend of ρ_f/ρ_g vs. Z_c for various fluids, especially for water. This may be the reason why Hauptmann and Lee's equation, as referred to Table 5-5, resulted in the highest errors when compared to water data. Note that CO_2 is included in Figs. 5-17—5-19 because Hauptmann and Lee derived their equation based on CO_2 and CFC-12 data as well as the water data.

It is noted that the UO CHF data for HCFC-123 and HFC-134a often result in larger Avg. and RMS errors than those of CFC-12 and HCFC-22 when compared with all non-dimensional

CHF equations. This is probably because that the derivations of all the non-dimensional CHF equations were not based on HFC-134a and HCFC-123 CHF data. In addition, the properties of the new fluids (HFC-134a and HCFC-123) are less well known than CFC-12 and HCFC-22. The property predictions for the new fluids are thus less accurate.

5.5 Assessment of CHF Theoretical Models

5.5.1 General

Theoretical CHF models are generally not-fluid specific, hence they can be applied to any fluid. The CHF data for various fluids obtained from the present work thus can be used to examine the suitability of the theoretical CHF models. As discussed in Section 2.4.3, the theoretical CHF models can be categorized as (1) subcooled flow models, i.e. for negative value of dryout quality (e.g. Lee and Mudawwar (1988) and Katto (1990a, 1990b and 1992)), (2) bubbly flow models, i.e. for low and intermediate dryout qualities (e.g. Weisman and Pei (1983) and Ying and Weisman(1986)), (3) annular flow models, i.e. for high dryout quality (e.g. Whalley et al. (1974 and 1978)). Since the dryout qualities of the test data are all greater than zero, the assessment of the subcooled flow model is omitted. From Tables 4-1—4-3, the dryout qualities of the present study range from 0 to 0.6, which cover the ranges of those for the bubbly flow model and the annular flow model. Therefore, both models will be examined in the following sections.

5.5.2 Comparison against the Bubbly Flow Model

The Weisman and Pei's model (1983) described in Section 2.4.3.3 was originally derived

for the subcooled-to-low dryout quality condition. Later, Ying and Weisman (1986) (described in Section 2.4.3.4) extended this model to void fractions in the bubbly region near the wall of up to 82%, which corresponds to the intermediate dryout quality. Ying and Weisman's model is thus used to compare with the present test data. The graphical comparisons are shown in Figs. 5-20—5-26, which illustrate the effect of X_e on the CHF of the test data and Ying and Weisman's prediction for various mass flux and pressure conditions. These figures show that Ying and Weisman's model predicts a constant X_e (X_e≈0.17 at ρ_f/ρ_g=20.3 and X_e≈0.25 at ρ_f/ρ_g=12.4), which is the upper limit of the thermodynamic quality prediction and corresponds to a void fraction in the bubbly layer reaching 82%. At low flows, before the constant quality condition is reached, the model generally underpredicts the data. The model is not applicable to higher qualities because the flow regime is no longer a bubbly flow. For G>3 Mg m^{-2} s^{-1} and X_e<0.25 at ρ_f/ρ_g=12.4, the model shows an overprediction of the CHF and the trend increases when the X_e decreases from 0.2 to 0.1. However, the difference between the test data and predictions decreases with decreasing X_e between 0.1 and 0. Generally, for conditions away from the maximum quality limit of the model, CHF vs. X_e trends are the same for the model and the experimental CHF data and the model predictions are roughly in agreement.

5.5.2.1 Mass Flux Effect

From Figs. 5-20—5-26, at low mass flux conditions (G≤4 Mg m^{-2} s^{-1}), the CHF test data fall along distinct curves for different mass flux conditions and the data tend to merge together when the mass flux increases. At high mass flux conditions (G>4 Mg m^{-2} s^{-1}), the mass flux effect on CHF can also be seen in the higher X_e conditions (X_e>0.05), but it becomes less significant at

the lower quality conditions ($X_e \leq 0.05$). Compared with the CHF data, the mass flux effect from Ying and Weisman's model is much less significant: the model shows almost no mass flux effect, especially at high flows.

5.5.2.2 Pressure Effect

The pressure effect on CHF for the experimental data and Ying and Weisman's model is illustrated in Figs. 5-27—5-32: as expected, the experimental CHF decreases with increasing pressure (i.e. from 7 to 10 MPa water-equiv.) for all fluids at $G \leq 4$ Mg m^{-2} s^{-1}. For $G > 4$ Mg m^{-2} s^{-1} as shown in Figs. 5-30—5-32, the above trend becomes less pronounced when the X_e decreases. For $G > 6$ Mg m^{-2} s^{-1}, the test CHF shows no pressure effect. However, Ying and Weisman's model generally shows no pressure effect on CHF for all fluids and most mass flux conditions. In some cases, as shown in Figs. 5-27(d), 5-29(d) and 5-31(a), the model predicts an opposite trend (compared to the CHF data) for the pressure effect.

5.5.2.3 Diameter Effect

As shown in Eqs. (2-79) and (2-80), two slightly different forms of the diameter effect on CHF have been presented by the USSR Academy of Science (1977) and Groeneveld et al. (1986a), respectively. The HCFC-22 data for 4.38 and 8 mm from MR-7A loop are used to examine Ying and Weisman's model for the diameter effect. Figure 5-33 shows that the diameter effect on the CHF for the test data and Ying and Weisman's model are similar but are not identical. Ying and Weisman's model shows a similar trend to Eq. (2-80); however, the experimental data are more likely to agree with Eq. (2-79) for the mass flux conditions shown

in these figures.

5.5.2.4 Quantitative Comparison

A numerical comparison of Ying and Weisman's prediction with the test CHF is illustrated in Table 5-6, where the CHF predictions with $X_e \geq 0.17$ at $\rho_f/\rho_g=20.3$ and $X_e \geq 0.25$ at $\rho_f/\rho_g=12.4$ are omitted as the model does not apply for the higher qualities. This result is observed in 487 out of the 799 test data used in the comparison. Table 5-6 shows that generally the model, which has not been derived for these data, predicts the data surprisingly well. Ying and Weisman's model resulted in better agreement with the CHF data at high pressure conditions (10 MPa water-equiv.), where it generally overpredicts the data, than at low pressure conditions (7 MPa water-equiv.), where it tends to underpredict the data.

5.5.3 Comparison against the Annular Flow Model

Whalley et al.'s (1974, 1978) model is the most frequently used model for annular film dryout. Their model calculates CHF due to liquid film depletion (dryout) on the heated channel wall (see Section 2.4.3.5). However, Govan et al. (1988) reported that Whalley et al.'s model predicts incorrect rates of liquid entrainment and droplet deposition using Eqs. (2-124) and (2-122) and the data shown in Fig. 2-19. Govan et al. then developed new correlations for the entrainment rate (E_E) and the coefficient of the deposition rate (k_1), i.e.

$$\frac{E_E}{G_G} = 5.75\times10^{-5}\left[(G_{LF} - G_{LFC})^2 \frac{D\,\rho_f}{\sigma\,\rho_g^2}\right]^{0.316} \qquad (5\text{-}21)$$

$$k_1\sqrt{\frac{\rho_g D}{\sigma}} = 0.18 \quad if \quad \frac{c}{\rho_g} < 0.3 \tag{5-22}$$

and

$$k_1\sqrt{\frac{\rho_g D}{\sigma}} = 0.083\left(\frac{c}{\rho_g}\right) \quad if \quad \frac{c}{\rho_g} > 0.3 \tag{5-23}$$

where c is the mass concentration of liquid droplets in the vapour core defined in Eq. (2-123) and G_{LFC} is the critical film flow rate at the onset of entrainment, i.e.

$$\frac{G_{LFC} D}{\mu_f} = e^{\left(5.8504+0.4249\frac{\mu_f}{\mu_g}\sqrt{\frac{\rho_f}{\rho_g}}\right)} \tag{5-24}$$

Once the k_1 is calculated from Eq. (5-22) or (5-23), the deposition rate can be calculated from Eq. (2-122) and the entrainment rate is calculated directly from Eq. (5-21). If $G_{LF} < G_{LFC}$, there is no entrainment.

5.5.3.1 Comparison of Model with Water CHF Data

Before Govan et al.'s new correlations were developed, the rates of entrainment and deposition relied on the same parameter (i.e. k_1). However, using Eqs. (5-21)—(5-24), the rates of deposition and entrainment can be calculated from different equations. The comparisons of our CHF test data with Whalley et al.'s original model and with Govan et al.'s correlations are illustrated in Figs. 5-34 and 5-35, where the water CHF data from the MR-1A loop are used. In both figures, the boundary condition that 99% of the fluid is entrained as droplets (ε_o) at a quality of 0.01 is used as recommended by Whalley et al. (1974, 1978). Both models predict the

correct trend of CHF variation with critical quality and mass flux.

Figure 5-34 shows that Whalley et al.'s original model overpredicts the CHF for all mass flux and pressure conditions. The overprediction trend also increases with the increasing mass flux. In Fig. 5-35, Whalley et al.'s model using Govan et al.'s correlations underpredicts the CHF for most pressure and mass flux conditions, but the prediction error is much smaller.

5.5.3.1.1 ε_0 and k_1 Effects

Figurers 5-34 and 5-35 show that the new correlations for E_E and k_1 have strong effects on the CHF prediction for the annular flow model. As shown in Table 5-7(a), Govan et al.'s correlations predict the CHF much better than Whalley et al.'s model. However, the better prediction of the CHF data at the high mass velocities, low quality at 7 MPa using the new correlations as shown in Fig. 5-35 contradicts the intended application range (high quality) of the original annular flow model (Whalley et al.'s).

Govan et al. (1988) found that a lower value of ε_0 (i.e. ε_0=0.9) can improve the CHF prediction. Therefore, the effect of the ε_0 on the CHF prediction is also tested using the water CHF data from the MR-1A loop. Figures 5-36 and 5-37 show the comparisons of the CHF data with Whalley et al.'s model using Govan et al.'s new correlations for ε_0=0.95 and ε_0=0.9. In both figures, the CHF is overpredicted at higher mass velocities for both pressures and the overprediction increases with decreasing quality. This is more likely a correct trend, which is similar to the result of the original annular flow model as shown in Fig. 5-34. In Table 5-7(a), despite Govan et al.'s correlations resulting in the best prediction for ε_0=0.99, their correlations also showed a similar accuracy of CHF prediction for ε_0=0.95 compared to ε_0=0.99 while a

reasonable parametric trend can be retained with ε_0=0.95.

The equations for k_f (i.e. Eqs. (5-22) and (5-23)) from Govan et al. were obtained from curve fitting based on large amount of disperse data. The equation form of k_f would probably change if a larger data base were employed. Therefore, the effect of k_f on the CHF prediction was tested by varying the value of k_f as calculated from either the Eq. (5-22) or (5-23). Figures 5-38 and 5-39 show the comparisons of the CHF data with the predictions from Whalley et al.'s model using Govan et al.'s correlations for $k_f \pm 10\%$ with ε_0=0.99. From these two figures, the model results in a further improvement in CHF prediction with the higher value of k_f.

5.5.3.1.2 Quantitative Comparison

A quantitative comparison of the CHF data with the prediction from Whalley et al.'s original model and Govan et al.'s modification as well as the ε_0 and k_f effects is shown in Table 5-7. The table shows that Govan et al.'s correlations improve the CHF prediction for the entire mass flux range over the present test, and underpredicts the data slightly. The change of ε_0 from 0.99 to 0.95 will increase the CHF prediction but does not change the RMS error. However, for ε_0=0.9 the RMS error is increased significantly. The k_f effect also affects the comparison of the CHF prediction with the test data. The table shows that the predicted CHF increases with the increasing k_f and a better agreement with the data was found for a 10% increase of k_f.

5.5.3.2 Comparison of Model with Non-aqueous Fluid Data

5.5.3.2.1 Mass Flux Effect

The comparison of the CHF data for non-aqueous fluids obtained from the UO and MR-7A

loops with the CHF predictions from Whalley et al.'s model using Govan et al.'s correlations is shown in Figs. 5-40—5-45. Whalley et al.'s model using Govan et al.'s correlations does not show the limiting quality effect at high pressure, low mass flux (≈1.4 Mg m^{-2} s^{-1}) condition, which is typical of the data. Unlike the comparison with water, the model results in overpredictions of CHF for non-aqueous fluids at the low mass flux condition (G≤3 Mg m^{-2} s^{-1}) except for the results shown in Fig. 5-41(a). Again, these figures show better agreement between the data and the predicted CHF at higher mass velocities. Similar to Ying and Weisman's bubbly flow model, Whalley et al.'s annular flow model is less sensitive to mass flux. At high mass flux conditions (G>4 Mg m^{-2} s^{-1}), the model predicts no mass flux effect.

5.5.3.2.2 Pressure Effect

Figures 5-46—5-51 illustrate the pressure effect on CHF vs. X_e for both the test data and Whalley et al.'s model using Govan et al.'s correlations. Unlike Ying and Weisman's model, the annular flow model shows that CHF increases with the decreasing pressure between 7 and 10 MPa water-equiv. for all mass flux conditions, which is in agreement with the observed experimental trend. The difference of the predicted CHF between low and high pressures increases slightly with the increasing mass flux. However, the CHF test data showed a declining effect of pressure on mass flux and no pressure effect at very high mass flux conditions.

5.5.3.2.3 Diameter Effect

Similar to the analysis studied for Ying and Weisman's model, the diameter effect is also studied for the annular flow model. Figures 5-52 and 5-53 compare the diameter effect on CHF

vs. X_e between the test CHF and the predicted CHF from Whalley et al.'s model using Govan et al.'s correlations, where the test data of the 4.2 and 8 mm diameters for HCFC-22 from the UO and MR-7A loops are used. In general, both the model prediction and the data show the usual increasing CHF trend with decreasing diameter. The figures show that the annular flow model agrees with the form shown in Eq. (2-79) rather than in Eq. (2-80), which is more likely to agree with Ying and Weisman's model.

5.5.3.2.4 Quantitative Comparison

A comparison of the prediction accuracies is shown in Table 5-8 for Whalley et al.'s model using Govan et al.'s correlations for all fluids. The table shows that the annular flow model overpredicts the CHF for most non-aqueous fluids and underpredicts the CHF for water for the test conditions of the present study. The model generally predicts the data with a relatively low RMS error for a total of about 800 points. This good accuracy supports the validity of the model which was originally developed for water but predicts in many cases the non-aqueous fluids better than the water data.

5.6 Discussions

According to Fig. 5-17 and Table 5-5, the comparison results of Shah's and Hauptmann and Lee's equations against the test data show that the use of P_r as a pressure scaling parameter differs from the use of ρ_f/ρ_g or ρ_g/ρ_f. To improve the relation between ρ_g/ρ_f (or ρ_f/ρ_g) and P_r, the use of P_rZ_c probably is a good choice but not $P_r^bZ_c^c$.

HCFC-123 and HFC-134a are new fluids and their thermophysical properties such as the

viscosities and thermal conductivities are less known. More work is still to be done in providing more accurate property predictions so that the CHF fluid-to-fluid scaling technique will be more reliable..

In general, the comparison between the bubbly flow CHF model (by Ying and Weisman) and the test CHF data from the present work shows satisfactory agreement for conditions where the model is applicable at low and intermediate qualities (i.e. bubbly flow pattern). The model slightly overpredicted the CHF of most data sources within the model's application range as concluded by Weisman and Ileslamlou (1988). However, the bubbly flow model also resulted in some unexpected trends:

(1) The mass flux effect on CHF is much less significant compared to the present test data within its application range.

(2) The model showed a minor pressure effect on CHF for all fluids in its application range. In some cases, the model obtained a different trend than the CHF data, i.e. the CHF increases with increasing pressure between 7 and 10 MPa water-equiv. pressure.

(3) The model agrees with Eq. (2-80) for the diameter effect on CHF.

The use of Govan et al.'s correlations in Whalley et al.'s annular flow model showed an improvement from the original annular flow model when compared with the present test CHF data. However, the improvement was more significant at low quality conditions (i.e. bubbly flow region) and this was not expected. Unlike the present CHF data, the annular flow model showed no limiting quality effect in high pressure, high quality conditions. Similar to the bubbly flow model, the annular flow model showed a less pronounced mass flux effect on CHF than the experimental data. The annular flow model also predicted the correct pressure effect on CHF and

obtained good agreement with Eq. (2-79) for the diameter effect on CHF. Finally, the ε_o=0.95 and k_l+10%k_l is recommended for Govan et al.'s correlation when used by Whalley et al.'s model.

Based on the statistical comparison shown in Table 5-3–5-8, the fluid-to-fluid scaling techniques, using the new mass flux scaling parameter ψ_B in conjunction with the CHF look-up table, provides the best overall CHF prediction. From all the CHF prediction methods which have been assessed, the fluid-to-fluid scaling techniques can be applied for the range wider than the other methods and are not restricted by flow pattern. However, this type of application (CHF scaling) may have its limitation. The limitations of the scaling techniques will be discussed in the next chapter.

Table 5-1 Equation functions for non-dimensional CHF equations.

Equation derived by	Equation function
Ahmad (1973)	$\frac{\phi_c}{G\lambda} = f\left(\psi_{CHF}, \frac{\Delta H_i}{\lambda}, \frac{\rho_f}{\rho_g}, \frac{L}{D}, \frac{D_{he}}{D}\right)$
Shah (1987)	$\frac{\phi_c}{G\lambda} = f\left(Y, \frac{L}{D}, P_r, X_{in}, X_c\right)$
Katto and Ohno (1984)	$\frac{\phi_c}{G\lambda} = f\left(\frac{\rho_g}{\rho_f}, \frac{\Delta H_i}{\lambda}, \frac{\sigma\rho_f}{G^2 L}, \frac{L}{D}\right)$
Green and Lawther (1981)	$\frac{\phi_c D}{\mu_g \lambda} = f\left(Re_v, Pr_g, \frac{\sigma}{\rho_g D\lambda}, \frac{\rho_f}{\rho_g}, \frac{\mu_f}{\mu_g}, \frac{k_f}{k_g}, \frac{Cp_f}{Cp_g}, \frac{L_b}{D}\right)$
Hauptmann and Lee (1983)	$\frac{\phi_c}{\left(\frac{\bar{R}T_c P_c^2}{M}\right)} = f\left(P_r, Re_f, \frac{L_b}{D}, Z_c\right)$

Table 5-2 Functional forms of dimensionless groups.

Parameter	Functional form	Reference Eq.
ψ_σ	$\psi_\sigma = \left(\frac{GD^{1/2}}{\rho_f^{1/2}\sigma^{1/2}}\right)^{4/3} \times \left(\frac{GD}{\mu_f}\right)^{-2/15} \times \left(\frac{GD}{\mu_g}\right)^{-1/5}$	Eq. (2-45)
ψ_γ	$\psi_\gamma = \left(\frac{GD}{\mu_f}\right) \times \left(\frac{\gamma^{1/2}\mu_f}{D\,\rho_f^{1/2}}\right)^{2/3} \times \left(\frac{\mu_f}{\mu_g}\right)^{1/8}$	Eq. (2-46)
ψ_k	$\psi_k = \frac{G\,D^{1/2}}{\rho_f^{1/2}\,\sigma^{1/2}}$	Eq. (2-81)
Y	$Y = G^{1.8}D^{0.6}\left(\frac{Cp_f}{k_f\rho_f^{0.8}g^{0.4}}\right)\left(\frac{\mu_f}{\mu_g}\right)^{0.6}$	Eq. (2-70)
ψ_L	$\psi_L = \frac{\sigma\,\rho_f}{G^2 L}$	Eq. (2-56)
Re_f	$Re_f = \frac{G\,D}{\mu_f}$	Eq. (2-76)
Re_v	$Re_v = \frac{\rho_g U_\infty D}{\mu_g} = \frac{D\,G\,[x+(1-x)(\rho_g/\rho_f)]}{\mu_g}$ *(for slip ratio of 1)*	Eq. (2-72)
ψ_B	$\psi_B = \frac{G\,D^{1/3}\,k_f^{1/3}\,\mu_f^{1/8}}{\sigma^{2/3}\,\rho_f^{2/3}\,Cp_f^{1/3}\,\mu_g^{1/8}}$	Eq. (5-8)
ψ_λ	$\psi_\lambda = (2\pi/\sqrt{g})^{1/2}\frac{G}{\rho_f^{1/2}\,\sigma^{1/4}\,(\rho_f-\rho_g)^{1/4}}$	Eq. (5-18)

Table 5-3 Comparison of CHF test data against CHF values from table method using different scaling parameters in method A.

Fluid	Pressure (MPa)	No. of data	ψ_σ			ψ_γ			ψ_k		
			Avg. error (%)	Mean error (%)	RMS error (%)	Avg. error (%)	Mean error (%)	RMS error (%)	Avg. error (%)	Mean error (%)	RMS error (%)
Data from UO loop, D=4.2 mm, L/D=155–238, G=1.5–4 Mg m^{-2} s^{-1}											
HFC-134a	1.13 (7)†	65	-5.82	6.08	6.92	-0.35	3.33	4.03	0.69	3.48	4.14
	1.66 (10)	73	-12.03	12.03	12.43	-8.54	8.54	8.92	-7.59	7.59	7.96
HCFC-22	1.34 (7)	68	-9.99	9.99	10.82	-3.29	4.39	5.23	-3.42	4.45	5.31
	1.96 (10)	61	-11.80	11.88	12.78	-6.67	6.67	7.69	-6.96	7.05	7.96
CFC-12	1.06 (7)	58	-7.85	7.88	8.70	-5.75	6.04	6.86	-1.90	3.51	4.25
	1.58 (10)	69	-11.52	11.54	12.08	-10.70	10.71	11.25	-7.45	7.48	8.05
HCFC-123	0.98 (7)	60	-8.85	8.85	9.07	-3.98	3.98	4.48	-1.52	1.92	2.62
Data from MR-7A loop, D=4.38 mm, L/D=155–333, G=4–8 Mg m^{-2} s^{-1}											
HCFC-22	1.34 (7)	56	0.91	4.92	6.16	7.09	8.44	9.48	6.98	8.36	9.39
	1.96 (10)	78	3.89	8.53	10.58	5.88	8.50	10.60	5.78	8.49	10.58
Data from MR-7A loop, D=8 mm, L/D=84–199, G=1–6 Mg m^{-2} s^{-1}											
HCFC-22	1.34 (7)	79	-3.0	5.69	7.09	5.76	7.25	8.69	5.59	7.16	8.57
	1.96 (10)	77	-3.89	7.57	9.03	1.70	5.54	6.85	1.42	5.51	6.83
Data from MR-1A loop, D=8 mm, L/D=219, G=2.5–7.7 Mg m^{-2} s^{-1}											
Water	7	31	1.15	3.02	3.50	1.15	3.02	3.50	1.15	3.02	3.50
	10	24	-2.95	3.01	3.57	-2.95	3.01	3.57	-2.95	3.01	3.57
Total	-	799	-5.83	8.26	9.59	-1.48	6.49	7.84	-0.66	5.80	7.18

† The number inside the parentheses referred to water-equivalent pressure.

Table 5-3 (Continued)

Fluid	Pressure (MPa)	No. of data	Ψ_B			Y			Ψ_λ		
			Avg. error (%)	Mean error (%)	RMS error (%)	Avg. error (%)	Mean error (%)	RMS error (%)	Avg. error (%)	Mean error (%)	RMS error (%)
Data from UO loop, D=4.2 mm, L/D=155–238, G=1.5–4 Mg m^{-2} s^{-1}											
HFC-134a	1.13 (7)†	65	2.20	3.82	4.73	-11.55	11.55	12.09	26.15	26.15	26.91
	1.66 (10)	73	-6.75	6.75	7.12	-13.81	13.81	14.27	11.40	11.40	12.09
HCFC-22	1.34 (7)	68	-6.14	6.44	7.35	-11.34	11.34	12.09	18.88	18.88	19.53
	1.96 (10)	61	-9.67	9.75	10.60	-12.17	12.24	13.17	12.25	12.26	13.69
CFC-12	1.06 (7)	58	-3.25	4.22	5.01	-11.12	11.12	11.72	22.80	22.80	23.39
	1.58 (10)	69	-8.48	8.50	9.05	-13.66	13.67	14.28	11.63	11.63	12.68
HCFC-123	0.98 (7)	60	0.68	1.99	2.36	-14.40	14.40	14.64	23.97	23.97	24.51
Data from MR-7A loop, D=4.38 mm, L/D=155–333, G=4–8 Mg m^{-2} s^{-1}											
HCFC-22	1.34 (7)	56	4.49	6.70	7.63	-0.38	4.59	6.08	27.12	27.12	27.74
	1.96 (10)	78	4.78	8.48	10.52	3.71	8.55	10.60	14.80	14.80	15.84
Data from MR-7A loop, D=8 mm, L/D=84–199, G=1–6 Mg m^{-2} s^{-1}											
HCFC-22	1.34 (7)	79	1.93	5.39	6.69	-4.75	6.74	8.02	36.24	36.24	37.86
	1.96 (10)	77	-1.40	6.14	7.50	-4.37	7.89	9.40	23.82	23.82	25.22
Data from MR-1A loop, D=8 mm, L/D=219, G=2.5–7.7 Mg m^{-2} s^{-1}											
Water	7	31	1.15	3.02	3.50	1.15	3.02	3.50	1.15	3.02	3.50
	10	24	-2.95	3.01	3.57	-2.95	3.01	3.57	-2.95	3.01	3.57
Total	-	799	-1.82	6.04	7.39	-7.76	9.96	11.36	19.35	19.60	22.36

† The number inside the parentheses referred to water-equivalent pressure.

Table 5-4 Comparison of CHF test data against CHF values from table method using different scaling parameters in method B.

Fluid	Pressure (MPa)	No. of data	ψ_σ			ψ_γ			ψ_k		
			Avg. error (%)	Mean error (%)	RMS error (%)	Avg. error (%)	Mean error (%)	RMS error (%)	Avg. error (%)	Mean error (%)	RMS error (%)
Data from UO loop, D=4.2 mm, L/D=155–238, G=1.5–4 Mg m^{-2} s^{-1}											
HFC-134a	1.15 (7)†	65	-2.37	2.69	3.44	4.08	4.40	5.30	12.47	12.47	13.33
	1.66 (10)	73	-10.30	10.30	10.48	-6.29	6.29	6.54	0.09	1.59	1.98
HCFC-22	1.34 (7)	68	-6.66	6.66	7.12	0.95	2.91	3.40	7.76	7.76	8.72
	1.96 (10)	61	-11.02	11.02	11.33	-4.58	4.64	5.47	1.22	3.28	3.81
CFC-12	1.06 (7)	58	-4.46	4.46	5.06	-1.96	2.54	3.19	9.65	9.65	10.39
	1.58 (10)	69	-9.87	9.87	10.17	-8.89	8.89	9.22	0.45	2.40	2.97
HCFC-123	0.98 (7)	60	-5.59	5.59	5.99	0.03	1.74	2.13	9.68	9.68	10.19
Data from MR-7A loop, D=4.38 mm, L/D=155–333, G=4–8 Mg m^{-2} s^{-1}											
HCFC-22	1.34 (7)	56	-1.55	3.73	5.51	5.09	6.16	6.88	10.63	10.63	11.42
	1.96 (10)	78	-3.02	4.87	6.07	0	3.64	4.20	2.75	3.94	4.60
Data from MR-7A loop, D=8 mm, L/D=84–199, G=1–6 Mg m^{-2} s^{-1}											
HCFC-22	1.34 (7)	79	-3.03	5.73	7.13	5.71	7.25	8.69	5.43	7.10	8.50
	1.96 (10)	77	-3.88	7.63	9.09	1.71	5.58	6.91	1.36	5.54	6.89
Data from MR-7A loop, D=8 mm, L/D=219, G=2.5–7.7 Mg m^{-2} s^{-1}											
Water	7	31	1.15	3.02	3.50	1.15	3.02	3.50	1.15	3.02	3.50
	10	24	-2.95	3.01	3.57	-2.95	3.01	3.57	-2.95	3.01	3.57
Total	-	799	-5.26	6.41	7.63	-3.75	4.87	5.99	4.88	6.28	7.91

† The number inside the parentheses referred to water-equivalent pressure.

Table 5-4 (Continued)

Fluid	Pressure (MPa)	No. of data	Ψ_B			Y		
			Avg. error (%)	Mean error (%)	RMS error (%)	Avg. error (%)	Mean error (%)	RMS error (%)
Data from UO loop, D=4.2 mm, L/D=155–238, G=1.5–4 Mg m^{-2} s^{-1}								
HFC-134a	1.13 (7)†	65	6.81	6.82	7.82	-9.21	9.21	9.41
	1.66 (10)	73	-4.42	4.46	4.78	-12.55	12.55	12.73
HCFC-22	1.34 (7)	68	-2.25	2.88	3.65	-8.24	8.24	8.59
	1.96 (10)	61	-8.17	8.17	8.60	-11.56	11.56	11.86
CFC-12	1.06 (7)	58	1.01	2.49	3.00	-8.44	8.44	8.73
	1.58 (10)	69	-6.31	6.36	6.80	-12.63	12.63	12.88
HCFC-123	0.98 (7)	60	5.16	5.24	5.81	-12.14	12.14	12.39
Data from MR-7A loop, D=4.38 mm, L/D=155–333, G=4–8 Mg m^{-2} s^{-1}								
HCFC-22	1.34 (7)	56	2.27	4.67	5.41	-2.91	4.01	6.17
	1.96 (10)	78	-1.67	4.05	5.04	-3.28	5.06	6.29
Data from MR-7A loop, D=8 mm, L/D=84–199, G=1–6 Mg m^{-2} s^{-1}								
HCFC-22	1.34 (7)	79	1.90	5.41	6.72	-4.78	6.79	8.06
	1.96 (10)	77	-1.40	6.20	7.56	-4.36	7.94	9.46
Data from MR-1A loop, D=8 mm, L/D=219, G=2.5–7.7 Mg m^{-2} s^{-1}								
Water	7	31	1.15	3.02	3.50	1.15	3.02	3.50
	10	24	-2.95	3.01	3.57	-2.95	3.01	3.57
Total	-	799	-0.74	5.02	6.03	-7.56	8.52	9.63

† The number inside the parentheses referred to water-equivalent pressure.

Table 5-5 Comparison of CHF test results against non-dimensional CHF equations based on constant inlet condition.

Fluid	Pressure (MPa)	NO. of data	Ahmad		Shah		Katto and Ohno		Green and Lawther		Hauptmann and Lee	
			Avg. error (%)	RMS error (%)	Avg. error (%)	RMS error (%)	Avg. error (%)	RMS error (%)	Avg. error (%)	RMS error (%)	Avg. error (%)	RMS error (%)
Data from UO loop, D=4.2 mm, L/D=155–238, G=1.5–4 Mg m^{-2} s^{-1}												
HFC-134a	1.13 (7)†	65	16.63	16.86	4.25	15.01	16.23	17.15	1.79	3.50	-17.84	18.36
	1.66 (10)	73	41.72	42.43	11.39	17.74	14.84	15.09	3.54	4.33	-14.62	15.14
HCFC-22	1.34 (7)	68	13.61	13.82	1.58	11.93	10.52	11.20	-15.47	15.78	-13.28	13.61
	1.96 (10)	61	48.09	48.52	12.32	19.55	14.82	15.27	-9.15	9.70	-9.27	10.22
CFC-12	1.06 (7)	58	9.04	9.55	1.47	11.50	11.77	12.49	-6.62	7.01	-11.77	12.18
	1.58 (10)	69	37.65	38.43	8.31	14.36	14.23	14.66	0	3.43	-9.42	10.20
HCFC-123	0.98 (7)	60	11.30	12.14	0.50	10.01	15.12	15.93	18.78	19.61	-17.06	18.02
Data from MR-7A loop, D=4.38 mm, L/D=155–333, G=4–8 Mg m^{-2} s^{-1}												
HCFC-22	1.34 (7)	56	4.98	8.09	9.63	20.48	9.24	12.77	-10.10	11.76	-7.64	12.57
	1.96 (10)	78	21.66	25.95	7.55	18.76	3.86	11.46	-11.45	14.59	-5.08	10.53
Data from MR-7A loop, D=8 mm, L/D=84–199, G=1–6 Mg m^{-2} s^{-1}												
HCFC-22	1.34 (7)	79	20.10	21.20	3.62	10.64	9.78	12.43	-2.11	8.85	25.62	28.42
	1.96 (10)	77	51.37	53.28	10.26	14.89	8.11	11.97	-4.29	7.90	25.12	26.88
Data from MR-1A loop, D=8 mm, L/D=219, G=2.5–7.7 Mg m^{-2} s^{-1}												
Water	7	31	4.84	7.62	13.21	20.65	1.82	8.80	-1.15	4.92	27.87	28.33
	10	24	29.62	33.63	18.18	28.02	1.36	8.85	3.09	7.47	29.12	30.59
Total	-	799 417‡	25.23 12.53‡	30.88 14.41‡	7.13	16.10	10.81	13.45	-3.02	10.55	-1.70	18.62

† The number inside the parentheses referred to water-equivalent pressure. ‡ Data for 10 MPa water-equivalent pressure were excluded.

Table 5-6 Comparison of the CHF test data against the predictions from Ying and Weisman's model

Fluid	P=7 MPa water-equiv.			P=10 MPa water-equiv.		
	No. of data	Avg. Error (%)	RMS error (%)	No. of data	Avg. error (%)	RMS error (%)
Data from UO loop, D=4.2 mm, L/D=155–238, G=1.5–4 Mg m^{-2} s^{-1}						
HFC-134a	14	-3.25	13.41	52	1.24	9.10
HCFC-22	10	-14.88	18.82	33	5.79	10.03
CFC-12	10	-12.52	19.94	42	1.66	8.85
HCFC-123	31	-13.12	21.48	0	–	–
Data from MR-7A loop, D=4.38 mm, L/D=155–333, G=4–8 Mg m^{-2} s^{-1}						
HCFC-22	56	-1.01	15.81	78	11.71	13.39
Data from MR-7A loop, D=8 mm, L/D=84–199, G=1–6 Mg m^{-2} s^{-1}						
HCFC-22	53	-2.94	26.70	60	14.29	21.98
Data from MR-1A loop, D=8 mm, L/D=219, G=2.5–7.7 Mg m^{-2} s^{-1}						
water	24	-4.58	12.43	24	4.19	7.56
Subtotal	198	-5.30	20.08	289	7.60	13.83
Total	487†	2.36†	16.65†			

† these numbers combine the 7 and 10 MPa water-equiv. data

Table 5-7 Comparison of the water CHF data with Whalley et al.'s model and Govan et al.'s modification as well as the effects of (a) ε_o and (b) k_1.

(a)

Pressure (MPa)	ε_o	k_1	Avg. error (%)	RMS error (%)
7	0.99	Whalley et al.'s model	18.85	21.37
10			19.72	20.65
7	0.99	Govan et al.'s correlation	-8.69	9.84
10			-4.97	8.41
7	0.95	Govan et al.'s correlation	-0.12	9.25
10			7.64	9.30
7	0.9	Govan et al.'s correlation	8.76	15.17
10			19.01	19.90

(b)

Pressure (MPa)	ε_o	k_1	Avg. error (%)	RMS error (%)
7	0.99	Govan et al.'s correlation+10%	-3.56	5.46
10			-0.05	7.83
7	0.99	Govan et al.'s correlation-10%	-13.94	15.03
10			-9.89	11.57

Table 5-8 Comparison of the CHF test data against the CHFs predicted from Whalley et al.'s model using Govan et al.'s correlations.

Fluid	Pressure (MPa)	No. of data	Avg. error (%)	RMS error (%)
Data from UO loop, D=4.2 mm, L/D=155–238, G=1.5–4 Mg m^{-2} s^{-1}				
HFC-134a	1.13 (7)†	65	6.04	7.22
	1.66 (10)	73	9.22	12.67
HCFC-22	1.34 (7)	68	1.61	5.39
	1.96 (10)	61	13.37	15.49
CFC-12	1.06 (7)	58	2.80	4.97
	1.58(10)	69	9.26	12.84
HCFC-123	0.98 (7)	60	2.32	5.52
Data from MR-7A loop, D=4.38 mm, L/D=155–333, G=4–8 Mg m^{-2} s^{-1}				
HCFC-22	1.34 (7)	56	1.21	4.68
	1.96 (10)	78	-0.25	7.61
Data from MR-7A loop, D=8 mm, L/D=84–199, G=1–6 Mg m^{-2} s^{-1}				
HCFC-22	1.34 (7)	79	-5.25	9.38
	1.96 (10)	77	2.03	12.12
Data from MR-1A loop, D=8 mm, L/D=219, G=2.5–7.7 Mg m^{-2} s^{-1}				
water	7	31	-8.69	9.84
	10	24	-4.97	8.41
Total	–	799	2.92	9.69

† The number inside the parentheses referred to water-equivalent pressure.

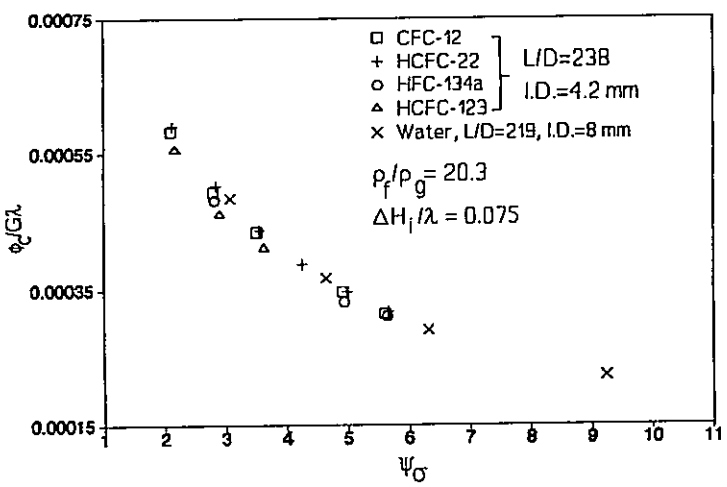

(a)

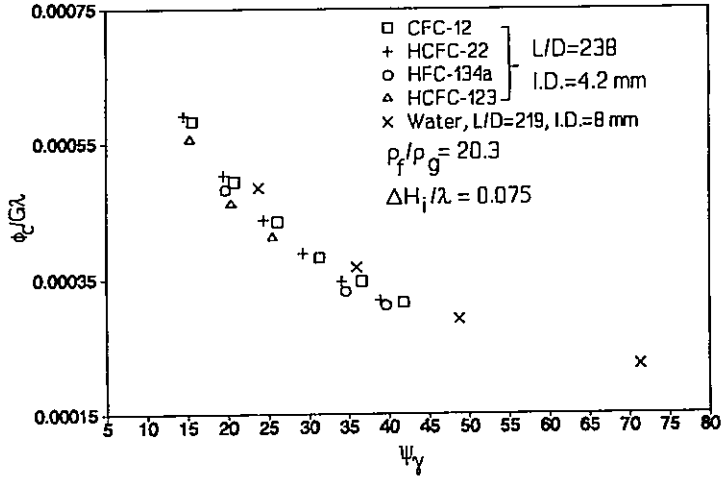

(b)

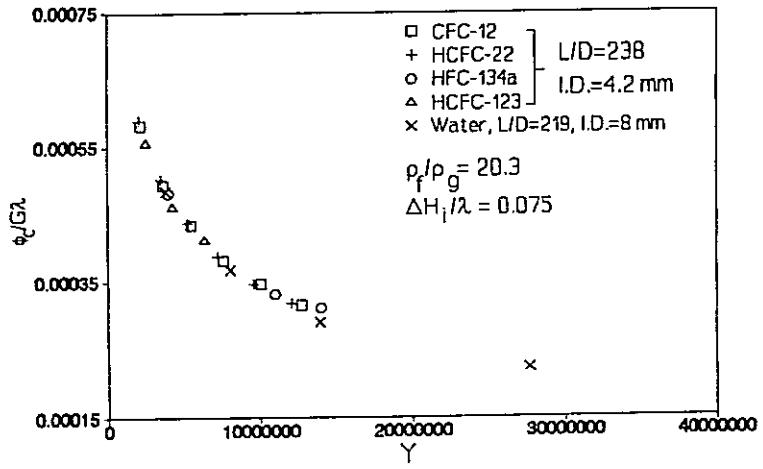

(c)

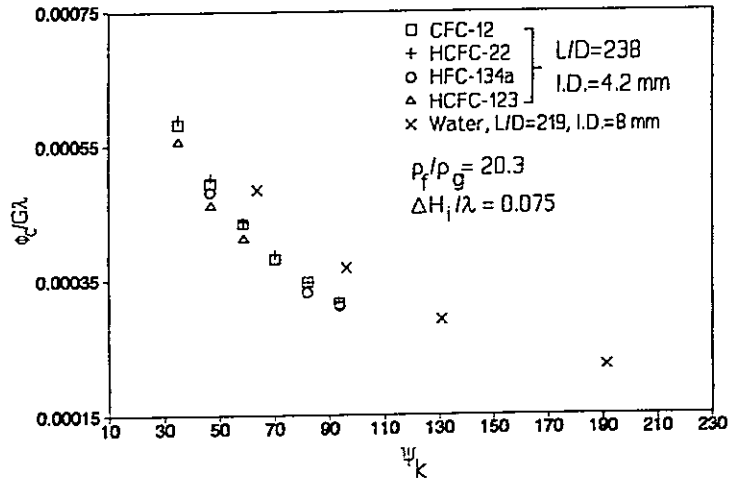

(d)

Figure 5-1 Effects of (a) ψ_σ, (b) ψ_γ, (c) Y and (d) ψ_k on Bo at ρ_f/ρ_g= 20.3 and $\Delta H_i/\lambda$=0.075.

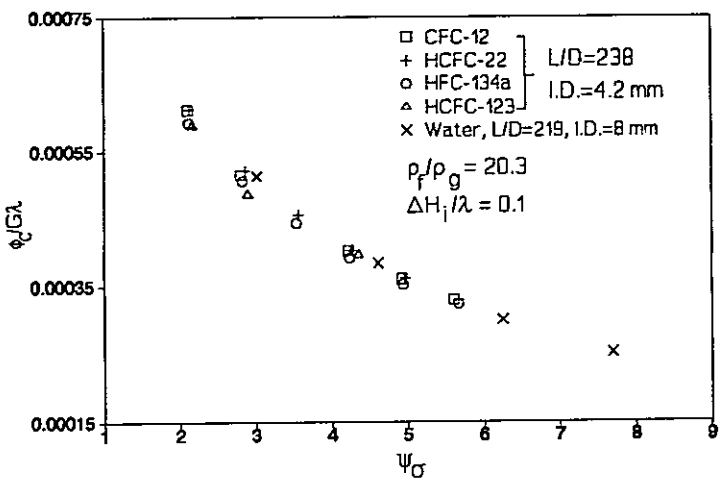

(a)

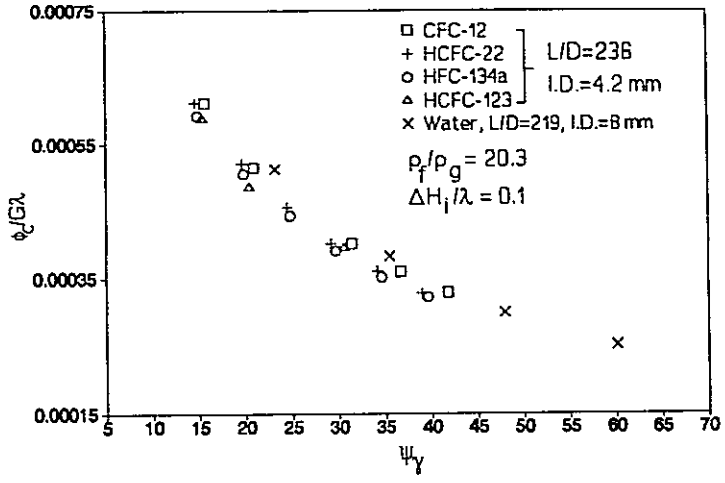

(b)

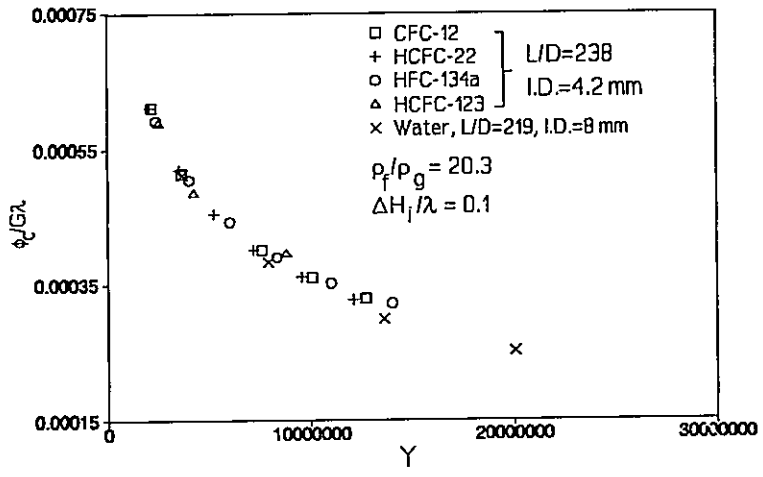

(c)

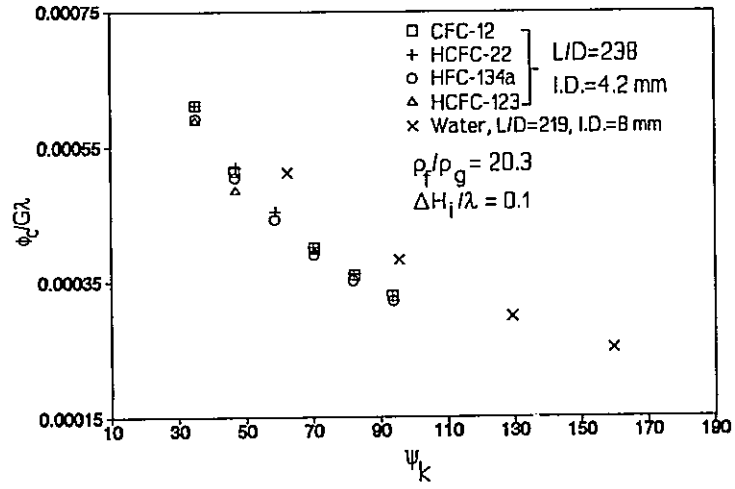

(d)

Figure 5-2 Effects of (a) ψ_σ, (b) ψ_γ, (c) Y and (d) ψ_k on Bo at ρ_f/ρ_g= 20.3 and $\Delta H_i/\lambda$=0.1.

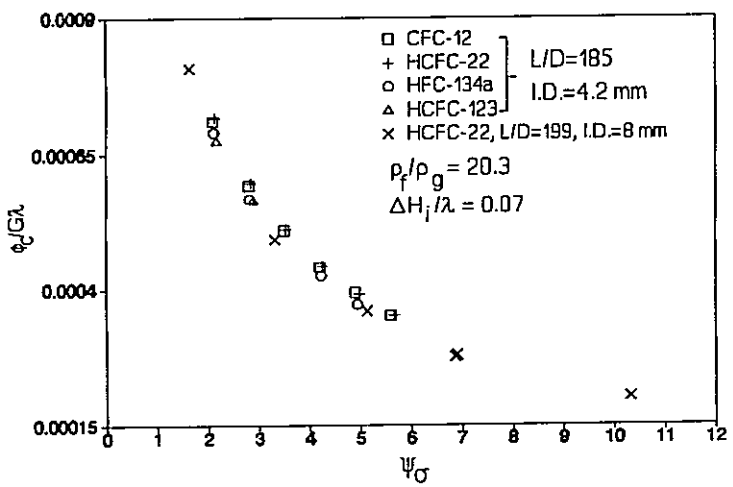

(a)

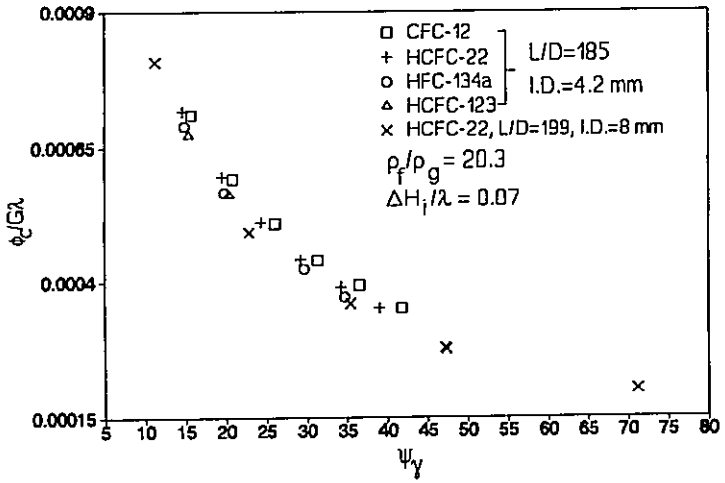

(b)

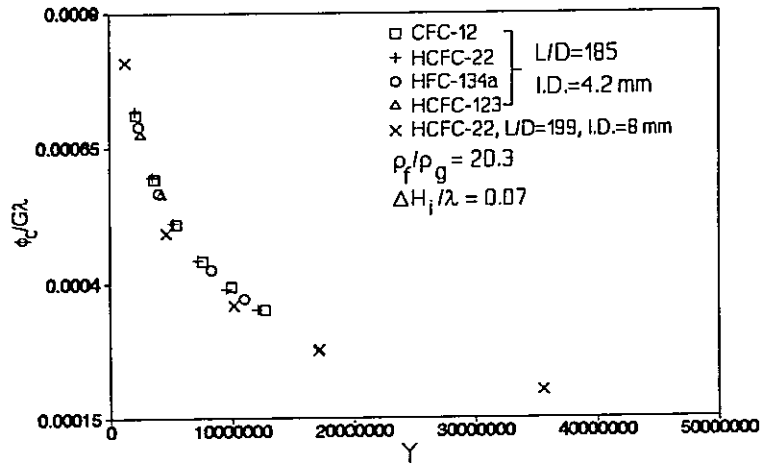

(c)

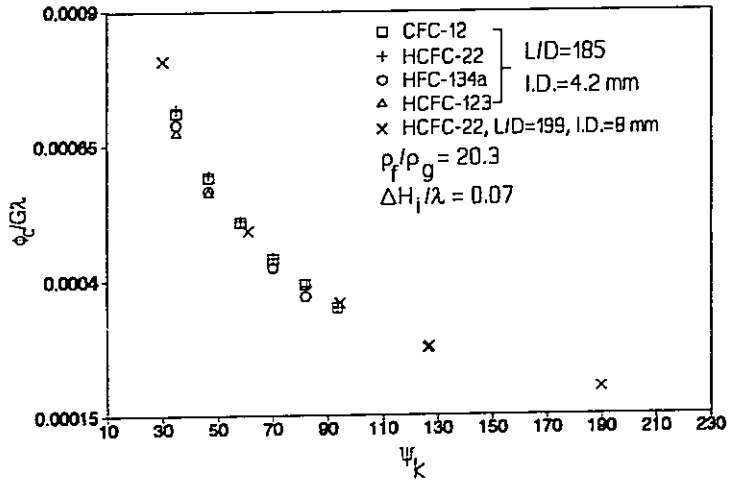

(d)

Figure 5-3 Effects of (a) ψ_σ, (b) ψ_γ, (c) Y and (d) ψ_k on Bo at ρ_f/ρ_g= 20.3 and $\Delta H_i/\lambda$=0.07.

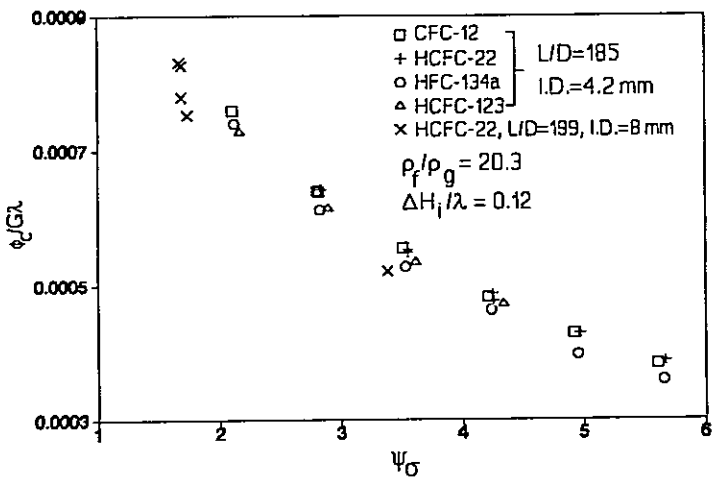

(a)

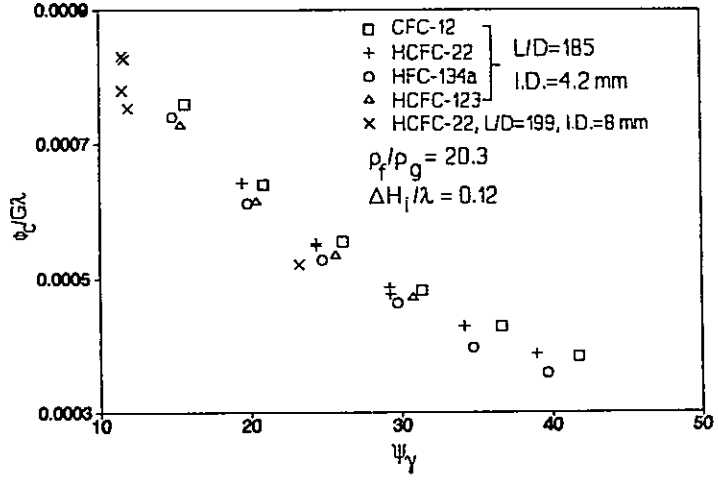

(b)

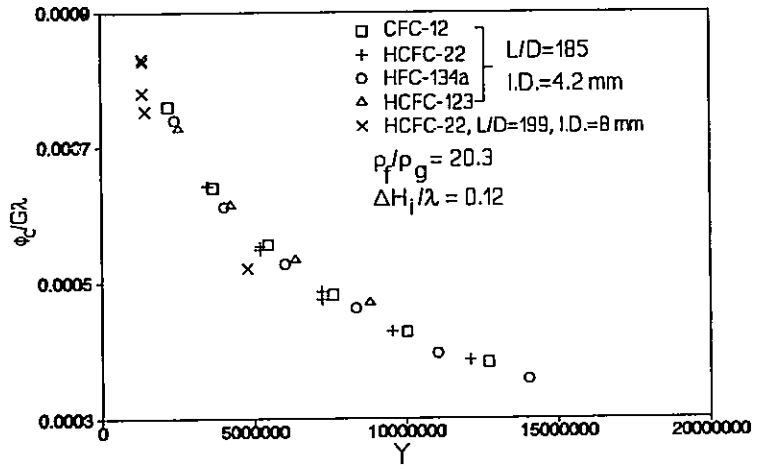

(c)

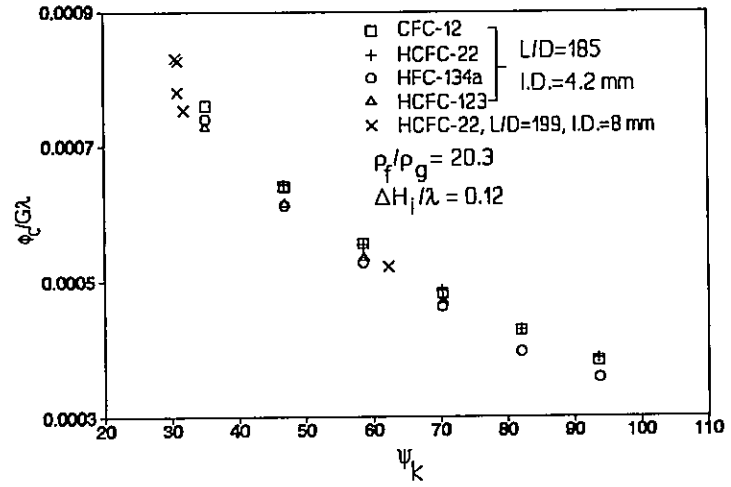

(d)

Figure 5-4 Effects of (a) ψ_σ, (b) ψ_γ, (c) Y and (d) ψ_k on Bo at ρ_f/ρ_g= 20.3 and $\Delta H_i/\lambda$=0.12.

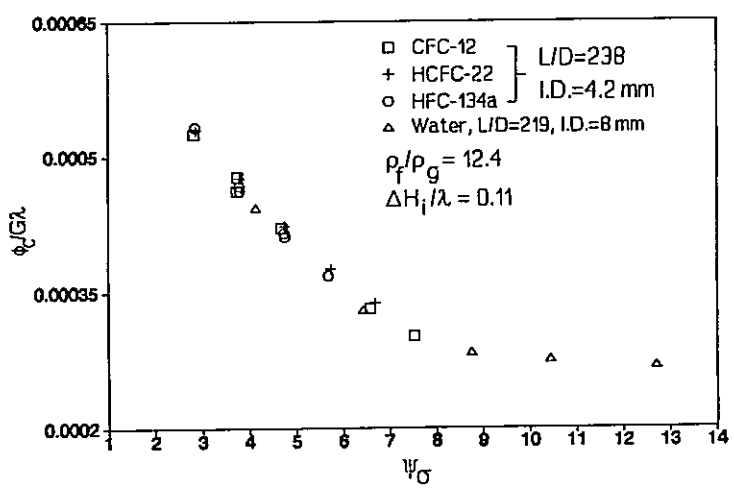

(a)

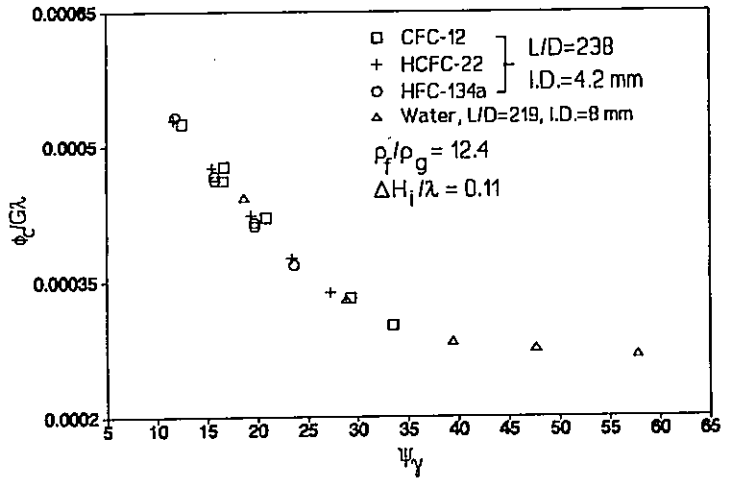

(b)

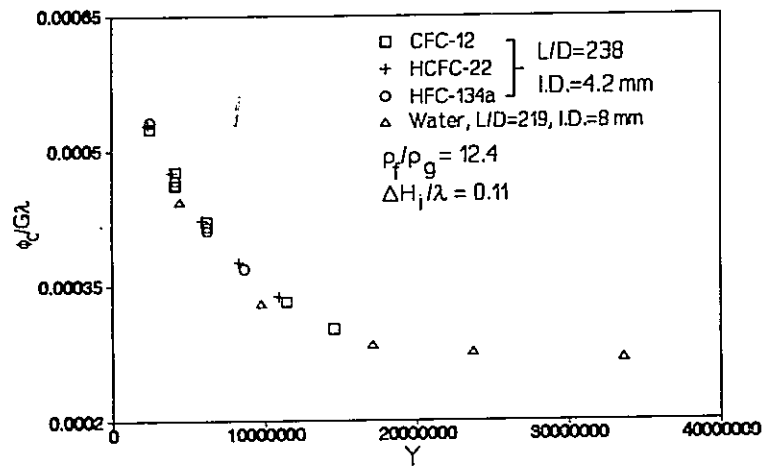

(c)

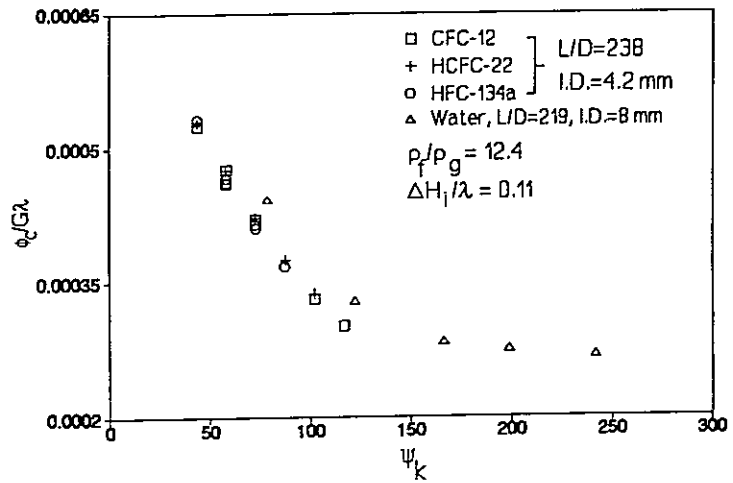

(d)

Figure 5-5 Effects of (a) ψ_σ, (b) ψ_γ, (c) Y and (d) ψ_k on Bo at ρ_f/ρ_g= 12.4 and $\Delta H_i/\lambda$=0.11.

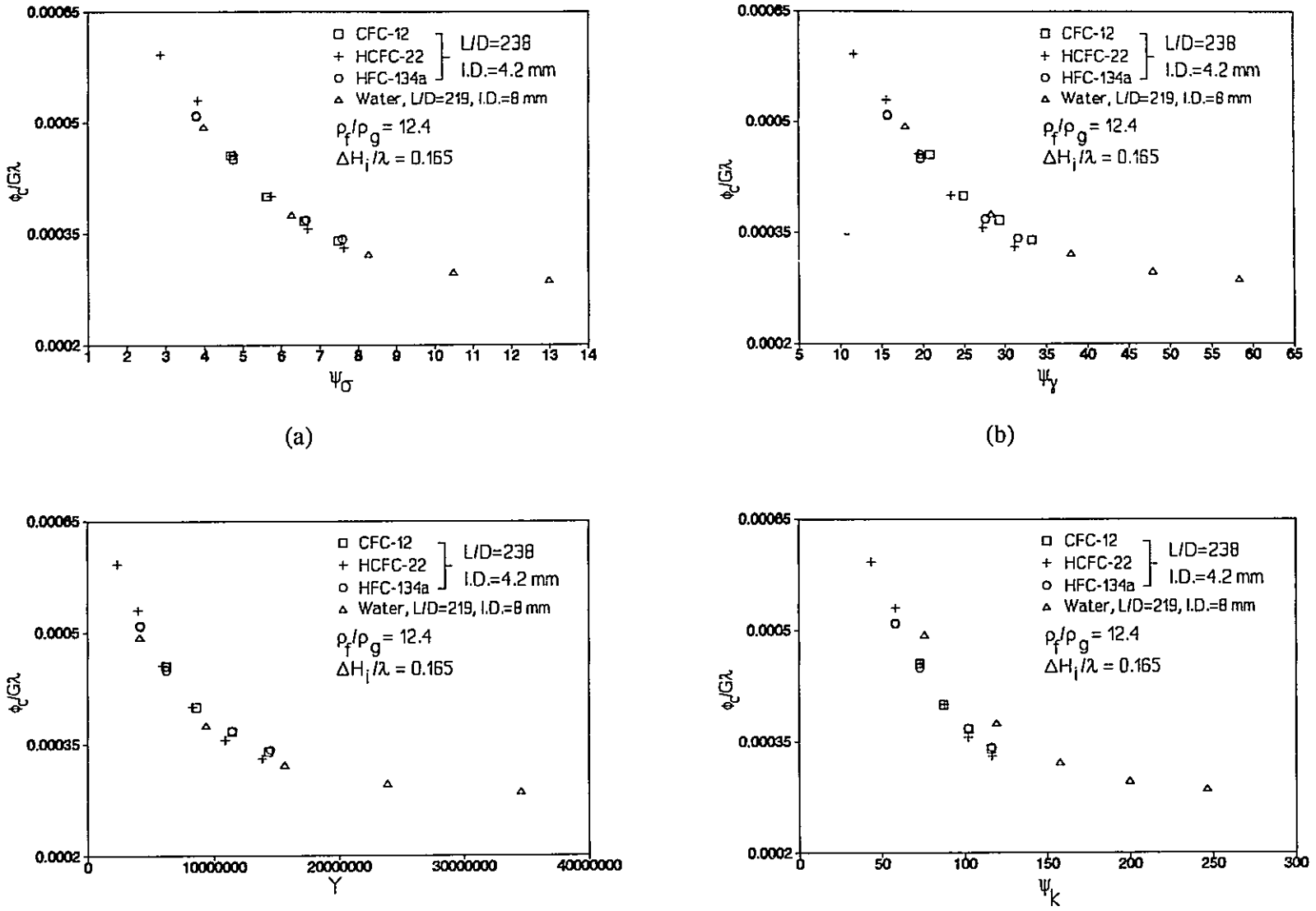

Figure 5-6 Effects of (a) ψ_σ, (b) ψ_γ, (c) Y and (d) ψ_k on Bo at ρ_f/ρ_g= 12.4 and $\Delta H_i/\lambda$=0.165.

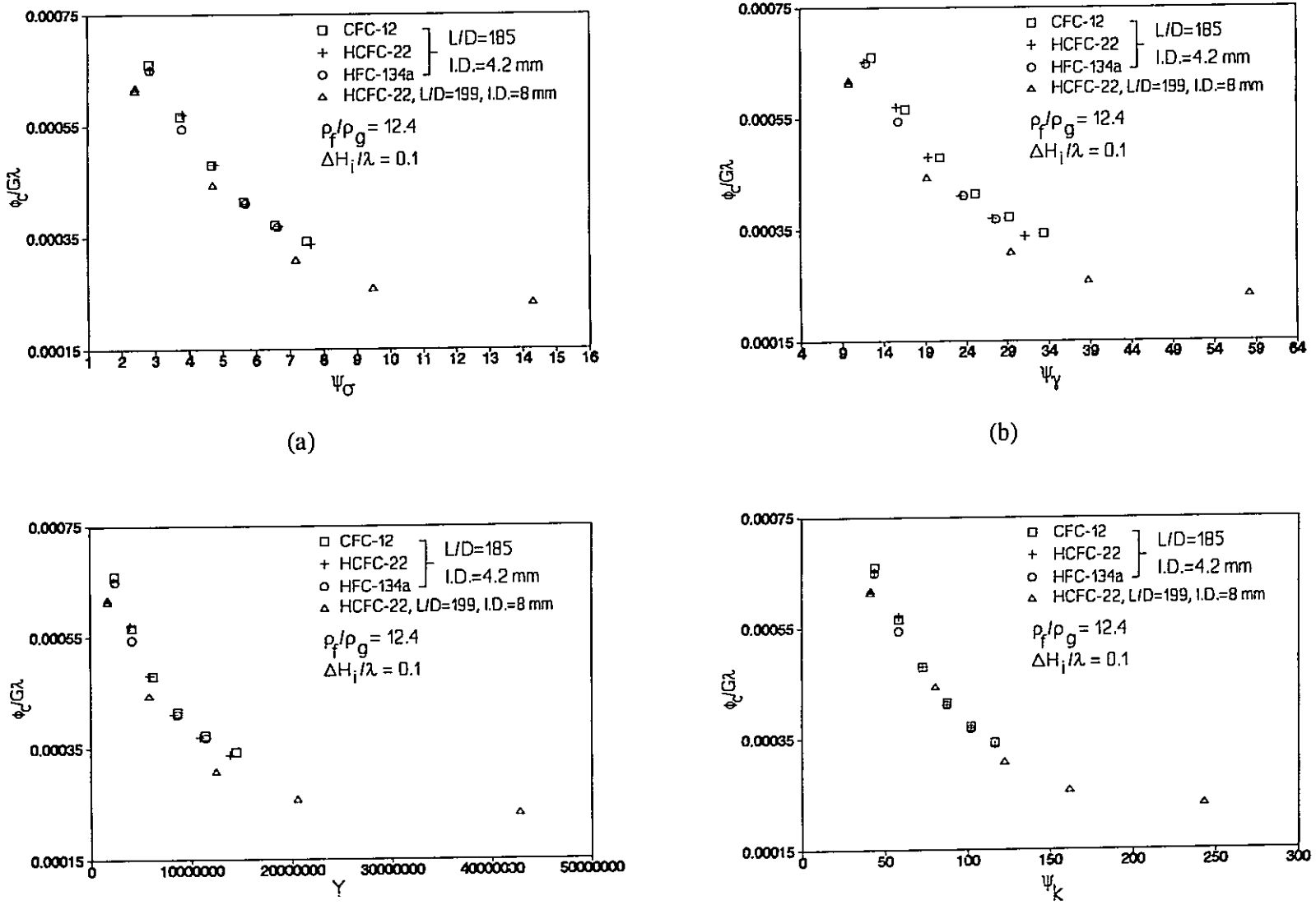

Figure 5-7 Effects of (a) ψ_σ, (b) ψ_γ, (c) Y and (d) ψ_k on Bo at ρ_f/ρ_g= 12.4 and $\Delta H_i/\lambda$=0.1.

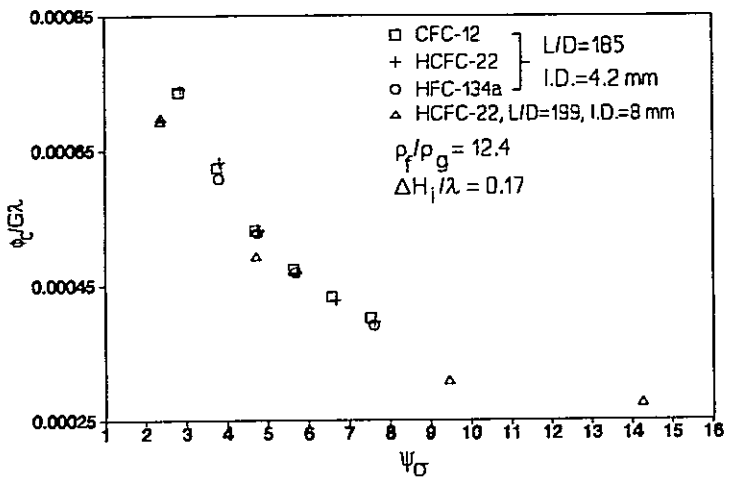

(a)

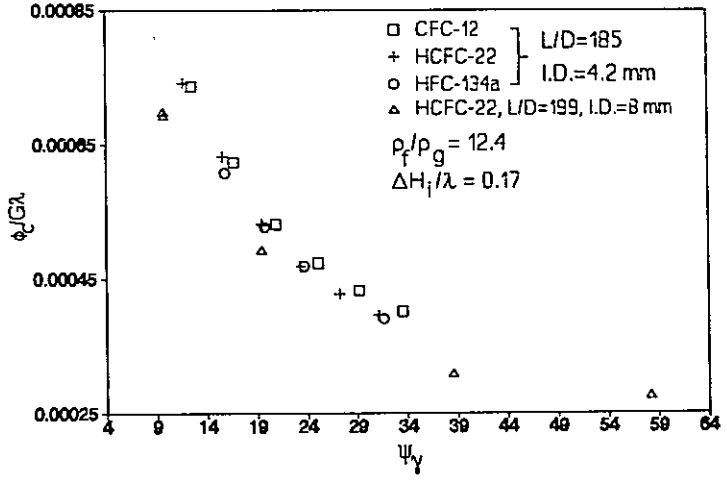

(b)

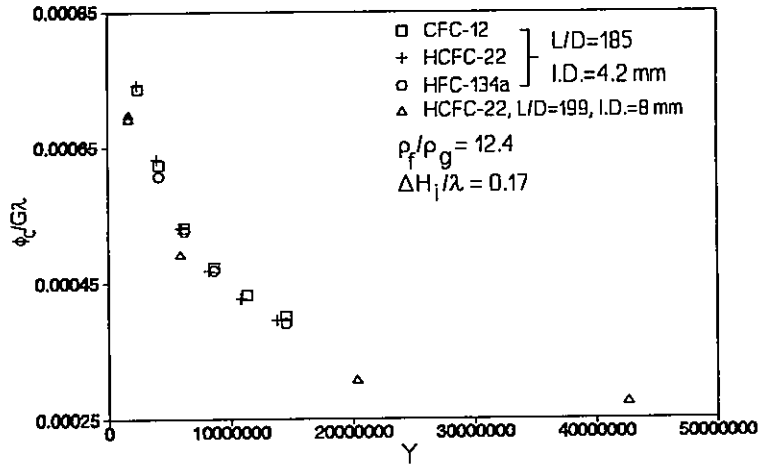

(c)

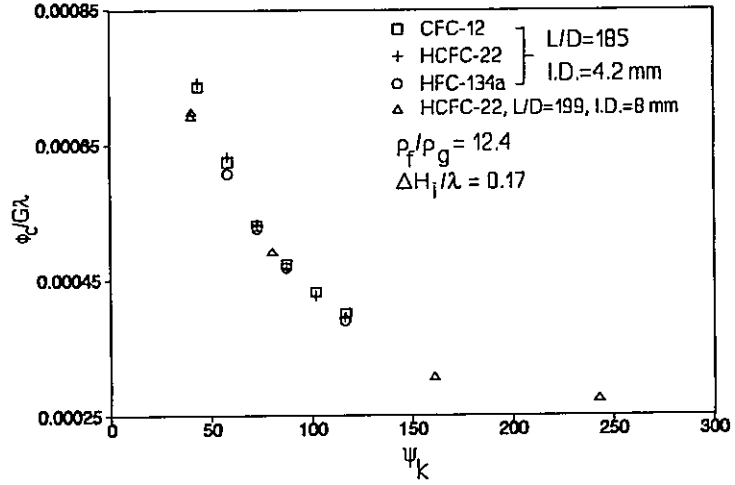

(d)

Figure 5-8 Effects of (a) ψ_σ, (b) ψ_γ, (c) Y and (d) ψ_k on Bo at ρ_f/ρ_g= 12.4 and $\Delta H_i/\lambda$=0.17.

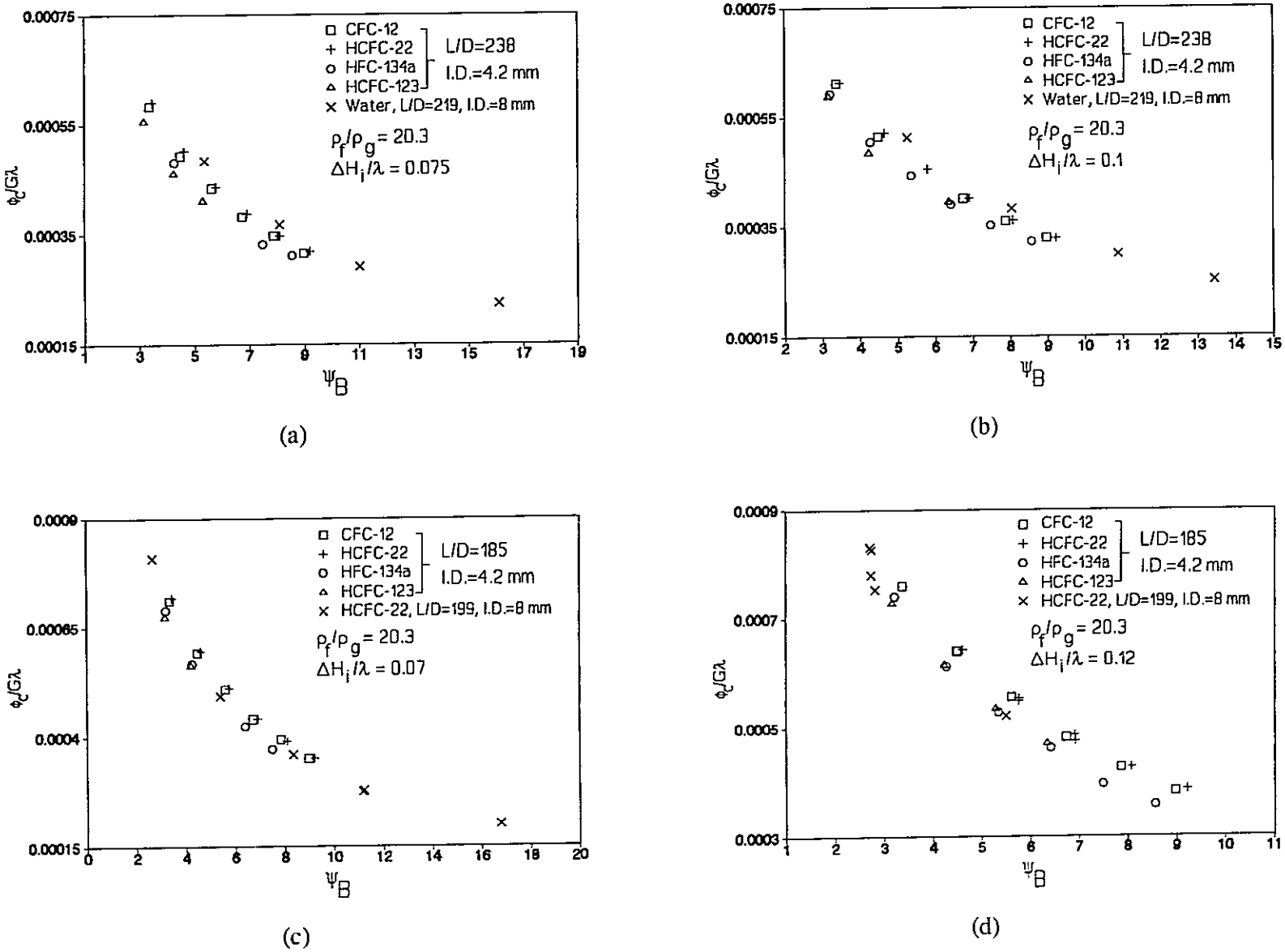

Figure 5-9 Effect of ψ_B on Bo at ρ_f/ρ_g= 20.3 and $\Delta H_i/\lambda$= (a) 0.075, (b) 0.1, (c) 0.07 and (d) 0.12.

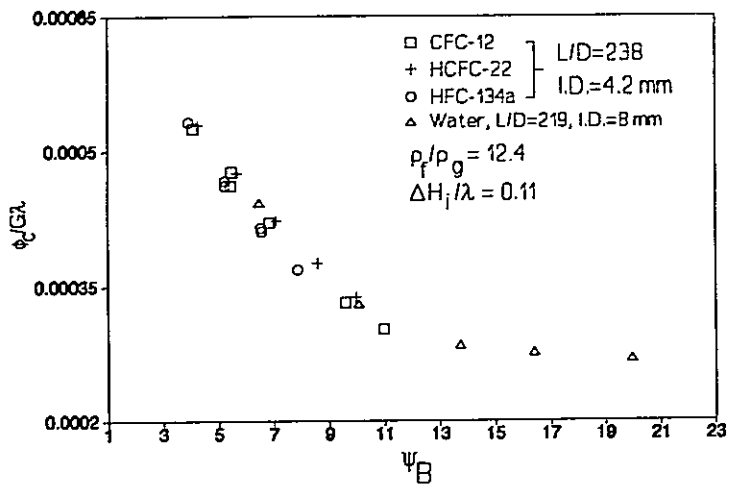

(a)

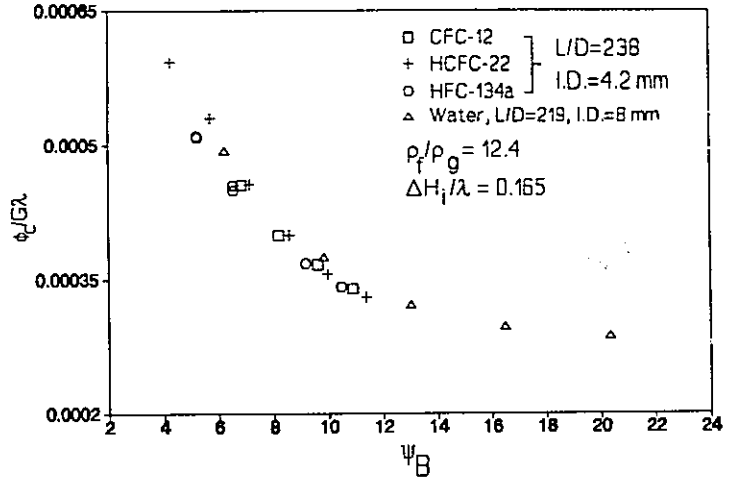

(b)

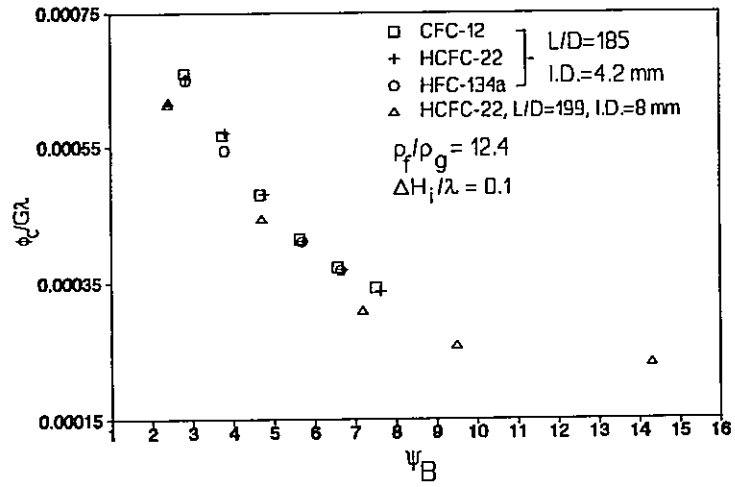

(c)

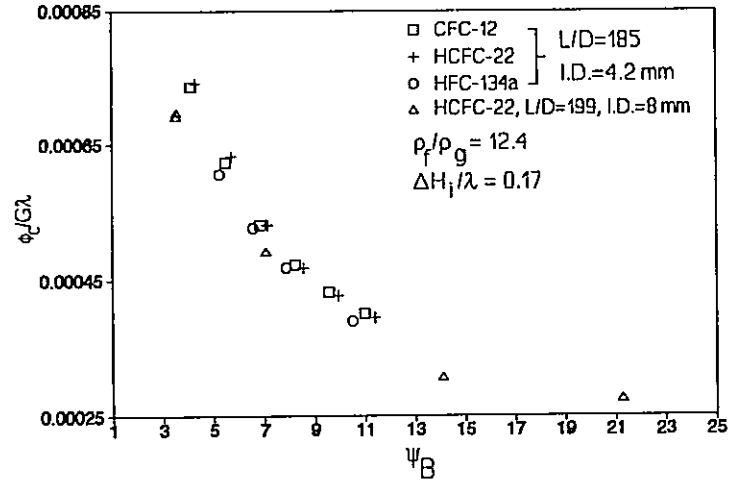

(d)

Figure 5-10 Effect of ψ_B on Bo at ρ_f/ρ_g= 12.4 and $\Delta H_i/\lambda$= (a) 0.11, (b) 0.165, (c) 0.1 and (d) 0.17.

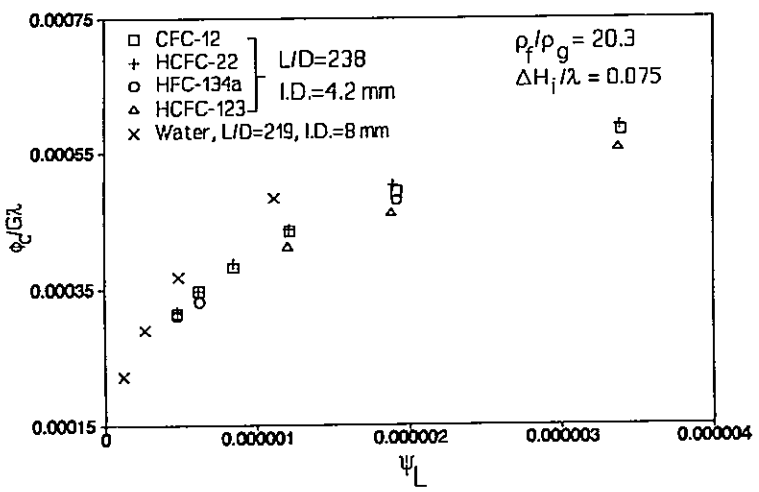

(a)

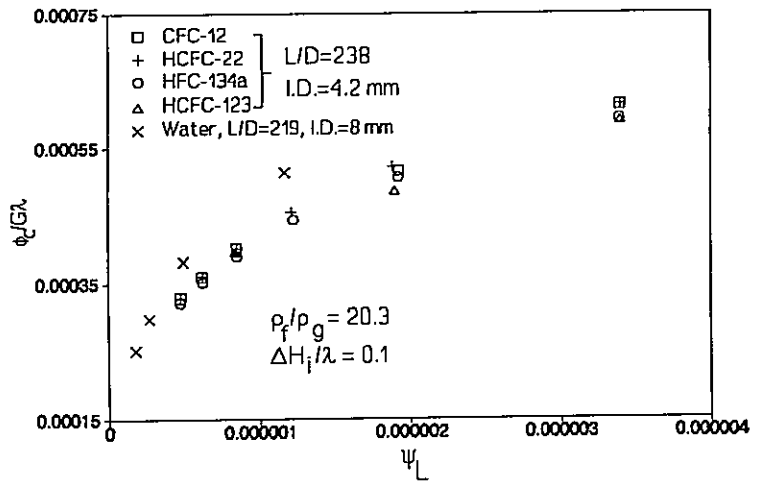

(b)

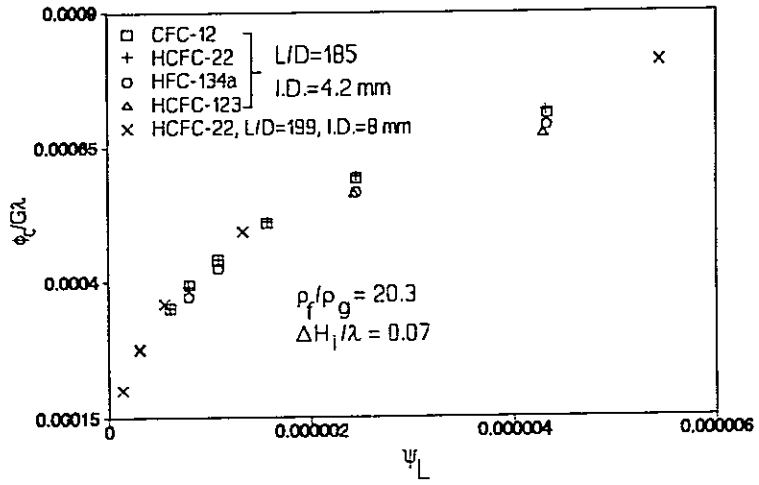

(c)

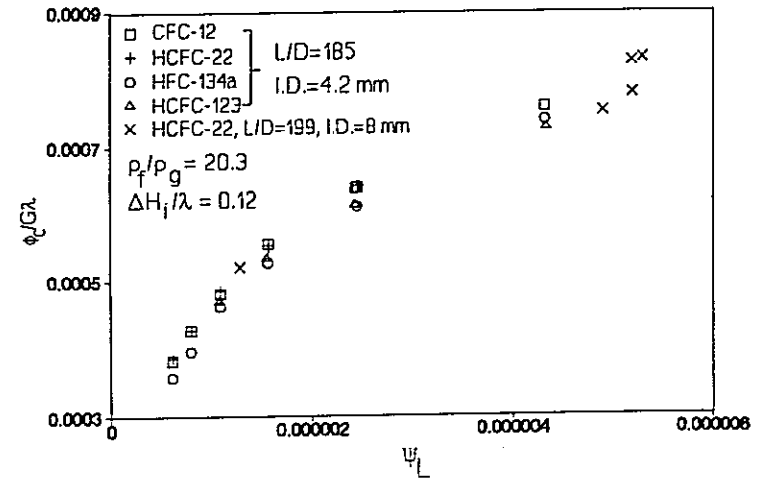

(d)

Figure 5-11 Effect of ψ_L on Bo at ρ_f/ρ_g= 20.3 and $\Delta H_i/\lambda$= (a) 0.075, (b) 0.1, (c) 0.07 and (d) 0.12.

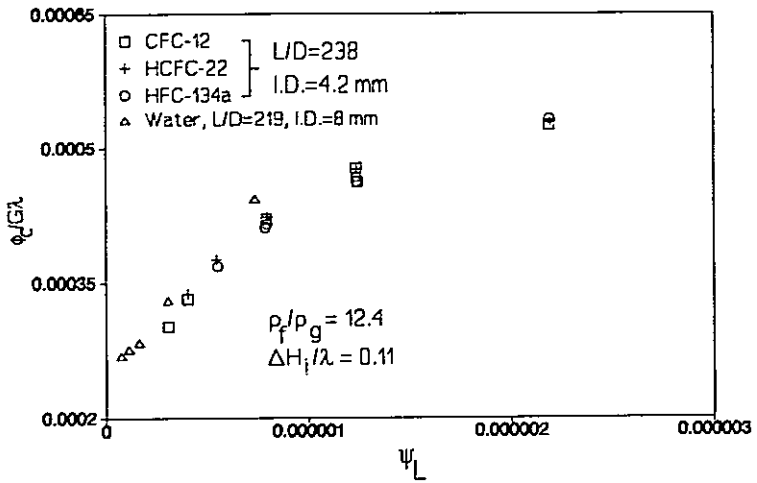

(a)

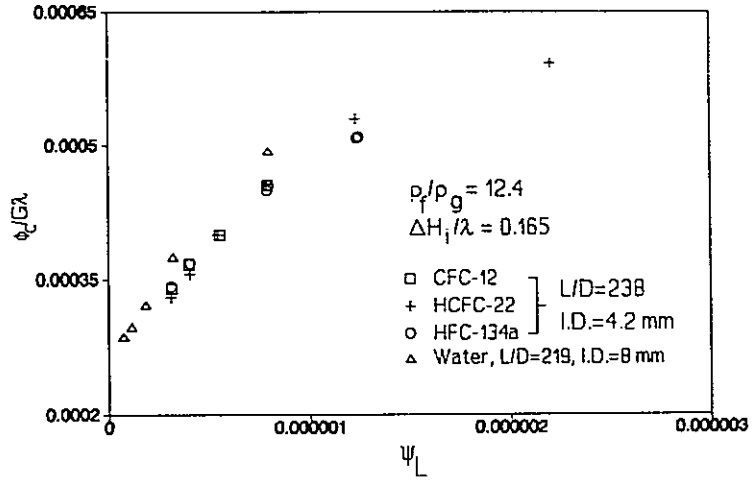

(b)

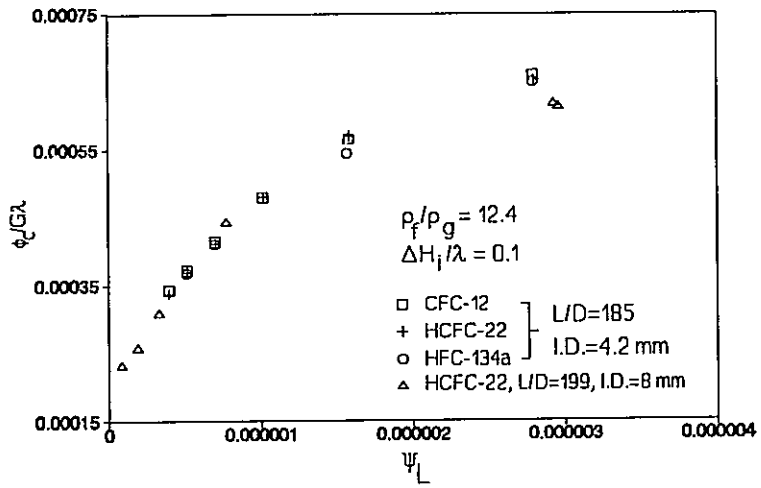

(c)

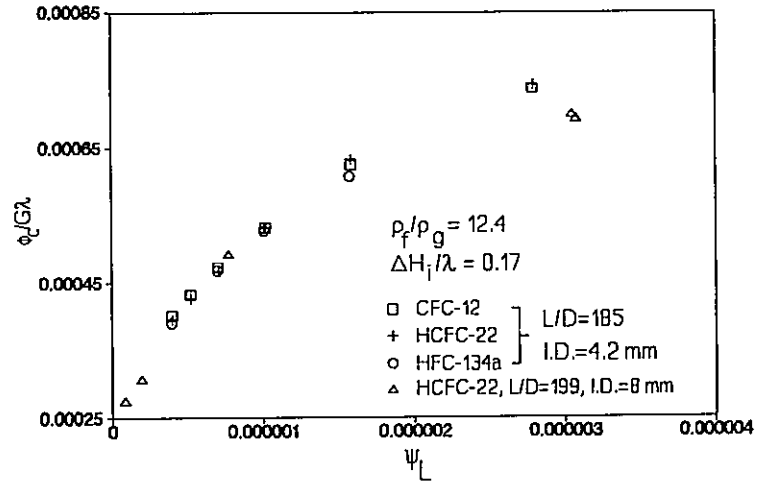

(d)

Figure 5-12 Effect of ψ_L on Bo at ρ_f/ρ_g= 12.4 and $\Delta H_i/\lambda$= (a) 0.11, (b) 0.165, (c) 0.1 and (d) 0.17.

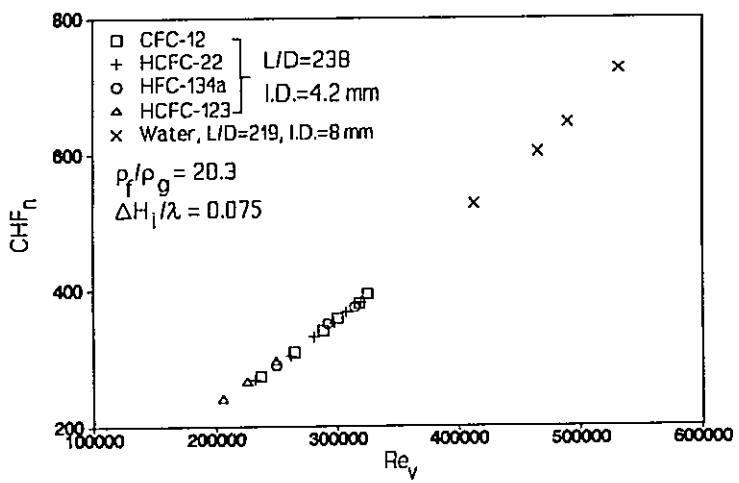

(a)

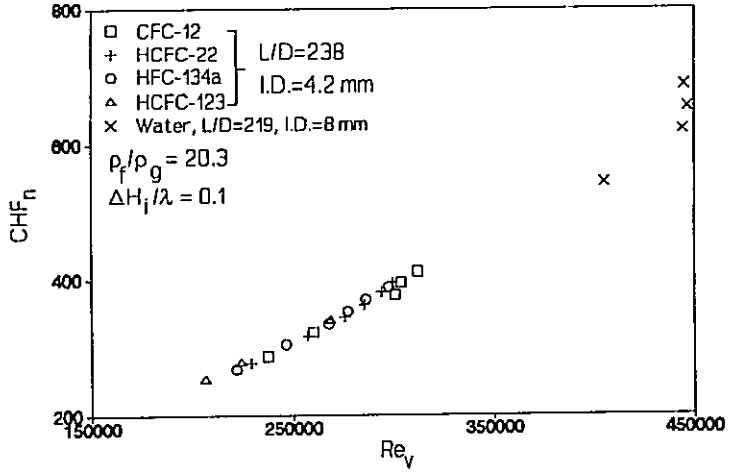

(b)

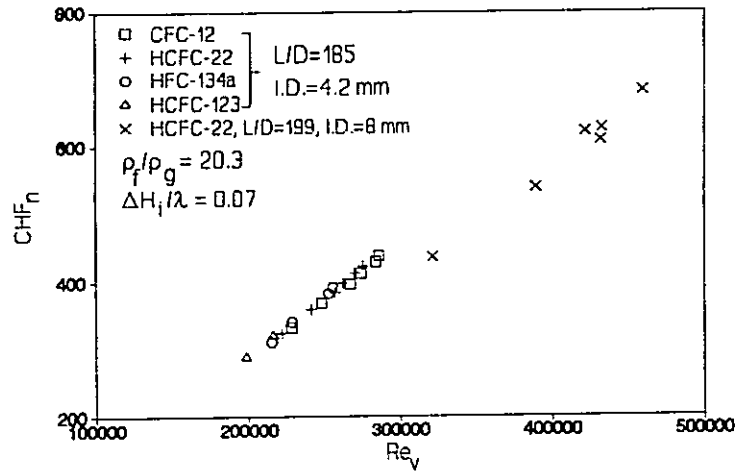

(c)

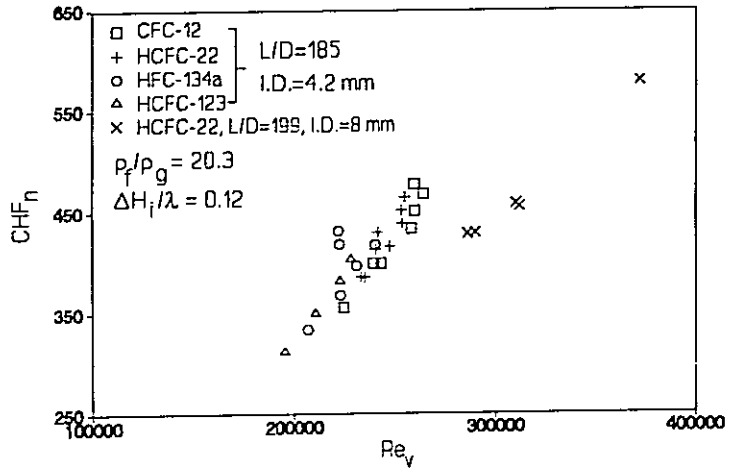

(d)

Figure 5-13 Effect of Re_v on CHF_n at ρ_f/ρ_g= 20.3 and $\Delta H_i/\lambda$= (a) 0.075, (b) 0.1, (c) 0.07 and (d) 0.12.

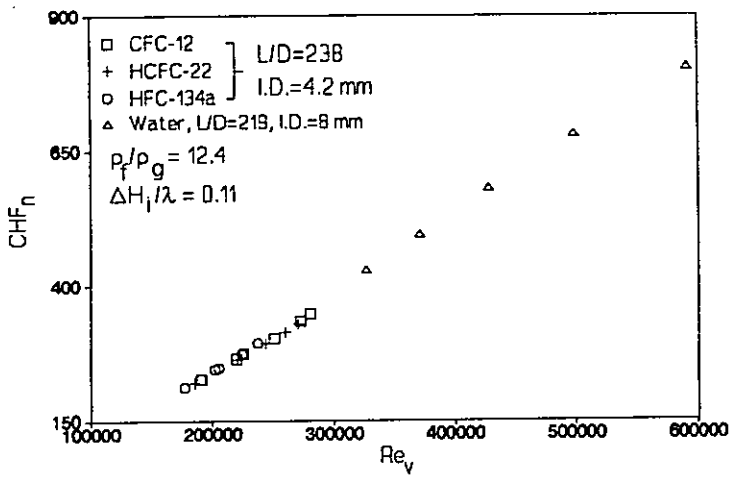

(a)

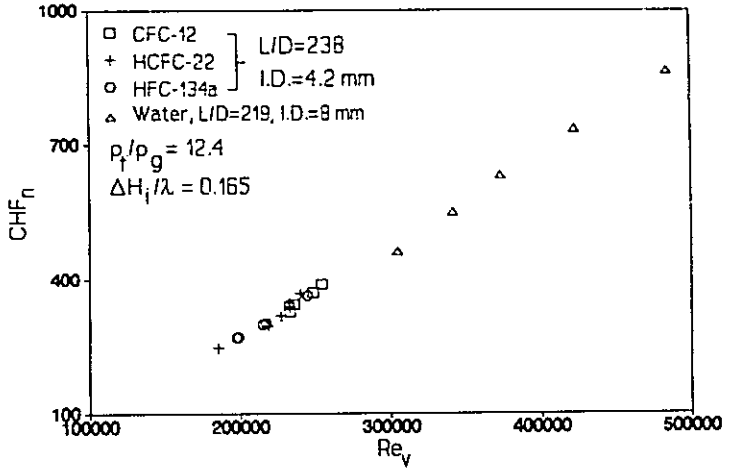

(b)

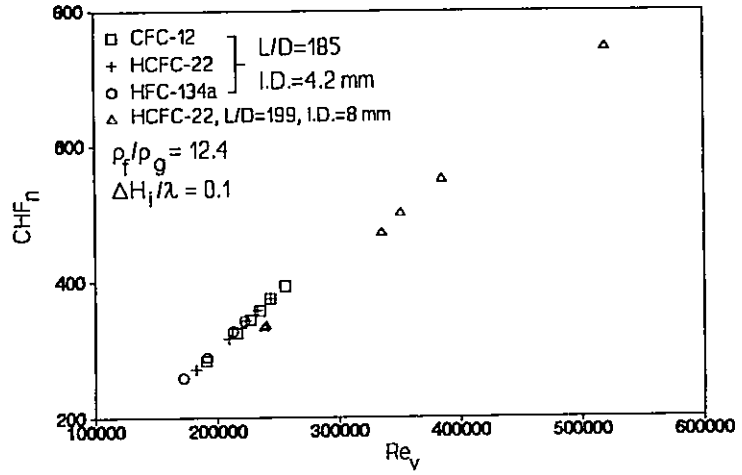

(c)

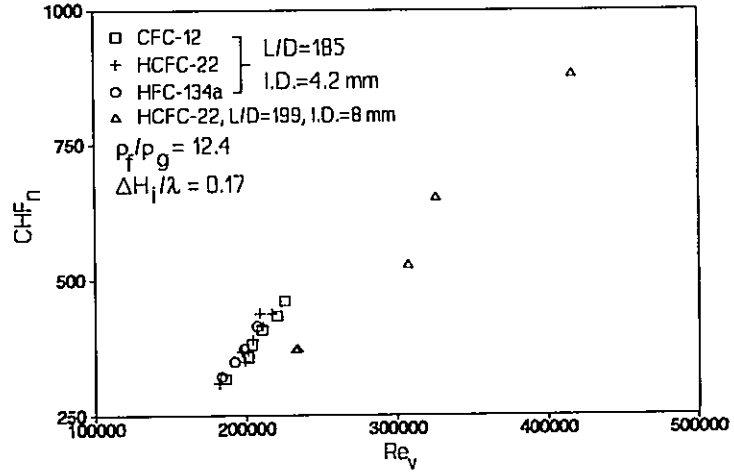

(d)

Figure 5-14 Effect of Re_v on CHF_n at ρ_f/ρ_g= 12.4 and $\Delta H_i/\lambda$= (a) 0.11, (b) 0.165, (c) 0.1 and (d) 0.17.

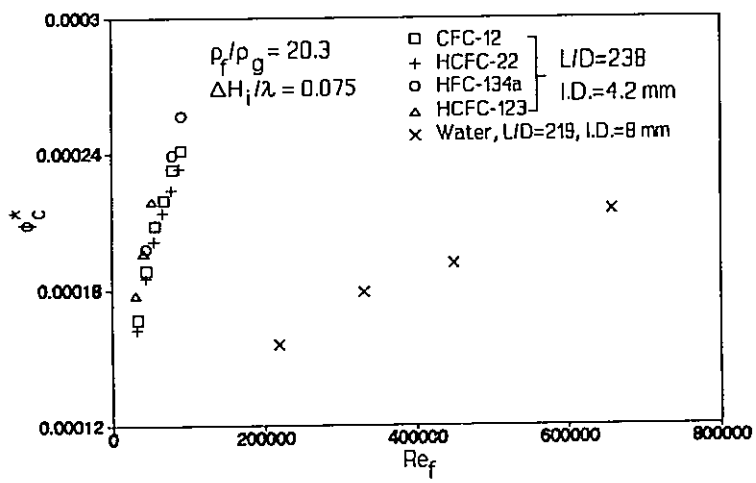

(a)

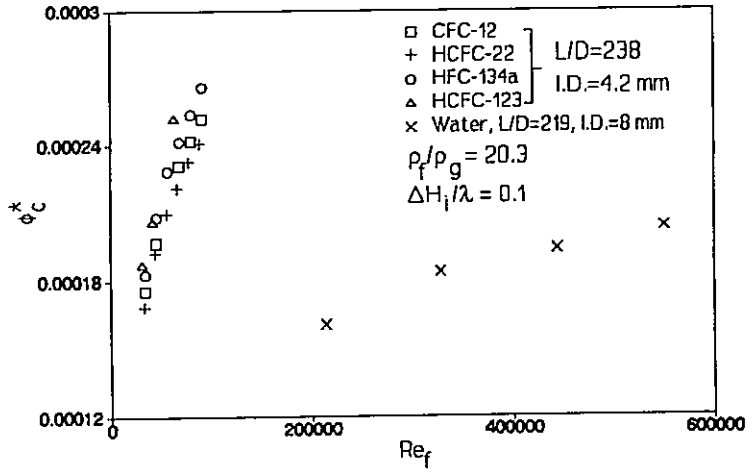

(b)

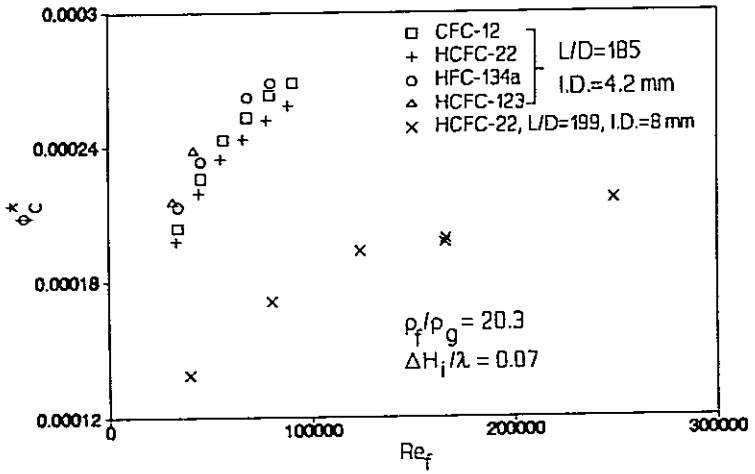

(c)

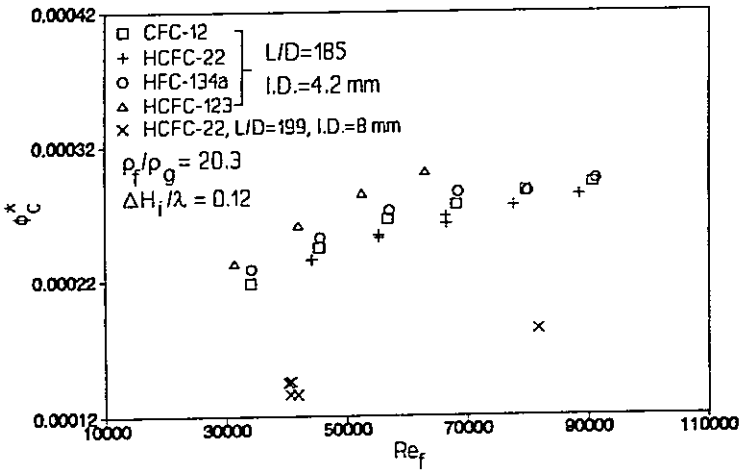

(d)

Figure 5-15 Effect of Re_f on ϕ_c^* at ρ_f/ρ_g= 20.3 and $\Delta H_i/\lambda$= (a) 0.075, (b) 0.1, (c) 0.07 and (d) 0.12.

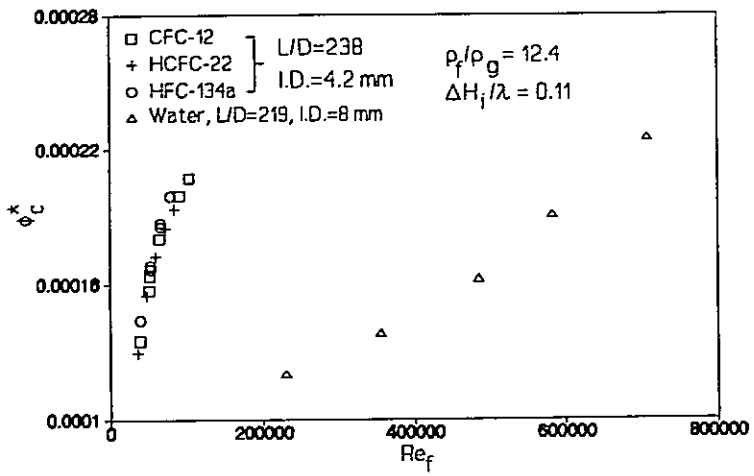

(a)

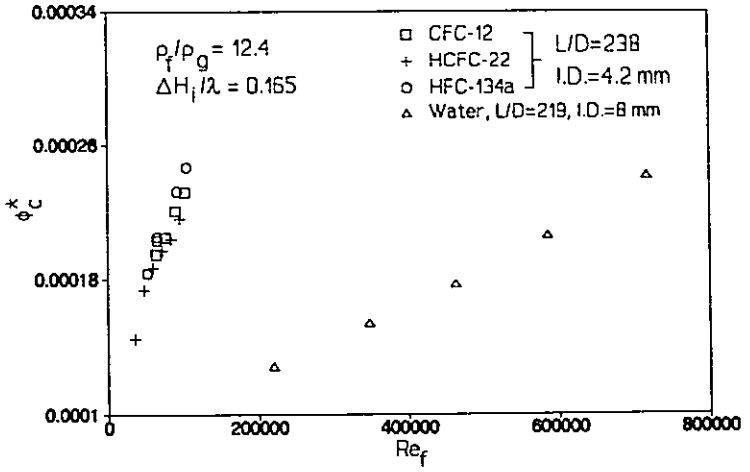

(b)

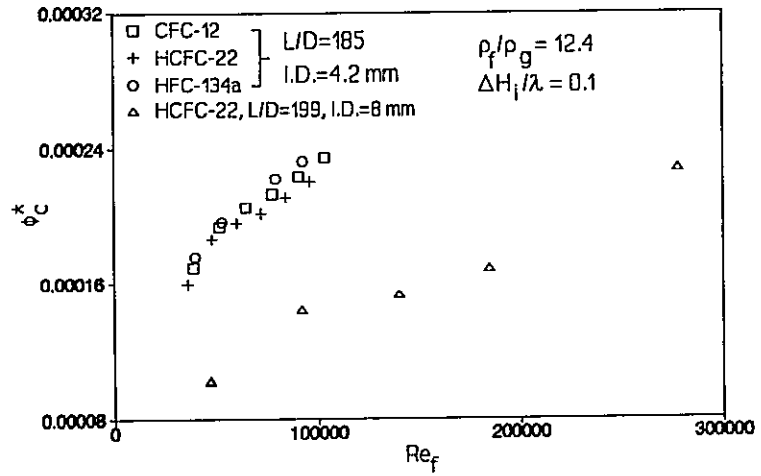

(c)

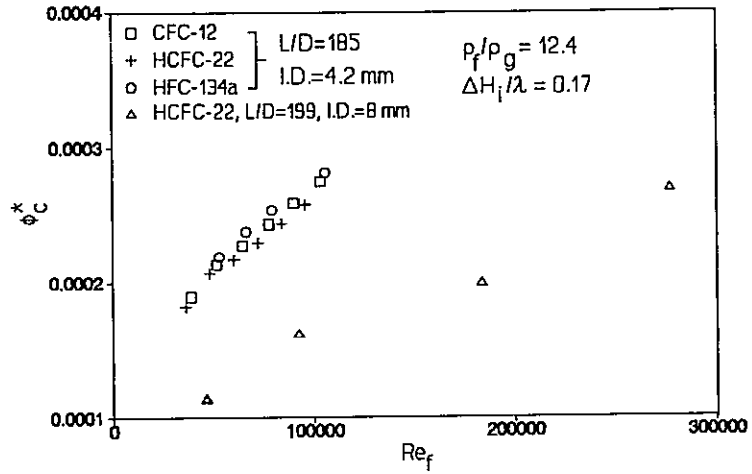

(d)

Figure 5-16 Effect of Re_f on ϕ_c^* at ρ_f/ρ_g= 12.4 and $\Delta H_i/\lambda$= (a) 0.11, (b) 0.165, (c) 0.1 and (d) 0.17.

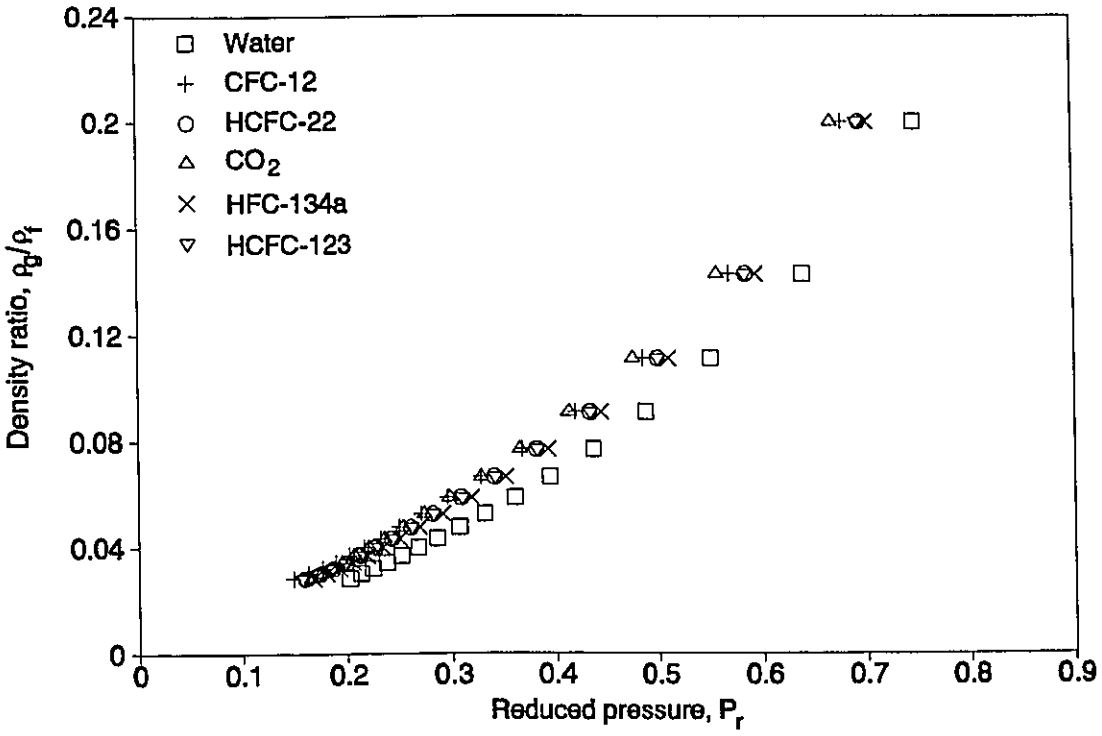

Figure 5-17 Relation between ρ_g/ρ_f and P_r for various fluids.

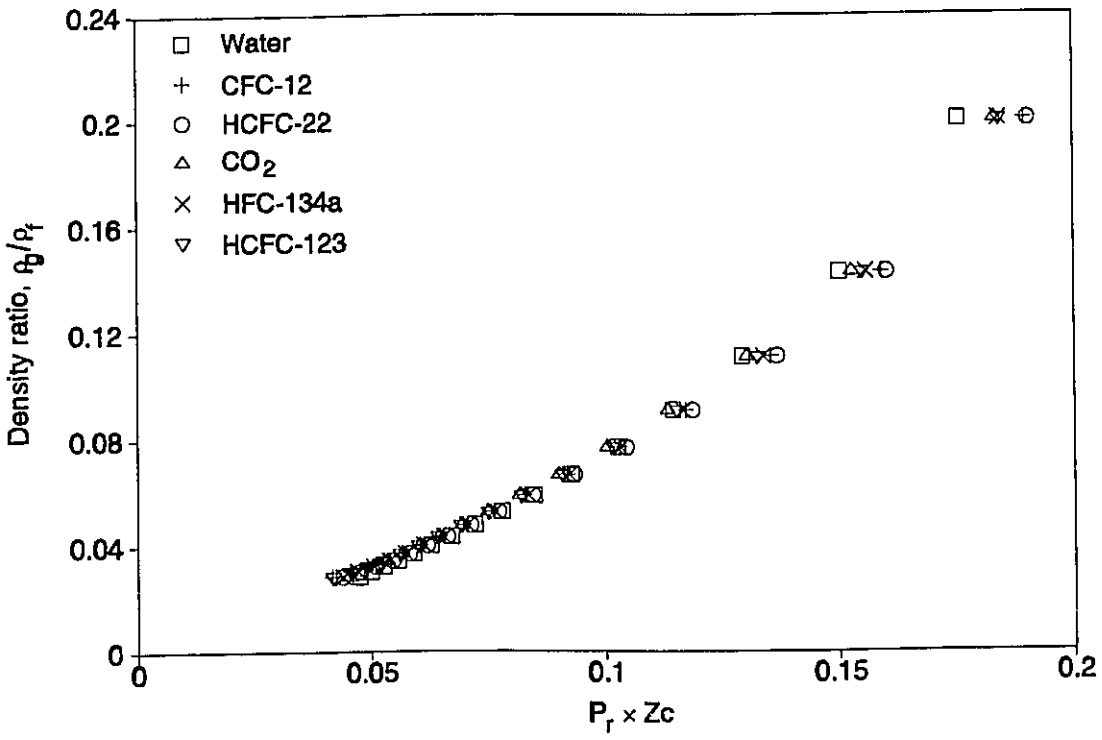

Figure 5-18 Relation between ρ_g/ρ_f and P_rZ_c for various fluids.

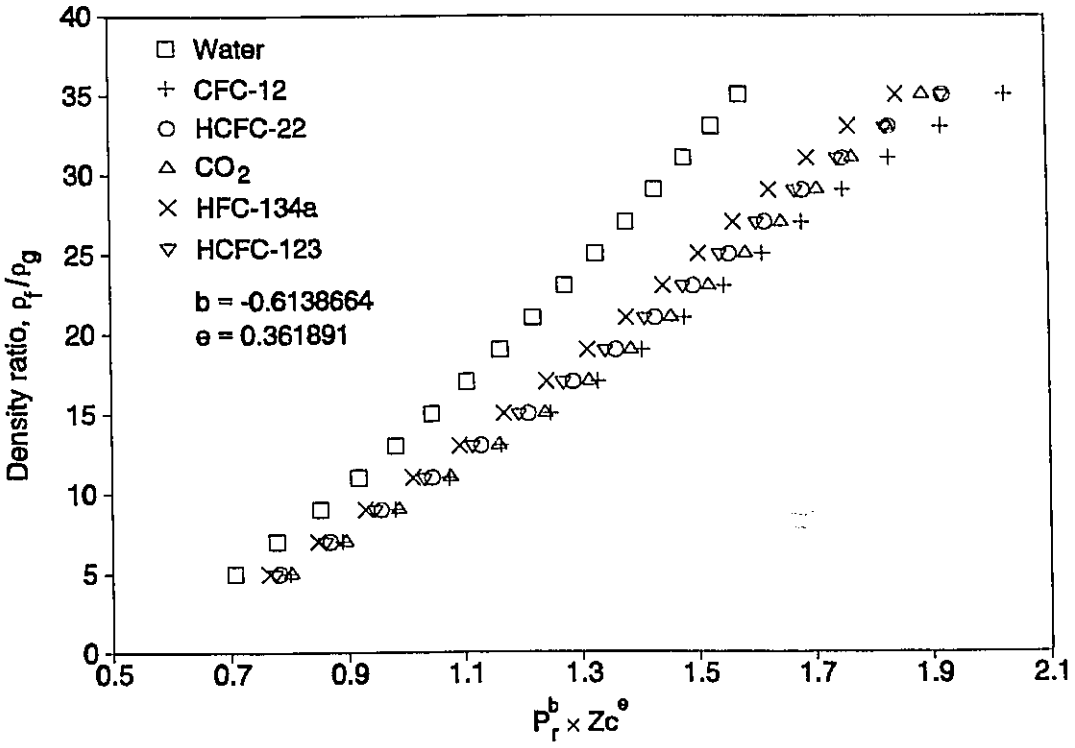

Figure 5-19 Relation between ρ_f/ρ_g and $P_r^b \times Z_c^e$ for various fluids.

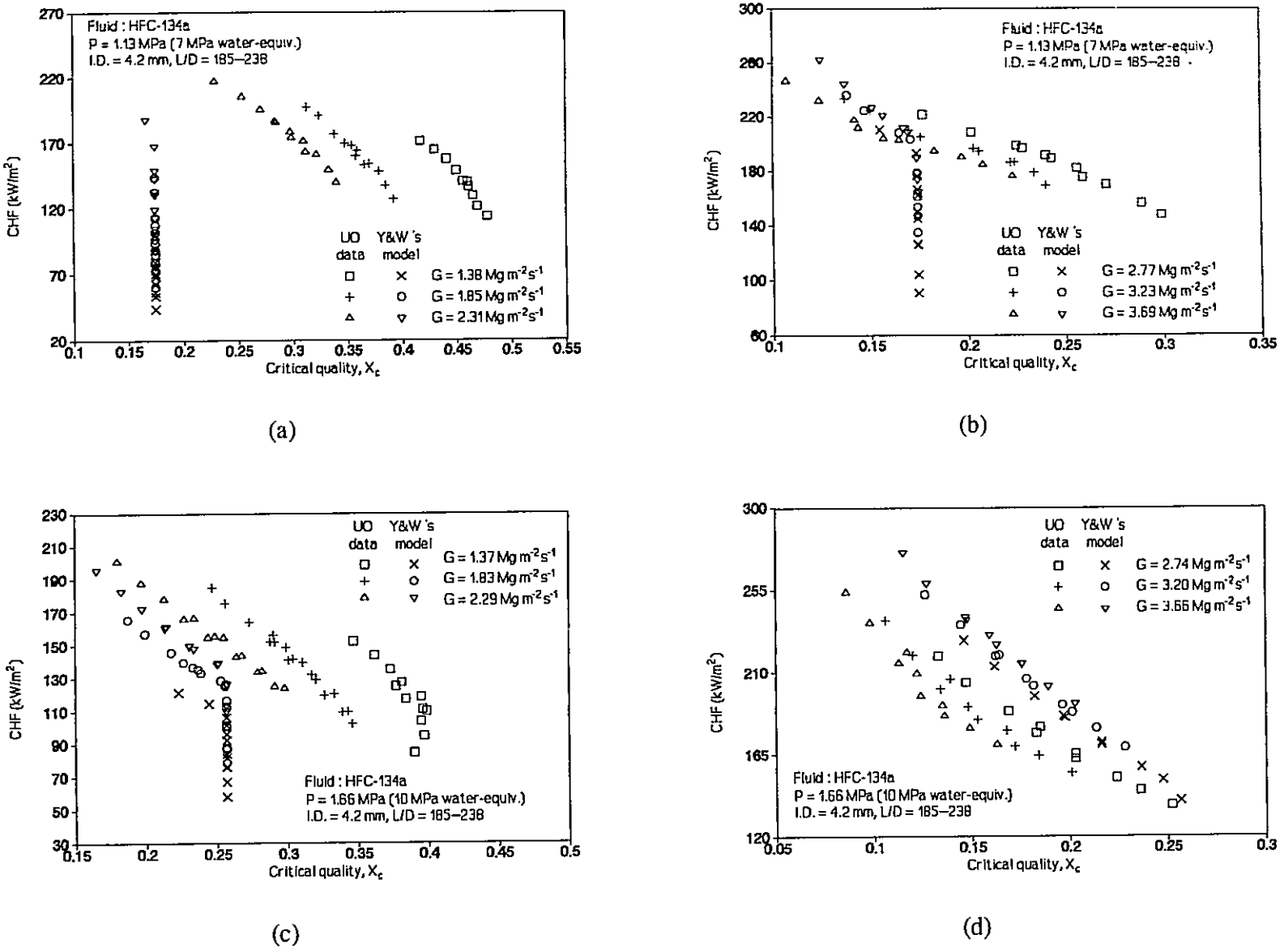

Figure 5-20 Comparison of the mass flux effect on CHF between UO data and Ying and Weisman's model for HFC-134a.

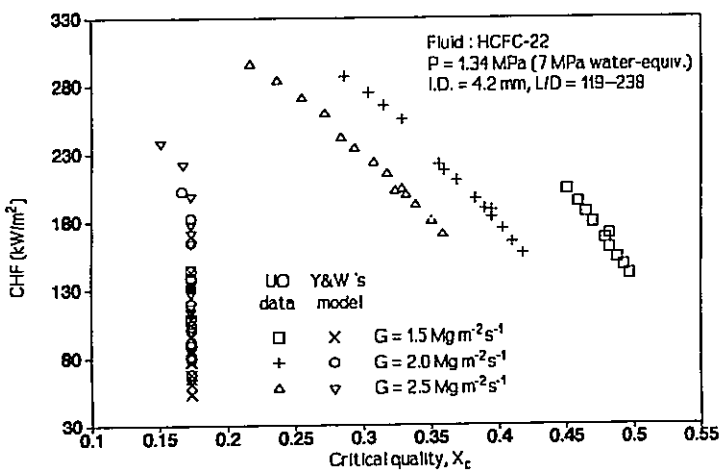

(a)

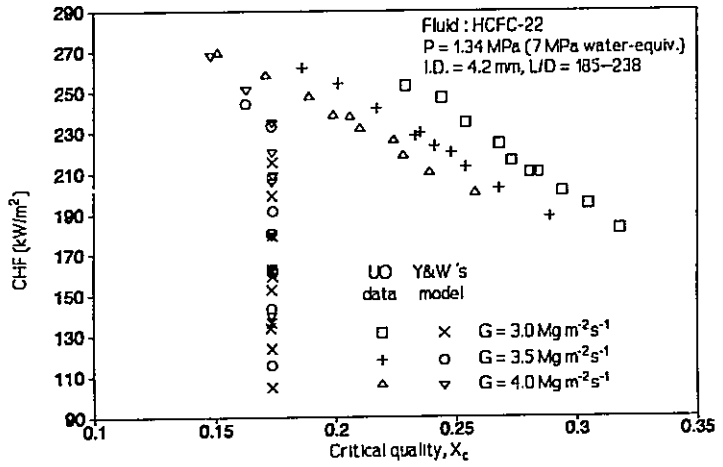

(b)

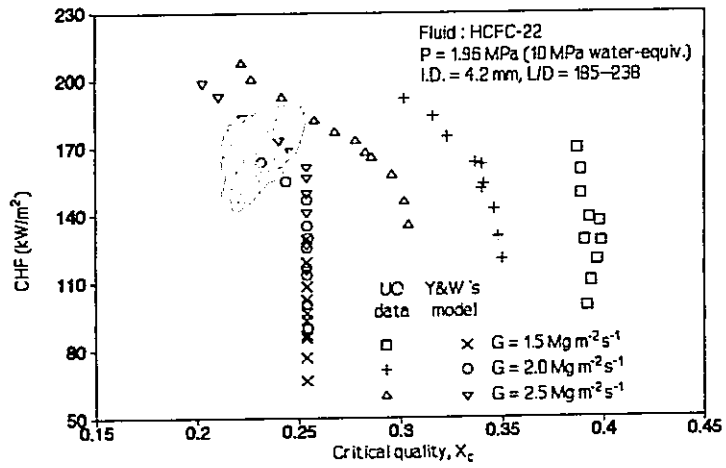

(c)

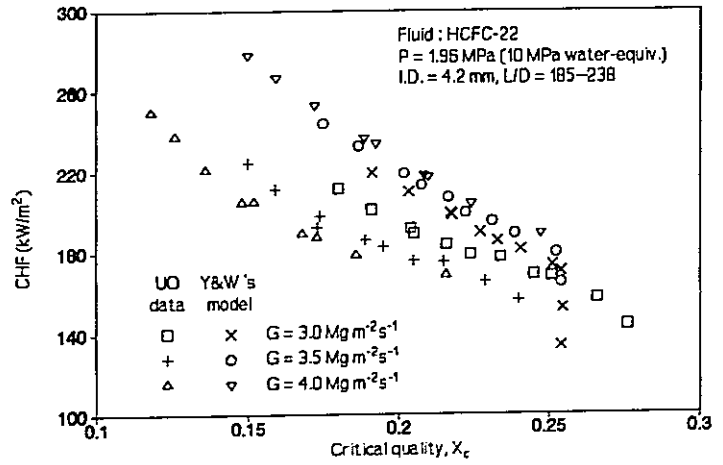

(d)

Figure 5-21 Comparison of the mass flux effect on CHF between UO data and Ying and Weisman's model for HCFC-22.

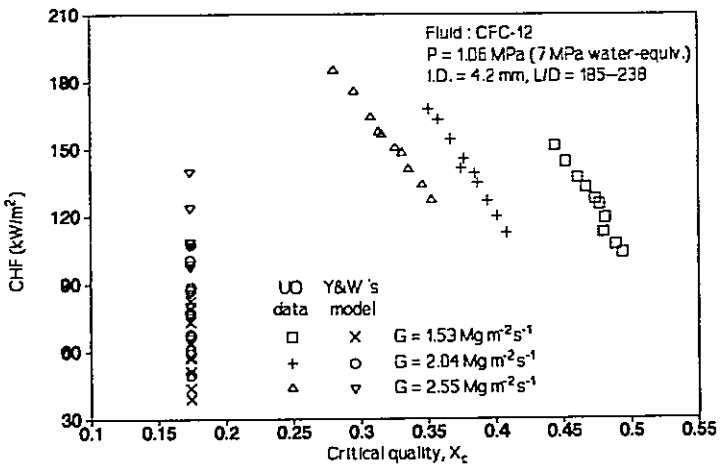

(a)

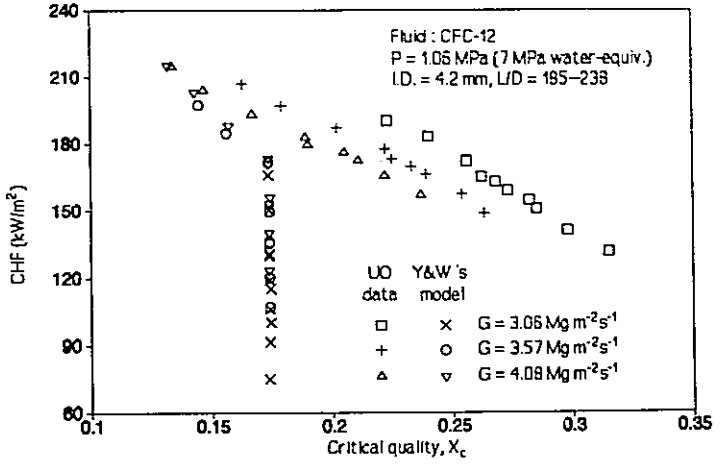

(b)

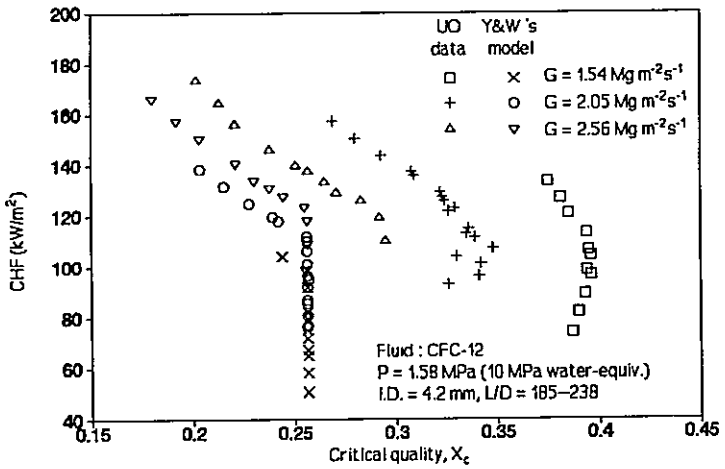

(c)

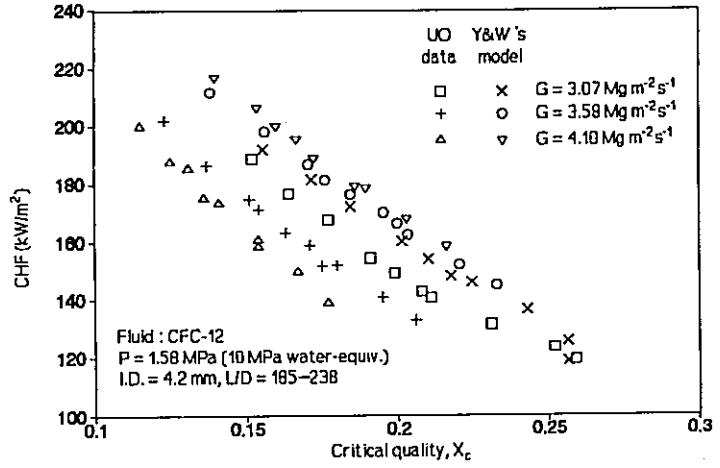

(d)

Figure 5-22 Comparison of the mass flux effect on CHF between UO data and Ying and Weisman's model for CFC-12.

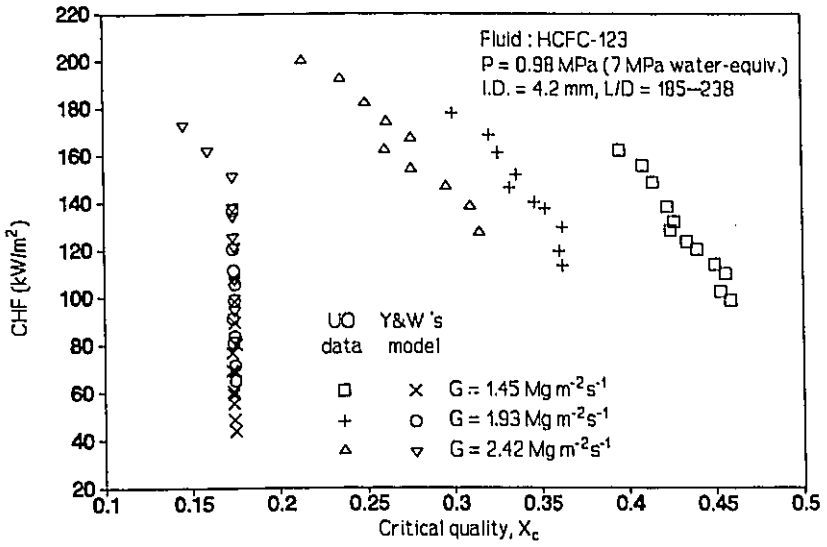

(a)

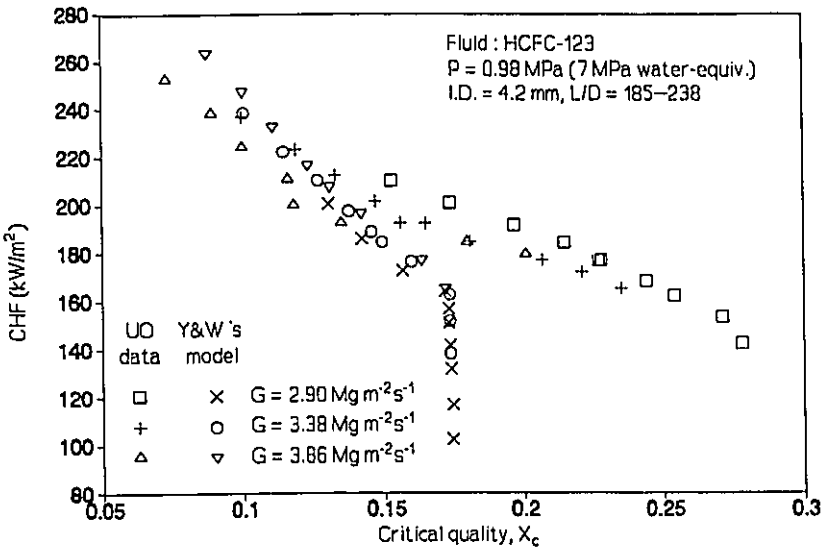

(b)

Figure 5-23 Comparison of the mass flux effect on CHF between UO data and Ying and Weisman's model for HCFC-123.

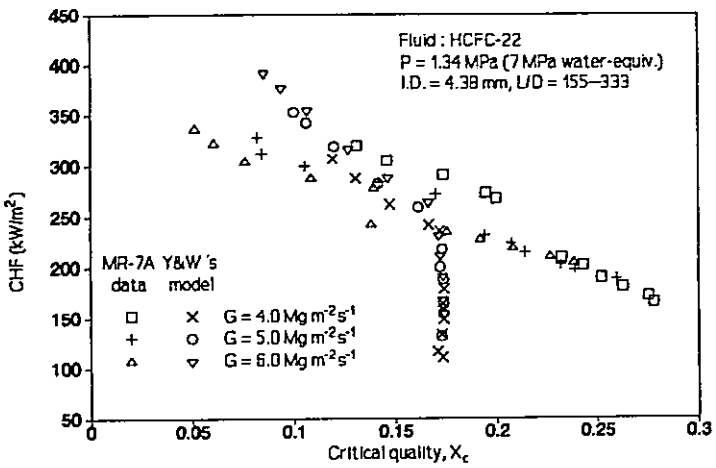

(a)

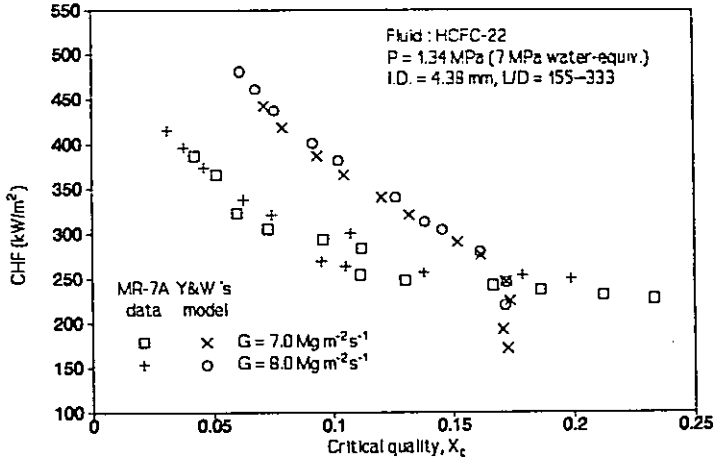

(b)

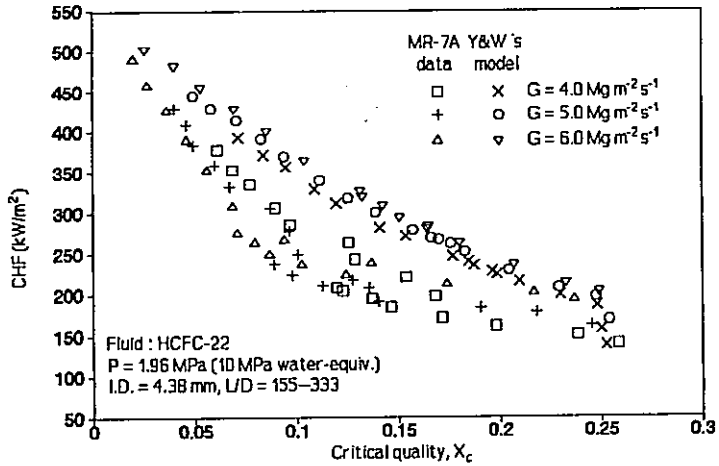

(c)

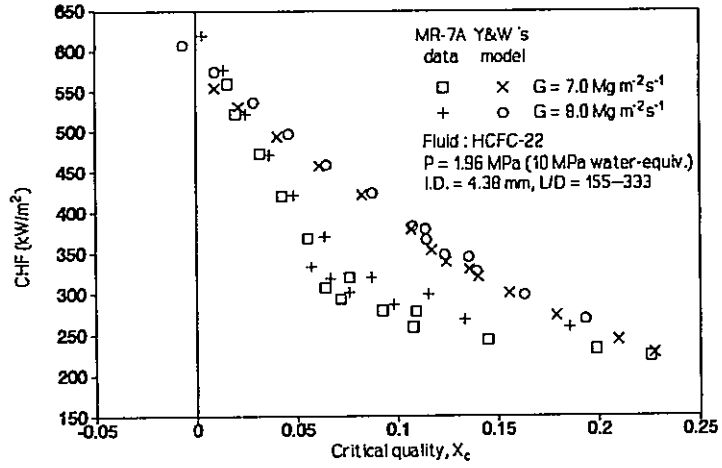

(d)

Figure 5-24 Comparison of the mass flux effect on CHF between MR-7A data and Ying and Weisman's model for HCFC-22.

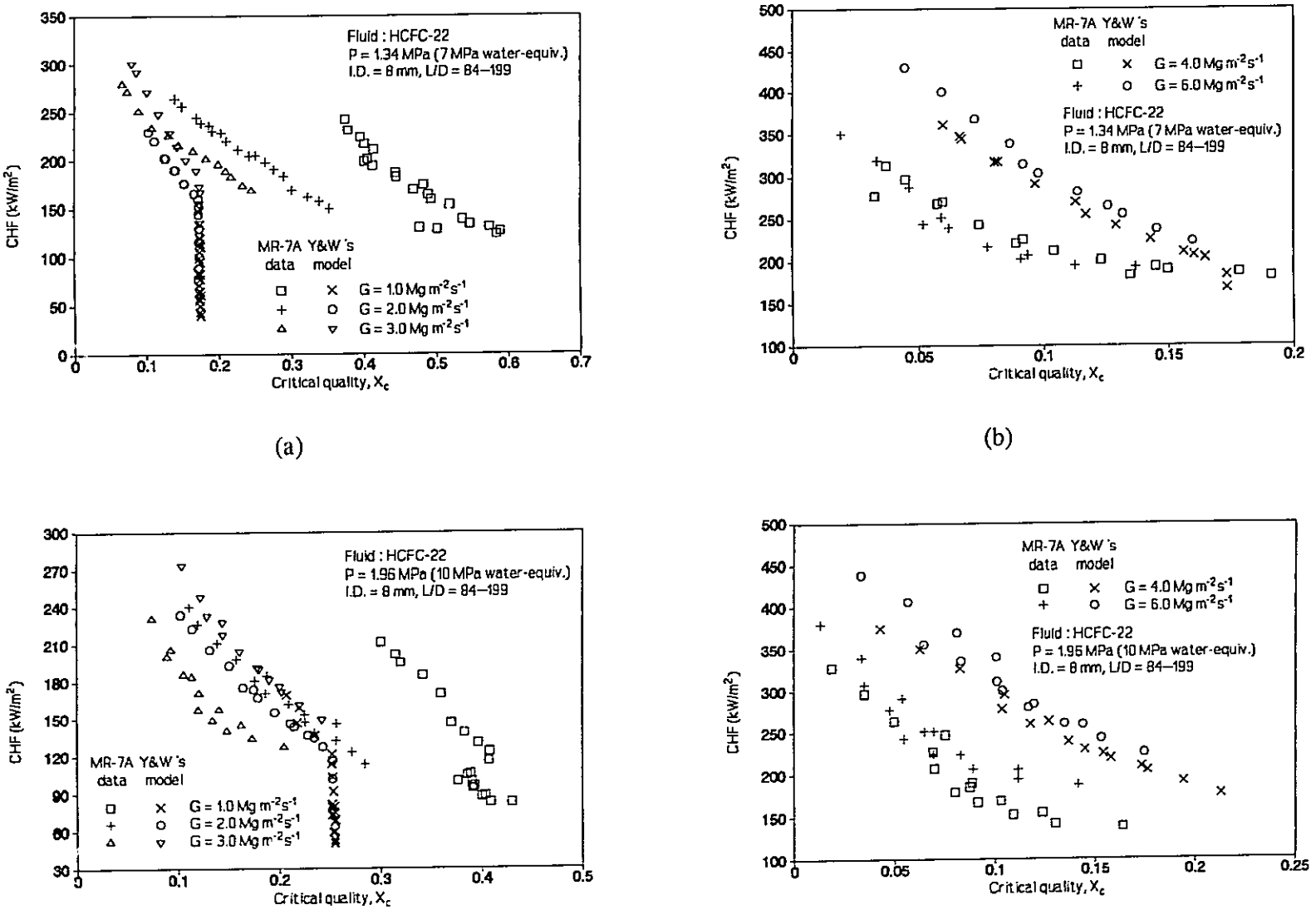

Figure 5-25 Comparison of the mass flux effect on CHF between MR-7A data and Ying and Weisman's model for HCFC-22.

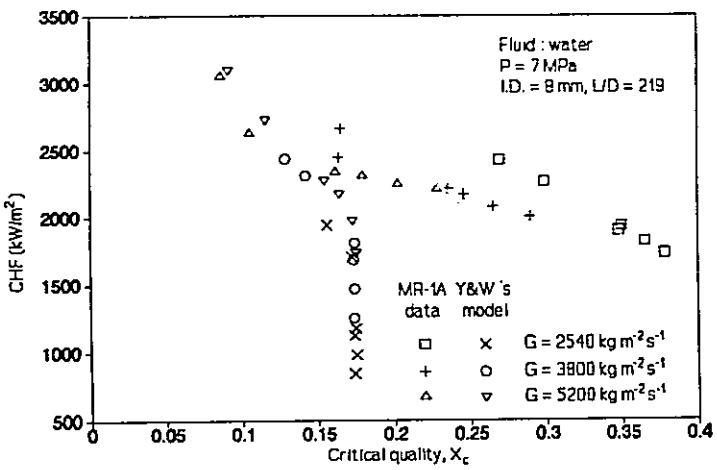

(a)

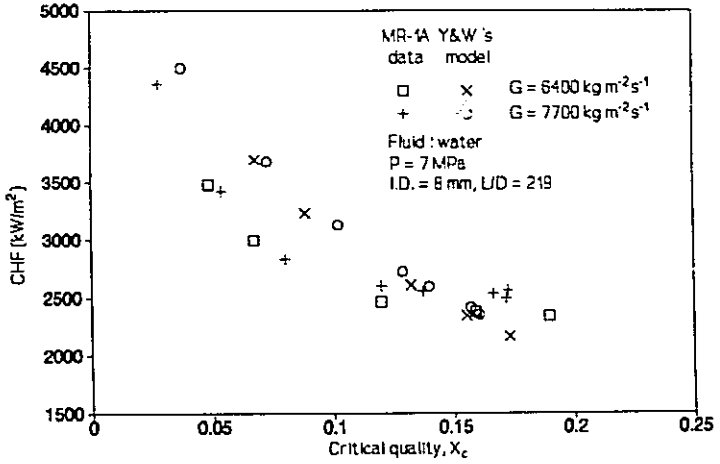

(b)

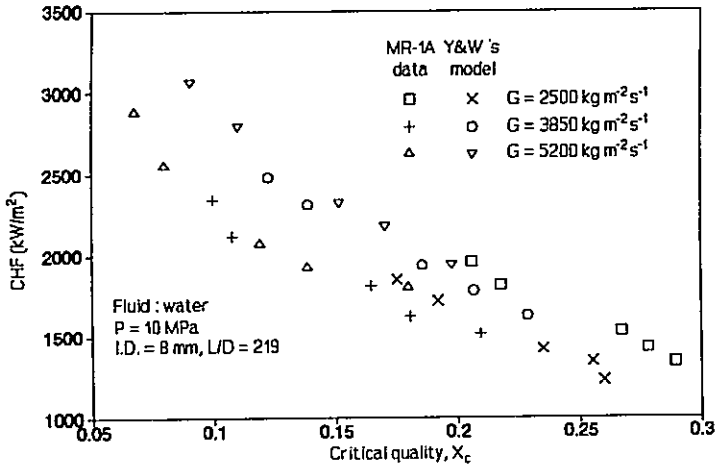

(c)

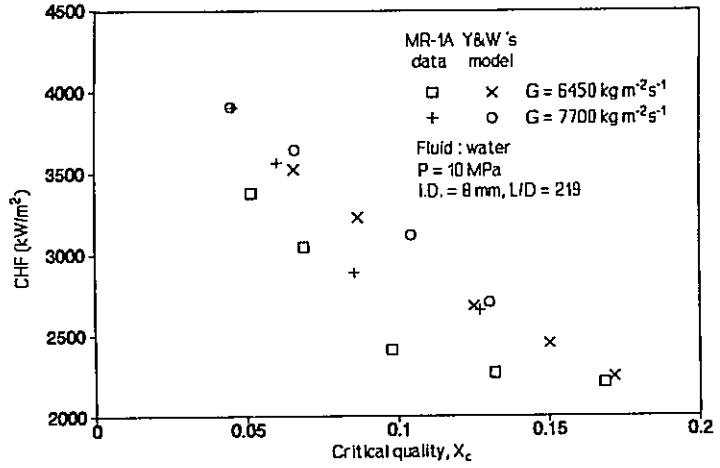

(d)

Figure 5-26 Comparison of the mass flux effect on CHF between MR-1A data and Ying and Weisman's model for water.

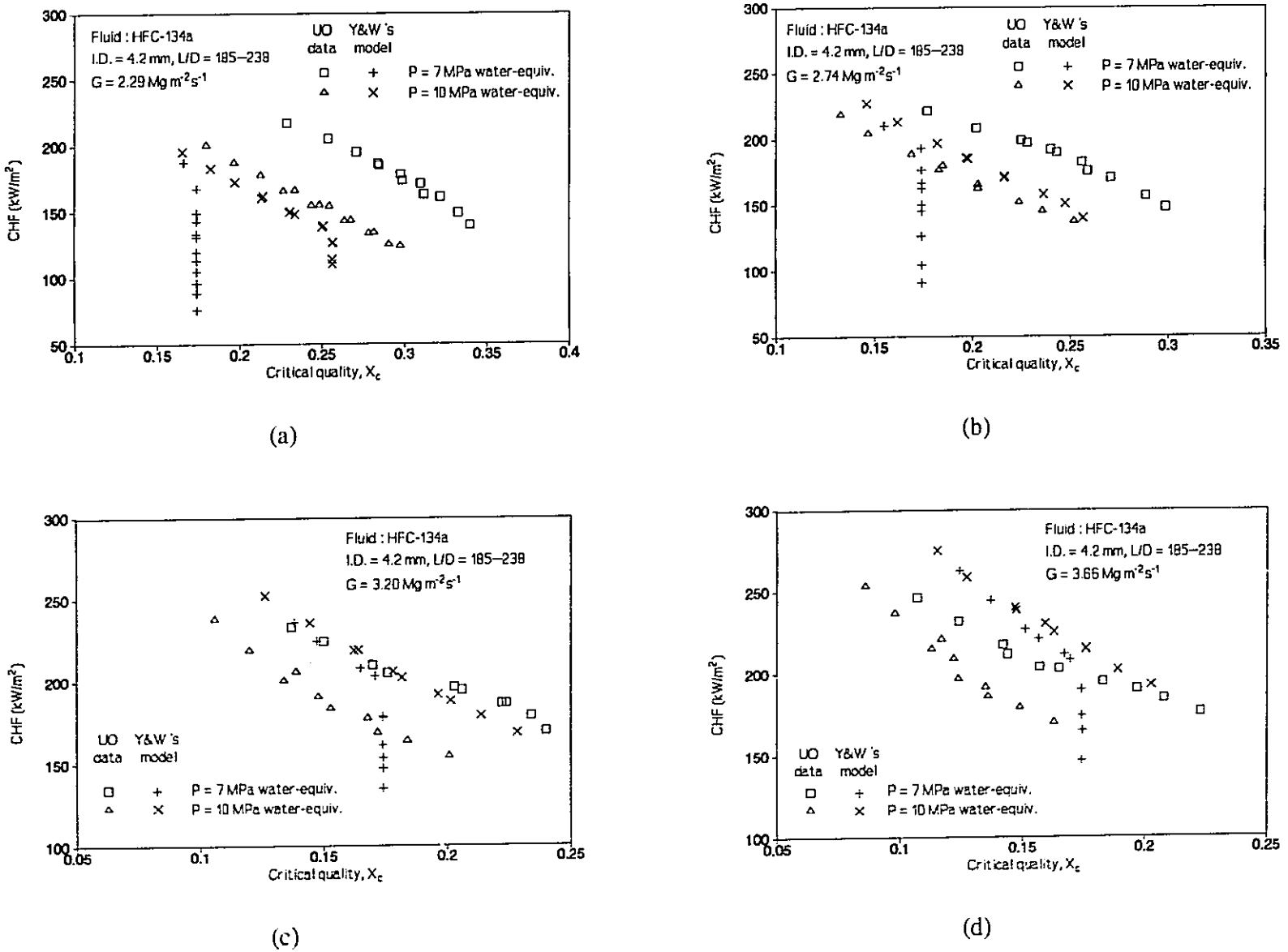

Figure 5-27 Comparison of the pressure effect on CHF between UO data and Ying and Weisman's model for HFC-134a.

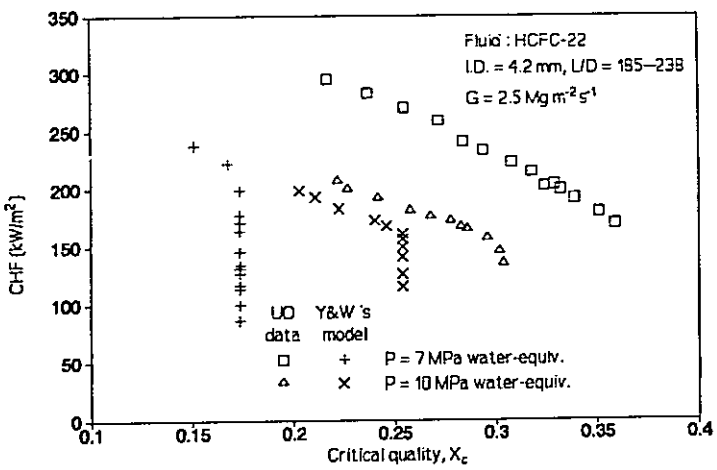

(a)

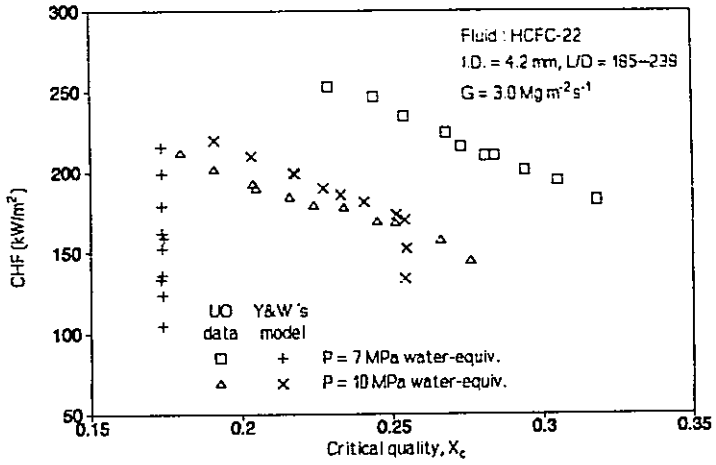

(b)

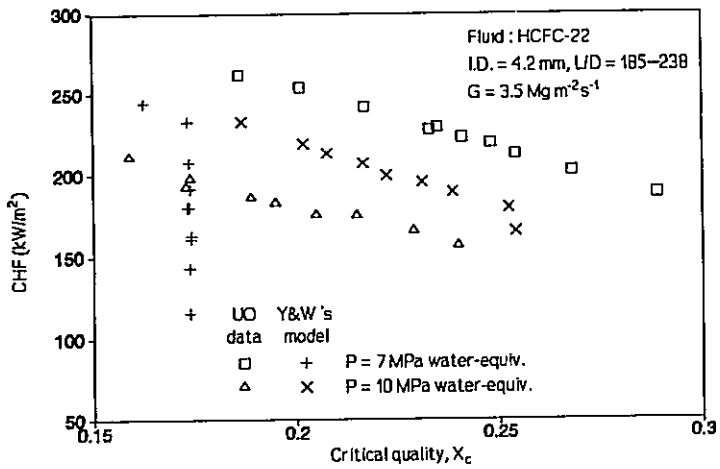

(c)

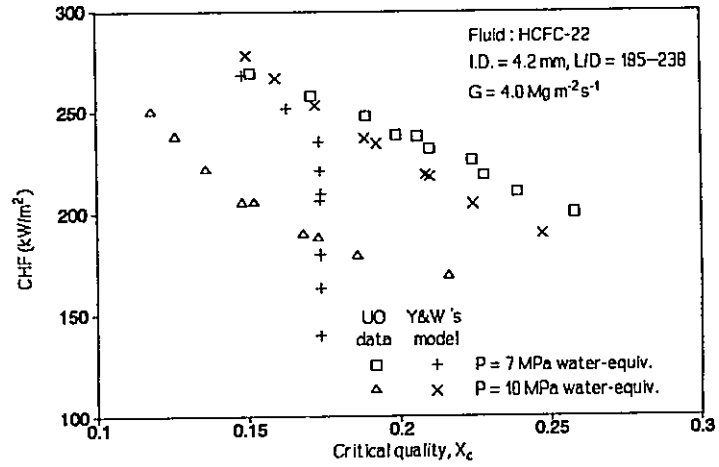

(d)

Figure 5-28 Comparison of the pressure effect on CHF between UO data and Ying and Weisman's model for HCFC-22.

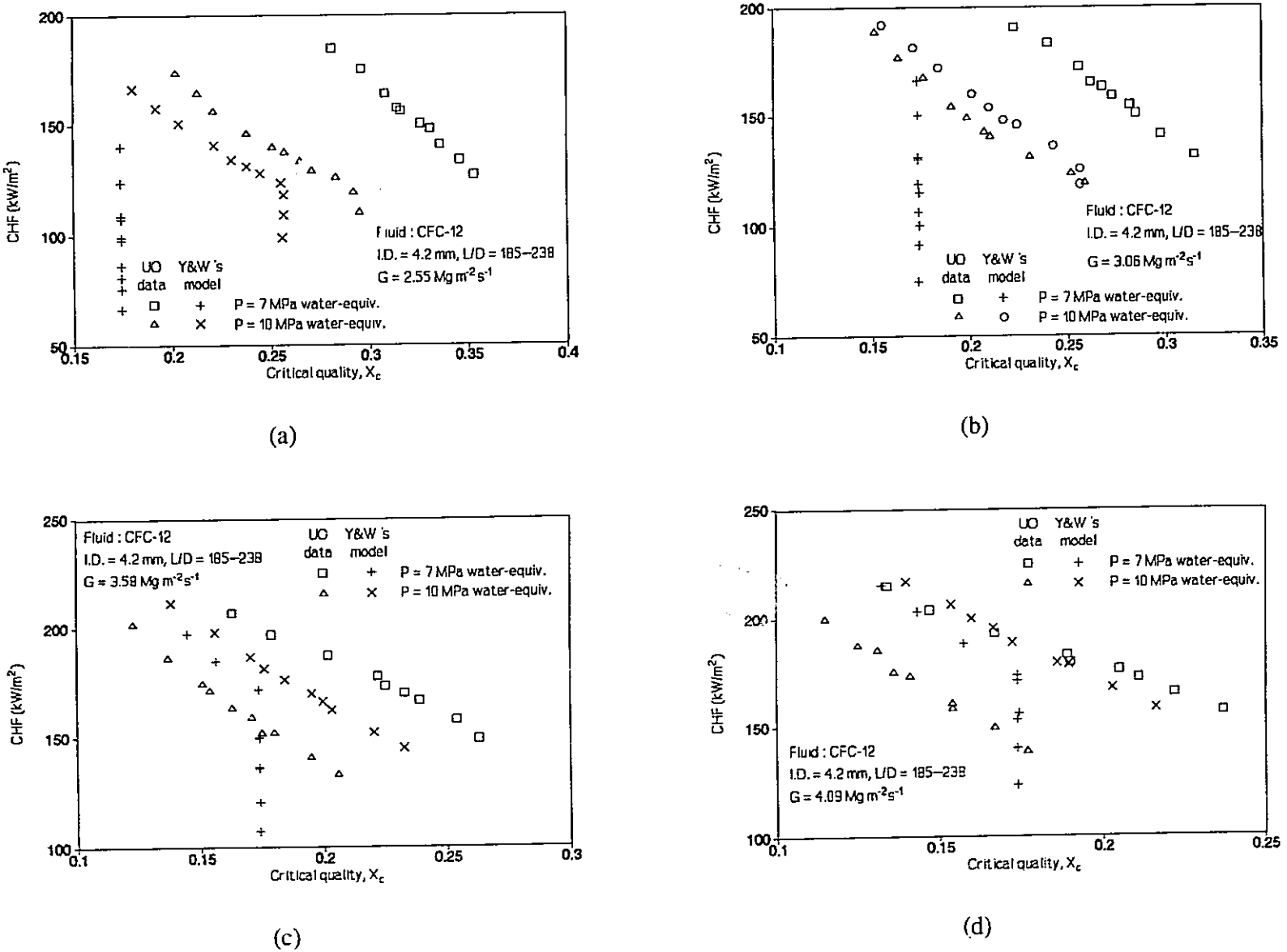

Figure 5-29 Comparison of the pressure effect on CHF between UO data and Ying and Weisman's model for CFC-12.

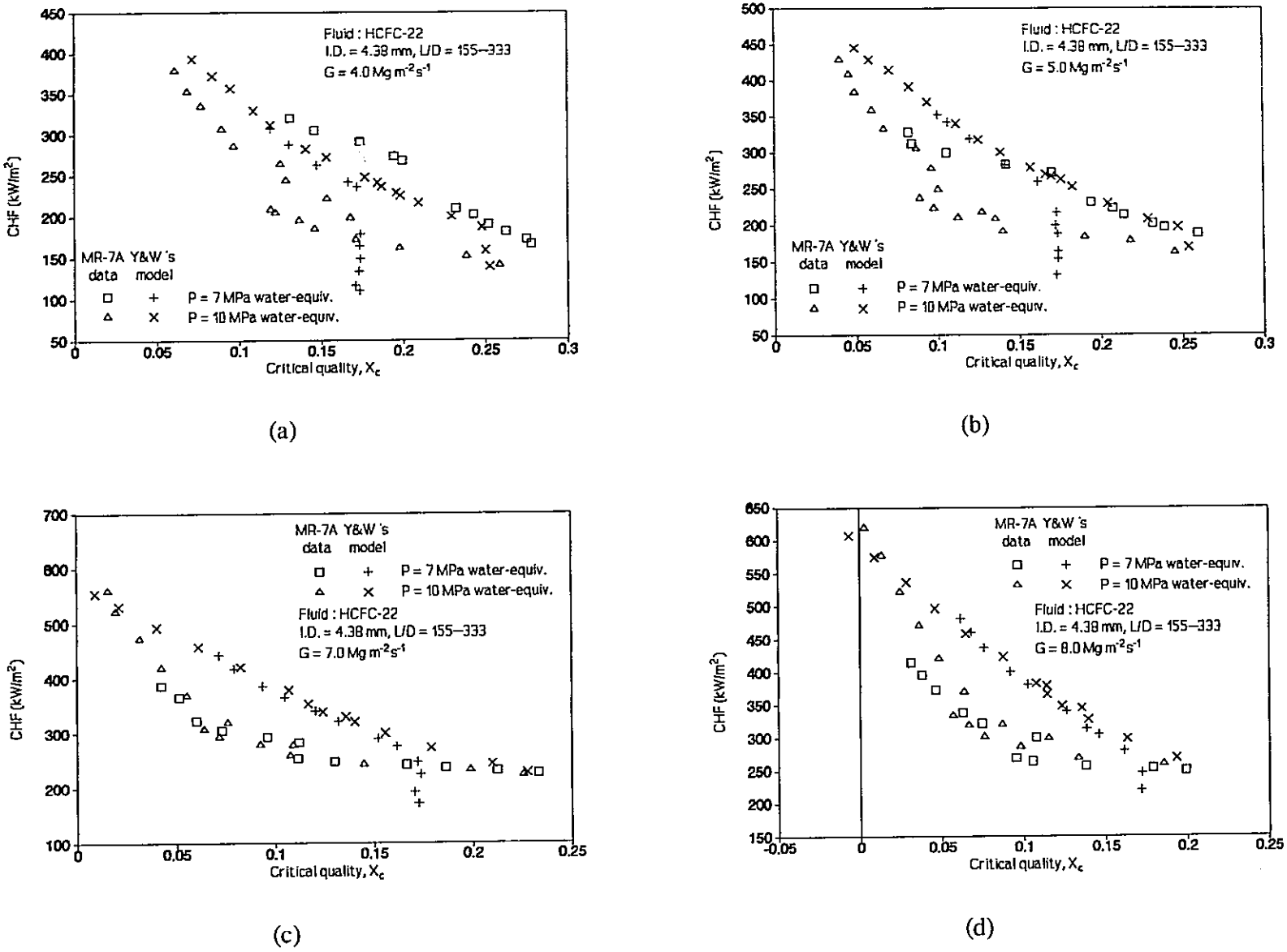

Figure 5-30 Comparison of the pressure effect on CHF between MR-7A data and Ying and Weisman's model for HCFC-22.

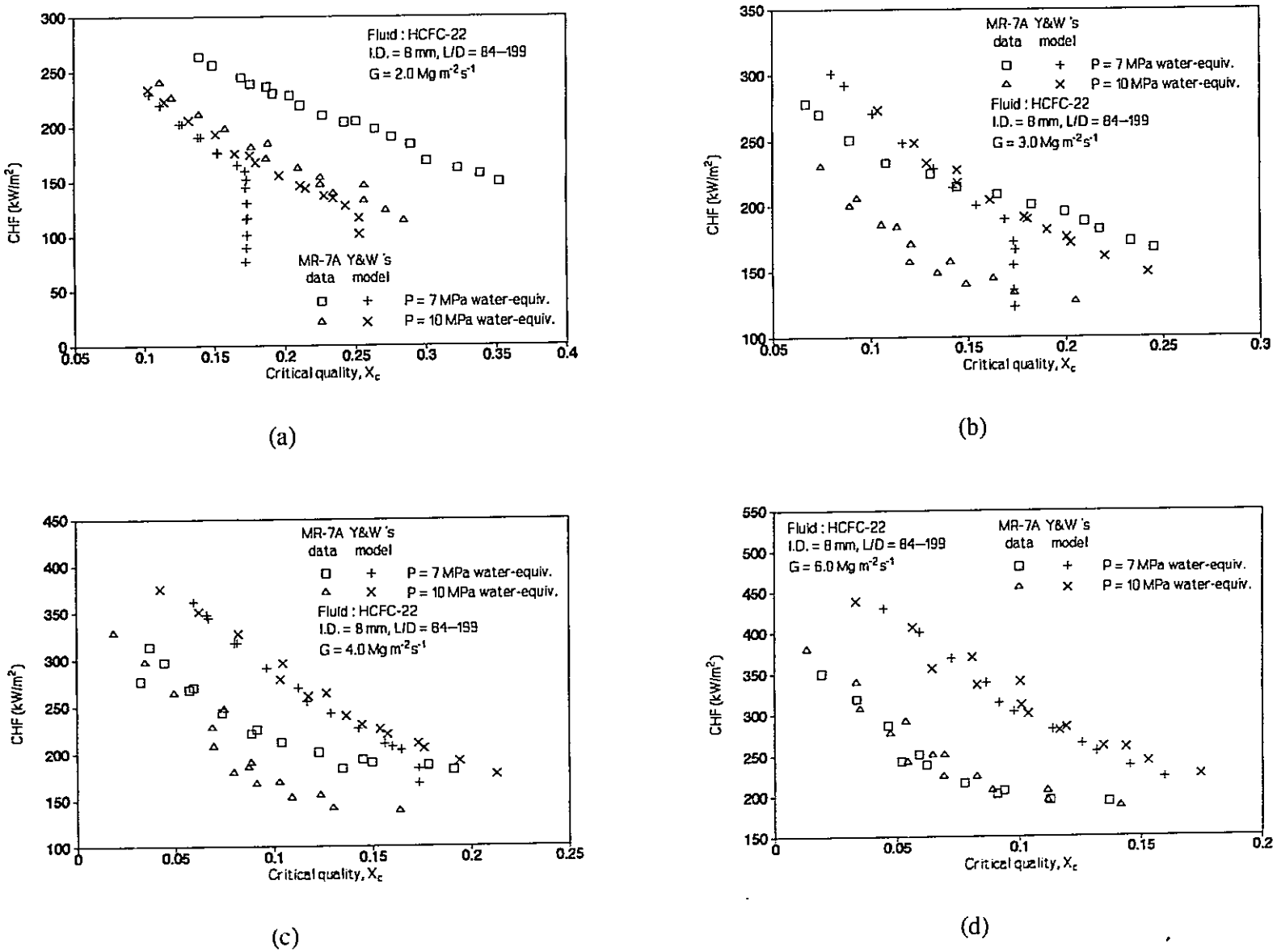

Figure 5-31 Comparison of the pressure effect on CHF between MR-7A data and Ying and Weisman's model for HCFC-22.

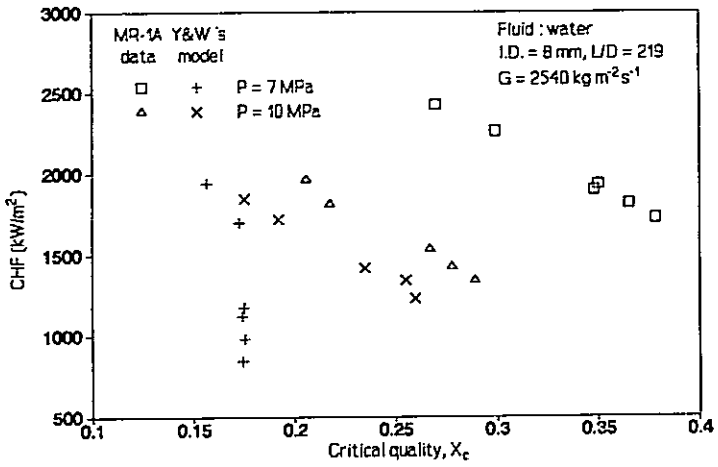

(a)

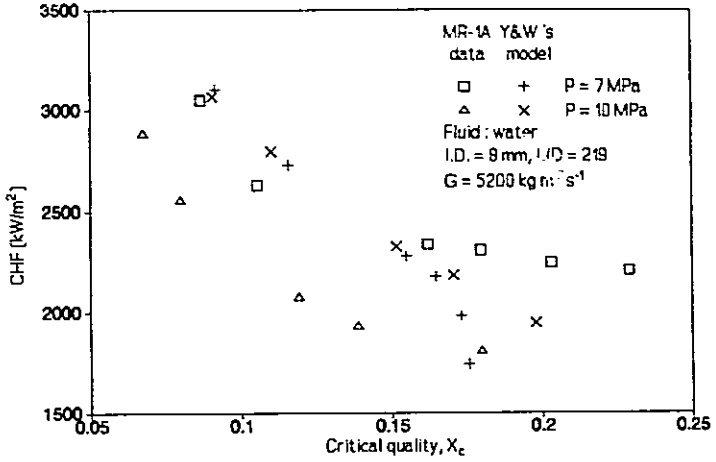

(b)

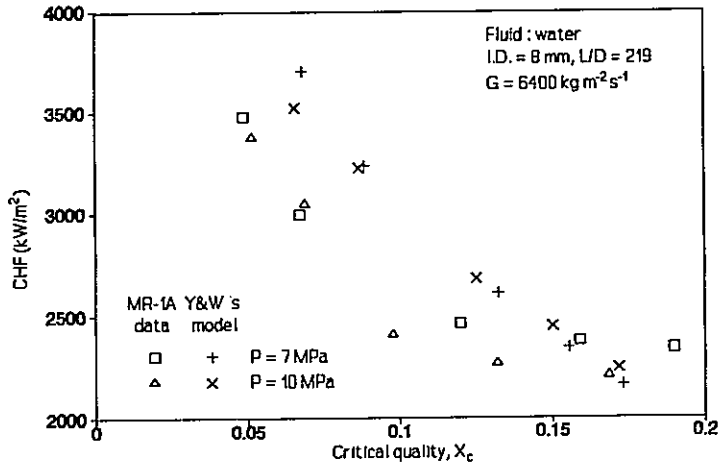

(c)

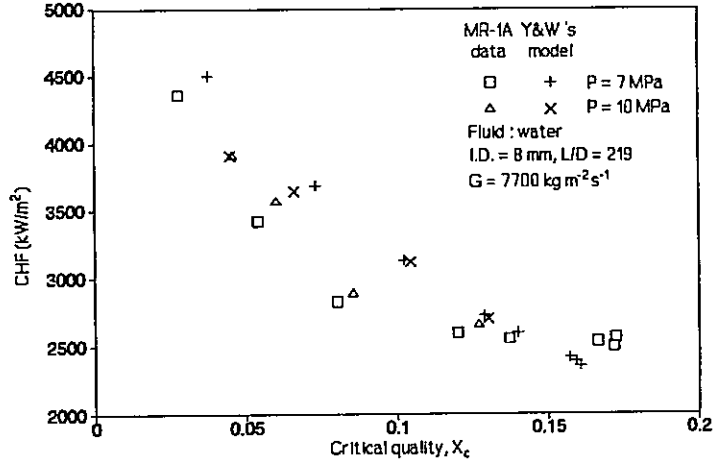

(d)

Figure 5-32 Comparison of the pressure effect on CHF between MR-1A data and Ying and Weisman's model for water.

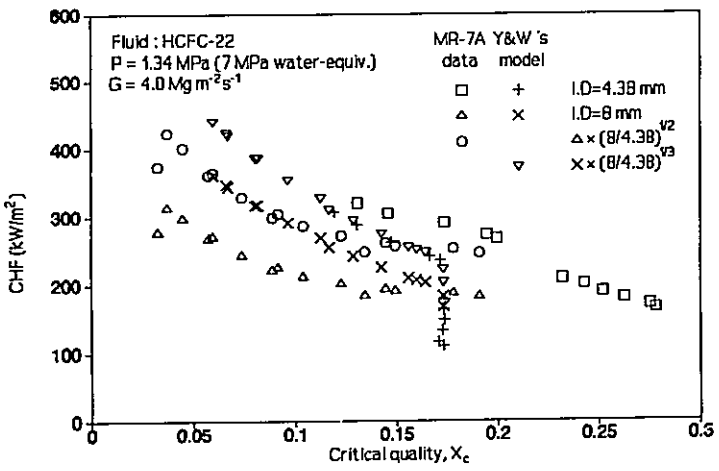

(a)

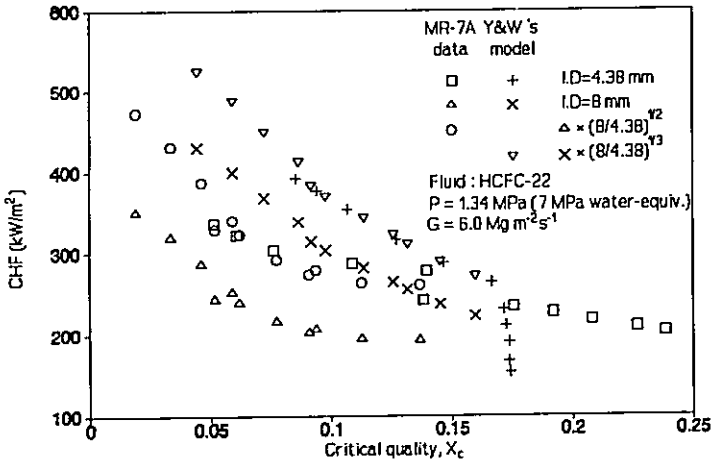

(b)

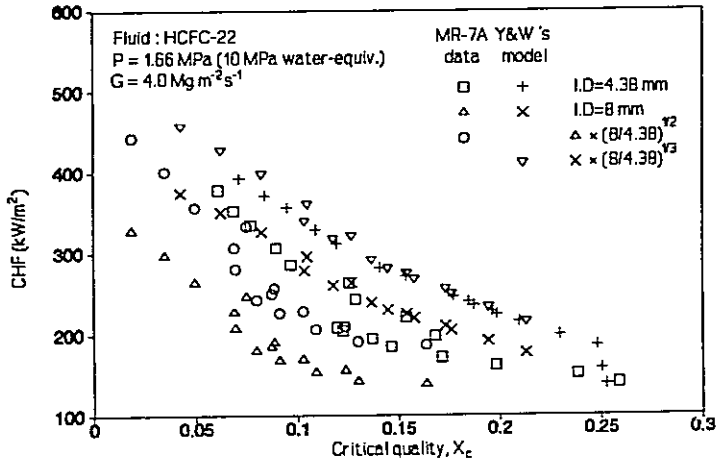

(c)

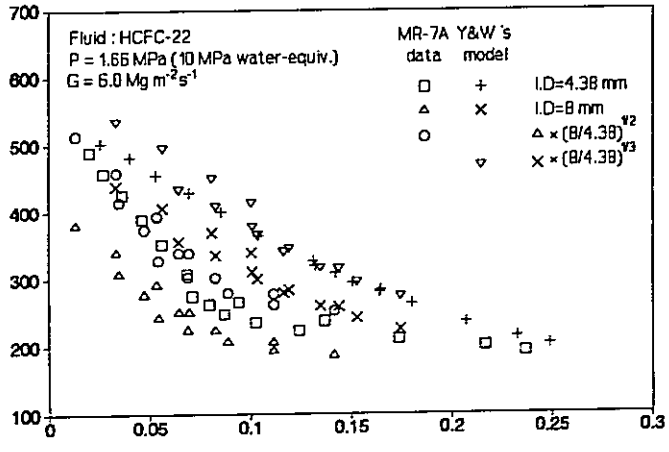

(d)

Figure 5-33 Comparison of the diameter effect on CHF between MR-7A data and Ying and Weisman's model for HCFC-22.

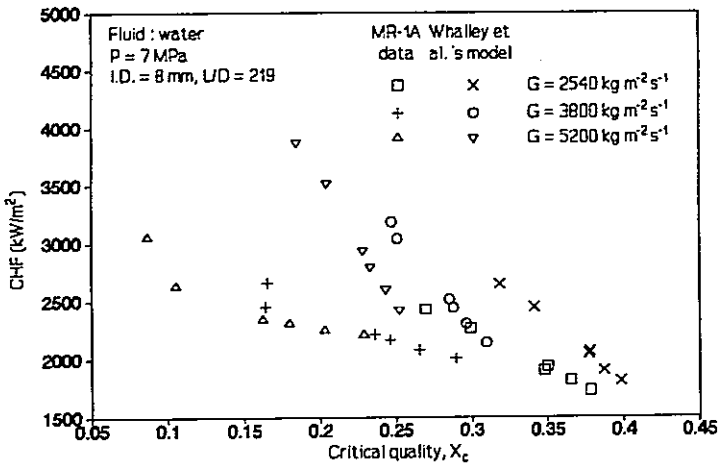

(a)

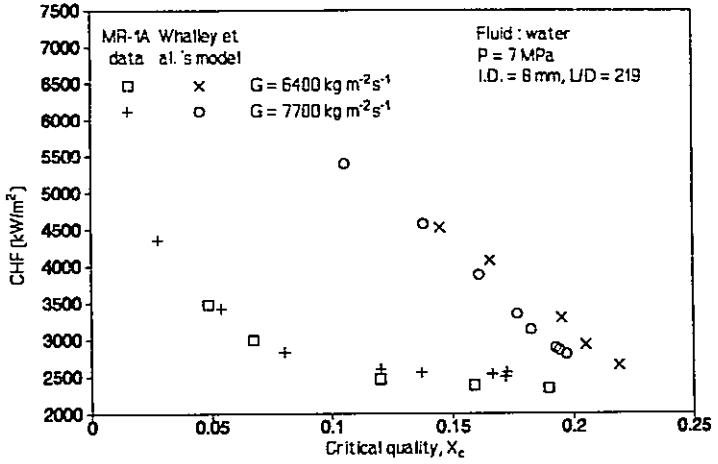

(b)

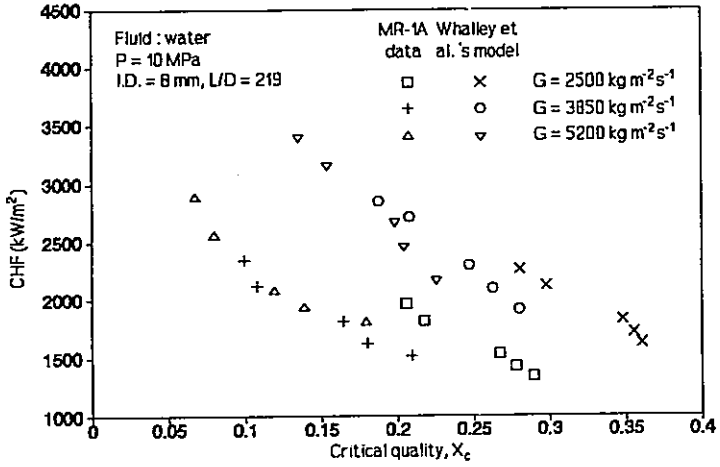

(c)

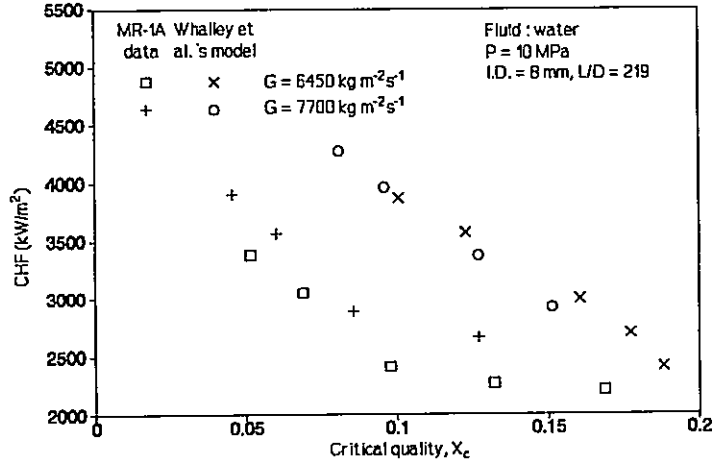

(d)

Figure 5-34 Comparison of the mass flux effect on CHF between MR-1A data and Whalley et al.'s model for water.

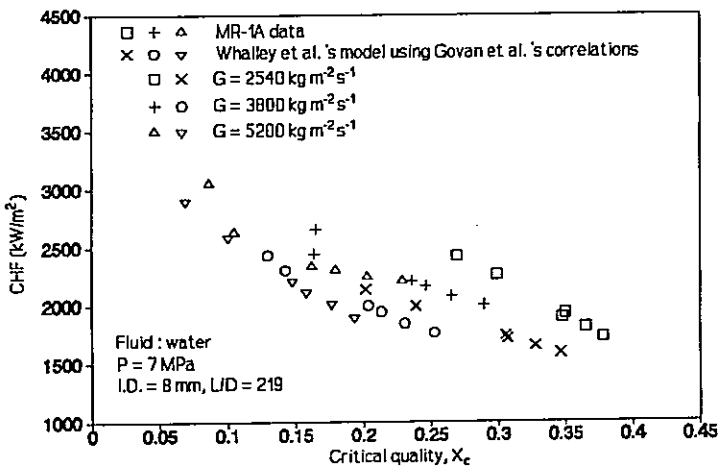

(a)

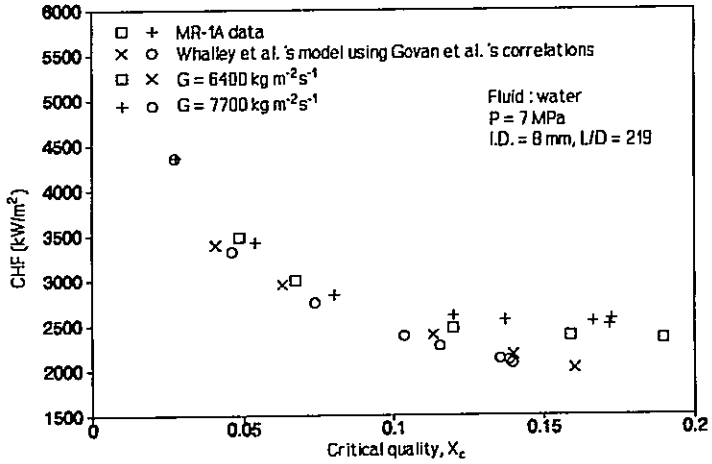

(b)

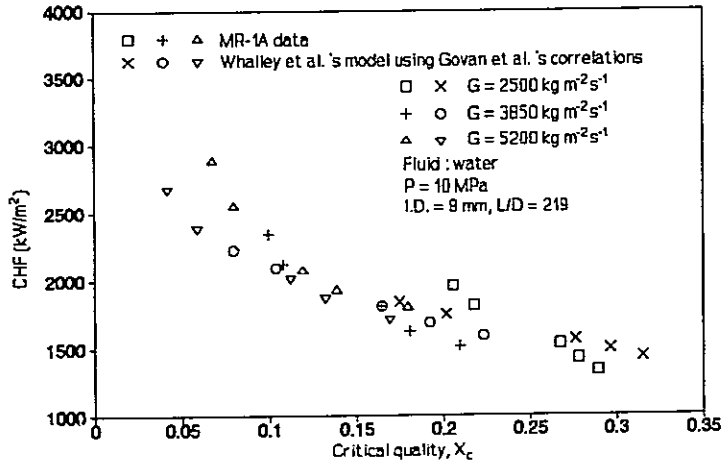

(c)

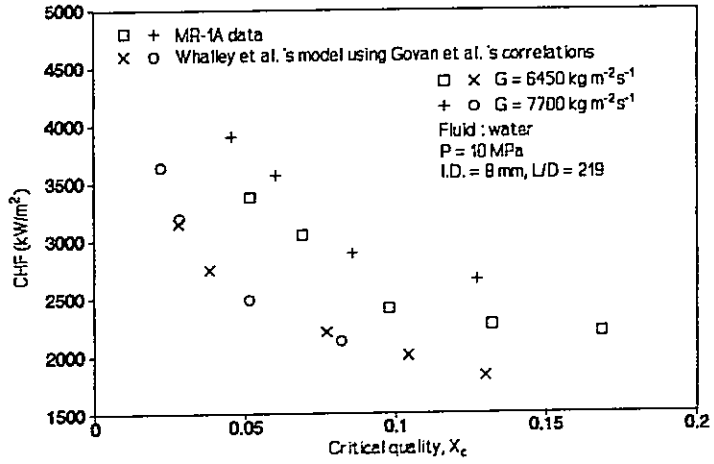

(d)

Figure 5-35 Comparison of the mass flux effect on CHF between MR-1A data and Whalley et al.'s model using Govan et al.'s correlations for water.

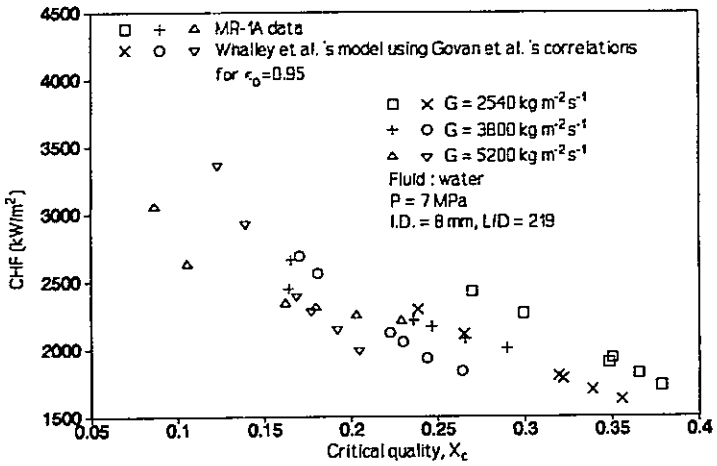

(a)

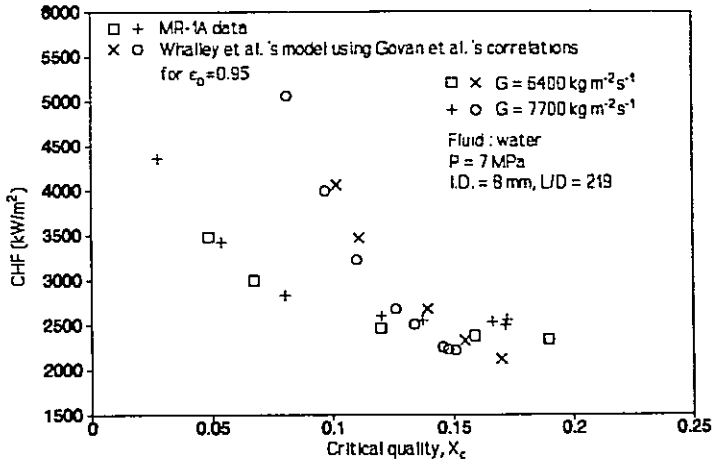

(b)

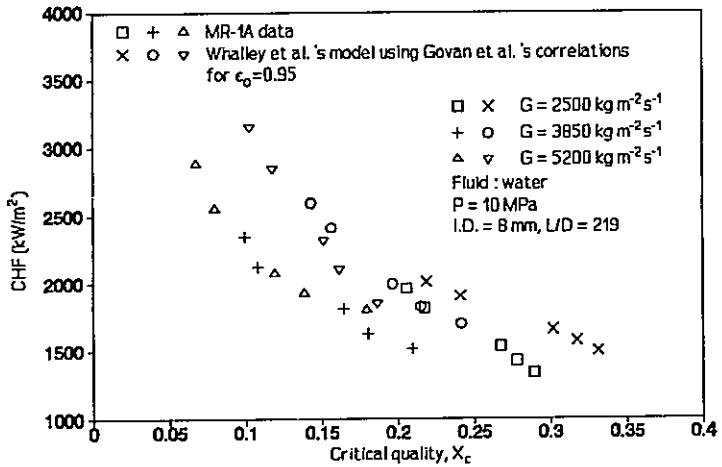

(c)

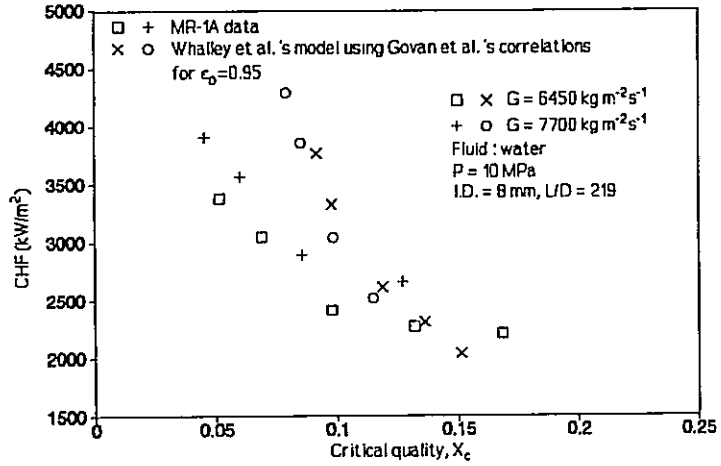

(d)

Figure 5-36 Comparison of the test CHF from MR-1A loop against Whalley et al.'s model using Govan et al.'s correlations for water when ε_o=0.95.

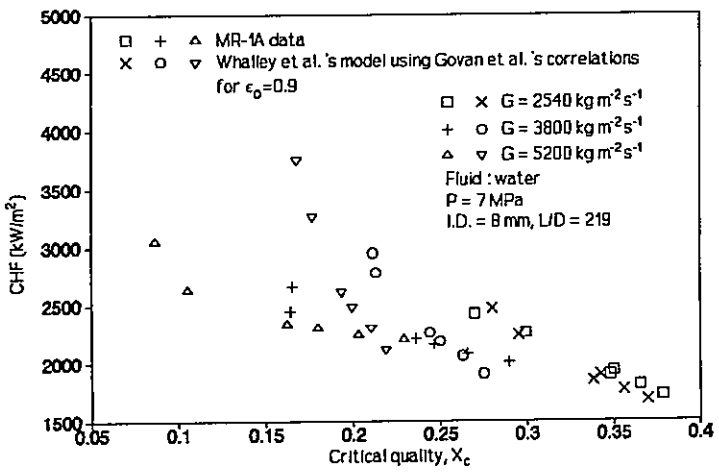

(a)

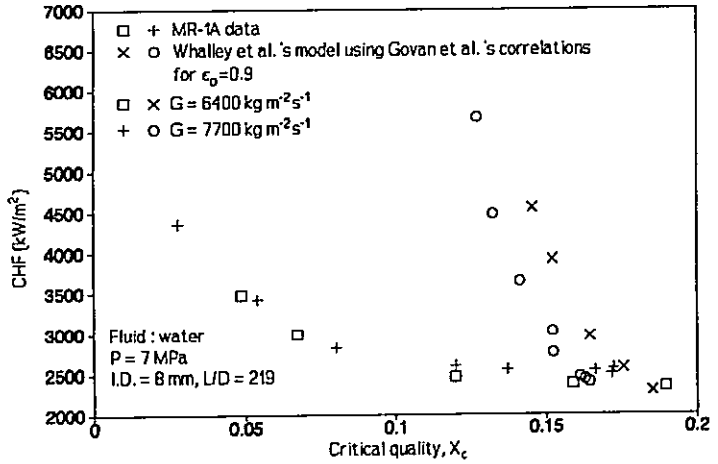

(b)

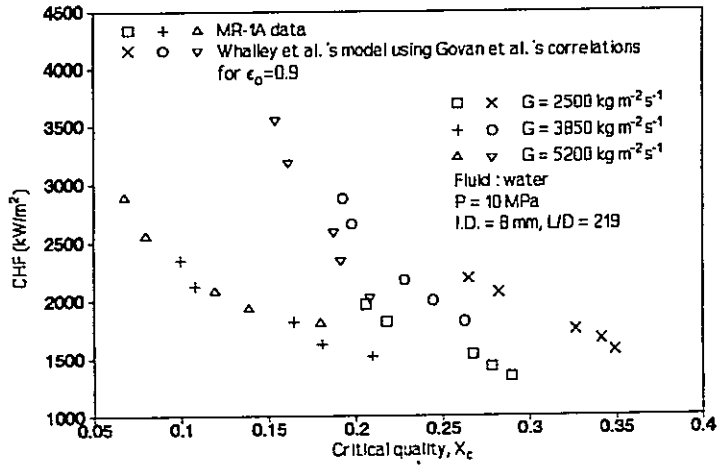

(c)

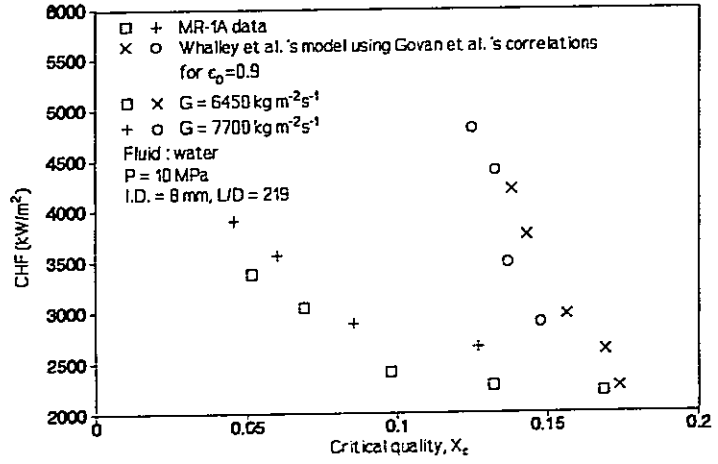

(d)

Figure 5-37 Comparison of the test CHF from the MR-1A loop against Whalley et al.'s model using Govan et al.'s correlations for water when ε_o=0.9.

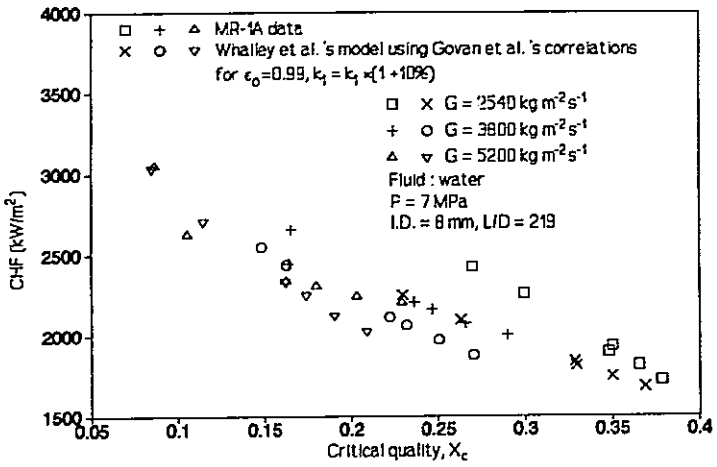

(a)

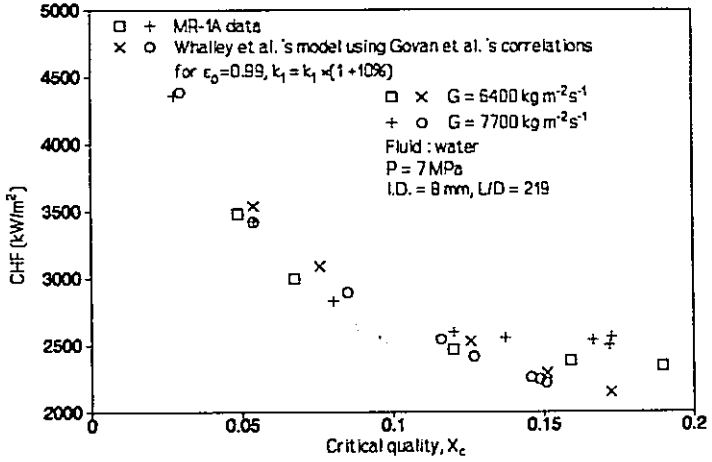

(b)

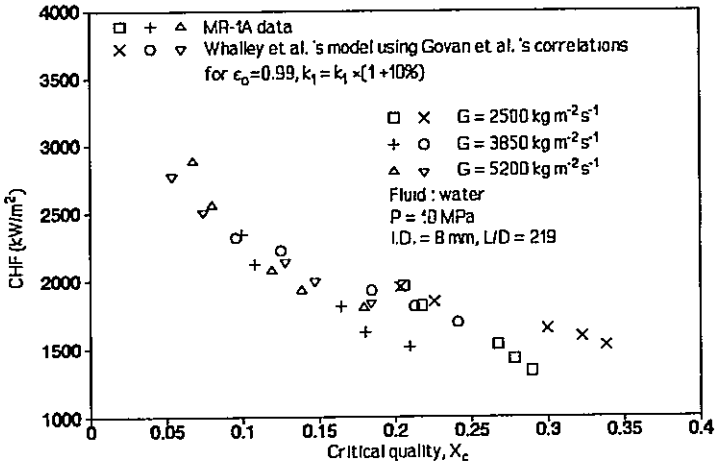

(c)

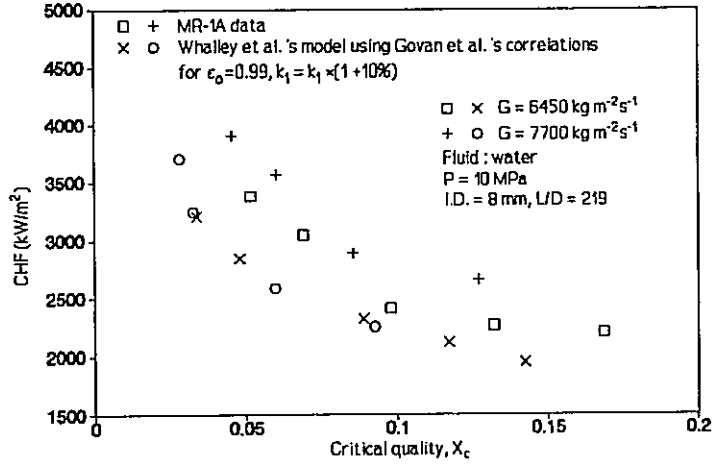

(d)

Figure 5-38 Comparison of the test CHF from the MR-1A loop against Whalley et al.'s model using Govan et al.'s correlations for water when $k_l=k_l\times(1+10\%)$ and $\epsilon_o=0.99$.

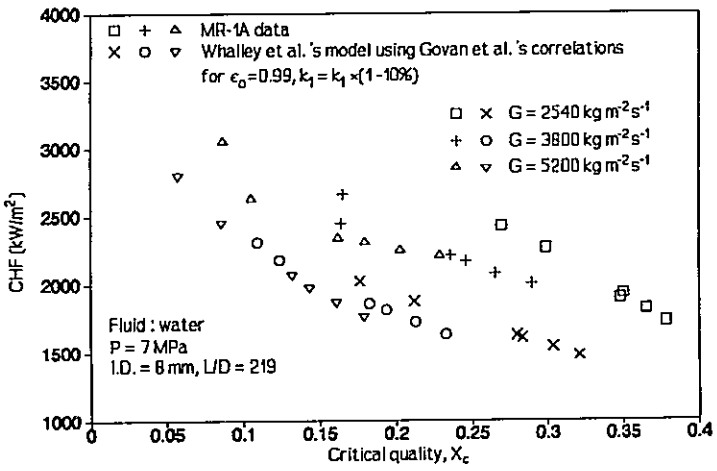

(a)

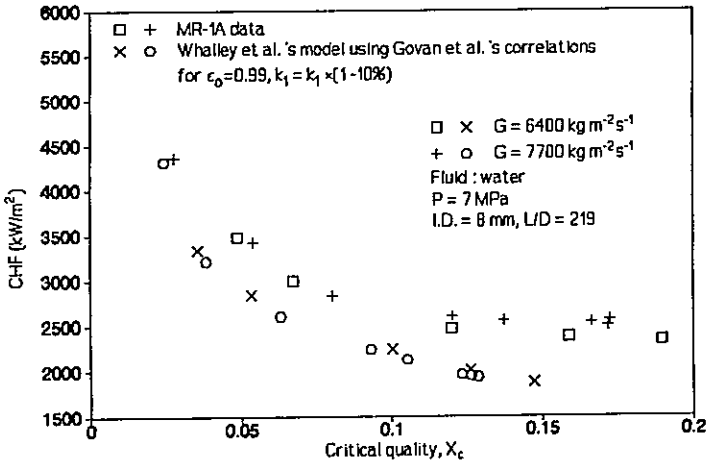

(b)

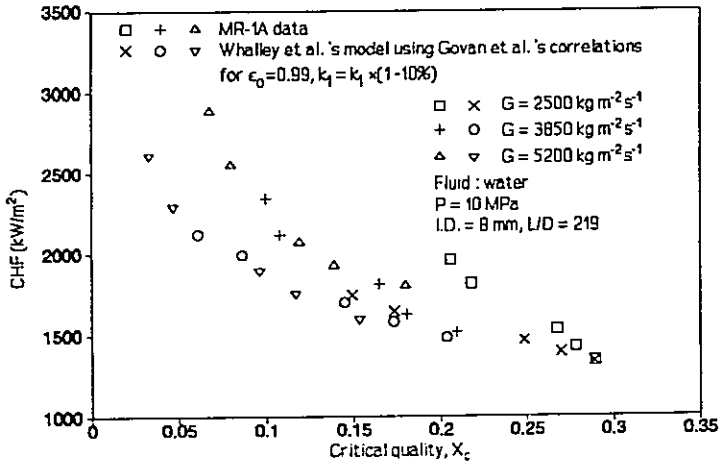

(c)

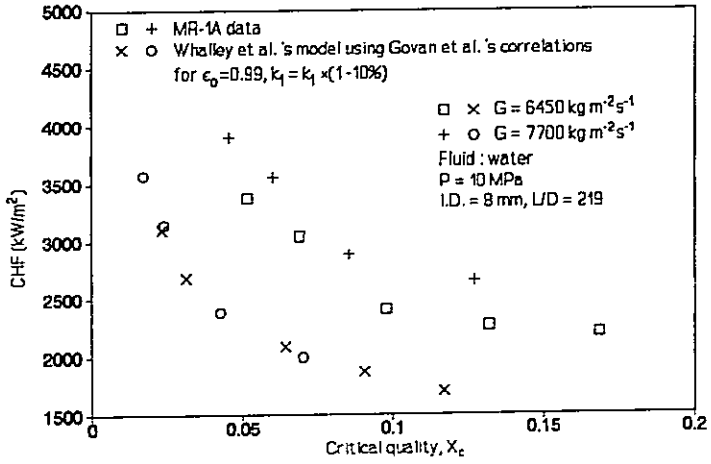

(d)

Figure 5-39 Comparison of the test CHF from the MR-1A loop against Whalley et al.'s model using Govan et al.'s correlations for water when $k_l=k_l\times(1\text{-}10\%)$ and $\varepsilon_o=0.99$.

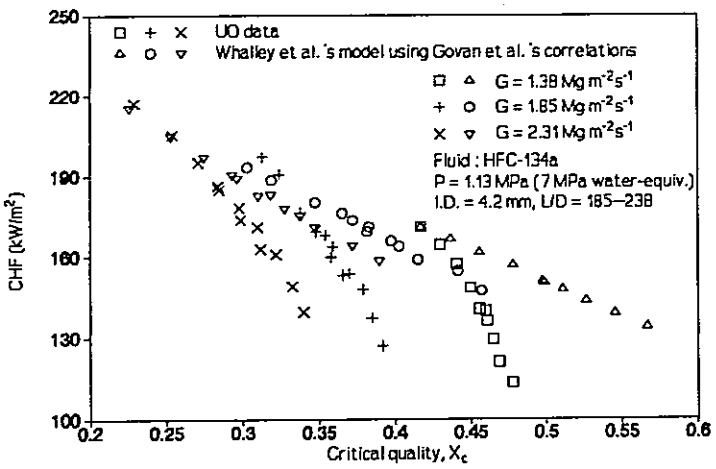

(a)

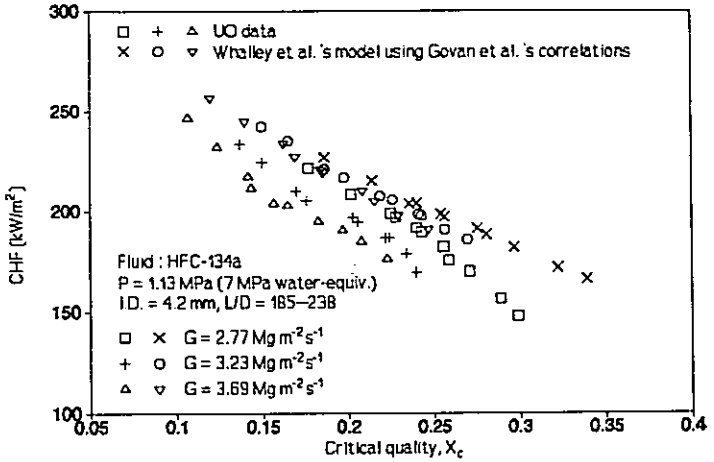

(b)

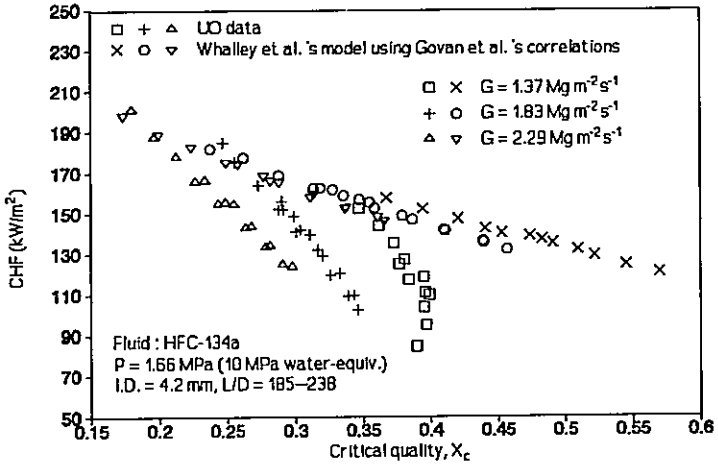

(c)

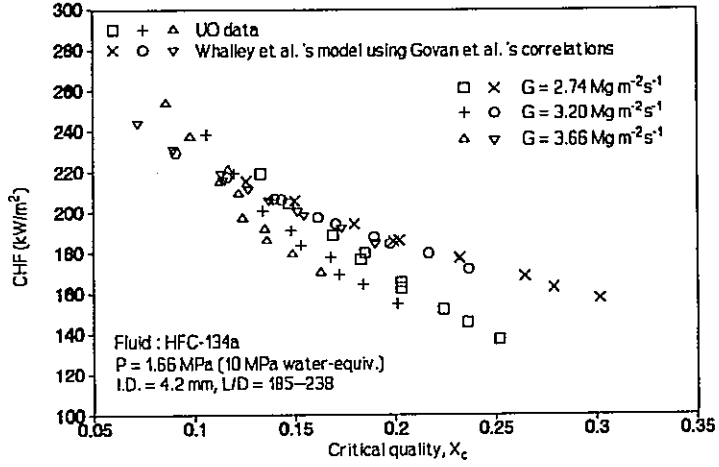

(d)

Figure 5-40 Comparison of the mass flux effect on CHF between UO data and Whalley et al.'s model using Govan et al.'s correlations for HFC-134a.

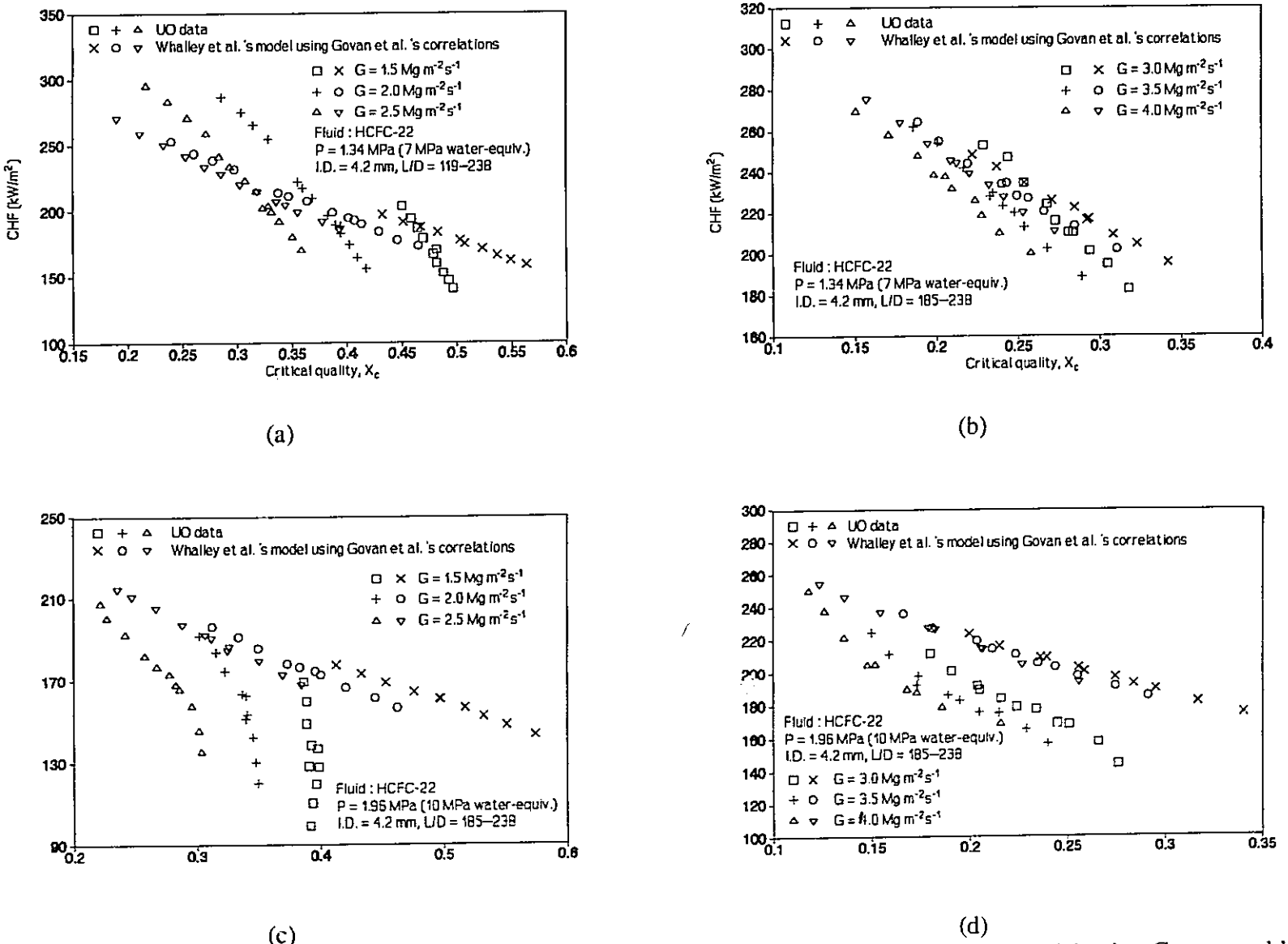

Figure 5-41 Comparison of the mass flux effect on CHF between UO data and Whalley et al.'s model using Govan et al.'s correlations for HCFC-22.

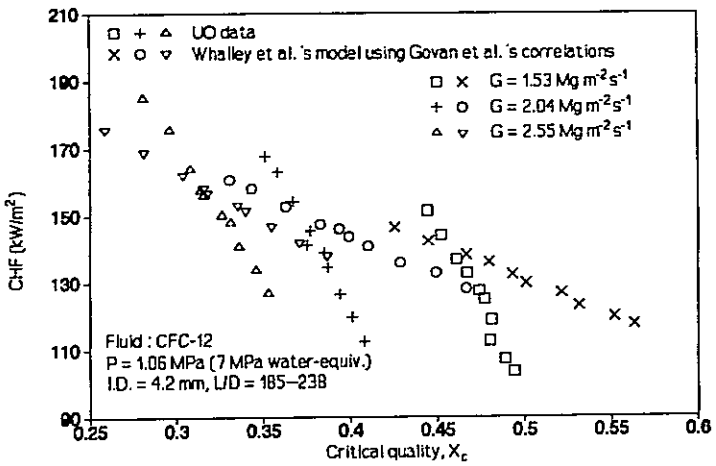

(a)

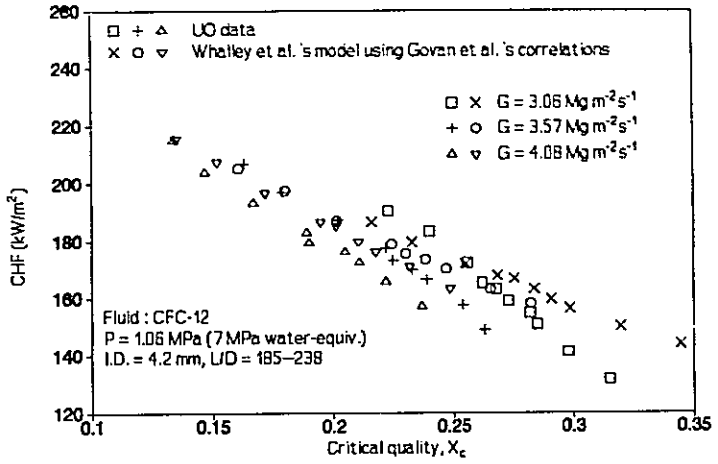

(b)

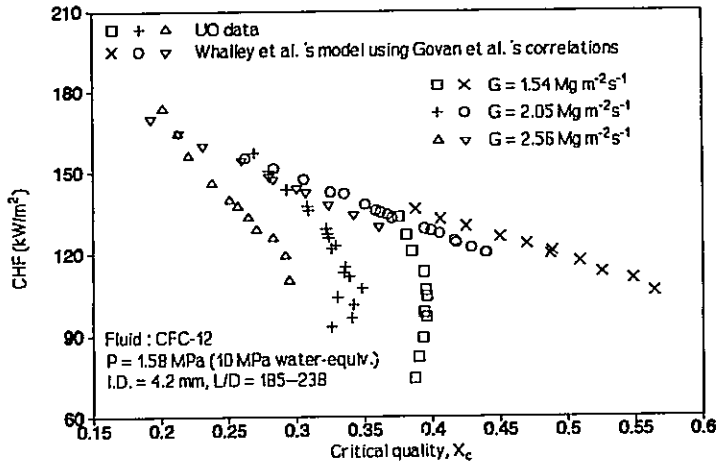

(c)

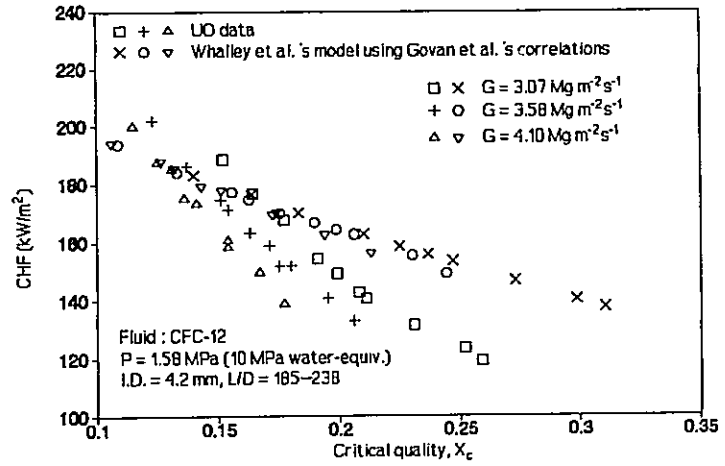

(d)

Figure 5-42 Comparison of the mass flux effect on CHF between UO data and Whalley et al.'s model using Govan et al.'s correlations for CFC-12.

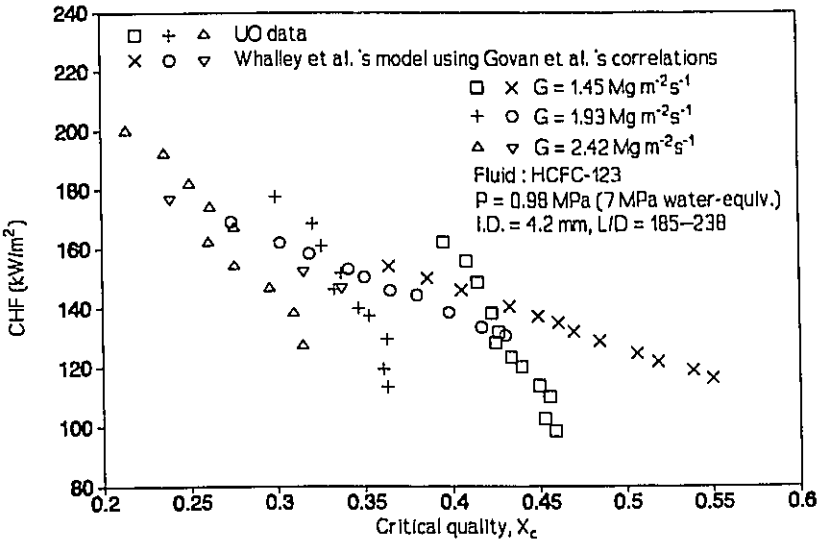

(a)

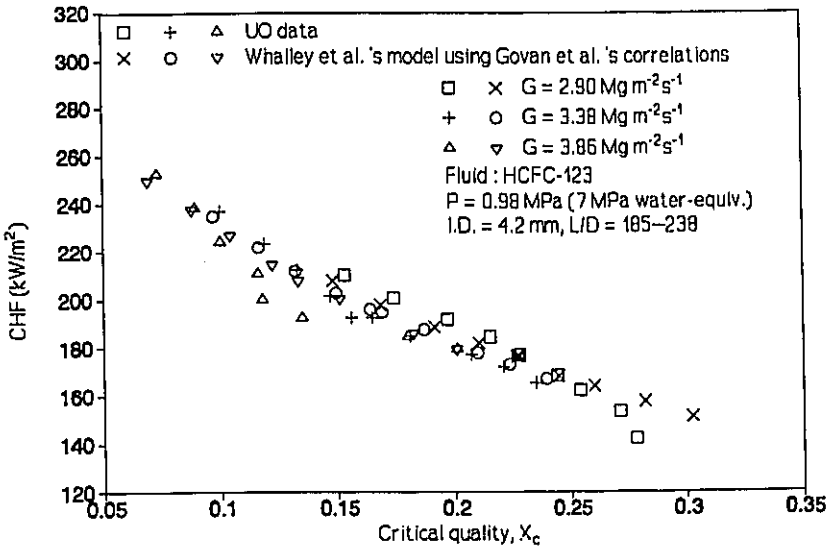

(b)

Figure 5-43 Comparison of the mass flux effect on CHF between UO data and Whalley et al.'s model using Govan et al.'s correlations for HCFC-123.

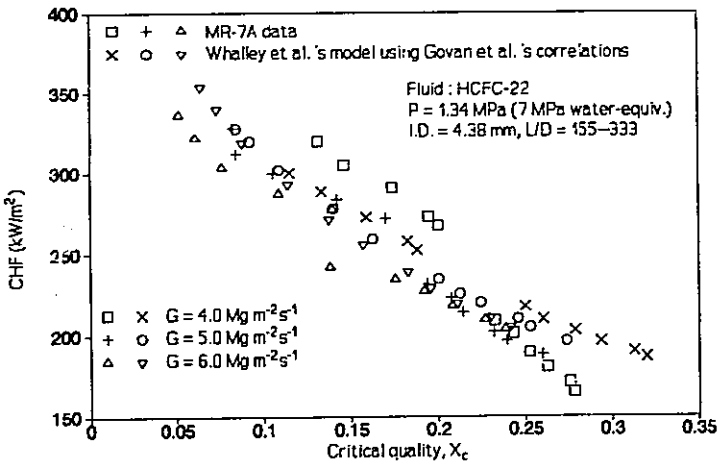

(a)

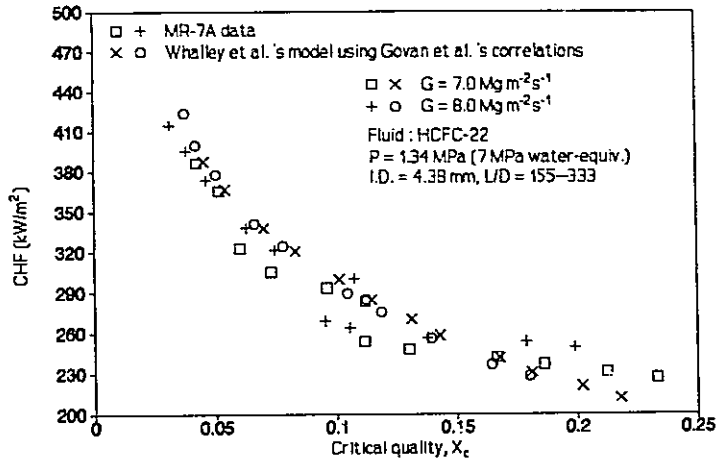

(b)

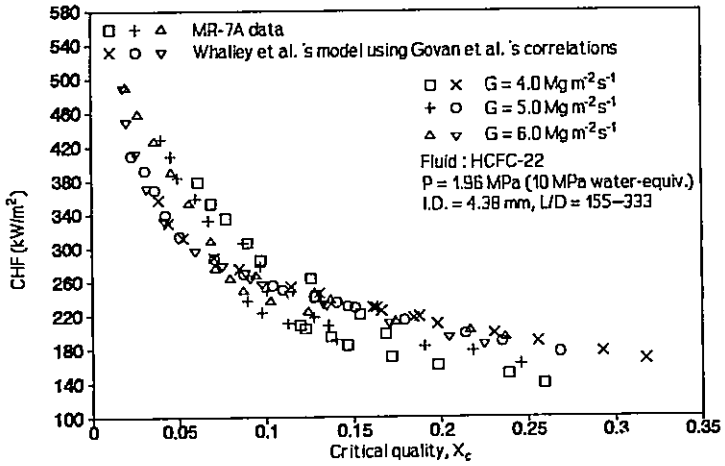

(c)

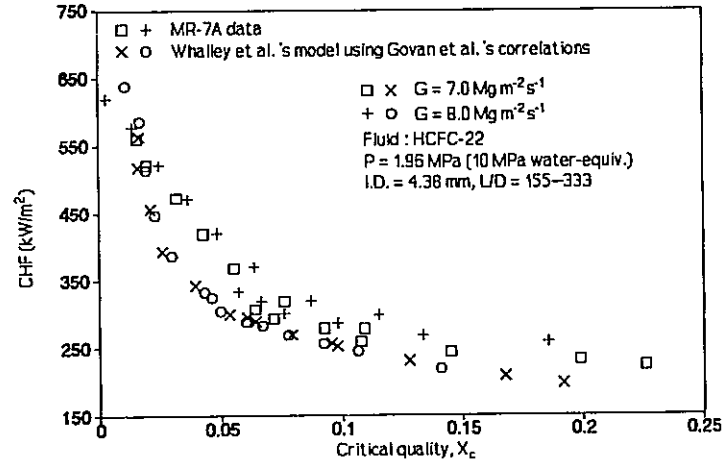

(d)

Figure 5-44 Comparison of the mass flux effect on CHF between MR-7A data and Whalley et al.'s model using Govan et al.'s correlations for HCFC-22.

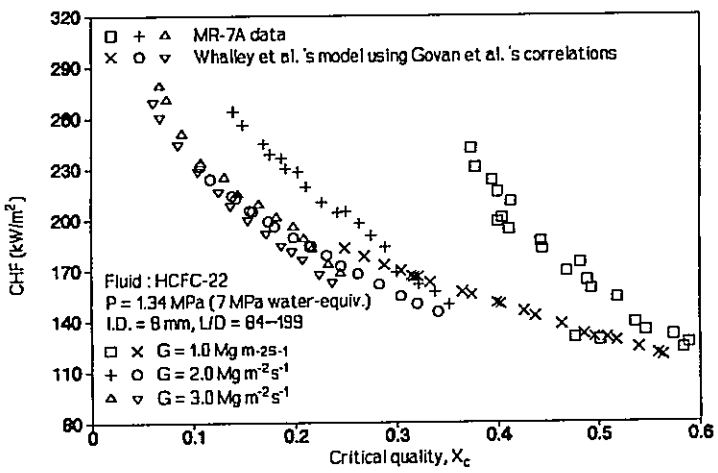

(a)

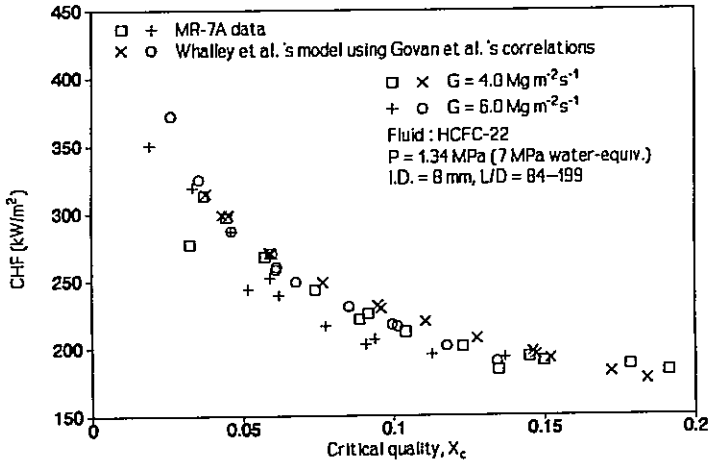

(b)

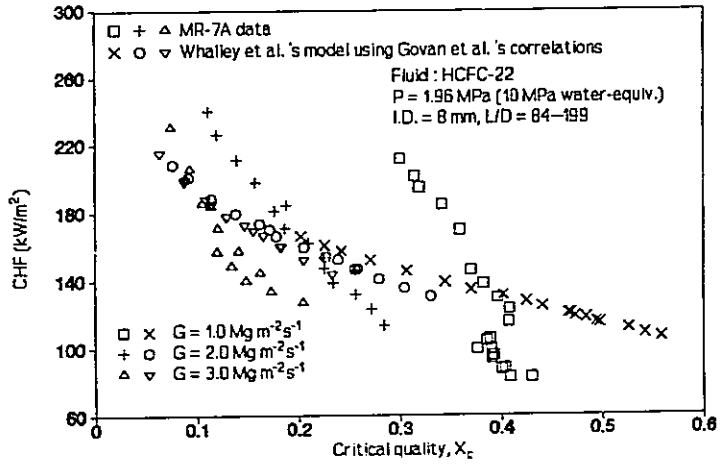

(c)

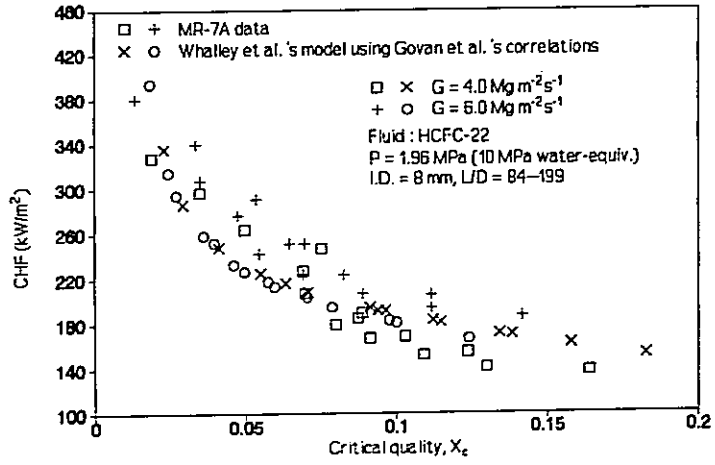

(d)

Figure 5-45 Comparison of the mass flux effect on CHF between MR-7A data and Whalley et al.'s model using Govan et al.'s correlations for HCFC-22.

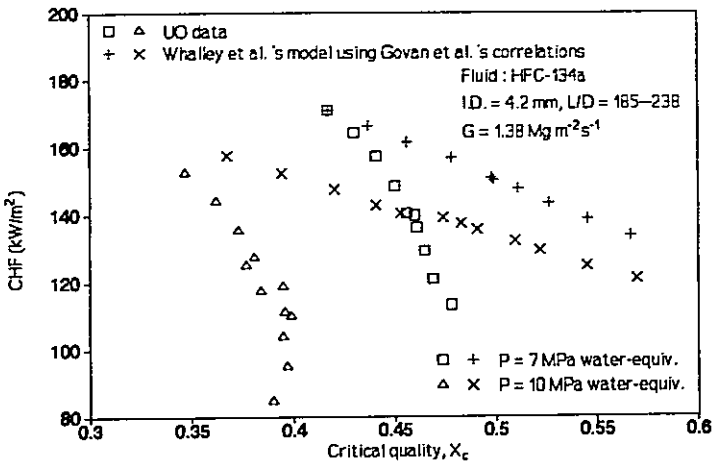

(a)

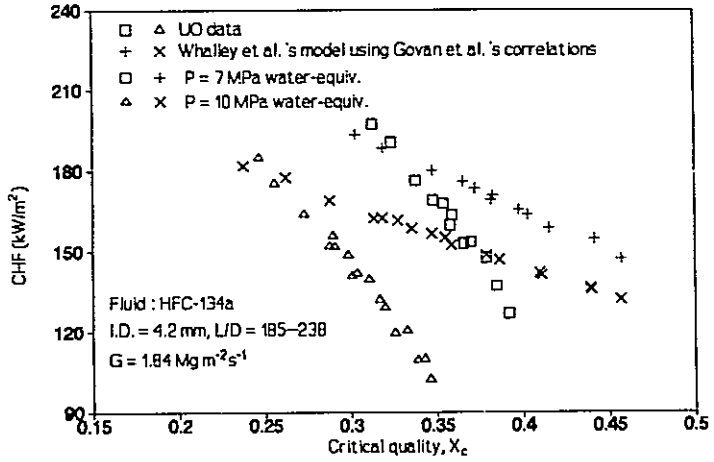

(b)

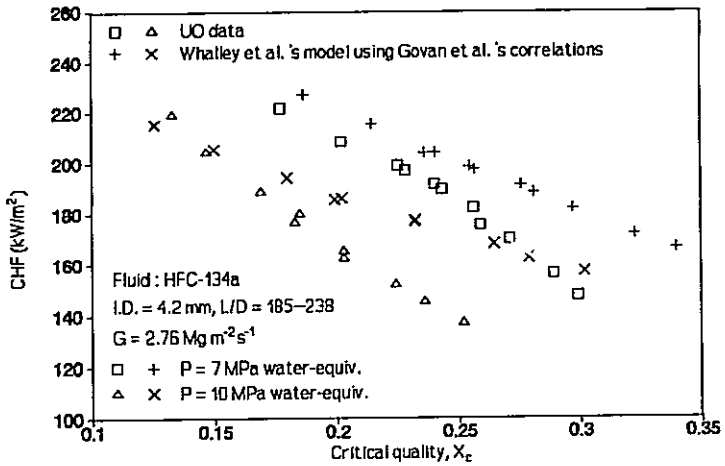

(c)

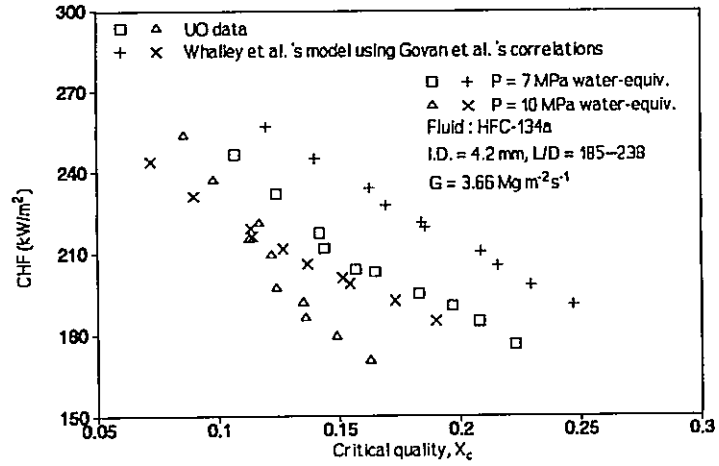

(d)

Figure 5-46 Comparison of the pressure effect on CHF between UO data and Whalley et al.'s model using Govan et al.'s correlations for HFC-134a.

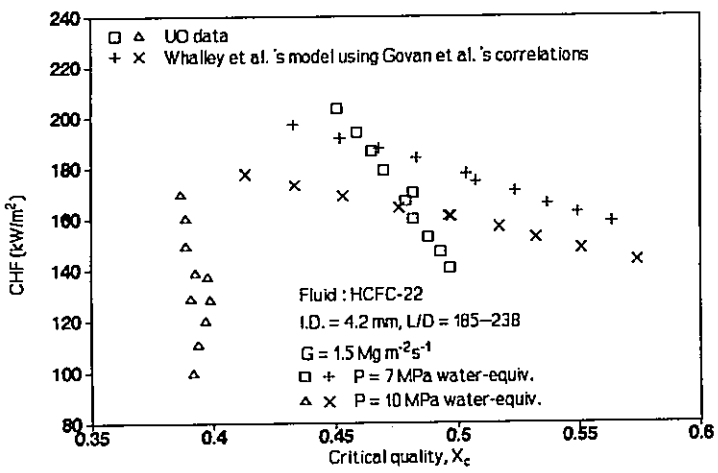

(a)

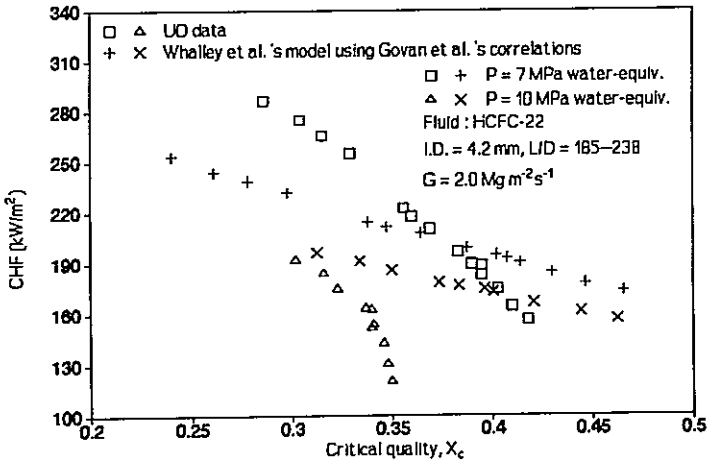

(b)

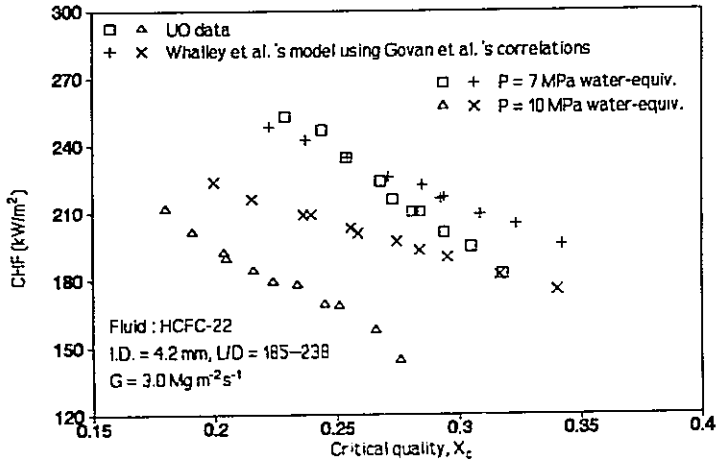

(c)

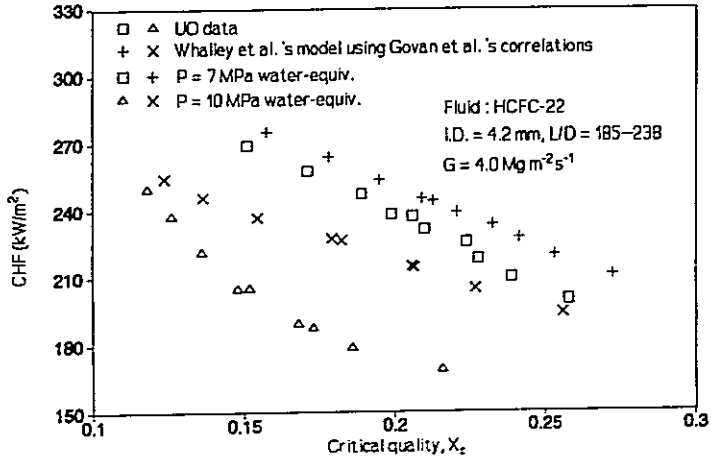

(d)

Figure 5-47 Comparison of the pressure effect on CHF between UO data and Whalley et al.'s model using Govan et al.'s correlations for HCFC-22.

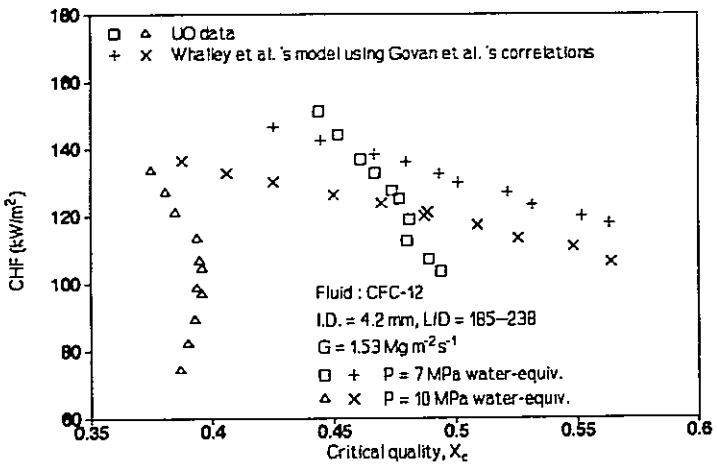

(a)

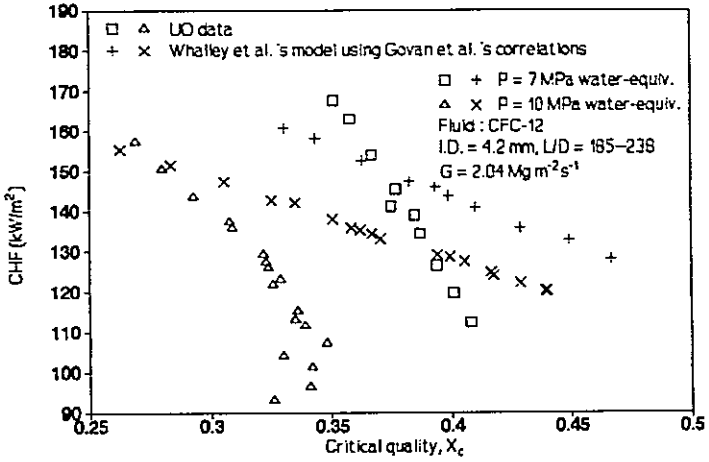

(b)

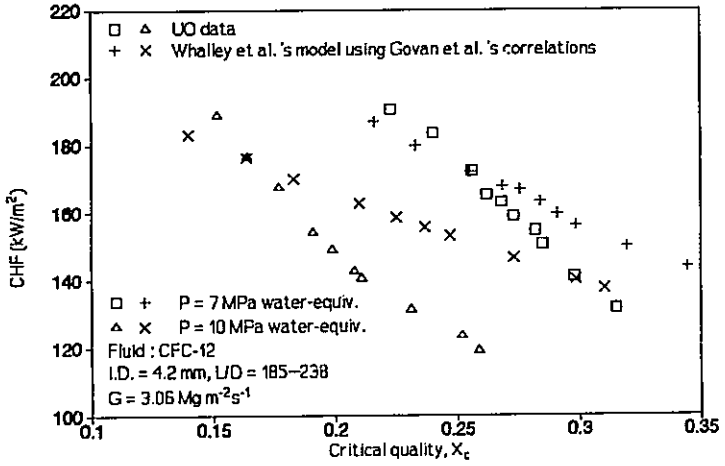

(c)

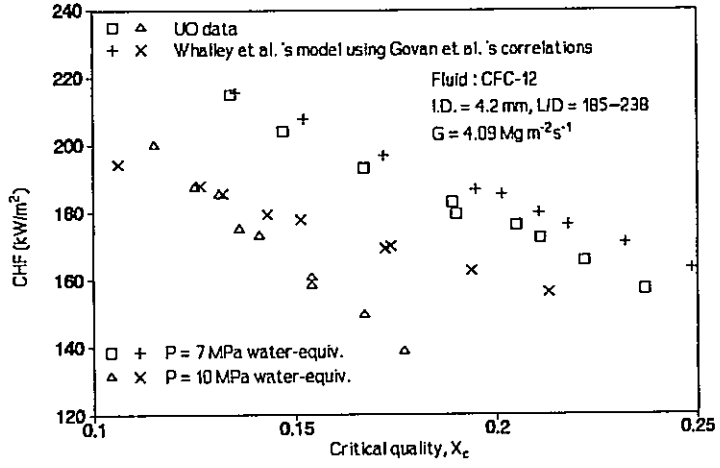

(d)

Figure 5-48 Comparison of the pressure effect on CHF between UO data and Whalley et al.'s model using Govan et al.'s correlations for CFC-12.

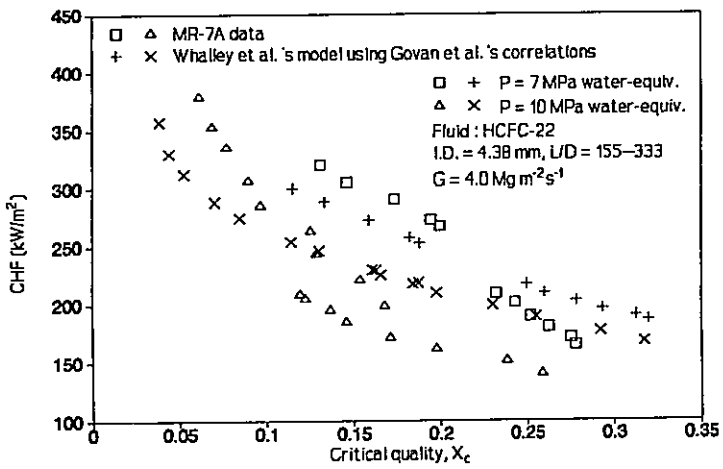

(a)

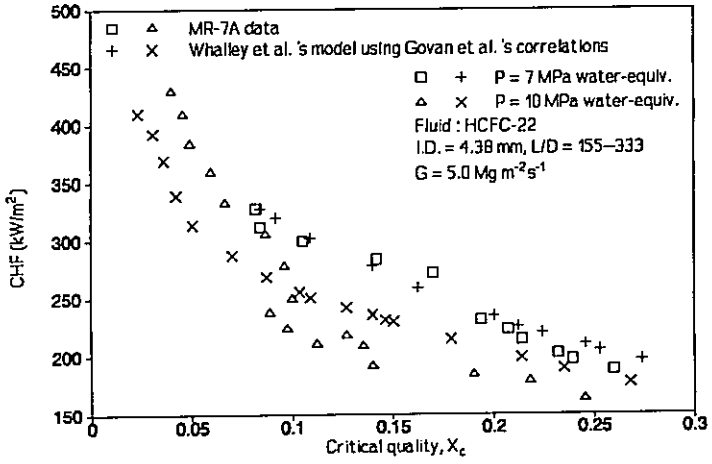

(b)

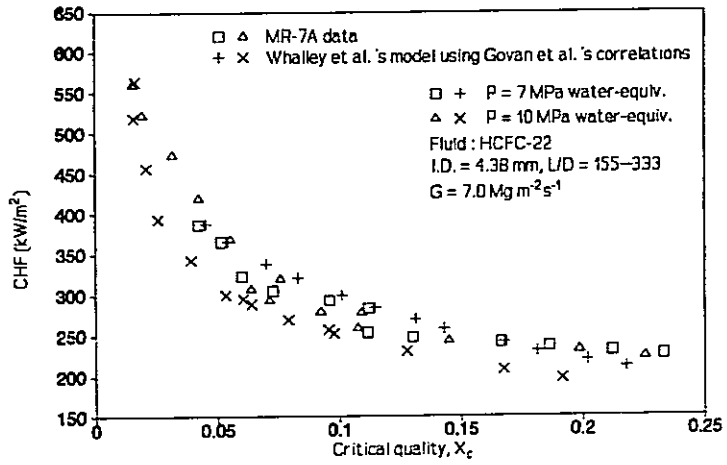

(c)

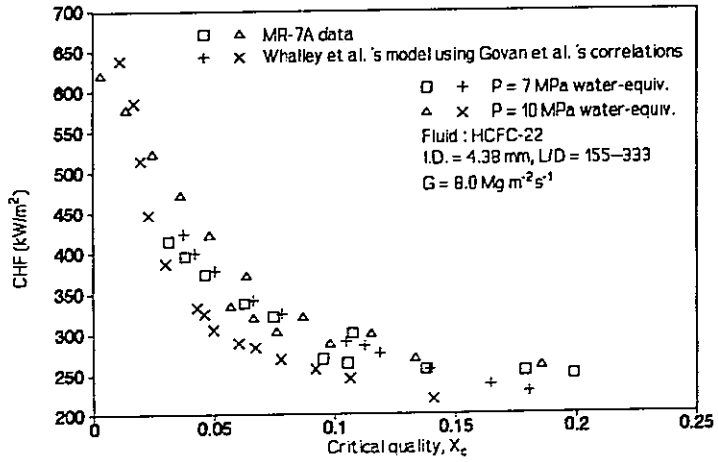

(d)

Figure 5-49 Comparison of the pressure effect on CHF between MR-7A data and Whalley et al.'s model using Govan et al.'s correlations for HCFC-22.

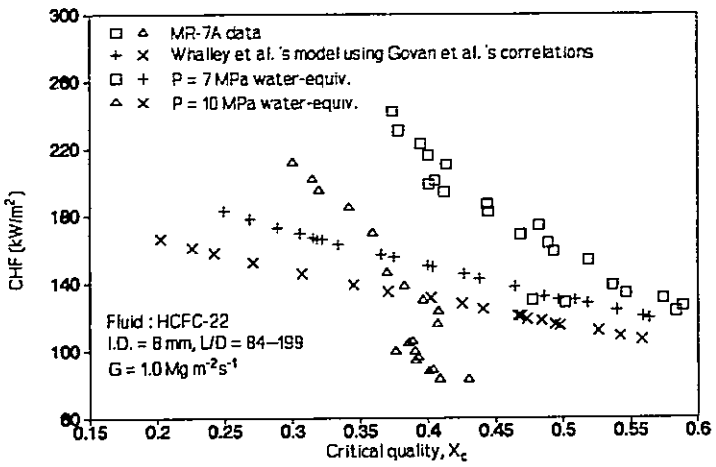

(a)

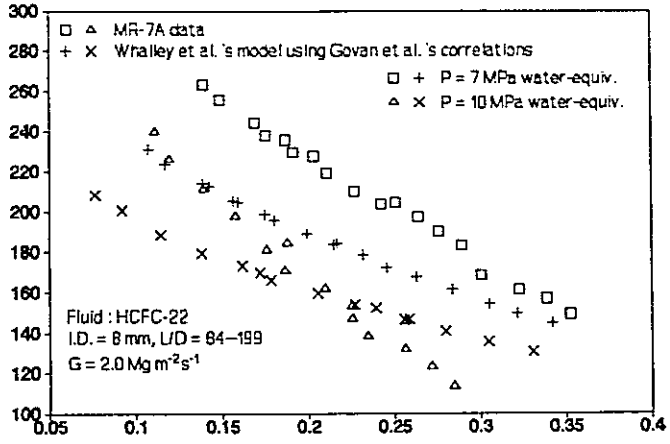

(b)

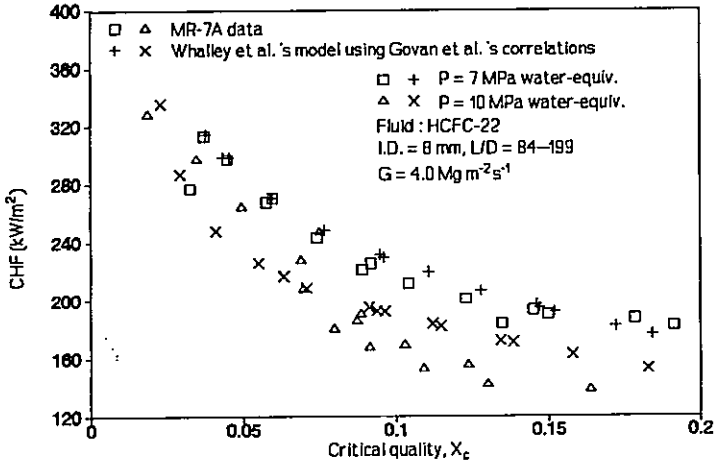

(c)

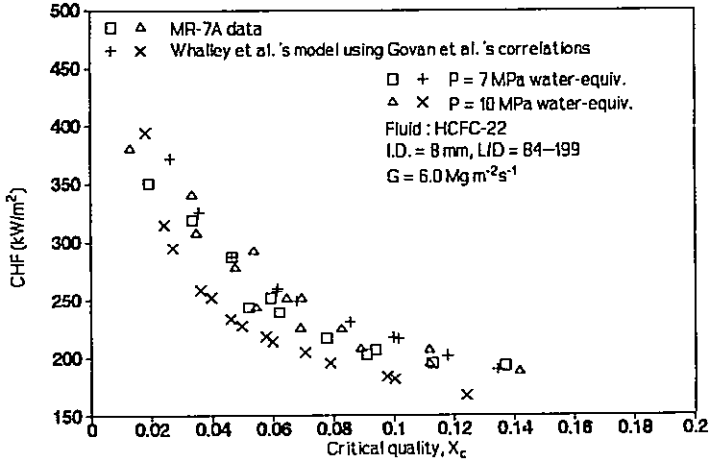

(d)

Figure 5-50 Comparison of the pressure effect on CHF between MR-7A data and Whalley et al.'s model using Govan et al.'s correlations for HCFC-22.

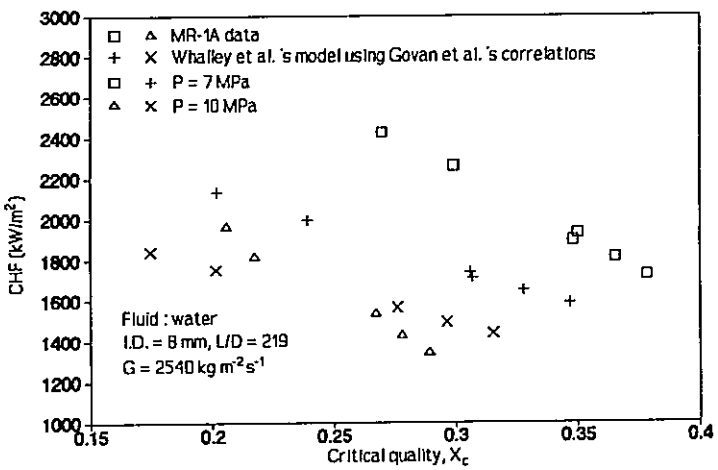

(a)

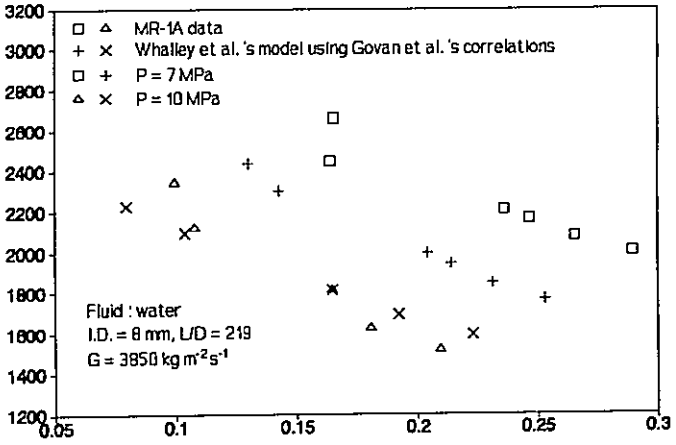

(b)

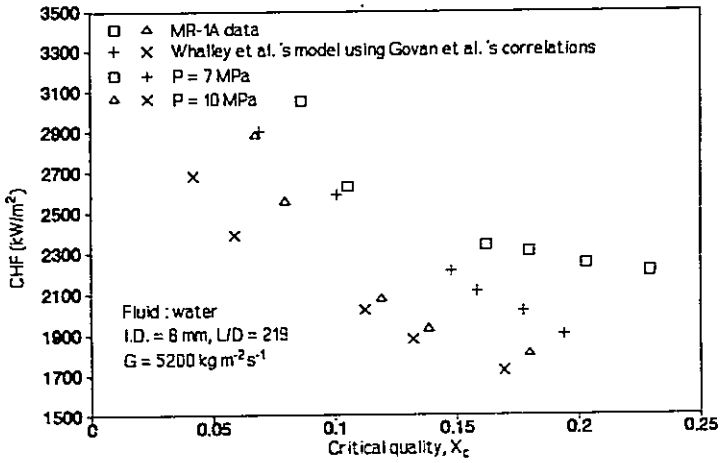

(c)

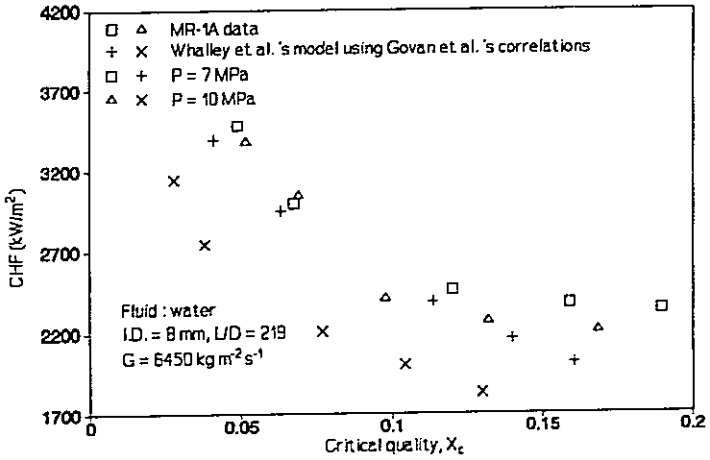

(d)

Figure 5-51 Comparison of the pressure effect on CHF between MR-1A data and Whalley et al.'s model using Govan et al.'s correlations for water.

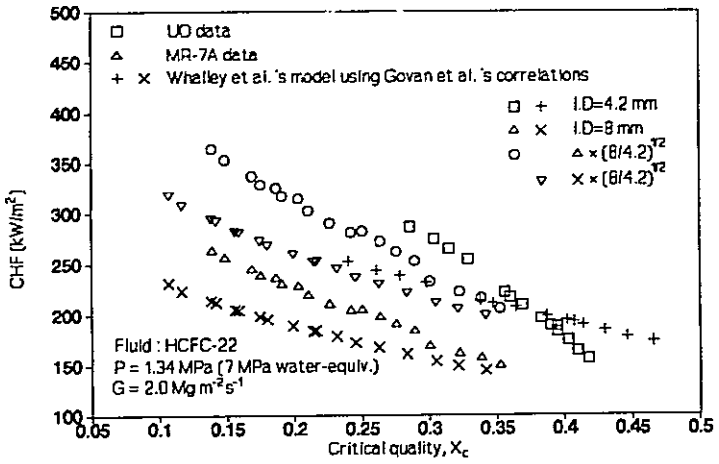

(a)

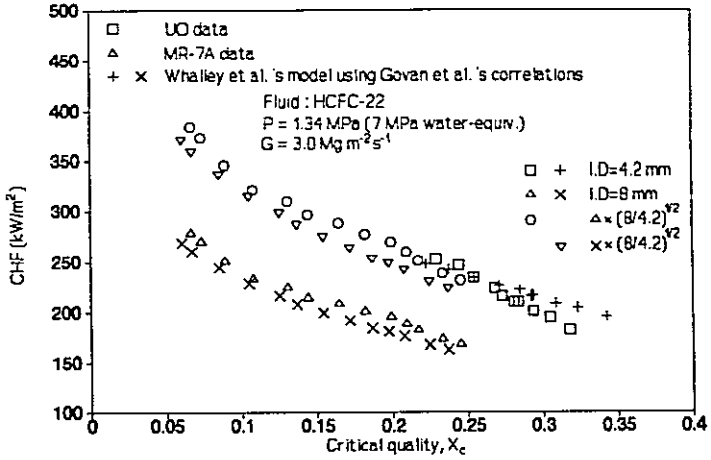

(b)

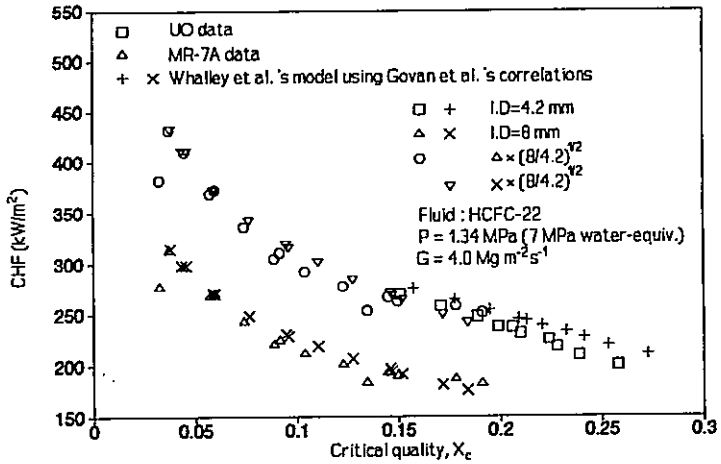

(c)

Figure 5-52 Comparison of the diameter effect on CHF for UO and MR-7A data against Whalley et al.'s model using Govan et al.'s correlations for HCFC-22 at 7 MPa water-equiv. pressure.

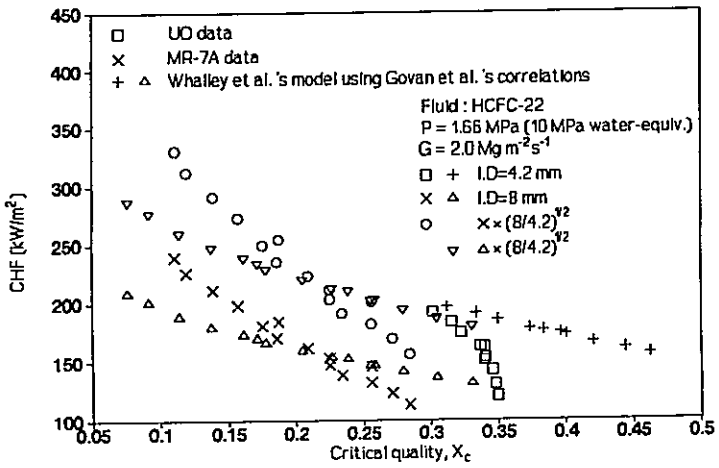

(a)

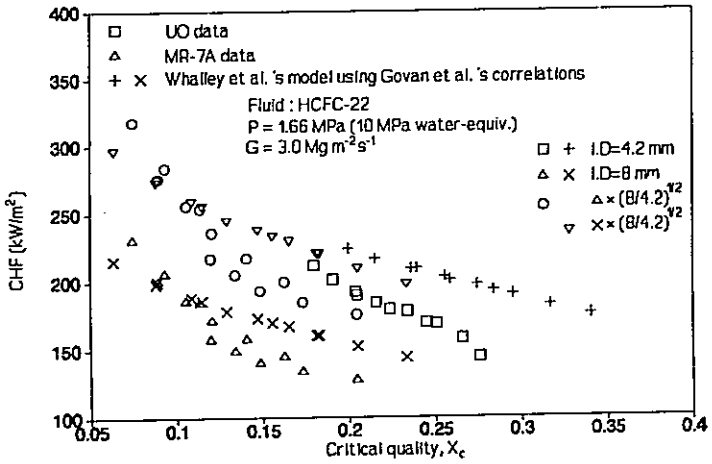

(b)

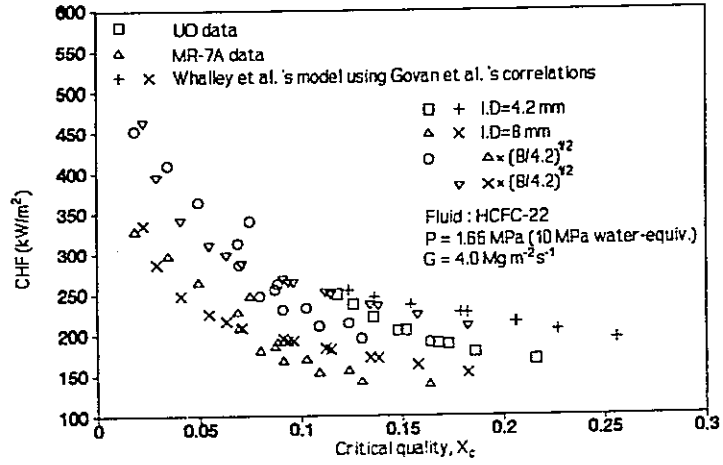

(c)

Figure 5-53 Comparison of the diameter effect on CHF for UO and MR-7A data against Whalley et al.'s model using Govan et al.'s correlations for HCFC-22 at 10 MPa water-equiv. pressure.

Chapter 6

LIMITATIONS OF THE SCALING TECHNIQUE

6.1 General

As shown in Eq. (2-15), the primary parameters governing the CHF prediction are geometries (L and D), pressure (P), mass flux (G) and inlet subcooling enthalpy (ΔH_i). For the purpose of fluid-to-fluid scaling, these parameters are converted into dimensionless quantities such as shown in Eqs. (2-3)–(2-9). The previous literature related to the CHF scaling technique simply report the scaling result or accuracy based on the experiments with the test conditions but do not provide any information regarding the limitation of this application. This chapter discusses the limitations of the fluid-to-fluid scaling techniques, especially for certain ranges of flow condition.

Among the dimensionless parameters (ρ_f/ρ_g, L/D, ψ_{CHF} or ψ_k, and X_e), ρ_f/ρ_g and ψ_{CHF} (or ψ_k) are calculated from the measured pressure and mass flow rate. The X_e (critical quality) is calculated based on L/D, pressure, mass flow rate and heat input. The quality is defined as a dimensionless enthalpy (i.e. $(h-h_f)/\lambda$), assuming thermal equilibrium is present and $x>0$; also is defined as the ratio of vapour mass flow rate to the total mass flow rate of the fluid. The vapour generated in a heated channel depends on contributions to enthalpy generation from the following

sources: heat input, flashing, wall friction and the changes in kinetic energy and potential energy. The difference in axial quality gradient due to the effects of friction, kinetic energy change and potential energy change between water and modelling fluids can cause a dissimilarity in phase distribution in both systems and thus may limit the application of the fluid-to-fluid scaling techniques. A better understanding of the limitation of the scaling technique may be obtained if we can formulate the axial quality gradient from various effects, e.g. friction, kinetic energy change, potential energy change and flashing. The following sections will discuss the details of these effects.

6.2 Wall Friction Heat

Rearranging Eq. (4-2), the critical quality is usually calculated from

$$X_c = \frac{h_{in}+\Delta h-h_f}{\lambda} \tag{6-1}$$

where h_{in} is the flow enthalpy at the inlet condition, Δh the enthalpy increase of the fluid in the heated channel, and h_f and λ the saturated liquid enthalpy and the heat of vaporization based on the outlet pressure. In most cases,

$$\Delta h = q \tag{6-2}$$

where q is the heat per unit mass added to the flow channel. As shown by Groeneveld (1972) in Fig. 6-1, which is a pressure-enthalpy diagram, path 1—3 is used by most investigators. They simply add the heat input (q) to the inlet enthalpy h_{in}. A more accurate calculation for Δh is the path 1—2, where W_f is the friction heat or the thermal equivalent of the work done by the

frictional pressure drop, defined as

$$dW_f = -v\,dP + v\,dP_g + v\,dP_a = -v\,dP_f \tag{6-3}$$

where v is the specific volume of the flow, dP the total pressure drop, dP_a the acceleration pressure drop, dP_g the gravitational pressure drop and dP_f the frictional pressure drop. The two terms vdP_g and vdP_a can reduce the quality by converting flow energy into potential energy and kinetic energy, i.e.,

$$v\,dP_g = -d(P.E.) \tag{6-4}$$

$$v\,dP_a = -d(K.E.) \tag{6-5}$$

where P.E. is the potential energy and K.E. is the kinetic energy. Complete mathematical expressions for dP_f, dP_g and dP_a are derived in Appendix V.

For water CHF, path 1—3 is accurate enough to calculate the critical quality because the heat of vaporization for water is much greater than Δ(P.E.), Δ(K.E.) and W_f, where

$$\Delta(P.E.) = \int_1^3 d(P.E.) = -\int_1^3 v\,dP_g \tag{6-6}$$

$$\Delta(K.E.) = \int_1^3 d(K.E.) = -\int_1^3 v\,dP_a \tag{6-7}$$

and

$$W_f = \int_1^3 dW_f = -\int_1^3 v\,dP_f \tag{6-8}$$

The effects of the friction heat and the changes of P.E. and K.E., which affect the calculation of the thermodynamic quality, can be neglected without a significant loss of accuracy for a

water-cooled system. However, in a refrigerant system, the effects of Δ(P.E.), Δ(K.E.) and W_f may have to be considered because the heat of vaporization for refrigerants is about 1/15 of that of water while the magnitudes of Δ(P.E.), Δ(K.E.) and W_f could be of the same order as those for water. At high mass flow rates and $\rho_f/\rho_g<30$, the friction heat W_f can be much greater than the sum of Δ(P.E.) and Δ(K.E.). This may have a significant consequence in fluid-to-fluid scaling when using refrigerants to simulate water CHF because the friction heat W_f can be considered as extra heat generated in the channel wall. This would have the same effect as reducing the heat flux required to cause CHF.

6.3 Energy Equation in an Irreversible Process

From the second law of thermodynamics for a control volume (Van Wylen and Sonntag, 1973), the entropy increase for a system can be written as

$$ds = \frac{\delta q}{T} + \frac{\delta LW}{T} \tag{6-9}$$

where δq is the heat input, T the system temperature and δLW the loss of work. In the present work, most of the loss of work is due to the friction, i.e.

$$\delta LW = \delta W_f \tag{6-10}$$

Rearranging the Eq. (6-9), it becomes

$$Tds = \delta q + \delta W_f \tag{6-11}$$

There are two important thermodynamic relations that can be used, i.e.

$$Tds = du + Pdv \tag{6-12}$$

and

$$Tds = dh - vdP \tag{6-13}$$

Comparing Eqs. (6-11) and (6-12), gives

$$\delta q + \delta W_f = du + Pdv \tag{6-14}$$

or

$$du = \delta q + \delta W_f - Pdv \tag{6-15}$$

Also comparing Eqs. (6-11) and (6-13), yields

$$\delta q + \delta W_f = dh - vdP \tag{6-16}$$

Employing the Eq. (V-6) in Appendix V in Eq. (6-16), we obtain

$$\delta q + \delta W_f = dh - vdP_f - vdP_a - vdP_g \tag{6-17}$$

Substituting dh=d(u+Pv) and Eqs. (6-3), (6-4), (6-5) into Eq. (6-17), it becomes

$$\delta q + \delta W_f = du + d(Pv) + \delta W_f + d(K.E.) + d(P.E.) \tag{6-18}$$

Cancelling the δW_f on both sides of Eq. (6-18), yields

$$\delta q = du + d(Pv) + d(K.E.) + d(P.E.) \tag{6-19}$$

Equation (6-19) is the energy equation of the first law of thermodynamics (no work in the flow channel) and is derived from Eq. (6-14) or (6-16). Integrating Eq. (6-14) on both sides, gives

$$q + W_f = \Delta u + \int P\,dv \tag{6-20}$$

The equivalence between RHS and LHS of Eq. (6-20) is illustrated in Fig. 6-1.

As mentioned previously, the magnitudes of Δ(K.E.), Δ(P.E.) and W_f could be of the same order for water and modelling fluids. However, the ratios of Δ(K.E.), Δ(P.E.) and W_f to λ could have large differences between water and modelling fluids, i.e.

$$\left[\frac{\Delta(K.E.)}{\lambda}\right]_W << \left[\frac{\Delta(K.E.)}{\lambda}\right]_M \tag{6-21}$$

$$\left[\frac{\Delta(P.E.)}{\lambda}\right]_W << \left[\frac{\Delta(P.E.)}{\lambda}\right]_M \tag{6-22}$$

and

$$\left[\frac{W_f}{\lambda}\right]_W << \left[\frac{W_f}{\lambda}\right]_M \tag{6-23}$$

The three factors can affect the dryout behaviours for both fluids and thus will determine the CHF similarity.

6.4 Flashing

Another dissimilarity in refrigerant and water is due to vapour flashing caused by a reduction in pressure (frictional and accelerational) and the corresponding reduction in saturation temperature along the channel, which results in the quality change. For example, for adiabatic two-phase flow at similar conditions of ρ_f/ρ_g, ψ_k and L/D for water and HCFC-22, the quality increase from inlet to outlet for HCFC-22 is approximately three times as high as for water. The

larger drop in saturation temperature and increase in quality for HCFC-22 results in a different upstream history than for water, i.e.

$$\left(\frac{dx}{dz}\right)_{HCFC\text{-}22,\ flashing} \neq \left(\frac{dx}{dz}\right)_{water,\ flashing} \tag{6-24}$$

This difference in x and dx/dz will also cause differences of axial and radial void fraction distributions and thus different dryout behaviours may occur in water and the modelling fluids.

The vapour generated in a heated channel depends on contributions to enthalpy generation from the following sources: heat input, flashing, friction and the changes in kinetic energy and potential energy, i.e.

$$\frac{dx}{dz} = \frac{dx}{dz}\Big)_F + \frac{dx}{dz}\Big)_H \tag{6-25}$$

where

$$\frac{dx}{dz}\Big)_H = \frac{dx}{dz}\Big)_q - \frac{dx}{dz}\Big)_{K.E.} - \frac{dx}{dz}\Big)_{P.E.} \tag{6-26}$$

The subscript "F", "H" and "q" represent the flashing effect, enthalpy increase and heat input, respectively. Although the frictional effect is not shown in Eq. (6-26), as illustrated in the later derivation (i.e. Eq. (6-27)), frictional heat has an effect on the internal energy calculation. Friction further changes the entropy, pressure and thus the fluid properties compared to the case without friction. For a high-pressure steam-water system, the effects of P.E., K.E., friction and flashing are negligible. However, in a low pressure refrigerant system, these effects become important at high flow and high quality conditions. Since the quality distribution (Eq. (2-4)) is one of the most important factors for the similarity in CHF between water and modelling fluids, caution should

be taken when converting high flow or high quality refrigerant CHF data to water CHF.

In the present study, the quality gradient along the flow channel thus will be studied by solving a differential energy equation including all the above effects. To achieve this, the energy equation for an irreversible process will be used because of the frictional effect.

6.5 Formulation of Quality Gradient

To derive the equation for the thermodynamic quality and quality gradient, the following assumptions are made:

1. The flow is one-dimensional with thermal equilibrium. This assumption is not valid for subcooled boiling but is reasonable for the high flow and high quality conditions of interest.
2. The pressure gradient can be evaluated using the homogeneous flow model. For the high flow and high quality conditions of interest, the flow approaches a homogeneous mixture.

Because the test sections used in the present experimental investigations are all uniformly heated, the constant heat flux condition will be used through out the following derivation. The δq in Eq. (6-15) is equal to $(q/L)\delta z$, that is, $\delta q/\delta z = q/L$. For the convenience of the equation derivation, the path dependent function δ is replaced by d in following derivations. Firstly, rewrite the Eq. (6-15) by dividing by dz (a differential increment):

$$\frac{du}{dz} = \frac{q}{L} - P\frac{dv}{dz} + \frac{dW_f}{dz} \qquad (6\text{-}27)$$

Substituting Eq. (6-3) for dW_f into Eq. (6-27), gives

$$\frac{du}{dz} = \frac{q}{L} - P\frac{dv}{dz} - v\frac{dP_f}{dz} \tag{6-28}$$

where -P(dv/dz) and -v(dP_f/dz) depend on whether the flow is single-phase or two-phase. From this point, the discussion will be divided into two sections: single-phase region and two-phase region.

6.5.1 Single-phase Region

The specific volume v can be determined by P_1 and T_1 as a subcooled liquid or can be approximated as a saturated liquid based on T_1, where the subscript "1" represents the upstream location of a finite increment (Δz) of distance. From Collier (1981), the compressibility of the liquid phase (dv/dz) can be neglected and the frictional pressure gradient (dP_f/dz) can be substituted by Eqs. (V-28) and (V-29). Therefore,

$$u_2 = u_1 + \Delta u = u_1 + \frac{q}{L}\Delta z + 0.158\left(\frac{G^2 v_f^2}{D}\right)\left(\frac{GD}{\mu}\right)^{-\frac{1}{4}}\Delta z \tag{6-29}$$

where the subscript "2" represents the downstream location of the finite increment of distance. When $u_2 \geq u_f$, the flow has entered the two-phase region.

6.5.2 Two-phase Region

In the two-phase region, the internal energy u in Eq. (6-28) is expressed as

$$u = u_f(1-x) + xu_g = u_f + xu_{fg} \tag{6-30}$$

where $u_{fg} = u_g - u_f$. The specific volume for homogeneous flow is calculated by

$$v_H = xv_g + (1-x)v_f = v_f + xv_{fg} \tag{6-31}$$

(based on Eqs. (V-15) and (V-16)). Substituting Eqs. (6-30) and (6-31) into Eq. (6-28), gives

$$\frac{du_f}{dz} + x\frac{du_{fg}}{dz} + u_{fg}\frac{dx}{dz} = \frac{q}{L} - P\left(\frac{dv_f}{dz} + x\frac{dv_{fg}}{dz} + v_{fg}\frac{dx}{dz}\right) - (v_f + xv_{fg})\frac{dP_f}{dz} \tag{6-32}$$

Expanding Eq. (6-32) and rearranging it, yields

$$(Pv_{fg} + u_{fg})\frac{dx}{dz} + \left(P\frac{dv_{fg}}{dz} + \frac{du_{fg}}{dz} + v_{fg}\frac{dP_f}{dz}\right)x + \left(P\frac{dv_f}{dz} + v_f\frac{dP_f}{dz} + \frac{du_f}{dz} - \frac{q}{L}\right) = 0 \tag{6-33}$$

where

$$P\frac{dv_{fg}}{dz} = P\left(\frac{dv_g}{dz} - \frac{dv_f}{dz}\right) \tag{6-34}$$

Again neglecting the compressibility of the liquid phase, Equation (6-33) becomes

$$(Pv_{fg} + u_{fg})\frac{dx}{dz} + \left(P\frac{dv_g}{dz} + \frac{du_{fg}}{dz} + v_{fg}\frac{dP_f}{dz}\right)x + \left(v_f\frac{dP_f}{dz} + \frac{du_f}{dz} - \frac{q}{L}\right) = 0 \tag{6-35}$$

where

$$\frac{du_{fg}}{dz} = \frac{du_{fg}}{dP}\frac{dP}{dz} = \frac{du_{fg}}{dP}\left(\frac{dP_f}{dz} + \frac{dP_a}{dz} + \frac{dP_g}{dz}\right) \tag{6-36}$$

$$\frac{du_f}{dz} = \frac{du_f}{dP}\frac{dP}{dz} = \frac{du_f}{dP}\left(\frac{dP_f}{dz} + \frac{dP_a}{dz} + \frac{dP_g}{dz}\right) \tag{6-37}$$

and

$$\frac{dv_g}{dz} = \frac{dv_g}{dP}\frac{dP}{dz} = \frac{dv_g}{dP}\left(\frac{dP_f}{dz}+\frac{dP_a}{dz}+\frac{dP_g}{dz}\right) \tag{6-38}$$

The relation of

$$\frac{dP}{dz} = \frac{dP_f}{dz} + \frac{dP_a}{dz} + \frac{dP_g}{dz} \tag{6-39}$$

can be seen in Appendix V (Eq. (V-6)). Therefore, Substituting Eqs. (6-36)–(6-38) into Eq. (6-35), yields

$$\begin{aligned}&(Pv_{fg}+u_{fg})\frac{dx}{dz}+\left[\left(\frac{dP_f}{dz}+\frac{dP_a}{dz}+\frac{dP_g}{dz}\right)\frac{du_{fg}}{dP}+P\frac{dv_g}{dP}\left(\frac{dP_f}{dz}+\frac{dP_a}{dz}+\frac{dP_g}{dz}\right)+v_{fg}\frac{dP_f}{dz}\right]x\\&+\frac{du_f}{dP}\left(\frac{dP_f}{dz}+\frac{dP_a}{dz}+\frac{dP_g}{dz}\right)+v_f\frac{dP_f}{dz}-\frac{q}{L}=0\end{aligned} \tag{6-40}$$

From Eq. (V-26), the accelerational pressure gradient for homogeneous flow is written as

$$\frac{dP_a}{dz} = -G^2\frac{dv_H}{dz} \tag{6-41}$$

Substituting Eq. (6-31) into Eq. (6-41) and neglecting the compressibility of the liquid phase, results in

$$\frac{dP_a}{dz} = -G^2\left(v_{fg}\frac{dx}{dz}+x\frac{dv_g}{dz}\right) \tag{6-42}$$

The gravitational pressure gradient is written as

$$\frac{dP_g}{dz} = -\frac{1}{v_H}g\cdot\sin\theta \tag{6-43}$$

For a vertical flow, $\theta = 90°$, Equation (6-43) becomes

$$\frac{dP_g}{dz} = -\frac{1}{v_H}g = -\rho_H g \tag{6-44}$$

Equation (6-42) can be further expanded into

$$\frac{dP_a}{dz} = -G^2\left(v_{fg}\frac{dx}{dz} + x\frac{dv_g}{dP}\frac{dP}{dz}\right) = -G^2\left[v_{fg}\frac{dx}{dz} + x\frac{dv_g}{dP}\left(\frac{dP_f}{dz} + \frac{dP_a}{dz} + \frac{dP_g}{dz}\right)\right] \tag{6-45}$$

Substituting Eq. (6-44) into Eq. (6-45) and rearranging it, gives

$$\left(1 + G^2 x\frac{dv_g}{dP}\right)\frac{dP_a}{dz} = -G^2\left[v_{fg}\frac{dx}{dz} + x\frac{dv_g}{dP}\left(\frac{dP_f}{dz} - \rho_H g\right)\right] \tag{6-46}$$

Collier (1981) has concluded that

$$\left|G^2 x\frac{dv_g}{dP}\right| << 1 \tag{6-47}$$

and an example of a calculation based on the present measurements has shown that, at ρ_f/ρ_g=20.3 and ψ_k=194, the values of $|G^2x(dv_g/dP)|$ are 0.019 and 0.037 for water and HCFC-22, respectively. Therefore, for simplification, we can neglect this term and reduce Eq. (6-46) to

$$\frac{dP_a}{dz} = -G^2\left[v_{fg}\frac{dx}{dz} + x\frac{dv_g}{dP}\left(\frac{dP_f}{dz} - \rho_H g\right)\right] \tag{6-48}$$

Now Eq. (6-40) can be further reduced by combining Eqs. (6-44) and (6-48):

$$\left(Pv_g + u_{fg} - PG^2 v_{fg} x\frac{dv_g}{dP} - G^2 x v_{fg}\frac{du_{fg}}{dP} - G^2 v_{fg}\frac{du_f}{dP}\right)\frac{dx}{dz} + \left[v_f + \frac{du_f}{dP} + x v_{fg}\right.$$
$$\left. + x\frac{du_{fg}}{dP} + Px\frac{dv_g}{dP} - PG^2 x^2\left(\frac{dv_g}{dP}\right)^2 - G^2 x\frac{du_f}{dP}\frac{dv_g}{dP} - G^2 x^2\frac{du_{fg}}{dP}\frac{dv_g}{dP}\right]\frac{dP_f}{dz} \qquad (6\text{-}49)$$
$$+\left[G^2 x^2\frac{du_{fg}}{dP}\frac{dv_g}{dP} + G^2 x\frac{du_f}{dP}\frac{dv_g}{dP} - x\frac{du_{fg}}{dP} - \frac{du_f}{dP} + PG^2 x^2\left(\frac{dv_g}{dP}\right)^2 - P\frac{dv_g}{dP}x\right]\rho_H g$$
$$-\frac{q}{L} = 0$$

For $-dP_f/dz$ in the two-phase region, Equations (V-30)–(V-32) in Appendix V may be used. Thus, Equation (6-49) becomes

$$(c_1 + c_2 x)\frac{dx}{dz} + c_3\frac{1 + c_4 x}{(1 + c_5 x)^{1/4}}(c_6 + c_7 x + c_8 x^2) + \frac{c_9 + c_{10} x + c_{11} x^2}{1 + c_4 x} - \frac{q}{L} = 0 \qquad (6\text{-}50)$$

where

$$c_1 = Pv_{fg} + u_{fg} - G^2 v_{fg}\frac{du_f}{dP} \qquad (6\text{-}51)$$

$$c_2 = -G^2 v_{fg}\frac{du_{fg}}{dP} - PG^2 v_{fg}\frac{dv_g}{dP} \qquad (6\text{-}52)$$

$$c_3 = -0.158\left(\frac{G^2 v_f}{D}\right)\left(\frac{GD}{\mu_f}\right)^{-\frac{1}{4}} \qquad (6\text{-}53)$$

$$c_4 = \frac{v_{fg}}{v_f} \tag{6-54}$$

$$c_5 = \frac{\mu_{fg}}{\mu_g} \quad where \quad \mu_{fg} = \mu_f - \mu_g \tag{6-55}$$

$$c_6 = v_f + \frac{du_f}{dP} \tag{6-56}$$

$$c_7 = \frac{du_{fg}}{dP} + v_{fg} - G^2 \frac{du_f}{dP}\frac{dv_g}{dP} + P\frac{dv_g}{dP} \tag{6-57}$$

$$c_8 = -G^2 \frac{du_{fg}}{dP}\frac{dv_g}{dP} - PG^2\left(\frac{dv_g}{dP}\right)^2 \tag{6-58}$$

$$c_9 = -\frac{du_f}{dP}\frac{g}{v_f} \tag{6-59}$$

$$c_{10} = \frac{g}{v_f}\left(G^2 \frac{du_f}{dP}\frac{dv_g}{dP} - \frac{du_{fg}}{dP} - P\frac{dv_g}{dP}\right) \tag{6-60}$$

$$c_{11} = \frac{g}{v_f}\left[G^2 \frac{du_{fg}}{dP}\frac{dv_g}{dP} + PG^2\left(\frac{dv_g}{dP}\right)^2\right] \tag{6-61}$$

and

$$g = 9.81 \tag{6-62}$$

The coefficients c_1—c_{11} are calculated based on local pressure and temperature conditions. Equation (6-50) is an ordinary differential equation, which can be solved by using a numerical method such as the Runge-Kutta method.

6.5.3 Results of Calculation

To use the Runge-Kutta method for Eq. (6-50), the increment of length is set for 1 cm. Once the quality (x) and quality gradient (dx/dz) along the heated length are calculated, the quality distribution from the inlet of heated length to CHF location can be seen by plotting the quality (x) against the dimensionless axial location (z/L). The data used for this calculation are HCFC-22 and water CHF data for 8 mm I.D. tubes obtained from the MR-7A and MR-1A loops. As noted from Table 3-2 and Table 3-3, the heated length of the HCFC-22 tests varies from 0.67 to 1.61 m and the heated length for the water test is 1.75 m. Since the purpose of making the x-vs-z graph is to compare the quality trajectories between water and the modelling fluid, identical geometries are required. The heated length of water test thus is trimmed artificially as illustrated in Fig. 6-2, where a new inlet quality of water flow is represented by the quality at the location of 14 cm or 60 cm away from the inlet of heated length. This can be achieved only for the homogeneous flow assumption.

For the present study, the heated length for the water test is trimmed from 1.75 m to 1.61 and 1.15 m, respectively, corresponding to the heated lengths of HCFC-22 test. In addition to the effect of identical geometry for the comparison of quality distribution between water and HCFC-22, the identical parameters such as ρ_f/ρ_g, ψ_k and X_i (inlet quality) are also used. The ranges of these parameters are:

ρ_f/ρ_g : 20.3 and 12.4 (7 and 10 MPa of water-equivalent pressure)

Mass flux for water: 2.6, 3.9, 5.2 and 7.8 Mg m^{-2} s^{-1}

Mass flux for HCFC-22: 2, 3, 4 and 6 Mg m^{-2} s^{-1}

ψ_k : 65, 97, 129 and 194 (for 7 MPa of water-equivalent pressure)

ψ_k : 80, 121, 161 and 241 (for 10 MPa of water-equivalent pressure)

L : 1.15 and 1.61 m

D : 8 mm

Figures 6-3—6-6 illustrate the comparison of the thermodynamic quality distribution vs. the dimensionless axial location between water and HCFC-22 with the identical L/D, and nearly identical ρ_f/ρ_g and ψ_k (because of impossibility of finding an exact match of experimentally scaled conditions). Since it is difficult to obtain an identical X_i experimentally, the values of $|X_{i,water}-X_{i,HCFC-22}|<0.01$ are used. Note that the X_i used in Figs. 6-3—6-6 is calculated based on the h_f and λ at inlet pressure conditions because the quality distribution represents the local phenomenon.

6.5.4 Comparison and Discussion

As discussed previously, the quality increase in a heated channel is attributed to the effects

of flashing and enthalpy increase, i.e., Eq. (6-25). The quality gradients due to the effects of flashing and enthalpy increase for water and HCFC-22 are also calculated separately and compared with each other. The comparison of $[dx/d(z/L)]_F$ at CHF location between water and HCFC-22 is illustrated in Fig. 6-7, where the $[dx/d(z/L)]_F$ for HCFC-22 is greater than that for water at all flow conditions and the trend increases with increasing ψ_k (i.e. mass flux). The dissimilarity of the flashing effect between water and HCFC-22 also results in a hydrodynamic dissimilarity in a flow channel: the change in density ratio over the whole heated channel, $\Delta(\rho_f/\rho_g)$, between water and HCFC-22 are compared as illustrated in Fig. 6-8, where the density ratio change over the whole heated length of HCFC-22 is greater than that of water for a given X_e and ψ_k for all flow conditions. This implies that perfect hydrodynamic similarity between water and HCFC-22 is hard to maintain.

The quality gradient due to friction, kinetic energy and potential energy changes affects the enthalpy gradient (i.e. Eq. (6-26)) for water and HCFC-22 and can be calculated, e.g.,

$$\left.\frac{dx}{dz}\right)_{W_f} = \frac{-v\,dP_f}{\lambda\,dz} \tag{6-63}$$

A comparison of the quality change over the whole heated length due to friction heat, kinetic energy change and potential energy change between water and HCFC-22 are illustrated in Figs. 6-9–6-11. All these figures have shown the larger quality changes for HCFC-22 than those of water. Figures 6-9 and 6-10 also show that the ΔX_{Wf} and $\Delta X_{K.E.}$ increase with increasing ψ_k at a fixed X_e, presumably because of the increase of friction and kinetic energy change with increasing mass flux. Figure 6-11 shows a constant $\Delta X_{P.E.}$ for various ψ_k because the potential energy change for unit mass in the same height of the heated channel does not change with the

mass velocities. Also the quality change over the whole heated length of the combined effect (i.e. $\Delta X_{Wf}+\Delta X_{K.E.}+\Delta X_{P.E.}$) of water and HCFC-22 are compared as illustrated in Fig. 6-12, where in general the quality change over the whole heated length of the combined effect for HCFC-22 is greater than that of water. Figure 6-12 also shows that the quality change increases with increasing mass flux for both fluids, probably because of an increase of friction heat and kinetic energy change with increasing mass flux.

The mass fluxes or ψ_k values of the present study result in a very small magnitude (order of 10^{-3}) of the quality change over the whole heated length of the combined effect compared to the effects of heat input (order of 10^{-1}) and flashing (order of 10^{-2}) over the whole heated length. Therefore, for the range of mass flux or ψ_k in the present study, the quality change over the whole heated length of enthalpy increase can be approximated by the effect of heat input and flashing: $\Delta X=\Delta X_q+\Delta X_F$. As shown in Fig. 6-13, the quality change over the whole heated length from the flashing effect (ΔX_F) for HCFC-22 is greater than that for water. This may affect the similarity of ΔX_q between the two fluids and thus results in different X_c and Bo for both fluids as shown in Figs. 6-3—6-6.

The Bo ratio of HCFC-22 to water as shown in Figs. 6-3—6-6 indicates the scaling accuracy of CHF from HCFC-22 to water, where the maximum error is about 15% under the highest mass flow (or ψ_k) condition. Assuming that the 15% difference of Bo between water and HCFC-22 is a maximum permissible error for HCFC-22 to scale the water CHF, the value of ψ_k at 194 for ρ_f/ρ_g=20.3 and ψ_k at 241 for ρ_f/ρ_g=12.4 correspond to the maximum ψ_k value that will keep the accuracy within 15%. Both ψ_k values (194 and 241) correspond to the mass flux of 6 Mg m^{-2} s^{-1} for HCFC-22 and about 8 Mg m^{-2} s^{-1} for water at both pressure conditions (7 and 10 MPa

water-equiv.). Therefore, for HCFC-22 at the conditions of mass flux beyond 6 Mg m^{-2} s^{-1} and ρ_f/ρ_g=12.4—20.3, caution must be exercised when converting the HCFC-22 CHF to water CHF for a satisfactory accuracy.

In Section 2.2.1, the scaling theory assumes that the equivalence of the local quality and the boiling number for both fluids can be obtained by using the Eq. (2-5) when L/D and $\Delta H_i/\lambda$ are the same. The use of Eq. (6-50) with the measured data has shown that this relationship (i.e. the local quality and the boiling number are correlated) can not be satisfied at high flow conditions when the effects of flashing, friction, etc. are included. This indicates that the local qualities are not equivalent with the use of the same $\Delta H_i/\lambda$ in identical geometry for both fluids. However, one may argue that Eq. (6-50) only puts a limit to the equivalence of the two variables but not to the scaling law itself. This could raise a question: If the local qualities are equivalent regardless of whether or not $\Delta H_i/\lambda$ is the same, will the boiling number be the same for both fluids? Figures 6-14—6-17 show the comparisons of the quality trajectory between water and HCFC-22, where X_e is the same or very close for both fluids but $\Delta H_i/\lambda$ is not the same.

The figures also show that the difference of boiling number for both fluids sometimes is more than 20%. However, from Figs. 6-3(c), 6-5(c) and 6-14(c), good agreement between boiling numbers in water and HCFC-22 is observed when the axial quality distribution for both fluids are nearly coincident. Therefore, not only the local quality but also the upstream history (e.g. flashing, friction, etc.) will influence the CHF scaling accuracy.

To calculate the quality gradient (dx/dz) and the thermodynamic quality by using the differential equation, the pressure distribution along the heated length is required. However, this was not available during the CHF test. The pressure distribution thus is calculated using the

existing pressure drop correlations (e.g. Eq. (V-28) for single-phase friction, Eq. (V-30) for two-phase friction and Eq. (6-39) considering for all effects). Separate pressure drop data for water measured by Leung (1994) have been used to assess the validity of the correlations. The average and RMS errors of the pressure drop calculation from the correlations are -7.87% and 9.65%, respectively, based on 18 measured data. A similar error is also present in evaluating the changes in the saturated liquid enthalpy and the enthalpy of vaporization. However, sensitivity studies show that the effect of this error on the calculation of quality change (<0.3%) as well as the CHF simulation (<2.5%) is small.

6.6 Critical Flow Rate

6.6.1 General

The previous analysis has shown that CHF prediction for water can be achieved by using fluid-to-fluid scaling with satisfactory accuracy for wide ranges of parameters. For example, the mass flux has been tested up to 6 Mg m^{-2} s^{-1} for HCFC-22 and 8 Mg m^{-2} s^{-1} for water in the present experiment and the dissimilarity caused by the effects of flashing, friction and the changes of kinetic energy and potential energy on CHF remains satisfactory (≤15%). However, at low pressure and high flow, critical flow or "choking" may occur when the flow rate can not be increased any further while the pressure drop is still increasing due to a upstream high pressure head and a very low downstream pressure. The maximum flow rate at choking is the critical flow rate or the critical mass flux (G_c). The critical mass flux may be quite different in water than in modelling fluid and this difference as well as the magnitude of G_c will be examined in this section.

The cause of the "choking" phenomenon in the two-phase flow is mainly due to the existence of vapour in the flow. For single phase (gas only), the phenomenon has been studied extensively and it may be considered as well understood. In two-phase flow, the critical flow phenomenon is more complex. According to Isbin (1980), there is no single, best estimate model for predicting the two-phase critical flow rate. The two-phase critical flow is often studied for the application in the blow-down condition of a high-pressure system containing a high-temperature liquid or two-phase mixture. In such an application, the flow passing through the pipe or the channel usually is not heated and the vapour generated in the flow channel is mainly due to the flashing effect. Most two-phase critical flow models thus are developed for such non-heating application. They are categorized as (1) homogeneous equilibrium models, (2) homogeneous non-equilibrium models, (3) two-fluid (separate flow) models. These models vary from very simple to very sophisticated for predicting the critical two-phase flow rate.

6.6.2 Parametric Trend and Calculation Procedure

As presented by Bouré (1978), the critical flow criterion for a two-phase mixture can be expressed by

$$G_c = G_c(\alpha, \gamma^*, P, T_g, T_f, z) \tag{6-64}$$

where α is the void fraction, γ^* the slip ratio of vapour to liquid, P the pressure, T_g the vapour temperature, T_f the liquid temperature and z the axial location. Bouré concluded that G_c depends on local values of slip and thermal non-equilibrium, and this conclusion is confirmed by experimental data. The following parametric trends of two-phase critical flow were also observed by Bouré:

1. For a given geometry and operating conditions, the critical flow rate increases with increasing pressure at constant void fraction or at constant equilibrium quality.
2. For a given geometry and operating conditions, the critical flow rate increases with decreasing thermal non-equilibrium at constant void fraction.
3. For a given geometry and operating conditions, the critical flow rate decreases sharply with increasing void fraction or equilibrium quality at constant pressure, in the ranges covered by $\alpha<0.75$ and $x<0.01$.

More details regarding the physics and mathematics of critical flow, may be found in Bouré (1978) and Giot (1981).

Figure 6-19 illustrates the comparison of critical mass flux at various pressure (density ratio) conditions between water and HCFC-22 based on Henry's (1970) model. This is a homogeneous non-equilibrium model developed to describe the two-phase critical flow rate of initially saturated and subcooled liquid through the channel with a sharp edge, a uniform cross-sectional area and $L/D \geq 12$. Henry assumes that the flow is characterized by a non-equilibrium mass transfer (i.e. flashing) process. In his model, a correction is developed and added to the quality gradient term used for a homogeneous equilibrium model. The formulation of Henry's model is summarized as follows:

$$P_o - P_t = G_c^2 \left[\frac{v_{fo}}{2C_H^2} + x_t (v_{gt} - v_{fo}) \right] \tag{6-65}$$

$$G_c = \left[\frac{x v_g}{P_t} - (v_g - v_{fo}) N \frac{dx_E}{dP} \right] \tag{6-66}$$

and

$$\frac{dx_E}{dP} = -\left[\frac{(1-x)\frac{ds_f}{dP} + x\frac{ds_g}{dP}}{s_g - s_f} \right] \tag{6-67}$$

where

$N = 20\ x_E$ for $x < 0.05$

$N = 1.0$ for $x \geq 0.05$

and

$$x_E = \left(\frac{s_o - s_f}{s_g - s_f} \right)_E \tag{6-68}$$

where the subscript 'E' represents the equilibrium condition, s_o the flow stagnation entropy, s_f the saturated liquid entropy, s_g saturated vapour entropy, P_o the stagnation pressure, P_t the pressure at the choking plane, G_c the critical mass flux and C_H=0.61. The calculation using Henry's formulation requires iterations or computation with small incremental steps of pressure until the maximum mass flux is found.

6.6.3 Discussion

In Fig. 6-19, the critical mass flux for HCFC-22 is less than the equivalent mass flux for HCFC-22 converted from water G_c at the same ψ_k value. The results show that modelling fluids

are more prone to "choking" or critical flow condition than water; where as the CHF mass flux scaling factor is in the 1.2—1.6 range, the critical mass flux scaling factor in the 2—3 range. However, Henry's and other models for critical flow may not be applicable to the CHF case because they do not consider the effect of heat input. The actual critical mass fluxes for water and HCFC-22 in a heated channel will be lower than those shown in Fig. 6-19 because of the presence of wall vapour generation. The effect of quality on the critical mass flux of HCFC-22 and water is illustrated in Fig. 6-20, based on Chisholm's equation (in Giot (1981)): G_c decreases with increasing quality for both fluids and G_c for HCFC-22 is less than that of water at the same quality condition.

Figure 6-19 also shows that the critical mass flux for HCFC-22 is less than that for water for all pressure conditions. This is due to the fact that HCFC-22 can generate more vapour than water from the flashing effect. As shown in Fig. 6-19, at ρ_f/ρ_g=20.3, the critical mass flux for HCFC-22 is about 27 Mg m^{-2} s^{-1}, which has exceeded the operating capability of most test rigs. However, at lower pressure (e.g. ρ_f/ρ_g=100), the critical mass flux is below 10 Mg m^{-2} s^{-1}, which is more likely to occur during the test. The critical flow phenomena is thus a physical limitation regardless of the thermodynamic, hydrodynamic and geometric similarities between the two fluids. More work needs to be done to provide better predictions of the two-phase critical mass flux, especially when heat input is involved.

6.7 Other Potential Limitations of the CHF Scaling Technique

6.7.1 Effect of Mixing

CHF fluid-to-fluid scaling may also be affected by transverse mixing in rod bundles and

flow stratification. The transverse mixing is the transport of mass, momentum and energy between the adjacent subchannels and is mainly caused by the radial pressure gradient. For two-phase flow in rod bundles, the radial pressure gradient between adjacent subchannels may be the result of differences in subchannel hydraulic resistance, in subchannel heat input, onset of boiling, etc. The turbulent mixing usually is expressed by a dimensionless parameter, β^*, which represents the ratio of transverse mass flux to axial mass flux. Doerffer and Cheng (1992) have evaluated various correlations for β^* and concluded that the general function form for β^* can be expressed as

$$\beta^* = f(D/L, Re) \tag{6-69}$$

where the ratio D/L is a general notation for the geometric similarity. For the same ρ_f/ρ_g, mass flux scaling parameter and geometry for water and HCFC-22, the viscosity used in the Reynolds number (Re) for water is about half of that of HCFC-22. This will result in a Re for water about 2.5 times as high as that for HCFC-22 and mixing will be more efficient in water. Doerffer and Cheng concluded that mixing in complex geometries may increase the CHF in water for that geometry and may further limit the CHF scaling technique although the impact is expected to be small.

6.7.2 Flow Direction

In a horizontal flow channel, stratification is due to the asymmetric phase distribution and possibly phase separation by the gravitational force. In intermediate and low flows, the stratification force, due to ρ_f-ρ_g, can lead to a maldistribution of void and thus result in a severe effect on CHF. Wong et al. (1990) has analyzed the ratio of the transit time for a droplet or a

bubble travelling across a horizontal channel (bottom to top) to the transit time for travelling along the channel length. The transit-time ratio, θ^*, is a function of the following parameters:

$$\theta^* = f(G, \sqrt{\rho_f} \text{ or } \sqrt{\rho_g}, 1/\sqrt{\rho_f - \rho_g}, \alpha, x, L, D^{1/2}) \tag{6-70}$$

At the same ρ_f/ρ_g for water and HCFC-22, the value of $\rho_f-\rho_g$ for HCFC-22 is higher (about 50% higher) than that of water and θ^* is smaller for HCFC-22 than that of water for an equivalent mass flux, void fraction and geometry. This indicates that the effect of the buoyancy force on CHF for HCFC-22 is larger than that of water for the same parameters. However, at high flows, stratification becomes suppressed because of the much higher turbulent forces; stratification can be safely ignored at water-equivalent mass velocities greater than 3 Mg m^{-2} s^{-1}.

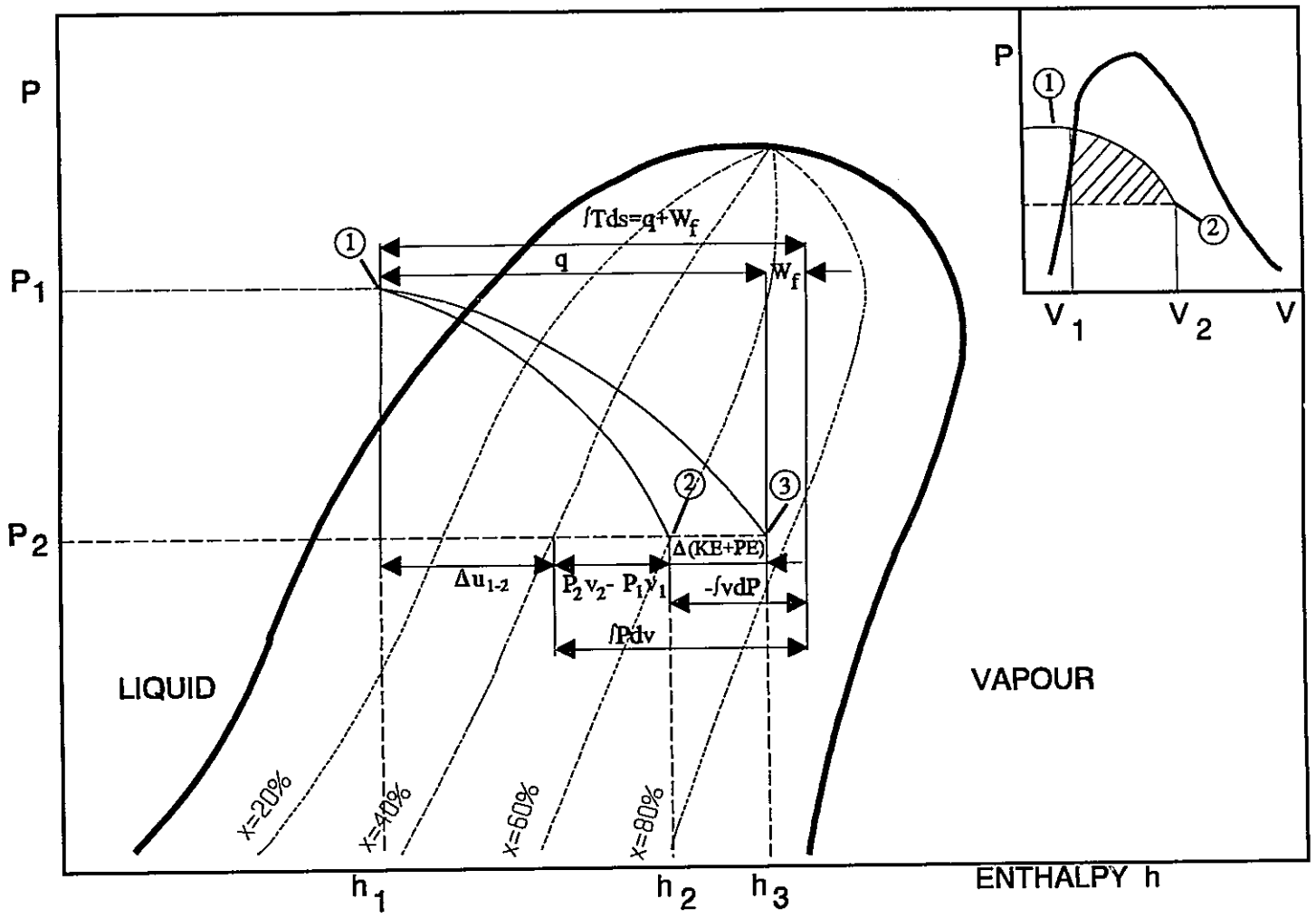

Figure 6-1 Enthalpy changes with pressure in a heated channel (Groeneveld, 1972)).

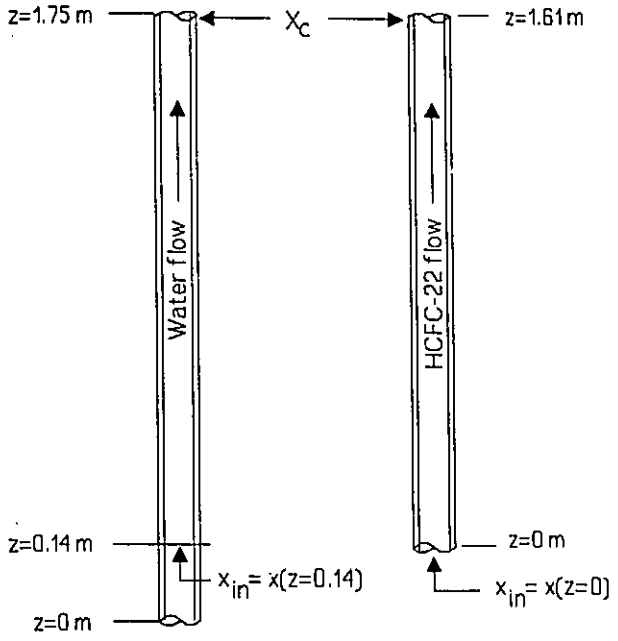

(a)

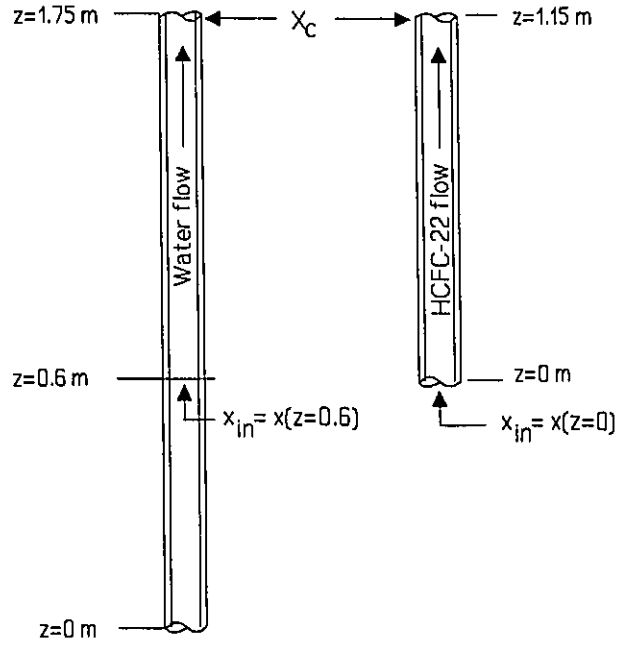

(b)

Figure 6-2 Determination of X_i for water test corresponding to HCFC-22 test (a) L=1.61 m (b) L=1.15 m

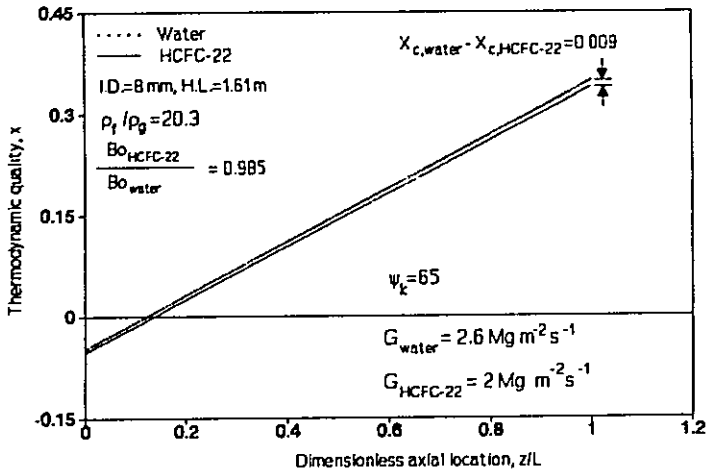

(a)

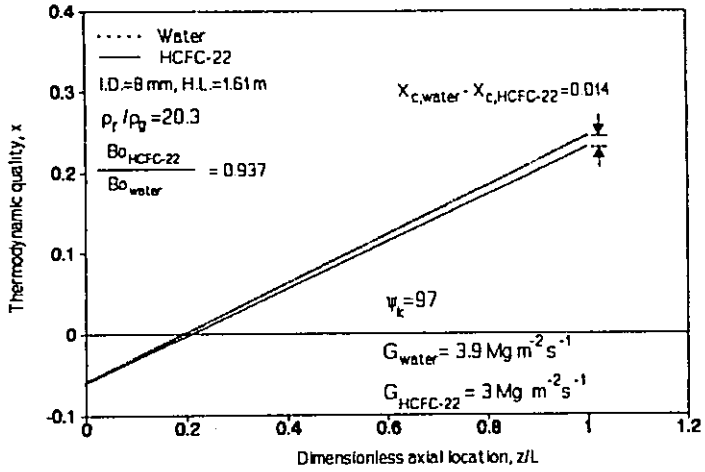

(b)

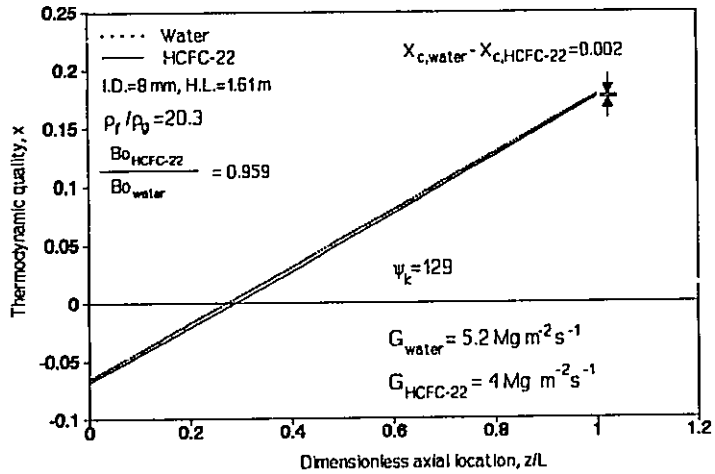

(c)

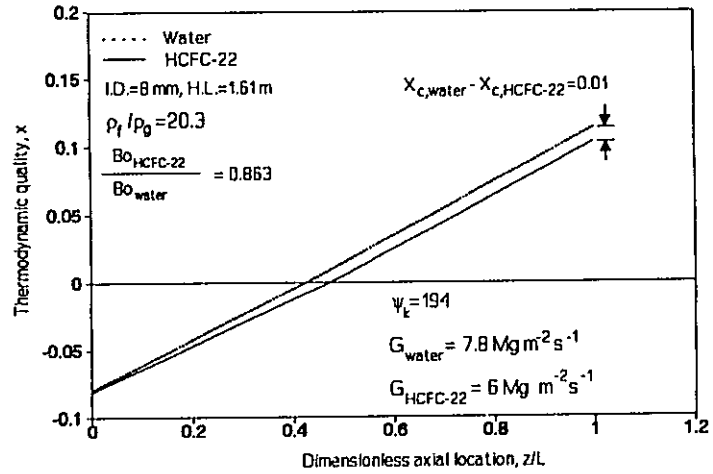

(d)

Figure 6-3 Quality distributions with constant X_i for water and HCFC-22 at ρ_f/ρ_g=20.3, H.L.=1.61 m and (a) ψ_k=65 (b) ψ_k=97 (c) ψ_k=129 (d) ψ_k=194.

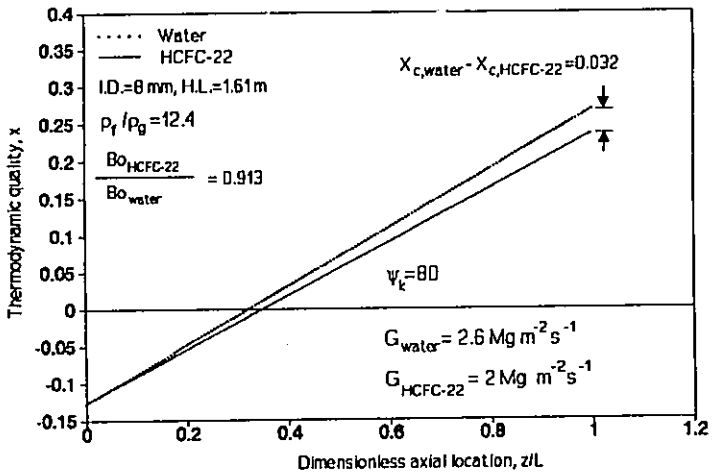

(a)

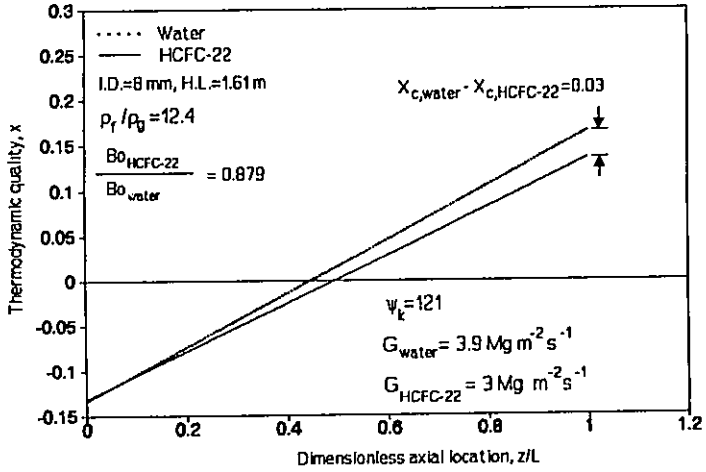

(b)

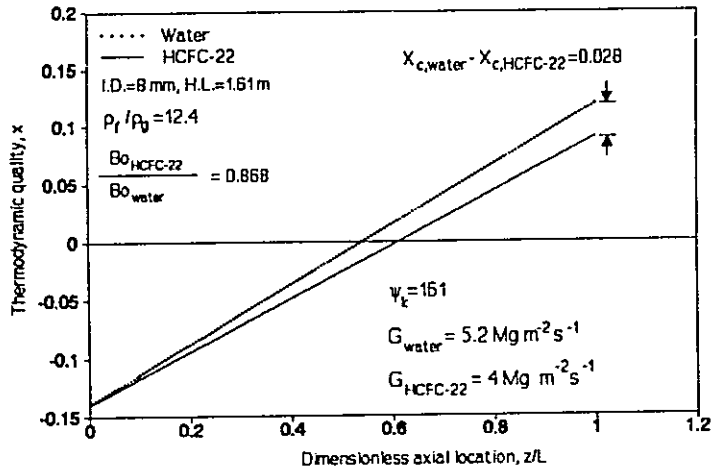

(c)

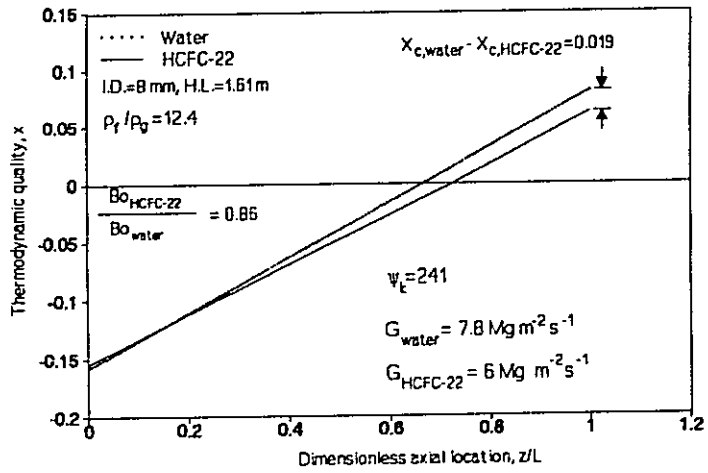

(d)

Figure 6-4 Quality distributions with constant X_i for water and HCFC-22 at ρ_f/ρ_g=12.4, H.L.=1.61 m and (a) ψ_k=80 (b) ψ_k=121 (c) ψ_k=161 (d) ψ_k=241.

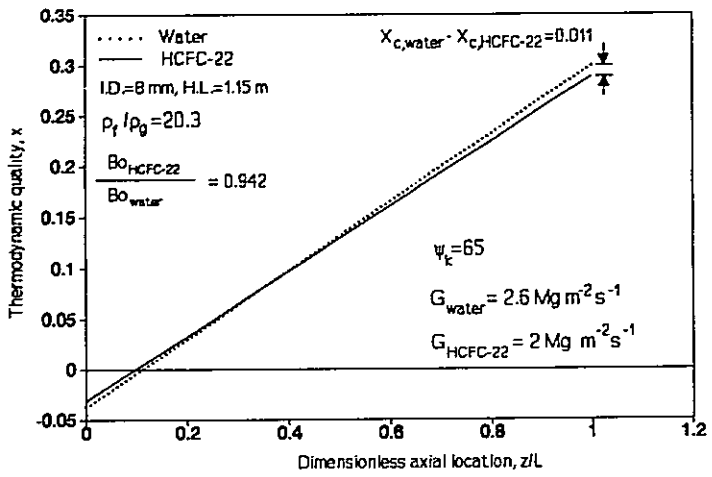

(a)

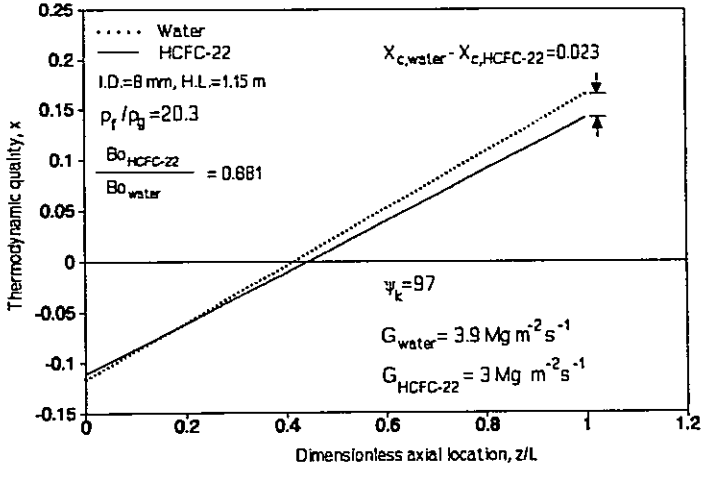

(b)

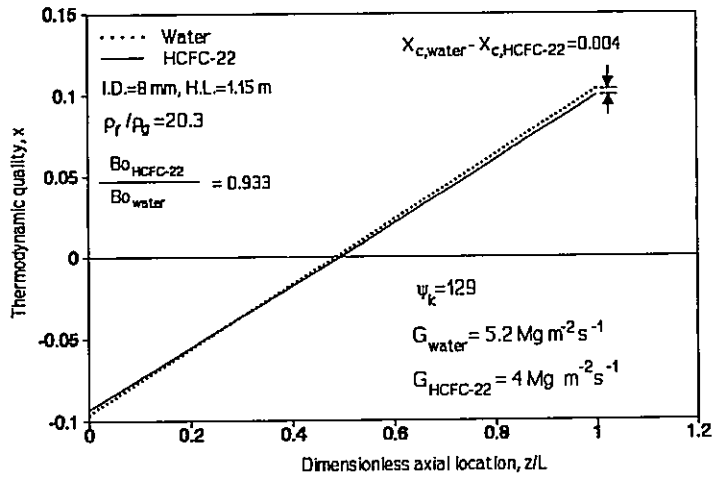

(c)

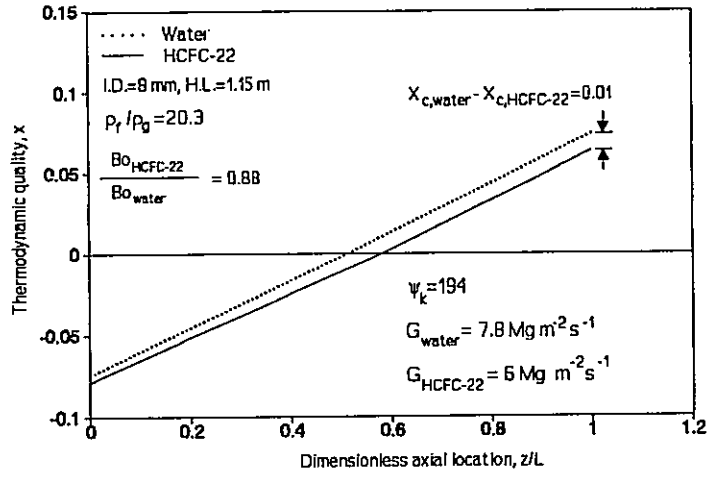

(d)

Figure 6-5 Quality distributions with constant X_i for water and HCFC-22 at ρ_f/ρ_g=20.3, H.L.=1.15 m and (a) ψ_k=65 (b) ψ_k=97 (c) ψ_k=129 (d) ψ_k=194.

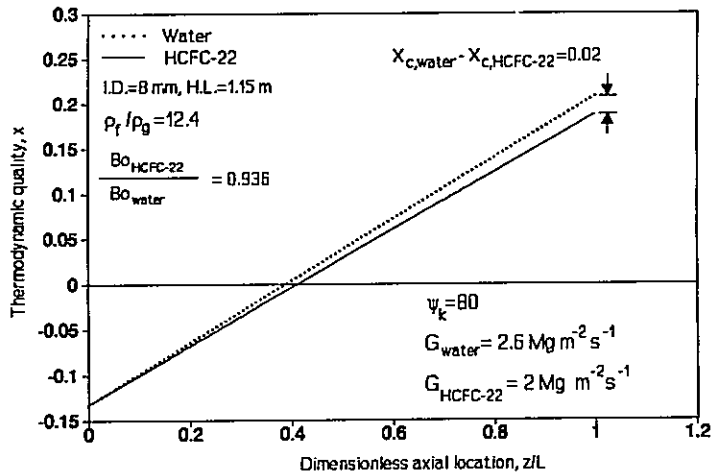

(a)

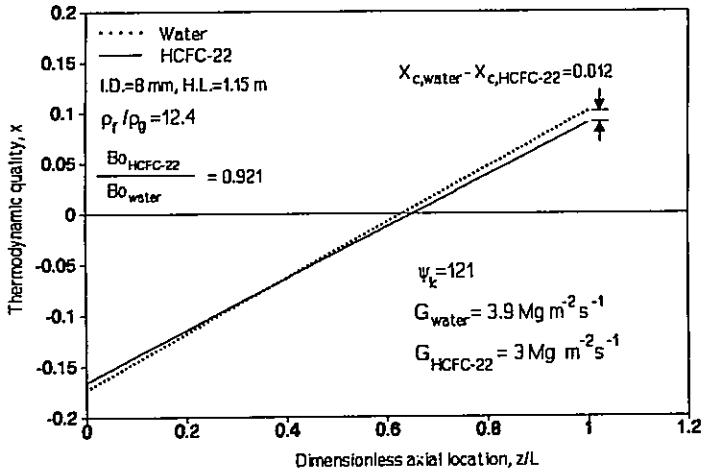

(b)

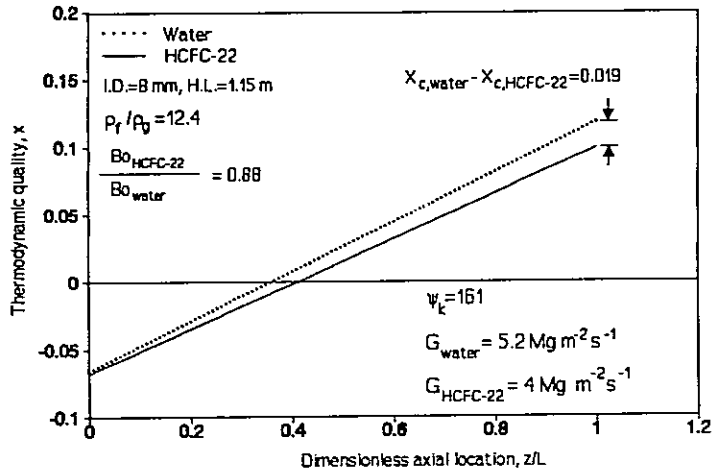

(c)

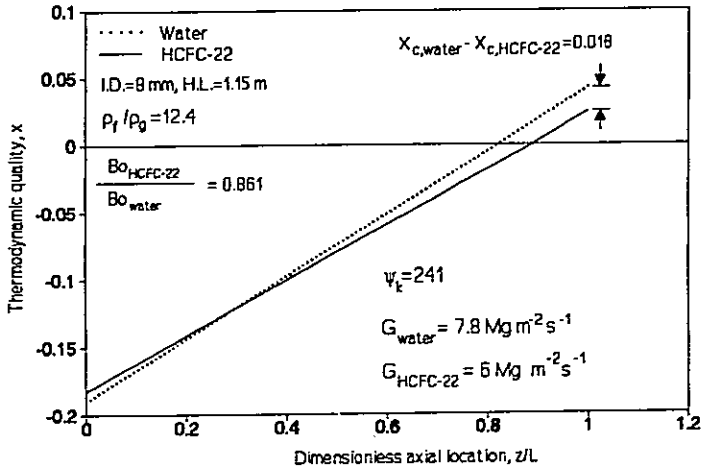

(d)

Figure 6-6 Quality distributions with constant X_i for water and HCFC-22 at ρ_f/ρ_g=12.4, H.L.=1.15 m and (a) ψ_k=80 (b) ψ_k=121 (c) ψ_k=161 (d) ψ_k=241.

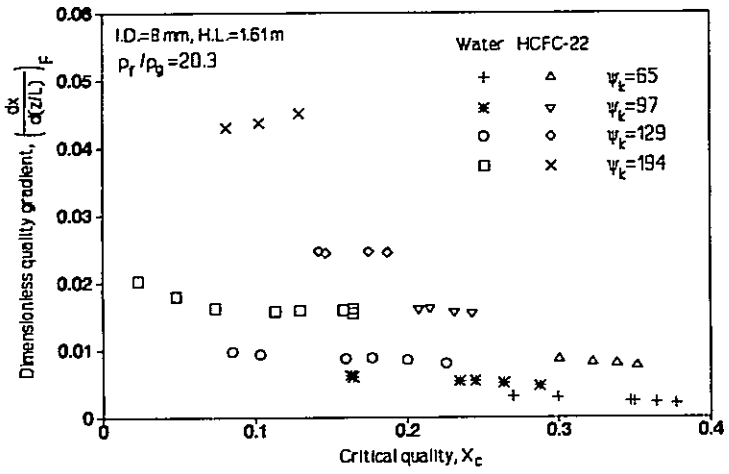

(a)

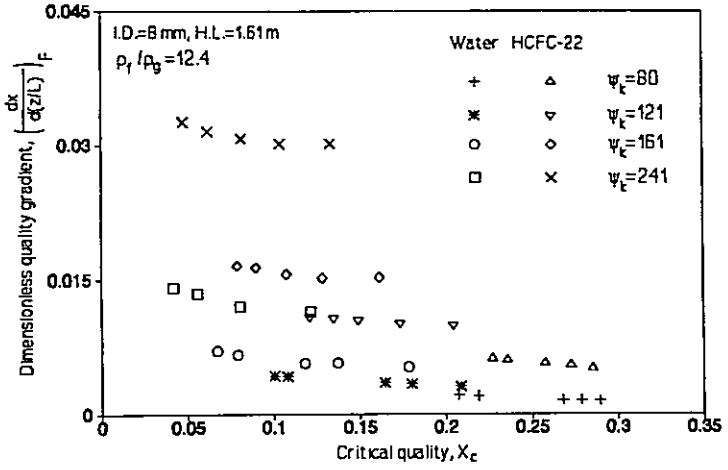

(b)

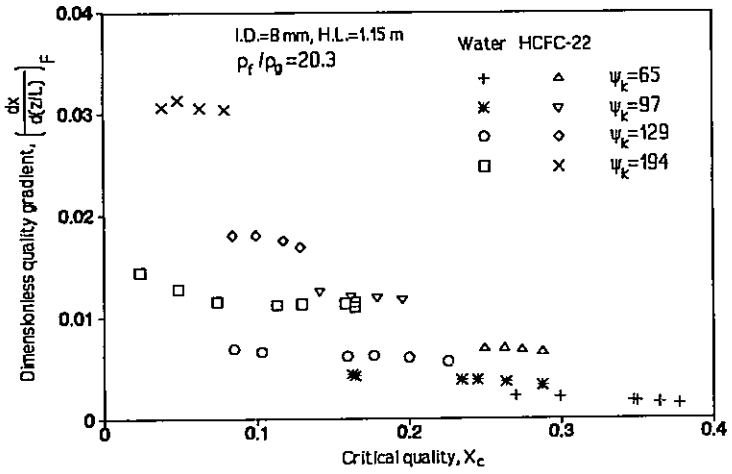

(c)

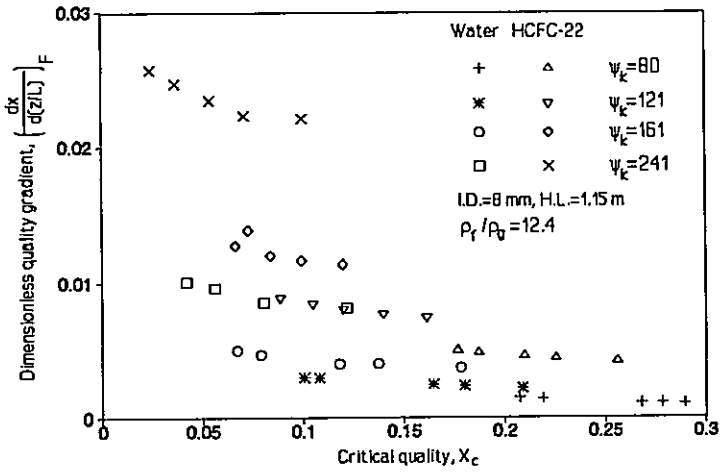

(d)

Figure 6-7 Comparison of the quality gradient for the flashing effect at the CHF location between water and HCFC-22 for various flow conditions.

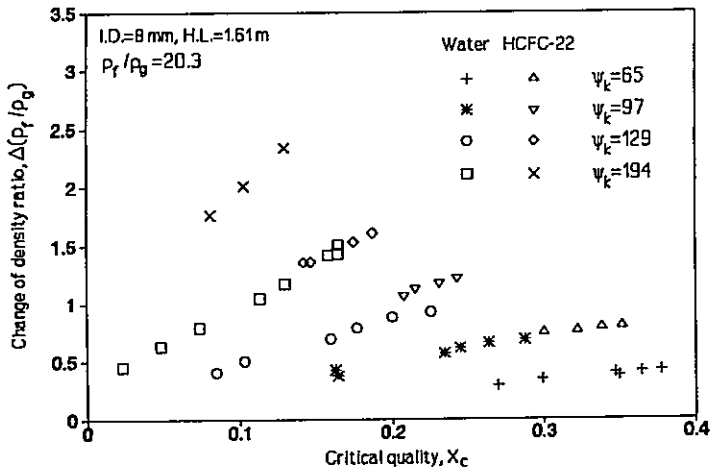

(a)

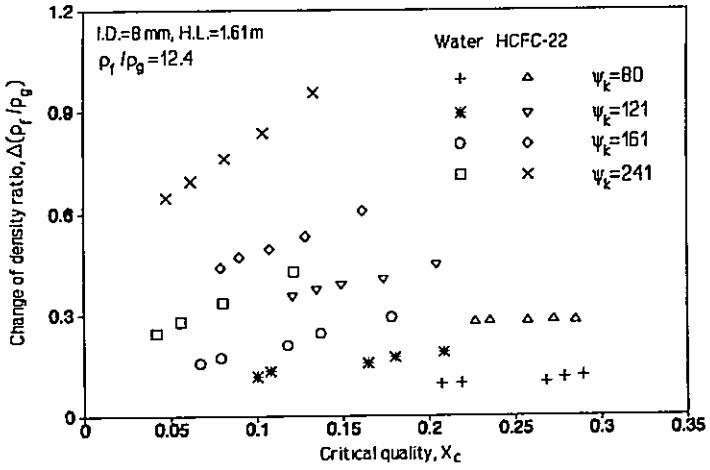

(b)

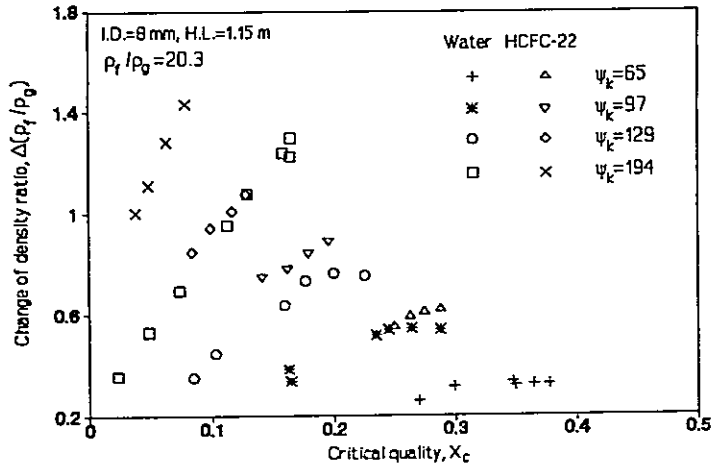

(c)

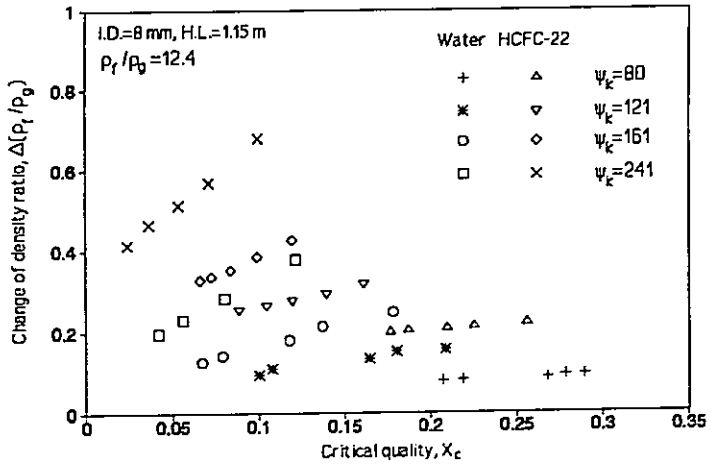

(d)

Figure 6-8 Comparison of the density ratio change over the whole heated length between water and HCFC-22 for various flow conditions.

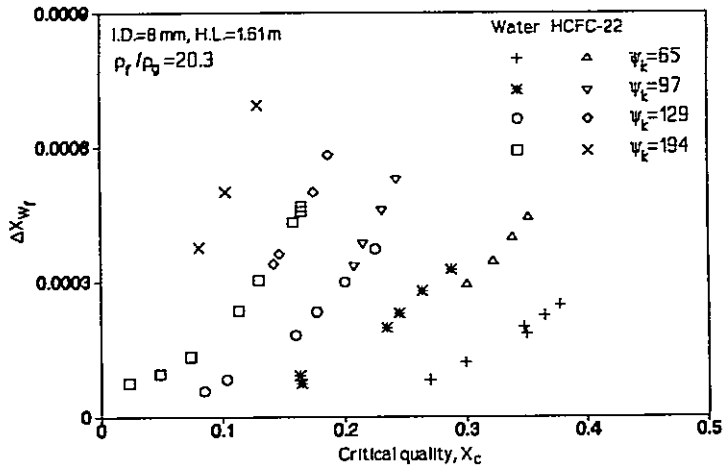

(a)

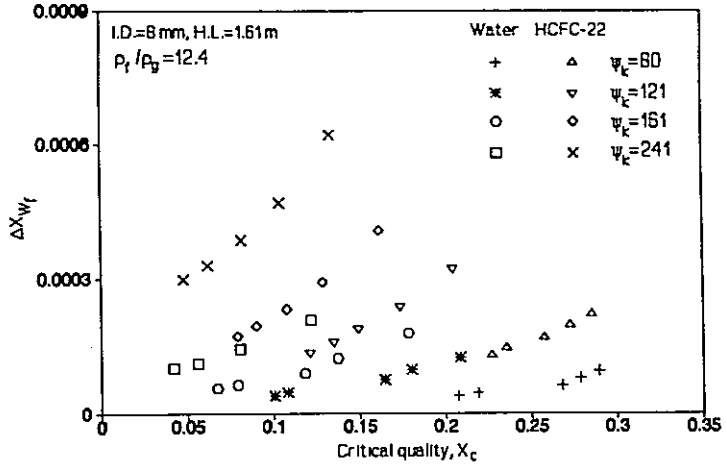

(b)

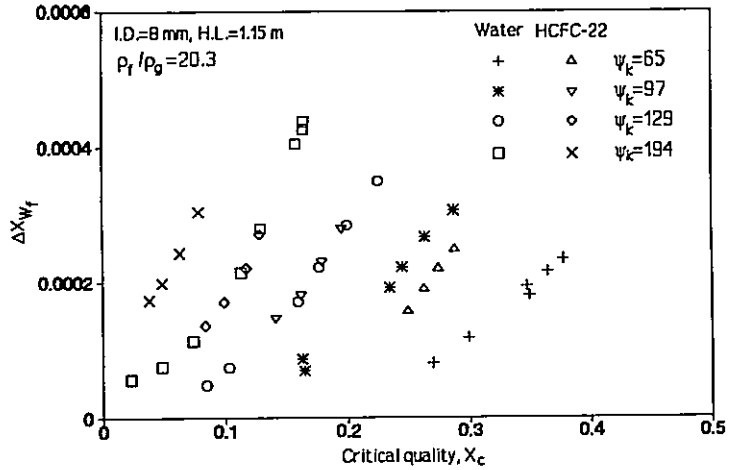

(c)

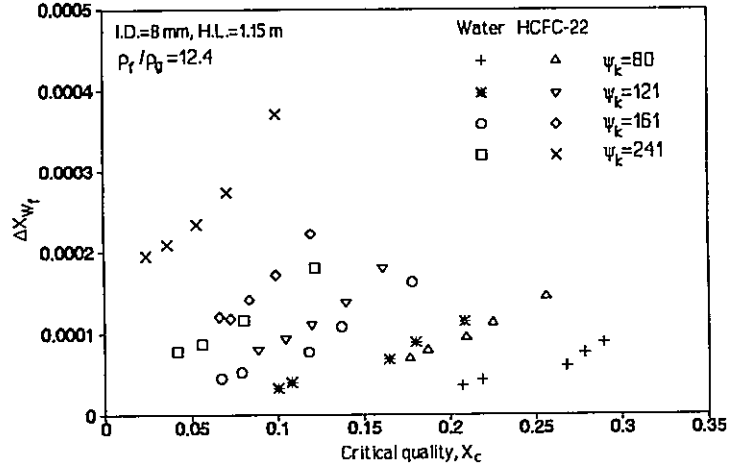

(d)

Figure 6-9 Comparison of the quality change for the frictional effect over the whole heated length between water and HCFC-22 for various flow conditions.

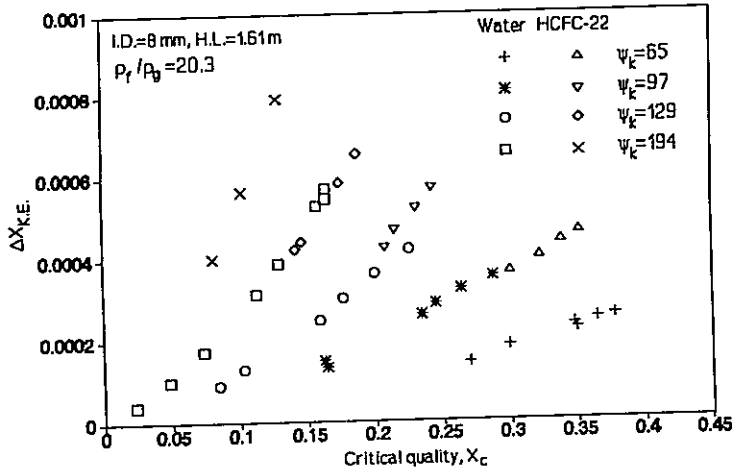

(a)

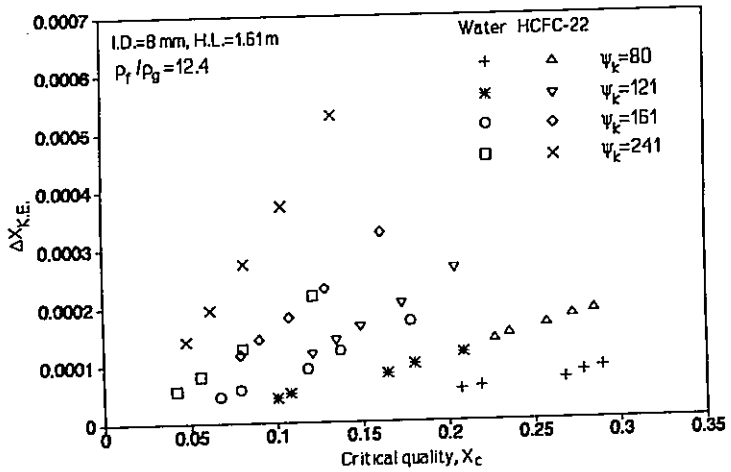

(b)

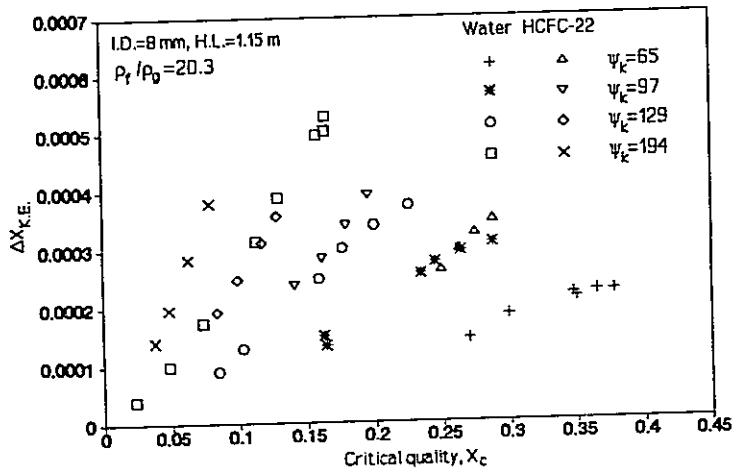

(c)

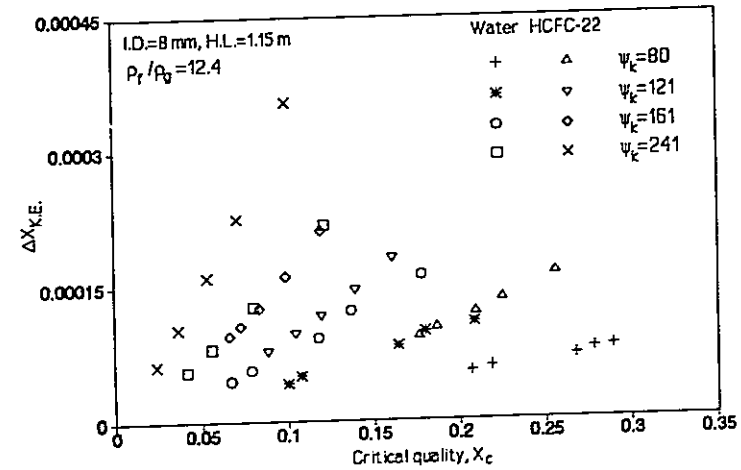

(d)

Figure 6-10 Comparison of the quality change for the kinetic energy change over the whole heated length between water and HCFC-22 for various flow conditions.

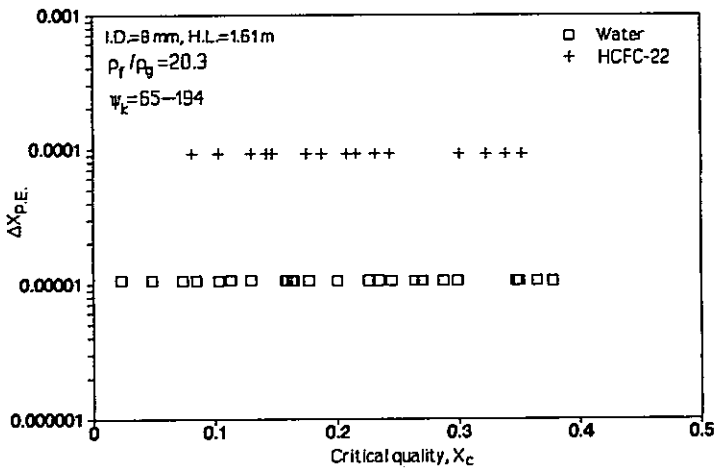

(a)

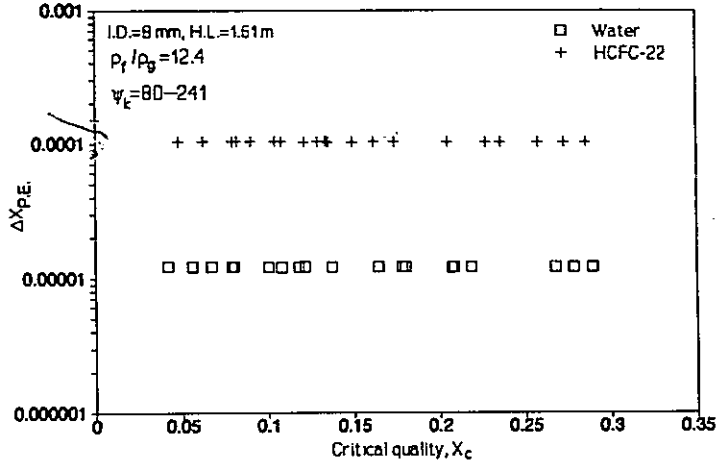

(b)

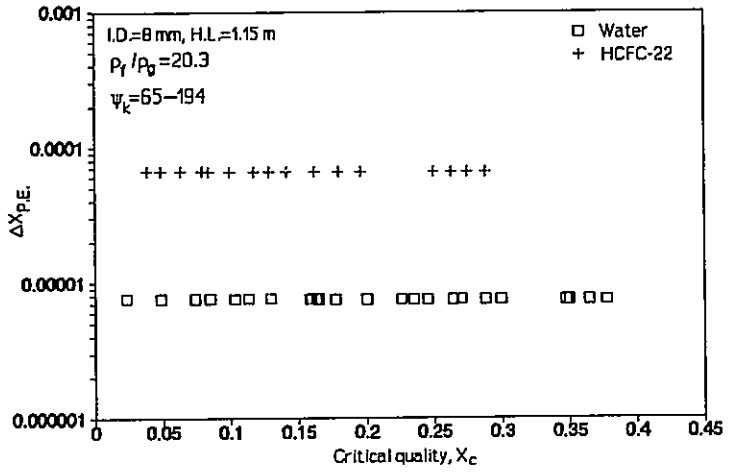

(c)

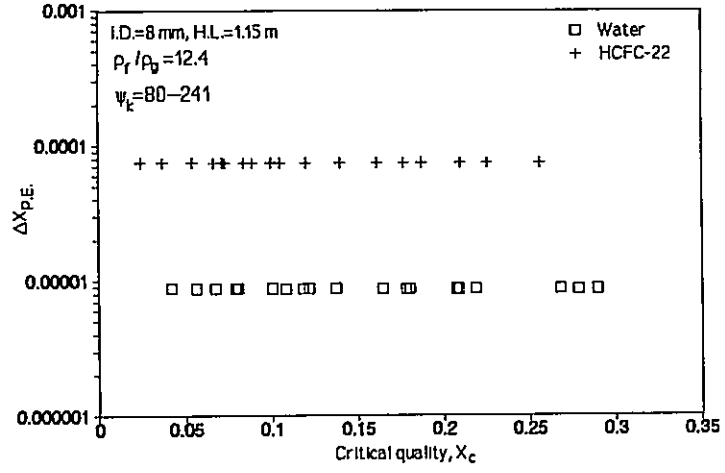

(d)

Figure 6-11 Comparison of the quality change for the potential energy change over the whole heated length between water and HCFC-22 for various flow conditions.

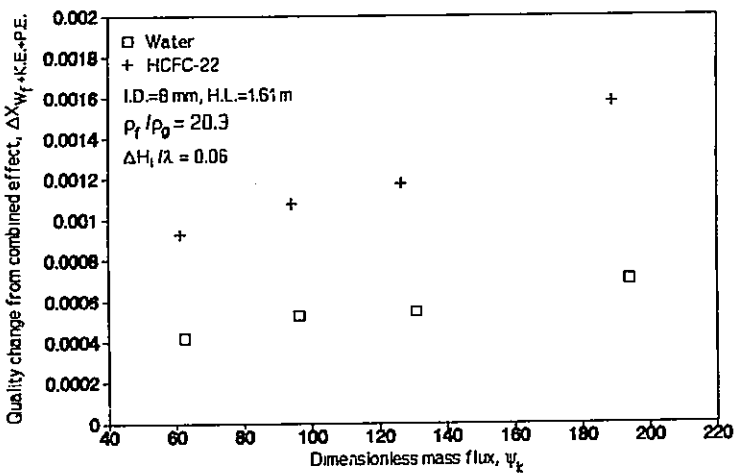

(a)

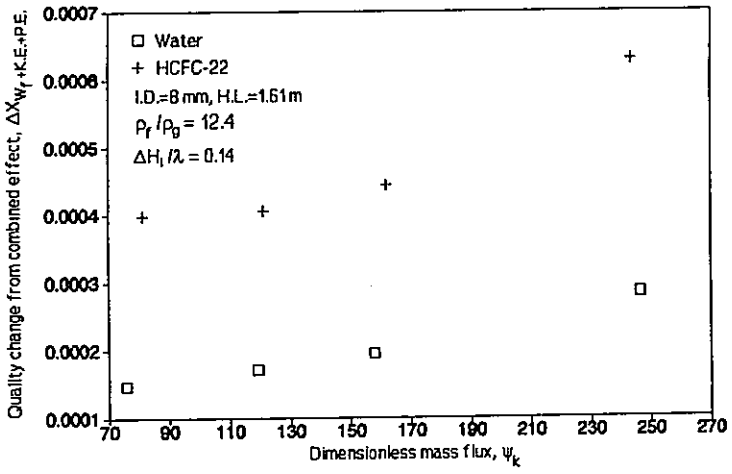

(b)

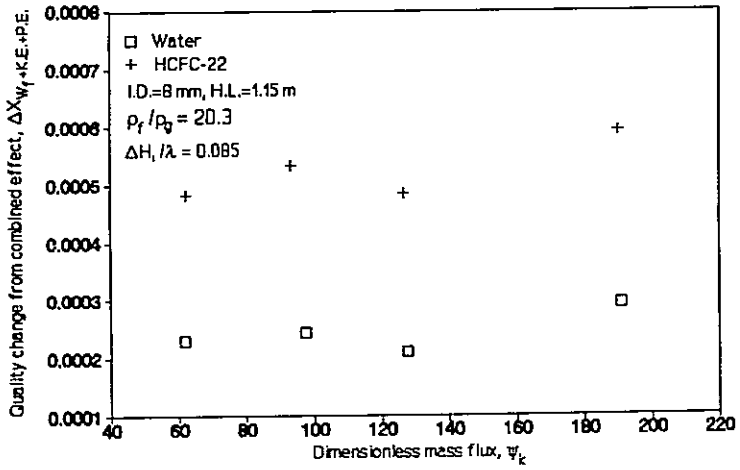

(c)

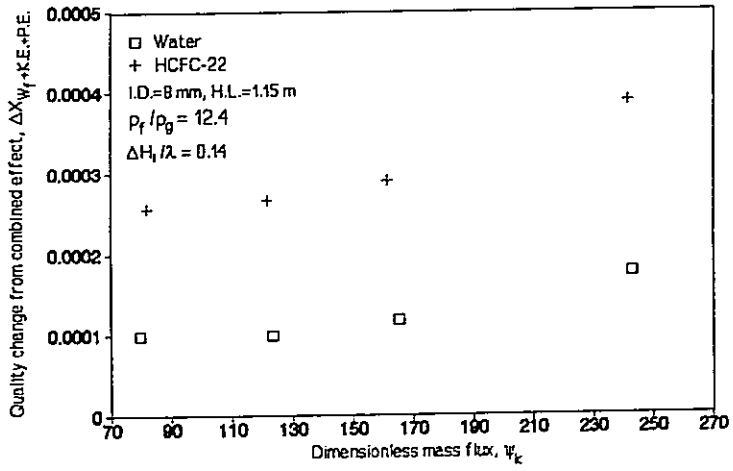

(d)

Figure 6-12 Comparison of the quality change for the combined effect over the whole heated length between water and HCFC-22 for various flow conditions.

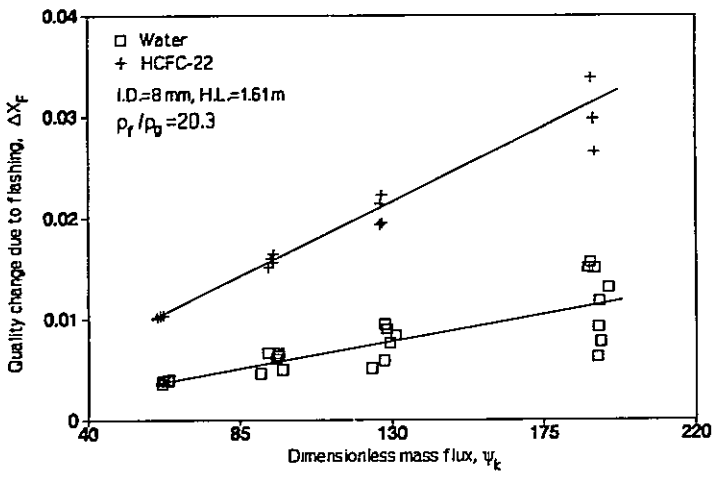

(a)

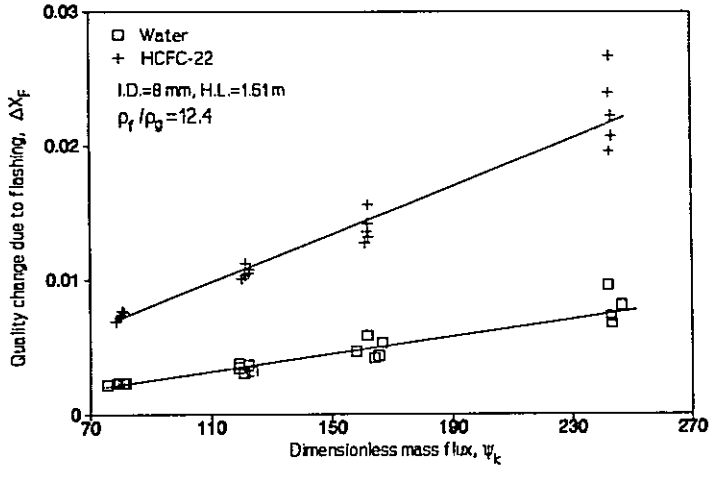

(b)

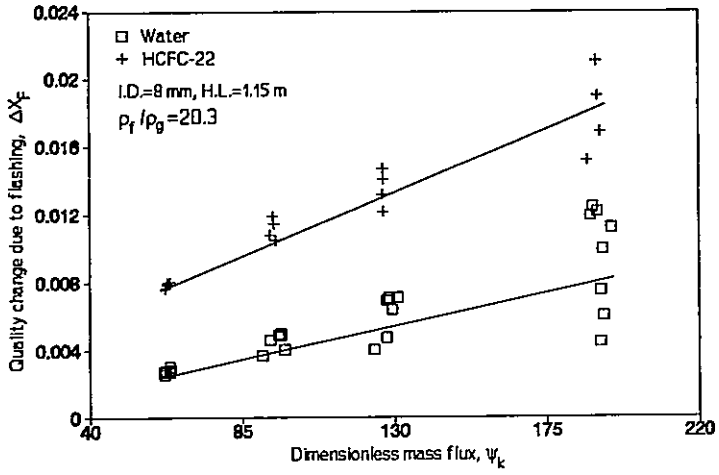

(c)

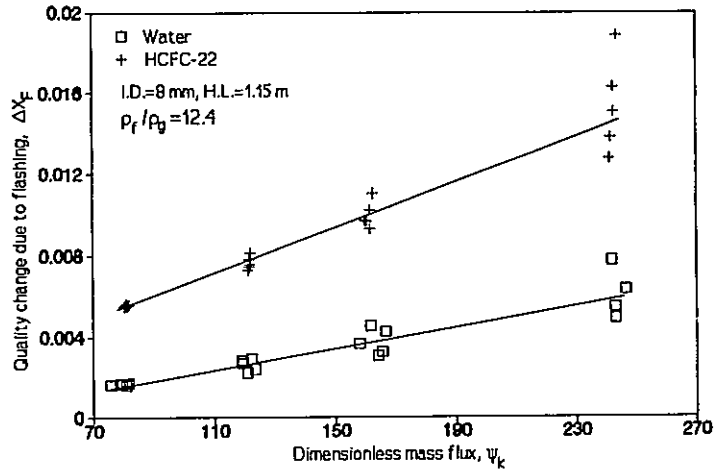

(d)

Figure 6-13 Comparison of the quality change for the flashing effect over the whole heated length between water and HCFC-22 for various flow conditions.

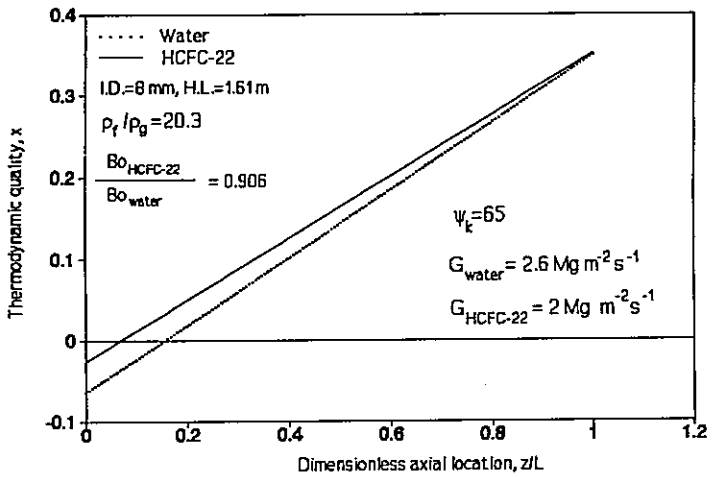

(a)

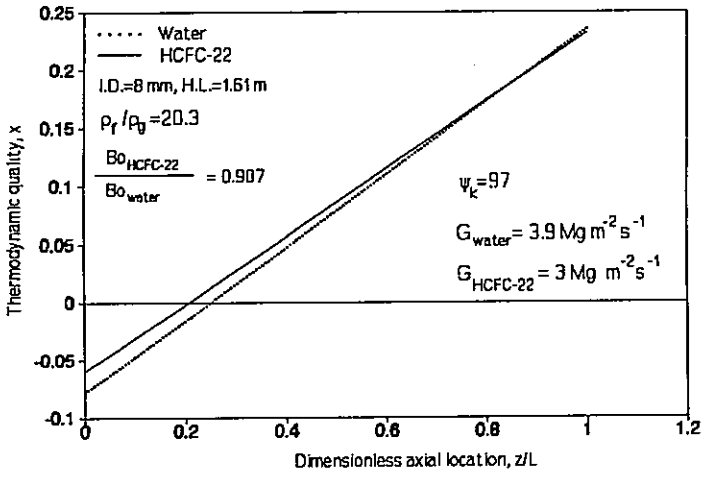

(b)

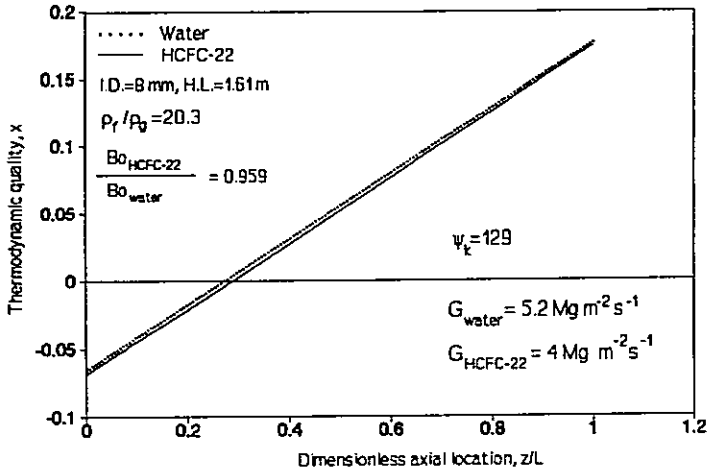

(c)

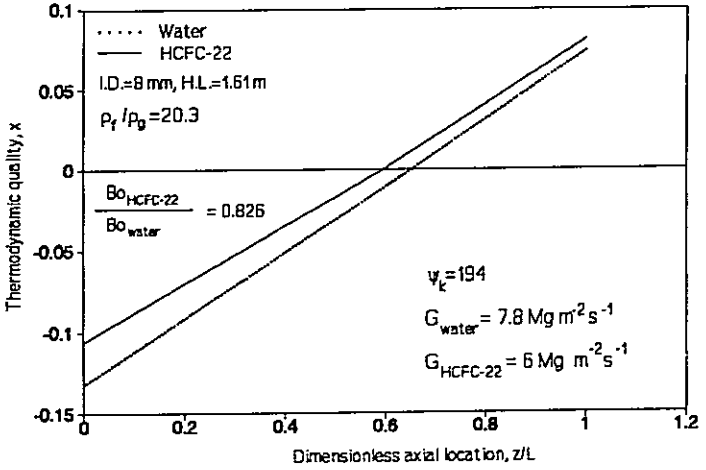

(d)

Figure 6-14 Quality distribution with constant X_c for water and HCFC-22 at ρ_f/ρ_g=20.3, H.L.=1.61 m and (a) ψ_k=65 (b) ψ_k=97 (c) ψ_k=129 (d) ψ_k=194.

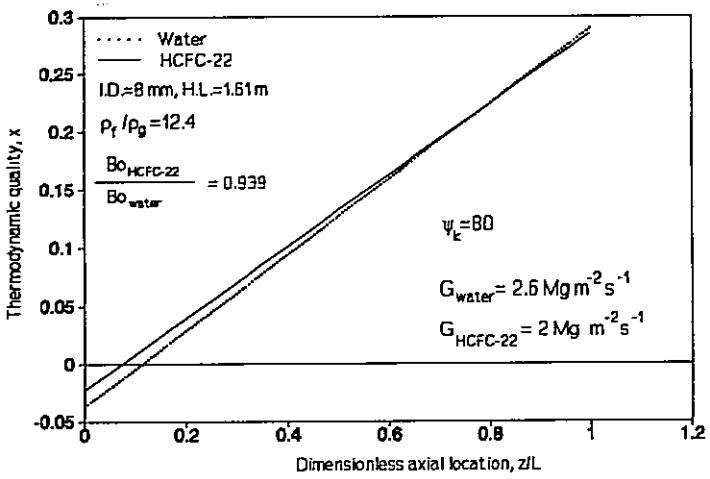

(a)

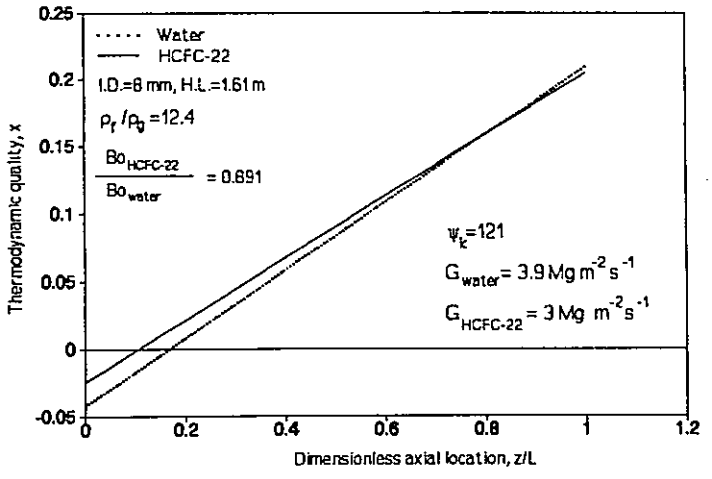

(b)

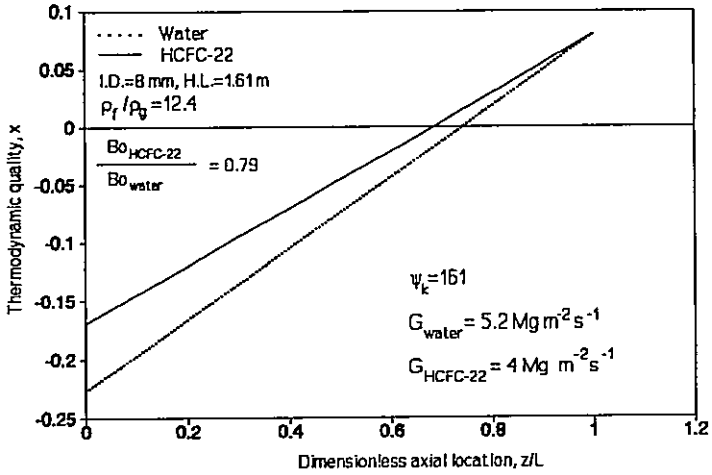

(c)

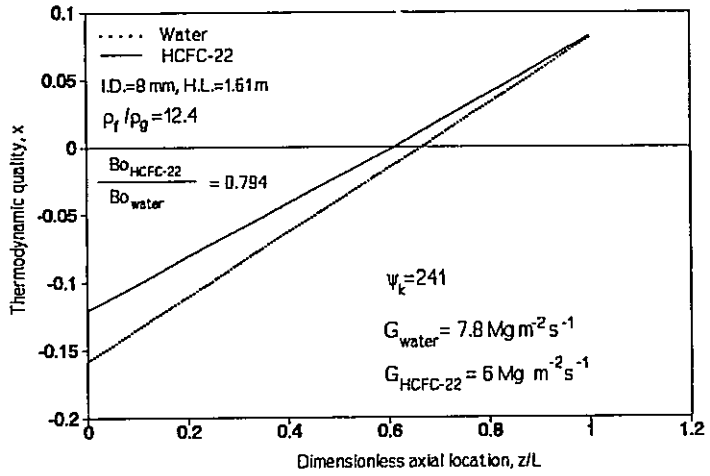

(d)

Figure 6-15 Quality distribution with constant X_c for water and HCFC-22 at ρ_f/ρ_g=12.4, H.L.=1.61 m and (a) ψ_k=80 (b) ψ_k=121 (c) ψ_k=161 (d) ψ_k=241.

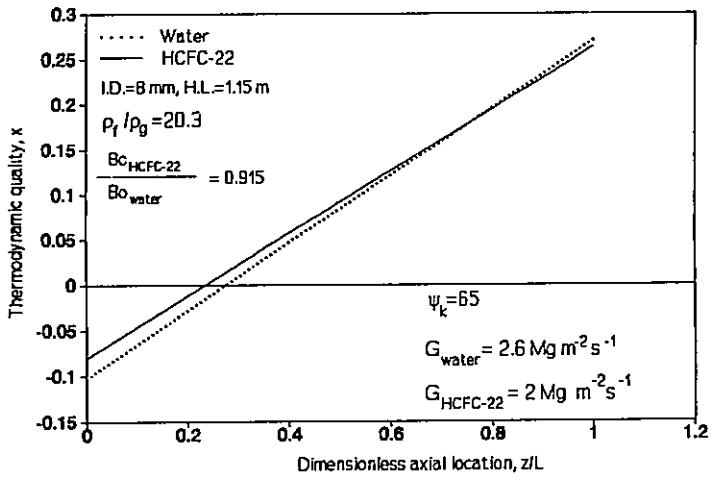

(a)

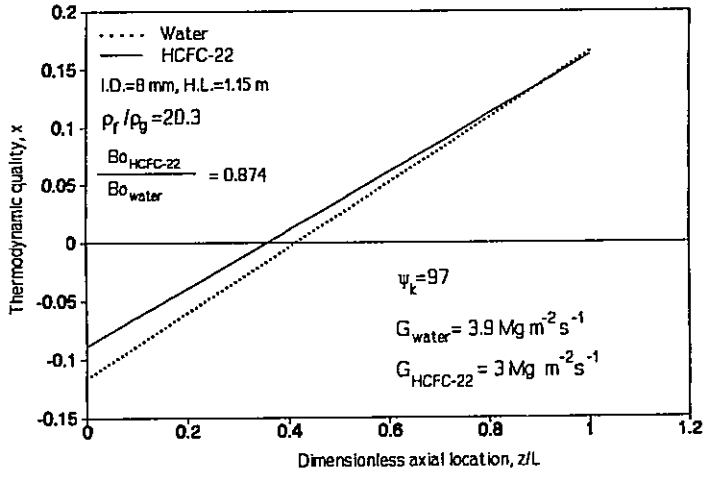

(b)

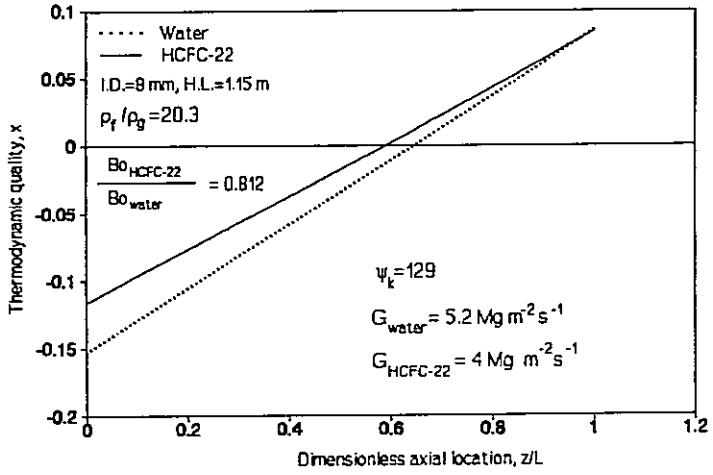

(c)

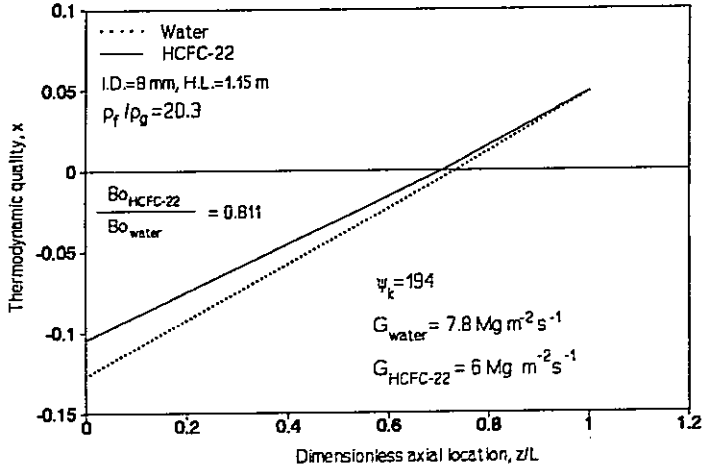

(d)

Figure 6-16 Quality distribution with constant X_c for water and HCFC-22 at ρ_f/ρ_g=20.3, H.L.=1.15 m and (a) ψ_k=65 (b) ψ_k=97 (c) ψ_k=129 (d) ψ_k=194.

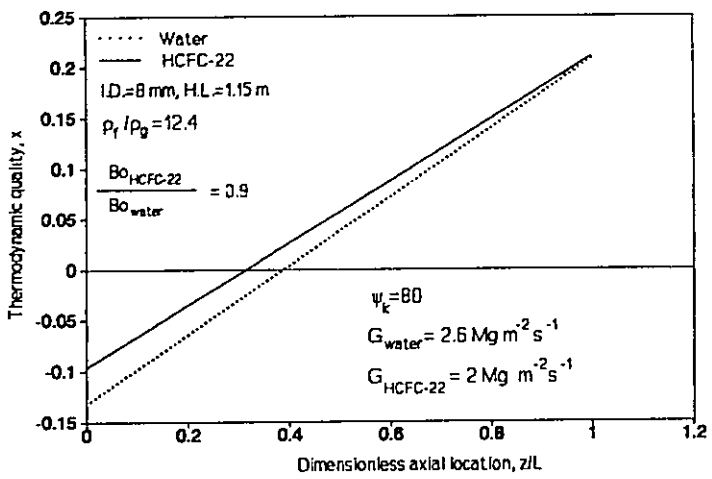

(a)

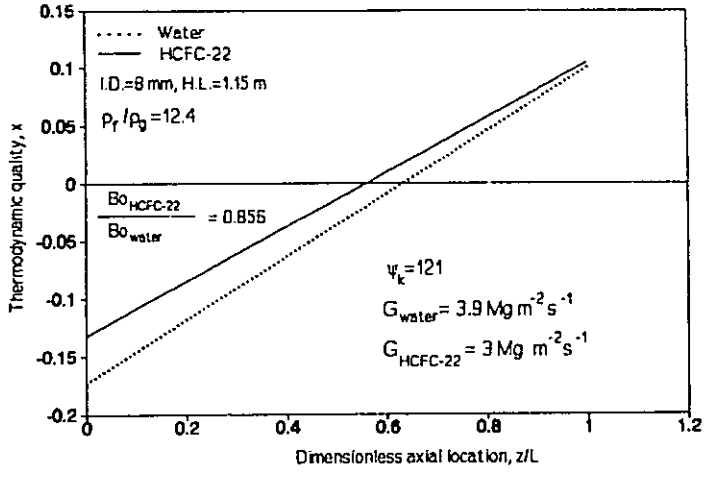

(b)

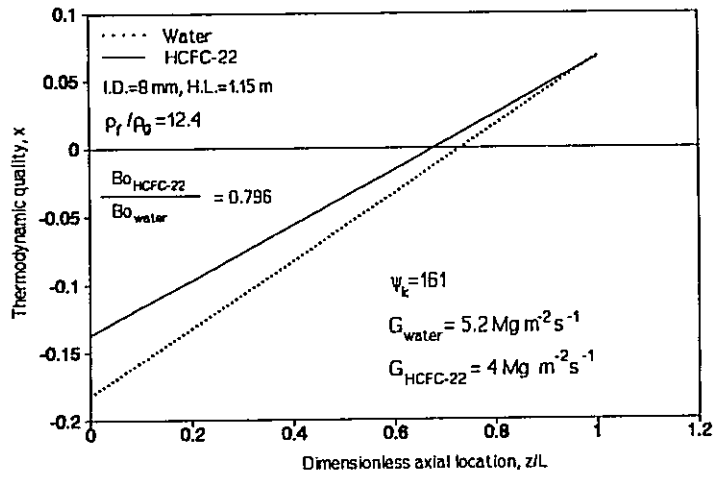

(c)

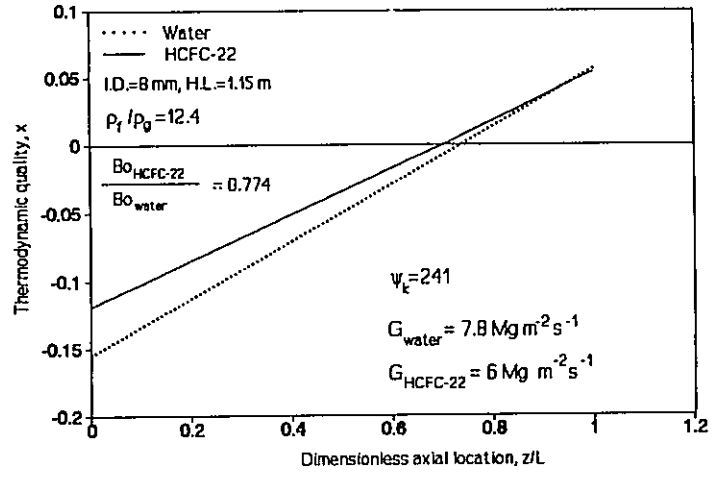

(d)

Figure 6-17 Quality distribution with constant X_c for water and HCFC-22 at ρ_f/ρ_g=12.4, H.L.=1.15 m and (a) ψ_k=80 (b) ψ_k=121 (c) ψ_k=161 (d) ψ_k=241.

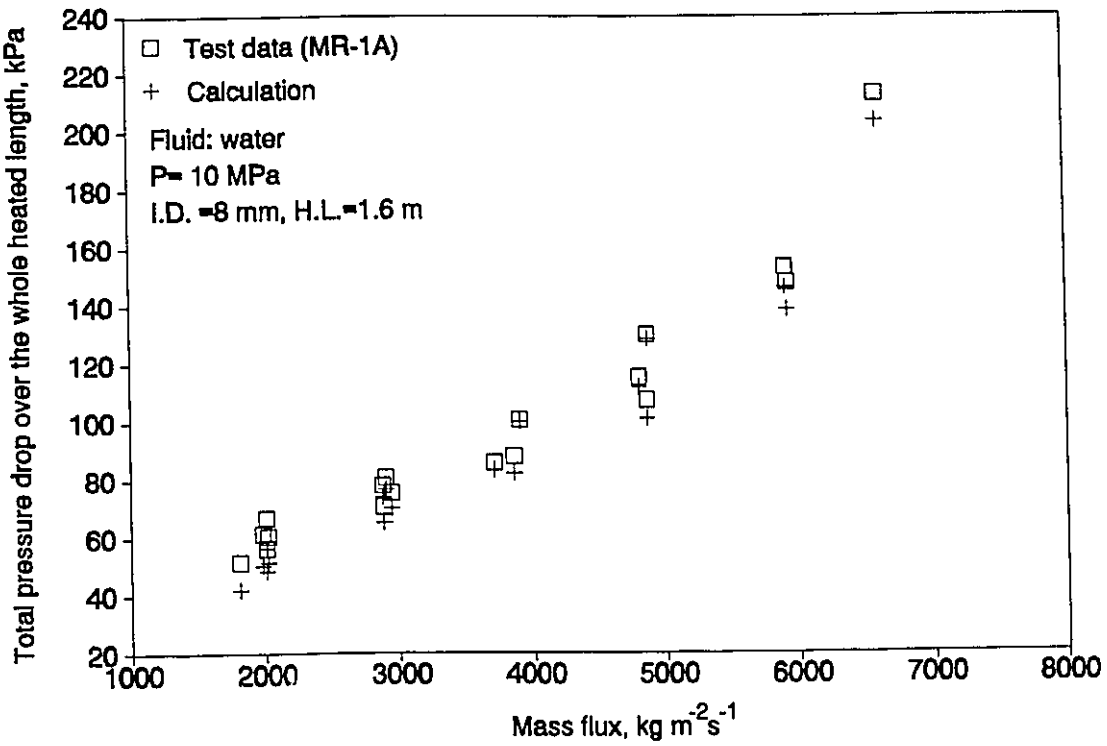

Figure 6-18 Comparison of measured and predicted total pressure drop values over the heated length.

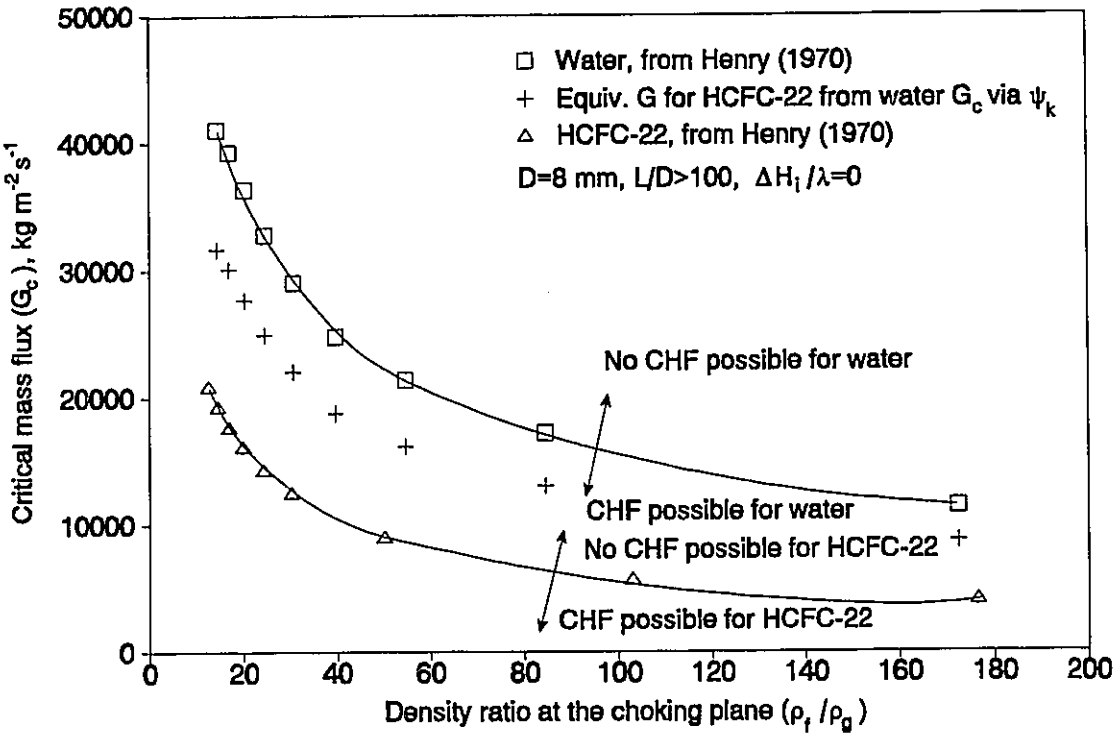

Figure 6-19 Comparison of the critical mass flux between water and HCFC-22 at the choking plane for various pressure conditions.

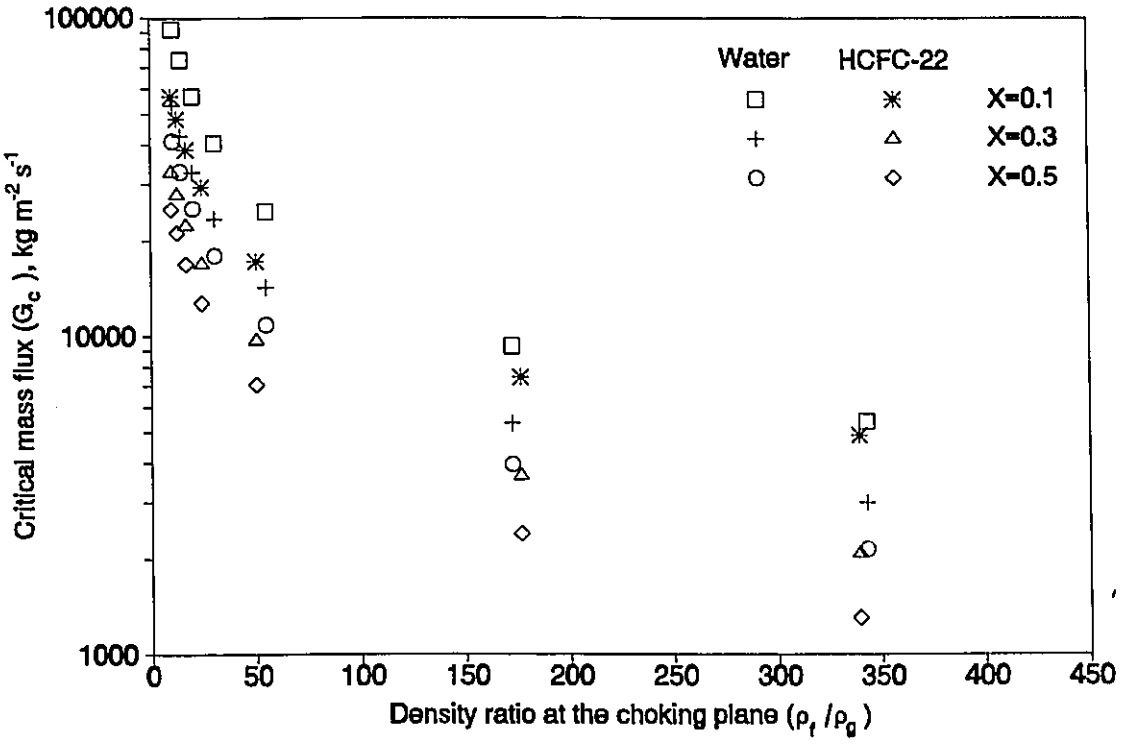

Figure 6-20 Effect of the quality on the critical mass flux for water and HCFC-22 at the choking plane for various pressure conditions (from Chisholm's equations in Giot (1981)).

Chapter 7

SUMMARY OF CONTRIBUTIONS, RECOMMENDATIONS FOR FUTURE WORK AND FINAL REMARK

7.1 Summary of Contributions

1. A multi-fluid boiling loop (i.e. the UO loop) was designed by the author and has been constructed with the assistance of a University of Ottawa technologist. The loop has subsequently been used extensively in CHF and post-CHF testing.

2. Over 450 CHF data were obtained with the UO loop using five fluids: CFC-11, CFC-12, HFC-134a, HCFC-123 and HCFC-22. The following ranges of test conditions were covered:

   pressure: 7 and 10 MPa water-equiv. (i.e. ρ_f/ρ_g=20.3 and 12.4);

   mass flux: 1.5—4 Mg m^{-2} s^{-1};

   quality at dryout: 0.07—0.58;

   test section inner diameter: 4.2 mm;

   heated length: 0.5—1 m.

   The CHF data of HFC-134a and HCFC-123 are the first ever obtained with these fluids

(see Tain et al., 1993); these fluids have either a zero or very low ozone depletion potential. The CHF test results in the UO loop are presented in Tables IV-1—IV-5. As reported in Chapter 4, a small number of CFC-11 data were obtained with the UO loop. The CFC-11 data were not used in the later analytical work simply because the number of data was too small to be used.

3. CHF tests for HCFC-22 and water were also performed by the author in the MR-7A Freon loop and the MR-1A water loop located at the Chalk River Laboratories of Atomic Energy Canada Limited. The following range of HCFC-22 test conditions was covered:

   pressure: 7 and 10 MPa water-equiv.;

   mass flux: 1—8 Mg m^{-2} s^{-1};

   quality at dryout: 0—0.6

   test section inner diameter: 4.38 and 8 mm;

   heated length: 0.67—1.61 m.

   The following range of water test conditions was covered,

   pressure: 7 and 10 MPa;

   mass flux: 2.5—7.7 Mg m^{-2} s^{-1};

   quality at dryout: 0.04—0.39

   test section inner diameter: 8 mm;

   heated length: 1.75 m.

   The CHF test results in MR-7A and MR-1A loops are presented in Tables IV-6—IV-8.

4. A new mass flux scaling parameter, ψ_B, was derived. This ψ_B was found to be more accurate than the existing scaling parameters (e.g. ψ_σ, ψ_k etc.), and gave the least RMS

error when applied to the test CHF data to predict the reference water CHF table.

5. The program subroutines for the properties of HFC-134a and HCFC-123 have been generated during the course of the study. The subroutines were then combined with the University of Ottawa property code to predict the thermophysical properties along with other 22 fluids.

6. Various empirical dimensionless CHF correlations were assessed during the course of this study. Green and Lawther's (1981) empirical dimensionless CHF correlation gave the best agreement with the measured data, obtained in five different fluids.

7. The theoretical CHF models for bubbly flow and annular flow were examined based on the CHF data from the present experimental work. CHF predictions from Ying and Weisman's (1986) bubbly flow model agreed reasonable well with the low quality CHF data. Whalley et al.'s (1974) annular flow model using Govan et al.'s (1988) correlations resulted in a excellent agreement with high quality CHF data, obtained in five different fluids. The effects of mass flux, pressure and diameter on the CHF from both models' predictions were also examined in the present study.

8. After comparing the analytical CHF models, the empirical dimensionless CHF correlations and the CHF table method (i.e. Groeneveld et al., 1986b) in conjunction with the ψ_B scaling parameter, the latter method was found to result in the best agreement with the CHF data.

9. A new methodology has been proposed to investigate the limitations of the CHF fluid-to-fluid scaling technique. A new derivation of the energy equation (i.e. Eq. (6-50)) showed that not only the local quality but also the upstream history (e.g. flashing, friction

heat, changes of kinetic energy and potential energy) influences the CHF scaling accuracy at high mass velocities. The analysis of the CHF similarity through the thermodynamic relationship has provided an insight into the fluid behaviour (flashing, friction, etc.) along a heated channel.

10. The limitation of the CHF fluid-to-fluid scaling due to the critical flow phenomenon had not been studied before. Although much work still needs to be done, a preliminary study of the choking phenomena at high mass flux has been made. This is very useful in providing information to the investigators designing a CHF experiment for certain flow conditions, some of which may not be attainable.

11. Several publications have been generated by this author as a result of his Ph.D. investigation. They have been listed in Appendix I.

7.2 Recommendations for Future Work

1. The density ratio of liquid to vapour (ρ_f/ρ_g) for the fluids examined in the present investigation covers a relatively narrow range (water-equiv. pressure: 7—10 MPa) corresponding to the CANDU power reactor's range of interest. To complete the study of pressure effect on CHF scaling, the lower and higher pressure conditions should also be continued in any future extension of this study.

2. The correlation used for the pressure gradient calculation as well as the differential energy equation are based on the homogeneous flow condition. The more complicated and accurate separate flow model for both the pressure gradient calculation and the differential energy equation should also be considered.

3. The mass flux condition for all fluids tested in the present work is not high enough to reach the critical flow condition. The choking problem in the CHF fluid-to-fluid scaling thus was not experimentally encountered in the present work. A CHF test associated with the choking problem should be considered as a future extension of this study.

7.3 Final Remark

A large amount of effort has been spent on finding suitable replacements for CFC's. This includes (1) determination of their thermophysical properties, (2) measurements of the thermalhydraulic properties such as heat transfer coefficient, CHF etc. and (3) examination of the compatibility of the new fluids with existing equipment. The underlying assumption is that CFC's are the leading cause of stratospheric ozone depletion.

Recently a number of scientists have begun to question the Ozone-depletion-by-CFC's (ODBC) theory (e.g. Ray and Guzzo, 1993). They have provided evidence that the ozone depletion and recovery in the stratosphere is a natural phenomenon rather than a man-made one. For instance, most of the chlorine present in the stratosphere comes from sea water evaporation and volcanic eruptions. Both produce hundreds of millions of tons of chloride per year. However, only hundreds of thousands of tons of chloride are produced from the annual world production of CFC's. On the other hand, the ODBC theory has only been proven in the laboratory rather than in a high altitude. In addition, the question of how the CFC rises when its molecules are four or eight times heavier than the air remains unanswered. The main point of the scientists who question the ODBC theory is that such theory is promulgated too soon through the media rather than through appropriate scientific justifications and thus leads to a sudden introduction of CFC

replacement by the government. Therefore, another concern is being introduced, that of health problems which may accompany the use of CFC replacement fluids. It is now known that some of the CFC replacements are hazardous. Also the cost of refrigeration has increased as a result of using less effective and more expensive replacement fluids, which is of particular concern to the third world countries.

The debate on the ODBC theory may change research priorities of funding agencies. The contribution of determining the CHF for CFC alternatives from the present investigation, however, is unaffected by this debate because this work is important and necessary at this stage due to the government's decision to phase out the use of CFC's. Nevertheless, the conclusion of the debate will send an important message to the researchers on both sides as to whether or not to continue or slow down the projects related to CFC replacements. So far, the conclusion of this debate is still far from being determined. It is the author's opinion that the decision regarding the phasing out the CFC's should be made based on the scientific facts and not due to exaggerated media rhetoric.

BIBLIOGRAPHY

Ahmad, S.Y., "Fluid to fluid modelling of critical heat flux: A compensated distortion model", Int. J. Heat Mass transfer, Vol. 16, pp. 641-662, 1973.

Armand, A.A., Isv Vsesoyuznogo Teploteckhnicheskogo Instituta, vol. 1, pp. 16-23, 1946.

Arpaci, V.S. and Larsen, P.S., *Convection Heat Transfer*, Prentice-Hall, Edgewood Cliffs, N.J., 1984.

Barnett, P.G., "The scaling of forced convection boiling heat transfer", AEEW-R134, 1963.

Barnett, P.G., "An experimental investigation to determine the scaling laws of forced convection boiling heat transfer. Part I: The preliminary examination using burnout data for water and arcton 12", AEEW-R363, 1964.

Barnett, P.G. and Wood, R.W., "An experimental investigation to determine the scaling laws of forced convection boiling heat transfer. Part II: An examination of burnout data for water, Freon-12 and Freon-21 in uniformly heated round tubes", AEEW-R443, 1965.

Barnett, P.G., "A correlation of burnout data for uniformly heated annuli and its use of predicting burnout in uniformly heated rod bundles", AEEW-R463, 1966.

Bergles, A.E., "Burnout in boiling heat transfer. Part II: Subcooled and low-quality forced-convection systems", Nuclear Safety, Vol.18, No. 2, March-April, 1977.

Bergles, A.E., "Burnout in boiling heat transfer. Part III: High-quality forced-convection systems", Nuclear Safety, Vol. 20, No. 6, Nov.-Dec. 1979.

Bertoletti, S., Gaspari, G.P., Lombardi, C., Peterlongo, G. and Tacconi, F.A., "A generalized correlation for predicting the heat transfer crisis with steam-water mixture", Energia Nucleare, 11, pp. 10-14, 1964a.

Bertoletti, S., Gaspari, G.P., Lombardi, C., Soldaini, G. and Zavattarelli, R, "Heat transfer crisis in steam-water mixtures. Experimental data in round tubes and vertical upflow obtained during the CAN-2 program", CISE report R 90, June, 1964b.

Beyerlein, S.W., Cossmann, R.K. and Richter, H.J., "Prediction of bubble concentration profiles in vertical turbulent two-phase flow", Int. J. Multiphase Flow, Vol.11, pp. 629-641, 1985.

Biasi, L., Clerici, G.C., Garribba, S., Sala, R. and Tozzi, A., "Studies on burnout, Part 3 -

A new correlation for round ducts and uniform heating and its comparison with world data", Energia Nuclear, 14, No.9, September 1967.

Blumenröhr, D., Doerffer, S., Groeneveld, D.C. and Katzenmaier, J., "Preliminary measurements of critical heat flux in an 8 mm tube using Chalk River's Multi-fluid loop', CRL Report, ARD-TD-332, 1991.

Boltienko, E.A., Private communication, 1991.

Bouré, J.A., "Two-phase flows and heat transfer with application to nuclear reactor design problems", Chapter 10, edited by J.J. Ginoux, McGraw-Hill Book Co., 1978.

Butterworth, D., "One-dimensional Flow", In *Two-phase Flow and Heat Transfer* (Edited by D. Butterworth and G.F. Hewitt), Chapter 3, Oxford University Press, New York, 1977.

Chan, B.K. and Prince, R.G.H., "Viscous drag on a gas bubble rise in a liquid", AIChE *Jl.* 11, pp. 188-192, 1965.

Cheng, S.C. and Nguyen, C., "U. O. property code for light water", Proceedings of the SCS Western Multiconference on Modeling and Simulation on Microcomputers, San Diego, California, pp. 138-141, Jan. 4-6, 1989.

Cheng, S.C., Tain, R.M., Hammouda, N., Doerffer, S.S., Osamusali, S. and Joober, K., "Development of Thermalhydraulic Relationships", Final report (1990-91), AECL contract, Purchase order CRD 26647/AF1, 226 pages, March 1991.

Cheng, S.C., Doerffer, S., Tain, R.M., Hammouda, N., Huang, X.C., "Experimental and analytical fluid-to-fluid modelling studies", Final Report, January-December 1993, AECL contract, Purchase order C83041, December 1993.

Cheng, X., Erbacher, F.J., Staron, E., Zeggel, W, "Critical heat flux in circular tubes at high pressures and high mass fluxes", Proceedings of NURETH-5, Salt Lake city, Utah, Vol. 2, pp. 832-838, Sept. 21-24, 1992.

Chin, S.K., "The comparison of prediction methods for flow boiling critical heat flux", M. Eng. thesis, Dept. of Mechanical Engineering, University of Ottawa, Ottawa, Canada, 1985.

Cicchitti, A. et al., "Two-phase cooling experiments — pressure drop, heat transfer and burnout measurements", Energia Nuclear, Vol. 7(6), pp. 407-425, 1960.

Coffield, R.D., Rohere, W.M. and Tong, L.S., "A subcooled DNB investigation of Freon-113 and its similarity to subcooled water DNB data", Nuclear Engineering and Design, Vol. 11, pp. 143-153, 1969.

Cole, R. and Rohsenow, W.R., "Correlation of bubble departure diameters for boiling of saturated liquids", Chem. Engng. Prog. Symp., 92, pp. 211-213, 1968.

Collier, J.G., *Convective Boiling and Condensation*, 2nd ed., Chapter 2, McGraw-Hill, London, 1981.

Cumo, M., Farello, G.E., Ferrari, G., Montanari, M. and Nozzi, P., "On two-phase thermal boundary layer along heated wall", Report to the National ATI annual Meeting, Cagliari, 1975.

Diller, D.E., Aragon, A.S. and Laesecke, A., "Measurement of Viscosities of Saturated and Compressed Liquid 1,1,1,2-tetrafluoroethane (R134a), 2,2-dichloro-1,1,1-trifluoroethane (R123) and 1,1-dichloro-1-1fluoroethane (R141b)", Proceedings of the 11th Symposium on Thermophysical Properties, Boulder, Colorado, June 23-27, 1991.

Dix, G.E., "Freon - water modelling of critical heat flux in round tubes", ASME paper No. 70-HT-26, 1970.

Doerffer, S. and Cheng, S.C., "A Comparison of Mixing in Tightly Spaced Bundle Geometries with Different Coolants", AECL Contract Report, ARD-TD-363, 1992.

Doroshchuk, V.E., Lantsman, F.P. and Levitan, L.L., "A Peculiar Type of Burnout in Evaporative Tubes", Proceedings of the 4th International Heat Transfer Conference, Vol. 6, Paper B6.1, Paris, 1970.

Dukler, A.E. et al., "Pressure drop and hold-up in two-phase flow. Part A - A comparison of existing correlations" and "Part B - An approach through similarity analysis", Paper presented at AIChe meeting help Chicago 2–6 Dec. 1962, also AIChe Journal, **10**(1), pp. 38-51, 1961.

Fiori, M.P. and Bergles, A.E., "Model of critical heat flux in subcooled flow boiling", Proceedings of the 4th International Heat Transfer Conference, Vol. 6, Paper B6.3, Paris, 1970.

Giot, M., "Thermohydraulics of two-phase system for industrial design and nuclear engineering", Chapter 18, edited by J.M. Delhaye, M. Giot and M.L. Tiethmuller, McGraw-Hill Book Co., 1981.

Govan, A.H. and Hewitt, G.F., Owen, D.G. and Bott, T.R., "An improved CHF modelling code", 2nd U.K. National Conference on Heat Transfer, Glasgow, 1988.

Green, W.J. and Lawther, K.R., "A flow boiling burnout correlation for water and Freon-12", Nuclear Engineering and Design, Vol. 67, pp. 13-25, 1981.

Green, W.J., "A flow boiling critical heat flux correlation for water and Freon-12 at low mass fluxes", Nuclear Engineering and Design, Vol. 72, pp. 381-389, 1982.

Groeneveld, D.C., "The thermal behaviour of a heated surface at and beyond dryout", Ph. D. Thesis, University of Western Ontario, London, Ontario, Canada, 1972.

Groeneveld, D.C., "The Mechanism of Upstream Dryout in Forced Convective Flow Boiling", Proceedings of the Fifth International Heat Transfer Conference, Tokyo, Japan, 4, pp. 265-269, 1974.

Groeneveld, D.C., Cheng, S.C. and Doan, T., "1986 AECL-UO critical heat flux lookup table", Heat Transfer Engineering, Vol. 7, Nos. 1-2, pp. 46-62, 1986a.

Groeneveld, D.C., Kiameh, B.P. and Cheng, S.C., "Prediction of critical heat flux (CHF) for non-aqueous fluids in forced convective boiling", Proceedings of the 8th International Heat Transfer Conference, San Francisco, 1986b.

Gungor, K.E. and Winterton, R.H.S., "A general correlation for flow boiling in tubes and annuli", Int. J. Heat Mass Transfer, Vol. 29, pp. 351-358, 1986.

Hammouda, N., Cheng, S.C. and Groeneveld, D.C., "Evaluation of Thermophysical Properties of Freon-22", Wärme- und Stoffübertragung, Vol. 28, pp. 387-395, 1993.

Haramura, Y. and Katto, Y., "A new hydrodynamic model of critical heat flux, applicable widely to both pool and forced convection boiling on submerged bodies in saturated liquids", Int. J. Heat Mass Transfer, Vol. 26, pp. 389-399, 1983.

Harmathy, T.Z., "Velocity of large drops and bubbles in media of infinite and restricted extent", AIChE J/. 6, pp. 281-288, 1960.

Hauptmann, E.G., Lee, V. and McAdam, D.M., "Two-phase fluid modelling of critical heat flux", Proc. International Meeting on Reactor Heat Transfer, Karlsruhe 1973.

Hauptmann, E.G. and Lee, V., "A thermodynamic similarity correlation for modelling of flow boiling dryout", Proc. on Nuclear Reactor Thermal-hydraulics, Vol. 1, pp. 352-355, 1983.

Hebel, W. and Detavernier, W., "Critical heat transfer rate to flowing cooling water", Kerntechnik, Vol. 19, No. 5, pp. 228-232, 1977.

Henry, R.E., "The two-phase critical discharge of initially saturated or subcooled liquid", Nuclear Science and Engineering, Vol. 41, pp. 336-342, 1970.

Hewitt, G.F., "Experimental studies on the mechanisms of burnout in heat transfer to steam-water mixtures", Proceedings of the 4th International Heat Transfer Conference, Vol. 6, Paper B6.6, Paris, 1970.

Hewitt, G.F., "Critical heat flux in flow boiling", Proceedings of the 6th International Heat

Transfer Conference, Vol. 6, pp. 143-171, 1978.

Hewitt, G.F. and Roberts, D.N., "Studies of two-phase flow pattern by simultaneous X-ray and flash photography", AERE-M2159, H.M.S.O., 1969.

Hewitt, G.F. and Hall-Taylor N.S., Annular Two-phase Flow, Pergamon Press, Oxford, 1970.

HOECHST, "Frigen - Informationen (Freon information)", report from HOECHST, Frankfurt, Germany, 1989.

Hutchinson, P. and Whalley, P.B., "A possible characterization of entrainment in annular flow", AERE-R7126, 1972.

Isbin, H.S., "Some observations on the status of two-phase critical flow models", Int. J. Multiphase Flow, Vol. 6, pp. 131-137, 1980.

Katto, Y., "A generalized correlation of critical heat flux for the forced convection boiling in vertical uniformly heated round tubes", Int. J. Heat Mass Transfer, Vol. 21, pp. 1527-1542, 1978.

Katto, Y., "A generalized correlation of critical heat flux for the forced convection boiling in vertical uniformly heated round tubes, a supplementary report", Int. J. Heat Mass Transfer, Vol. 22, pp. 783-794, 1979a.

Katto, Y., "An analysis of the effect of inlet subcooling on critical heat flux of forced convection boiling in vertical uniformly heated tubes", Int. J. Heat Mass Transfer, Vol. 22, pp. 1567-1575, 1979b.

Katto, Y., "General feature of CHF of forced convection boiling in uniformly heated vertical tubes with zero inlet subcooling", Int. J. Heat Mass Transfer, Vol. 23, pp. 493-504, 1980a.

Katto, Y., "Critical heat flux of forced convection boiling in uniformly heated vertical tubes (correlation of CHF in HP-regime and determination of CHF-regime map)", Int. J. Heat Mass Transfer, Vol. 23, pp. 1573-1580, 1980b.

Katto, Y., "On the relation between critical heat flux and outlet flow pattern of forced convection boiling in uniformly heated vertical tubes", Int. J. Heat Mass Transfer, Vol. 23, pp. 541-544, 1980c.

Katto, Y., "An analytical investigation on CHF of flow boiling in uniformly heated vertical tubes with special reference to governing dimensionless groups", Int. J. Heat Mass

Transfer, Vol. 25, pp. 1353-1361, 1982.

Katto, Y. "A Physical approach to critical heat flux of subcooled flow boiling in round tubes", Int. J. Heat Mass Transfer, Vol. 33, No. 4, pp. 611-620, 1990a.

Katto, Y., "Prediction of critical heat flux of subcooled flow boiling in round tubes", Int. J. Heat Mass Transfer, Vol. 33, No. 9, pp. 1921-1928, 1990b.

Katto, Y., "A Prediction model of subcooled water flow boiling CHF for pressure in the range 0.1—20 MPa", Int. J. Heat Mass Transfer, Vol. 35, No. 5, pp. 1115-1123, 1992.

Katto, Y. and Ohno, H., "An improved version of the generalized correlation of critical heat flux for the forced convection boiling in uniformly heated vertical tubes", Int. J. Heat Mass Transfer, Vol. 27, pp. 1641-1648, 1984.

Katto, Y. and Yokoya, S., "CHF of forced convection boiling in uniformly heated vertical tubes: experimental study of HP-regime by the use of refrigerant 12", Int. J. Multiphase Flow, Vol. 8, pp. 165-181, 1982.

Katto, Y. and Yokoya, S., "Critical heat flux of liquid helium (I) in forced convection boiling", Int. J. Multiphase Flow, Vol. 10, pp. 401-413, 1984.

Katto, Y. and Ashida, S., "CHF in high-pressure regime for forced convection boiling in uniformly heated vertical tubes of low length-to-diameter ratio", Proceedings of the 7th International Heat Transfer Conference, Vol. 4, pp. 291-296, 1982.

Kiameh, B.P., "Prediction of critical heat flux for non-aqueous fluids in forced convection boiling", M.A.Sc. Thesis, Dept. of Mechanical Engineering, University of Ottawa, Ottawa, Canada, 1986.

Kirby, G.J., Staniforth, R. and Kinneir, I.H., "A visual study of forced convection boiling. Part 2: Flow patterns and burnout for a round test section", UKRER Report No. AEEW-R506, 1967.

Kumagai, A. and Takahashi, S., "Viscosity of saturated liquid fluorocarbon refrigerants from 273 to 353 K", Int. J. of Thermophysics, Vol. 12, No. 1, pp. 107-117, 1991.

Kutateladze, S.S. and Leont'ev, A.I., "Some application of the asymptotic theory of the turbulent boundary layer", Proceedings of the 3rd International Heat Transfer Conference, Chicago, Vol. 3, pp. 1-6, 1966.

Lawther, K.R. and Miles, D.N., "Review of modelling flow boiling crisis conditions", J. Br. Nucl. Energy Soc., 12(3), pp. 309-321, 1973.

Lazarek, G.M. and Black, S.H., "Evaporative heat transfer, pressure drop and critical heat flux in a small vertical tube with R-113", Int. J. Heat Mass Transfer, Vol. 25, pp. 945-959, 1982.

Lee, C.H. and Mudawwar, I., "A mechanistic critical heat flux model for subcooled flow boiling based on local bulk flow conditions", Int. J. Multiphase Flow, Vol. 14, pp. 711-728, 1988.

Lee, D.H and Obertelli, J.D., "An experimental investigation of forced convection burnout in high pressure water, part I: round tubes with uniform flux distribution", AEEW-R213, 1963.

Leung, J.C., "Transient critical heat flux and blowdown heat-transfer studies", NUREGCR-1559 (ANL-80-53), 1980.

Levy, S., "Forced convection subcooled boiling - Prediction of vapour volumetric fraction", GEAP-5157, General Electric Company, 1966.

Levy, S., "Forced-convection subcooled boiling prediction of vapour volumetric fraction", Int. J. Heat Mass Transfer, Vol. 10, pp. 951-965, 1967.

Maroti, L., "Critical heat flux in subcooled and low quality boiling", Crip Budapest, Report No. KFKI-76-34, 1976.

Mayinger, F. and Langner, H., "Use of an optical measurement technique to determine the entrainment behaviour of a two-phase flow steady-state and non-stationary blowdown conditions", Proceedings of a Specialist Conference, Feb./march 1977, Hanover, Edited by P. Voj, INTERATOM internationale Atomreaktorbau GmbH, Berg-Gladbach, Oct. 1977.

McAdams, W.H. et al., "Vaporization inside horizontal tubes—II—Benzene—oil mixtures", Trans. ASME, Vol. 64, p. 193, 1942.

McLinden, M.O., Gallagher, J.S., Weber, L.A., Morrison, G., Ward, D., Goodwin, A.R.H., Moldover, M.R., Schmidt, J.W., Chae, H.B., Bruno, T.J., Ely, J.F. and Huber, M.L., "Measurement and Formulation of the Thermodynamic Properties of Refrigerants 134a (1,1,1,2-Tetrafluoroethane) and 123 (1,1-Dichloro-2,2,2-Trifluoroethane)", ASHRAE Trans., Vol. 95, Part 2, p. 263, 1989.

McPherson, G.D. and Ahmad, S.Y, "Fluid modelling of critical heat flux in an 18-element bundle", Nuclear Engineering and Design, Vol. 17, No. 3, pp. 409-427, 1971.

Molen, S.B. and Van Der Galjee, F.W.B.M., "Boundary layer and burnout phenomena in a subcooled two-phase flow", European Two-phase Flow group Meeting, Grenoble, June, Paper No. E1, 1977.

Moles, F.D. and Shaw, J.F.G., "Boiling heat transfer to subcooled liquids under conditions of forced convection", Trans. Instn. Chem. Engrs. 50, pp. 76-83, 1972.

Nabizadeh, H. and Mayinger, F., "Viscosity of gaseous R123, R134a and R142b", High Temperature–High Pressure, Vol. 24, pp. 221-230, 1992.

Nishikawa, K., Yoshida, S., Yamada, A. and Ohno, M., "Experimental investigation of critical heat flux in forced convection boiling of Freon in a tube at high subcritical pressure", Proceedings of the 7th International Heat Transfer Conference, Vol. 4, pp. 321-326, 1982.

Ogata, H. and Sato, S., "Critical Heat flux for two-phase flow of helium I", Cryogenics, Vol. 13, pp. 610-611, 1976.

Pappel, S.S., Simoneau, R.J. and Brown, D.D., "Buoyancy effects on critical heat flux of forced convective boiling in vertical flow", NASA Report, TN D-3672, 1966, Washington, D. C.

Pei, B.S., "Prediction of critical heat flux in flow boiling at low qualities", Ph.D. Thesis, University of Cincinnati, Cincinnati, Ohio, 1981.

Piao, C., Sato, H. and Watanabe, K., "Thermodynamic charts, tables, and equations for refrigerant HFC-134a", ASHRAE Transactions 1991, Vol. 97, Part 2, 1991.

Purcupile, J.C., Tong, L.S. and Gouse, Jr. S.W., "Refrigerant-water scaling of critical heat flux in round tubes – subcooled forced-convection boiling", J. Heat Transfer, Vol. 95, pp. 279-281, 1973.

Ray, D.L. and Guzzo, L., *Environmental overkill: whatever happened to common sense?*, Regnery Gateway Book Co., 1993.

Reid, R.C. and Sherwood, T.K., "The properties of gases and liquids, their estimation and correlation", McGraw-Hill Book Co., 1987.

Rotem, Z. & Hauptman, E.G., "Burnout in uniformly heated round tubes using CO_2 as working fluid, with reference to burnout in water", Report in Dept. of Mech. Eng., Univ. of British Columbia, 1969.

Semeria, R. and Hewitt, G.F., "Aspects of heat transfer in two-phase gas-liquid flow", in *Heat exchangers: Design and theory source-book*, edited by N. Afgan and E. Schlunder, Scripta Book Co., Washington, 1974.

Shah, M.M., "A general correlation for heat transfer during subcooled boiling in pipes and annuli", ASHRAE Trans. 83, pp. 202-217, 1977.

Shah, M.M., "A generalized graphical method for predicting CHF in uniformly heated vertical tubes", Int. J. Heat Mass Transfer, Vol. 22, pp. 557-568, 1979.

Shah, M.M., " Improved general correlation for critical heat flux during upflow in uniformly heated vertical tubes", J. Heat Fluid Flow, Vol. 8, No. 4, pp. 326-335, December 1987.

Shankland, I.R., "Transport properties of CFC alternatives", Proceedings of AIChE Spring National Meeting, Symp. on Global Climate Change and Refrigerant Properties, Olando, Florida, March 18-22, 1990.

Smogalev, I.P., "Calculation of critical heat fluxes with flow of subcooled water at low velocity", Thermal Engineering, 28, pp. 208-211, 1981.

Smolin, V.N., Shpanskii, V.S., Esikov, V.I., "Experimantal data and calculation methodology for boiling water circulating in tubes with uniform and nonuniform heating", Problems of Atomic Science and Technology, Ser. Physics and Technology of Nuclear Reactors, Vol. 9, No.5, 1979.

Staub, F.W., "Two-phase fluid modelling - the critical heat flux", Nuclear Science and Engineering, Vol. 35, pp. 190-199, 1969.

Stevens, G.F. and Kirby, G.J., "A quantitative comparison between burn-out data for water at 1000 lb/in^2 and Freon-12 at 155 lb/in^2 (ABS) uniformly heated round tubes, vertical upflow", AEEW-R327, 1964.

Stevens, G.F., Elliot, D.F. and Wood, R.W., "An experimental investigation into forced convection burnout in freon, with reference to burnout in water, uniformly heated round tubes with vertical upflow", AEEW-R321, 1964.

Subbotin, V.I., Sorokin, D.N, Nigmatulin, B.I., Milashenki, V.I. and Nikolayev, V.E., "Integrated investigation into hydrodynamic characteristic of annular-dispersed steam-liquid flows", Proceedings of the 6th International Heat Transfer Conference, Toronto, Aug. 1978.

Tain, R.M., Cheng, S.C. and Groeneveld, D.C., "Critical heat flux measurements in a round tube for CFCs and CFC alternatives", Int. J. Heat Mass Transfer, Vol. 36, No. 8, pp. 2039-2049, 1993.

Tanaka, Y., Nakata, M. and Makita, T., "Thermal conductivity of gaseous HFC-134a, HFC-143a, HCFC-141b and HCFC-142b", Int. J. of Thermophysics, Vol. 12, No. 6, pp. 949-963, 1991.

Thompson, B. and Macbeth, R.V., "Boiling water heat transfer—burnout in uniformly heated round tubes: A compilation of world data with accurate correlation", AEEW-R356, 1964.

Tong, L.S., "Boiling heat transfer and two-phase flow", p. 141, John Wiley, New York, 1965.

Tong, L.S., "Boiling crisis and critical heat flux", U.S. Atomic Energy Commission Report TID-25887, Washington, D.C., 1972.

Tong, L.S., Currin, H.B., Larsen, P.S. and Smith, D.G., "Influence of axially non-uniform heat flux on DNB", Westinghouse report No. WCAP-2767 (1965). Published in AIChE Symp. Ser. 64, 1965.

Tong, L.S., "Prediction of departure from nuclear boiling for an axially non-uniform heat flux distribution", J. Nuclear Energy, 6, pp. 21-27, 1967.

Tong, L.S. and Hewitt, G.F., "Overall viewpoint of film boiling CHF mechanisms", ASME Paper No. 72-HT-54, 1972.

Turner, J.M. and Wallis, G.B., "An analysis of the liquid film in annular flow", Dartmouth College, Report no. NYO-3114-13, 1965.

Ueno, Y., Kobayashi, Y., Nagasaka, Y. and Nagashima, A., "Thermal conductivity of CFC alternatives — measurements of HCFC-123 and HFC-134a in the liquid phase by the transient hot-wire method", Transactions of the Japan Society of Mechanical Engineers, Series B, 57(541), pp. 309-315, 1991.

U.S.S.R. Academy of Sciences, "Tabular data for calculating burnout when boiling water in uniformly heat round tubes", Thermal Engineering, 23, pp. 77-79, 1977.

Van Wylen, G.J. and Sonntag, R.E., *Fundamentals of classical thermodynamics*, Chapter 7, 2nd, ed., John Wiley and Son INC., 1973.

Wallis, G.B., "Annular two-phase flow. Part 1: A simple theory", Trans. ASME, Vol. 92, pp. 59-81, 1970.

Watanabe, K., "Current status of thermophysical properties research on CFC alternatives", Proceedings of 3rd International Energy Agency Heat Pump Conference, Tokyo, Japan, pp. 263-282, 1990.

Weisman, J. and Ileslamlou, S., "A phenomenological model for prediction of critical heat flux under highly subcooled conditions", Fusion Technology, Vol. 13, pp. 654-659, 1988.

Weisman, J. and Pei, B.S., "Prediction of critical heat flux in flow boiling at low qualities", Int. J. Heat Mass Transfer, Vol. 26, No. 10, pp. 1463-1477, 1983.

Whalley, P.B., Hutchinson, P. and Hewitt G.F., "The calculation of critical heat flux in forced convection boiling", Proceedings of the 5th International Heat Transfer Conference, Paper B6.11, pp. 290-294, Tokyo, Sept. 1974.

Whalley, P.B., Hutchinson, P. and James, P.W., "The calculation of critical heat flux in complex situations using an annular flow model", Proceedings of the 6th International Heat Transfer Conference, Nr-12, pp. 65-70, Toronto, Aug. 1978.

Wong, Y.L., Cheng, S.C. and Groeneveld, D.C., "Generalized thermodynamic and transport properties evaluation for nonpolar fluids", Heat Transfer Engineering, Vol. 11, p. 60, 1990.

Wong, Y.L., Groeneveld, D.C. and Cheng, S.C., "CHF Prediction for Horizontal Tubes", *Int. J. of Multiphase Flow*, Vol. 16, pp. 123-138, 1990.

Ying, S.H. and Weisman, J., "Prediction of the critical heat flux in flow boiling at intermediate qualities", Int. J. Heat Mass Transfer, Vol. 29, No. 11, pp. 1639-1648, 1986.

Zenkevich, B.A., Peskov, O.L., Petrishcheva, G.A. et al., "Analysis and correlation of experimental burnout data for forced flow of boiling water in tubes", Atomizdat, Moscow, 1969.

Zenkevich, B.A., Peskov, O.L. and Sergeev, N.D., "Burnout for internal water flow in uniformly heated long tubes", Report FEI-254, Obuivsk, Russia, 1971.

Zenkevich, B.A., "Analysis and generalization of experimental data on heat transfer crisis associated with forced convection of cooling water in tubes", AECL-tr-Misc.-304, 1974.

APPENDIX I

LIST OF PUBLICATIONS GENERATED DURING THE COURSE OF THE STUDY

1. Doerffer S.S., Tain, R.M., Groeneveld, D.C., Cheng, S.C. and Zeggel, W., "CHF Modelling of Simple and Complex Geometries Using Freon and Water", Final report (1989-91), Technische Universitat Braunschweig's Grant, 179 pages, February 1991.
2. Cheng, S.C., Tain, R.M., Hammouda, N., Doerffer, S.S., Osamusali, S. and Joober, K., "Development of Thermalhydraulic Relationships", Final report (1990-91), AECL contract, Purchase order CRD 26647/AF1, 226 pages, March 1991.
3. Cheng, S.C. and Tain, R.M., "Multi Fluid Boiling Loop and Preliminary Test Results", Proceedings of 13th Canadian Congress of Aplied Mechanics (CANCAM '91), Winnipeg, Minitoba, Vol. 2, pp. 590-591, June 2-6, 1991.
4. Blumenröhr, D., Tain, R.M., Groeneveld, D.C. and Doerffer, S., "Measurements of Critical Heat Flux in An 8 mm Diameter Tube Cooled by HCFC-22", AECL Report No. ARD-TD-340 or COG-91-299, Dec. 1991.
5. Doerffer, S.S., Groeneveld, D.C., Tain, R.M., Cheng, S.C. and Zeggel, W., "Fluid-to-fluid Modelling of The Critical Heat Flux in Simple and Complex Geometries", Trends in Heat, Mass and Momentum Transfer, Council of Scientific Research Integration, India, Vol. 1,

pp. 45-64, 1991.

6. Groeneveld, D. C., Blumenröhr, D., Cheng, S.C., Cheng, X., Doerffer, S., Erbacher, F.J., Tain, R.M., and Zeggel, W., "CHF Fluid-to-Fluid Modelling Studies in Three Laboratories Using Different Modelling Fluids", Proceedings of NURETH-5, Salt Lake city, Utah, Vol. 2, pp. 531-538, Sept. 1992.

7. Cheng, S.C., Doerffer, S.S., Tain, R.M., Hammouda, N., Wong, W. and Joober, K., "Development of Thermalhydraulic Relationships", Final Report (1991-92), AECL contract, Purchase order CRD 44309/AF1, 70 pages, March, 1992.

8. Tain, R.M., Cheng, S.C. and Groeneveld, D.C., "Critical Heat Flux Measurements for CFCs and CFC Alternatives in A Round Tube of Vertical Upflow", Proceedings of the 14th Canadian Congress of Aplied Mechanics (CANCAM '93), Kingston, Ontario, May 30 — June 4, pp. 655-656, 1993.

9. Tain, R.M., Cheng, S.C. and Groeneveld, D.C., "Critical Heat Flux Measurements in A Round Tube for CFCs and CFC Alternatives", Int. J. Heat Mass Transfer, Vol. 36, No. 8, pp. 2039-2049, 1993.

10. Tain, R.M., Cheng, S.C. and Groeneveld, D.C., "Limitations of the Fluid-to-Fluid Scaling Technique for Critical Heat Flux", in press by Int. J. Heat Mass Transfer.

APPENDIX II

HEAT LOSS AND HEAT BALANCE ANALYSES OF THE TEST SECTION IN THE UO LOOP

II.1 Heat Loss Test

A dry test of heat loss was performed by adding the power to the test section while the whole loop was evacuated. When all thermocouples on the test section show that the temperatures are stabilized, the power to the test section is then equal to the heat loss. Seven data points were obtained from the heat loss test. An equation to calculate the rate of the heat loss from the wall temperature was correlated based on these data points, i.e.

$$\dot{q}_{H.L.} = -1.74348 + 0.091563\, T_W + 0.000229\, T_W^2 \qquad \text{(II-1)}$$

The result of the test are presented in Table II-1.

II.2 Heat Balance Test

A heat balance test was performed by adding the power to the test section while a single-phase (from inlet to outlet) water flows through the test section. The power measured from the power supply, the mass flow rate of water and the temperatures at the inlet and the outlet of

the test section are thus recorded. The rate of heat carried away by the water flow is calculated as

$$\dot{q}_{water} = \dot{m}\, Cp_f (T_2 - T_1) \tag{II-2}$$

where the subscript "1" is the inlet temperature and the subscript "2" is the outlet temperature. The $\dot{q}_{water}$ then is compared with the $\dot{q}$ measured from the power supply ($\dot{q}_{P.S.}$). Figure II-1 shows the deviations of $\dot{q}_{water}$ with respect to the $\dot{q}_{P.S.}$, where

$$Deviation\ (\%) = \frac{\dot{q}_{water} - \dot{q}_{P.S.}}{\dot{q}_{P.S.}} \times 100\% \tag{II-3}$$

The total RMS deviation is 1.9%, which is calculated as

$$Total\ RMS\ Dev.\ (\%) = \sqrt{\frac{\sum_{1}^{n}\left(\frac{\dot{q}_{water} - \dot{q}_{P.S.}}{\dot{q}_{P.S.}}\right)^2}{N}} \times 100\% \tag{II-4}$$

II.3 Discussion

The maximum wall temperature for the CHF test in the UO loop does not exceed 150 °C, which corresponds to a heat loss of less than 20 W based on Eq. (II-1). Such heat loss does not exceed 1% of the power of most CHF tests. The heat balance test shows a deviation between the measured ($\dot{q}_{P.S.}$) and calculated ($\dot{q}_{water}$) powers, which is larger than the result of heat loss test. This is due to the measurement uncertainties of flow, temperature and power during the heat balance test. In general, both tests support the accuracy of CHF measurements in the UO loop.

Table II-1 Result of the heat loss test for the UO loop

Run No.	Wall Temperature (°C)	Power on the test section (W)
1	48.1	3.22
2	163.4	19.24
3	195.2	24.88
4	236.3	32.66
5	257.7	37.05
6	281.8	42.53
7	313.0	49.17

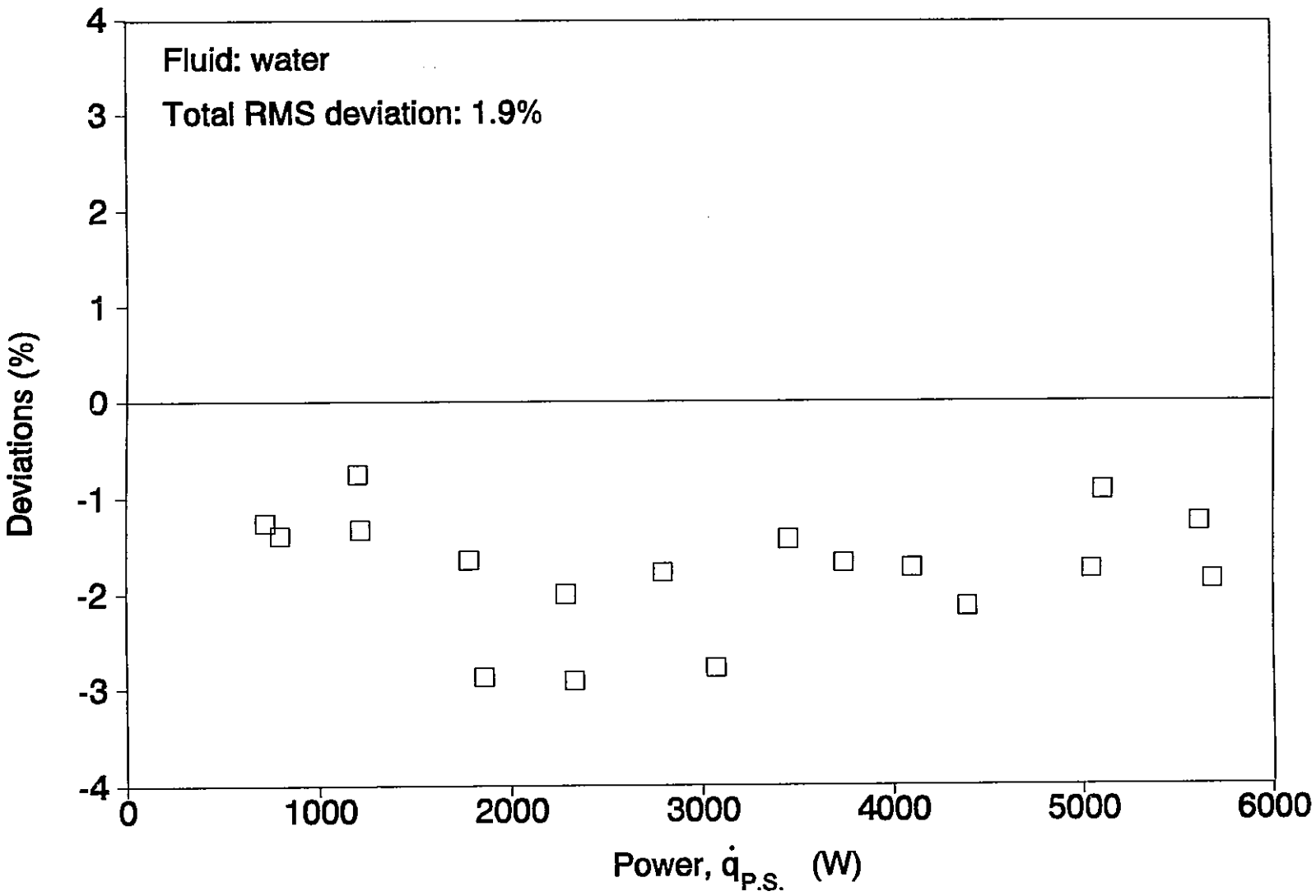

Figure II-1 Result of heat balance test of the test section in the UO loop.

APPENDIX III

PROPERTY SUBROUTINES USED IN THE PRESENT WORK

The development of subroutines to calculate the thermophysical properties of all fluids is an important part of the thesis work, especially for new refrigerants such as HCFC-123 and HFC-134a for which subroutines were not available. The work of the property subroutines was originated by Wong et al. (1990) and a computer code called the UO code was thus developed for the prediction of thermodynamic and transport properties. The original University of Ottawa property code (UO code) was developed for the prediction of nonpolar fluid properties. It was written in Fortran-77 and could be run on microcomputers. The UO code is divided into general and special codes. The general used simple correlations and equations to calculate fluid properties. The equations and correlations were chosen based on accuracy and simplicity. Each fluid of interest requires 21 constants for property evaluation. A list of such constants for 24 fluids is given in a data block in the program. The list of the 24 fluids is shown in Table III-1. The general code has a flexible structure, and hence can be updated easily upon the availability of new and more accurate correlations.

To improve the prediction accuracy of the properties, some special codes (different from the general code mentioned above) are used. In the UO code, the general code will predict the properties first based on input pressure (in kPa) and temperature (in °C). If the special code is

also available for the same pressure and temperature, its prediction will replace that from the general code. Note that the special code is normally valid over narrower ranges of pressure and temperature.

The subprograms for the special codes, which are listed in Table III-2, come from various sources. The CFC-12 subprogram is based on AECL's saturated Freon-12 code. The HCFC-22 subprogram comes from Hammouda et al. (1993). The subprograms for HCFC-123, HFC-134a (both created by the author) and water (Cheng and Nguyen, 1989) have been added recently. In general, most of the equations for the properties included in the UO code have been described by Cheng et al. (1993). and will not be repeated. In this Appendix, only the equations not included in Cheng et al. are listed.

III.1 Prediction for HCFC-123

III.1.1 General

This section presents saturation property equations of HCFC-123 suitable for direct application. All these equations were correlated based on the tabulation data of McLinden et al. (1989) for thermodynamic properties. For transport properties, papers from Kumagai and Takahashi (1991), Shankland (1990), Nabizadeh and Mayinger (1992) and Ueno et al. (1991) are used. A comparison with the data is shown in Table III-3.

III.1.2 Equations for HCFC-123

Critical temperature, T_c, in °C:

$$T_c = 185.045\,^{\circ}C \tag{III-1}$$

Saturation pressure, P_{sat}, in kPa:

for $-20 \le T \le 150^{\circ}C$

$$P_{sat} = 32.72292 + 1.467302\,T + 0.027118\,T^2 + 0.000278\,T^3 + 5.93\times10^{-7}\,T^4 \tag{III-2}$$

Saturation temperature, T_{sat}, in °C:

for $12 \le P \le 2102$ kPa

$$T_{sat} = 223.74276 \times P^{0.035036} \times e^{0.006272(\ln P)^2} - 273.15 \tag{III-3}$$

Saturated liquid density, ρ_f, in kg m^{-3}:

for $-20 \le T \le 150^{\circ}C$

$$\rho_f = 26651.42 - 9245.58\,TK^{1/3} + 920.9641\,TK^{2/3} - 0.34006\,TK^{5/3} \tag{III-4}$$

where

$$TK(^{\circ}K) = T + 273.15 \tag{III-5}$$

Saturated vapour density, ρ_g, in kg m^{-3}:

for $-20 \le T < 56.85^{\circ}C$

$$\rho_g = (724.0385 + 25.42679\,TM + 1.3801\,TM^2 - 0.00204\,TM^3 + 0.000109\,TM^4)/1000 \tag{III-6}$$

for $56.85 \le T < 150^{\circ}C$

$$\rho_g = (117867.9 - 4206.73\,TM + 58.16806\,TM^2 - 0.33678\,TM^3 + 0.000836\,TM^4)/1000 \quad \text{(III-7)}$$

where

$$TM(^\circ C) = T + 25 \quad \text{(III-8)}$$

Saturated liquid enthalpy, h_f, in J kg^{-1}:

for $-20 \leq T \leq 150^\circ C$

$$h_f = (13.32663 + 0.788026\,TM + 0.002349\,TM^2 - 5.3\times10^{-6}\,TM^3 + 4.53\times10^{-9}\,TM^4)\times1000 \quad \text{(III-9)}$$

Saturated vapour enthalpy, h_g, in J kg^{-1}:

for $-20 \leq T < 66.85^\circ C$

$$h_g = (199.2983 + 0.580677\,TM + 0.000546\,TM^2 - 1.9\times10^{-6}\,TM^3 - 1.2\times10^{-8}\,TM^4)\times1000 \quad \text{(III-10)}$$

for $66.85 \leq T \leq 150^\circ C$

$$h_g = (186.2571 + 0.982834\,TM - 0.00408\,TM^2 + 2.23\times10^{-5}\,TM^3 - 6.4\times10^{-8}\,TM^4)\times1000 \quad \text{(III-11)}$$

Latent heat of vaporization, λ, in J kg^{-1}:

$$\lambda = h_g - h_f \quad \text{(III-12)}$$

Saturated liquid specific heat, Cp_f, in J kg^{-1} °C^{-1}:

for $-20 \leq T \leq 51.85^\circ C$

$$Cp_f = 825.1858 + 2.533748\,TM + 0.012269\,TM^2 + 3.08\times10^{-5}\,TM^3 - 1.2\times10^{-6}\,TM^4 \quad \text{(III-13)}$$

for $51.85 < T \leq 101.85°C$

$$Cp_f = 1362.682 - 19.9606\,TM + 0.373735\,TM^2 - 0.00266\,TM^3 + 6.76\times10^{-6}\,TM^4 \quad \text{(III-14)}$$

for $101.85 < T \leq 150°C$

$$Cp_f = 1314.608 - 0.01906\,TM^2 + 6.21\times10^{-7}\,TM^4 \quad \text{(III-15)}$$

Saturated vapour specific heat, Cp_g, in J kg^{-1} $°C^{-1}$:

for $-20 \leq T \leq 91.85°C$

$$Cp_g = 624.0352 + 1.760523\,TM + 0.007401\,TM^2 - 0.00015\,TM^3 + 7.71\times10^{-7}\,TM^4 \quad \text{(III-16)}$$

for $91.85 < T \leq 150°C$

$$Cp_g = 966.4911 - 0.02176\,TM^2 + 9.54\times10^{-7}\,TM^4 \quad \text{(III-17)}$$

Surface tension, σ, in N m^{-1}:

for $-20 \leq T \leq 150°C$

$$\sigma = 0.058533\times(1 - T_r)^{1.26729} \quad \text{(III-18)}$$

where

$$T_r = \frac{T+273.15}{T_c+273.15} \qquad \text{(III-19)}$$

Saturated liquid viscosity, μ_f, kg m^{-1} s^{-1}:

for $0 \leq T \leq 80°C$

from Kumagai and Takahashi (1991)

$$\mu_{f,K} = \frac{e^{\left(-11.093+\frac{1603.2}{TK}+0.025615\,TK-3.1391\times10^{-5}\,TK^2\right)}}{1000} \qquad \text{(III-20)}$$

from Shankland (1990)

$$\mu_{f,S} = \frac{e^{\left(-0.7084+\frac{491.03}{TK}-5.6372\times10^{-3}\,TK\right)}}{1000} \qquad \text{(III-21)}$$

$$\mu_f = (\mu_{f,K} + \mu_{f,S})/2 \qquad \text{(III-22)}$$

Saturated vapour viscosity, μ_g, kg m^{-1} s^{-1}:

for $30 \leq T \leq 150°C$

from Nabizadeh and Mayinger (1992)

$$\mu_g = (-76.7857298+0.695347\times TK-0.00167254\times TK^2+5.563854\times10^{-7}\,TK^3 +1.79923\times10^{-9}\,TK^4)\times10^{-6} \qquad \text{(III-23)}$$

Saturated liquid thermal conductivity, k_f, W m^{-1} °C^{-1}:

for $35 \leq T \leq 69°C$

from Shankland (1990)

$$k_{f,S} = [81.1234\times(1 - 2.6878\times10^{-3}\,T)]/1000 \qquad \text{(III-24)}$$

from Ueno et al. (1991)

$$\begin{aligned} k_{f,U} = {} & 0.16269 + 4.479\times10^{-8}\,P - 4.741\times10^{-12}\,P^2 - 3.1076\times10^{-4}\times TK \\ & + 2.5567\times10^{-10}\times P\times TK + 4.1416\times10^{-14}\times P^2\times TK + 7.2009\times10^{-8}\times TK^2 \\ & + 3.2489\times10^{-12}\times P\times TK^2 - 1.0475\times10^{-16}\times P^2\times TK^2 \end{aligned} \qquad \text{(III-25)}$$

$$k_f = (k_{f,S} + k_{f,U})/2 \qquad \text{(III-26)}$$

Saturated vapour thermal conductivity, k_g, W m^{-1} °C^{-1}:

for $33 \le T \le 55$°C

from Shankland (1990)

$$k_g = 8.2342\times(1 + 1.05887\times10^{-2}\,T)/1000 \qquad \text{(III-27)}$$

III.1.3 Comparison with data

Table III-3 shows the results of the comparison of HCFC-123 predictions from special and general codes against McLinden et al's data (1989).

III.2 Prediction for HFC-134a

II.2.1 General

This section presents the saturation property equations of HFC-134a suitable for direct application. All these equations were correlated based on the tabulation data of McLinden et al. (1989) for thermodynamic properties. For transport properties, papers from Shankland (1990), Kumagai and Takahashi (1991), Nabizadeh and Mayinger (1992), Ueno et al. (1991) and Tanaka

et al. (1991) are used. A comparison with available data is shown in Table III-4.

III.2.2 Equations for HFC-134a

Critical temperature, T_c, in °C:

$$T_c = 101.15\,°C \tag{III-28}$$

Saturation Pressure, P_{sat}, in kPa:

for $-40 \le T \le 100$ °C

$$P_{sat} = 292.1935 + 10.62572 + 0.15203\,T^2 + 0.00087\,T^3 - 4.8597\times10^{-7}\,T^4 + 2.7245\times10^{-8}\,T^5 \tag{III-29}$$

Saturation temperature, T_{sat}, in °C:

for $52 \le P \le 3971$ kPa

$$T_{sat} = -84.9841 - 0.01335\,P + 14.19546\,P^{1/2} - 240.661\,P^{1/3} + 744.1678\,P^{1/4} - 524.819\,P^{1/5} \tag{III-30}$$

Saturated liquid density, ρ_f, in kg m^{-3}:

for $-40 \le T \le 100$°C

$$\rho_f = 1535.119 + 47.58204\,TN + 0.445156\,TN^2 - 108.87\,TN^{2/3} - 3.34549\,TN^{5/3} - 1.0823\times10^{-8}\,TN^5 \tag{III-31}$$

where

$$TN = T + 45 \tag{III-32}$$

Saturated vapour density, ρ_g, in kg m^{-3}:

for -40 ≤ T ≤ 100°C

$$\rho_g = 515.3 \times e^{a_1} \tag{III-33}$$

where

$$a_1 = -3.47966\,TA^{0.34} + 9.34904\,TA^{2/3} - 0.40186\,TA + 28.09001\,TA^{4/3} + 31.91004 \ln\left(\frac{T+273.15}{T_c+273.15}\right) \tag{III-34}$$

and

$$TA = 1 - \frac{T+273.15}{T_c+273.15} \tag{III-35}$$

Saturated liquid enthalpy, h_f, in J kg^{-1}:

for -40 ≤ T ≤ 100°C

$$h_f = (48.8174 + 1.319583\,T + 0.003524\,T^2 - 4.8\times10^{-6}\,T^3 - 6.4045\times10^{-7}\,T^4 + 7.08406\times10^{-9}\,T^5)\times1000 \tag{III-36}$$

Saturated vapour enthalpy, h_g, in J kg^{-1}:

for -40 ≤ T < 50°C

$$h_g = (247.7652 + 0.585009\,T - 0.00089\,T^2 - 9.6373\times10^{-6}\,T^3 - 1.0605\times10^{-7}\,T^4)\times1000 \tag{III-37}$$

for 50 ≤ T ≤ 100°C

$$h_g = (-73.5242+19.95118\,T-0.43351\,T^2+0.004245\,T^3 - 1.57109\times10^{-5}\,T^4)\times1000 \quad \text{(III-38)}$$

Latent heat of Vaporization, λ, in J kg^{-1}:

$$\lambda = h_g - h_f \quad \text{(III-39)}$$

Saturated liquid specific heat, Cp_f, in J kg^{-1} °C^{-1}:

for -40 ≤ T ≤ 50°C

$$Cp_f = (1.32009+0.004544\,T-4.5971\times10^{-6}\,T^2 + 1.7032\times10^{-7}\,T^3+3.6307\times10^{-9}\,T^4)\times1000 \quad \text{(III-40)}$$

for 50 < T ≤ 100°C

$$Cp_f = (1.429998+1.95723\times10^{-43}\,e^{T}+7.436\times10^{-9}\,e^{T/5} - 6.4739\times10^{-5}\,e^{T/10}+0.012937\,e^{T/20})\times1000 \quad \text{(III-41)}$$

Saturated vapour specific heat, Cp_g, in J kg^{-1} °C^{-1}:

for -40 ≤ T ≤ 60°C

$$Cp_g = (0.889972+0.00439\,T+1.9844\times10^{-5}\,T^2 + 2.863\times10^{-7}\,T^3+5.9531\times10^{-9}\,T^4)\times1000 \quad \text{(III-42)}$$

for 60 < T ≤ 100°C

$$Cp_g = (1.000027+2.6644\times10^{-43}\,e^{T}+9.355\times10^{-9}\,e^{T/5} - 3.2555\times10^{-5}\,e^{T/10}+0.01902\,e^{T/20})\times1000 \quad \text{(III-43)}$$

Surface tension, σ, in N m^{-1}:

for -40 ≤ T < 30°C

$$\sigma = 0.011714 - 0.00014\,T + 1.4393\times10^{-7}\,T^2 - 4.2338\times10^{-10}\,T^3 + 1.4501\times10^{-11}\,T^4 \quad \text{(III-44)}$$

for 30 < T ≤ 65°C

$$\sigma = 0.012621 - 0.00021\,T + 1.8878\times10^{-6}\,T^2 - 1.8913\times10^{-8}\,T^3 + 8.4796\times10^{-11}\,T^4 \quad \text{(III-45)}$$

for 65 < T ≤ 100°C

$$\sigma = -0.007457 + 0.000663\,T - 1.1996\times10^{-5}\,T^2 + 7.6262\times10^{-8}\,T^3 - 1.5151\times10^{-10}\,T^4 \quad \text{(III-46)}$$

Saturated liquid viscosity, μ_f, in kg m^{-1} s^{-1}:

for 0 ≤ T ≤ 70.15°C

from Shankland (1990)

$$\mu_{f,S} = \frac{e^{\left[-3.3528 + \frac{714.25}{T+273.15} - 0.0019969\,(T+273.15)\right]}}{1000} \quad \text{(III-47)}$$

from Kumagai and Takahashi (1991)

$$\mu_{f,K} = \frac{e^{\left(-7.639 + \frac{1054.3}{TK} + 0.016602\,TK - 2.7532\times10^{-5}\,TK^2\right)}}{1000} \quad \text{(III-48)}$$

$$\mu_f = (\mu_{f,S} + \mu_{f,K})/2 \quad \text{(III-49)}$$

Saturated vapour viscosity, μ_g, in kg m^{-1} s^{-1}:

for $30 \leq T \leq 105°C$

from Nabizadeh and Mayinger (1992)

$$\mu_g = (-335.231 + 3.599135\,TK - 0.01255326\,TK^2 + 1.471115\times10^{-5}\,TK^3) \times 10^{-6} \quad \text{(III-50)}$$

Saturated liquid thermal conductivity, k_f, W m^{-1} °C^{-1}:

for $39 \leq T \leq 69°C$

from Shankland (1990)

$$k_{f,S} = 90.9371\times(1 - 4.5904\times10^{-3}\,T) / 1000 \quad \text{(III-51)}$$

from Ueno et al. (1991)

$$\begin{aligned} k_{f,U} = {} & 0.20877 + 8.5903\times10^{-7}\,P - 2.9022\times10^{-11}\,P^2 - 4.1483\times10^{-4}\times TK \\ & - 5.9203\times10^{-9}\times P\times TK + 2.2909\times10^{-13}\times P^2\times TK - 3.4532\times10^{-8}\times TK^2 \\ & + 1.7278\times10^{-11}\times P\times TK^2 - 4.632\times10^{-16}\times P^2\times TK^2 \end{aligned} \quad \text{(III-52)}$$

$$k_f = (k_{f,S} + k_{f,U})/2 \quad \text{(III-53)}$$

Saturated vapour thermal conductivity, k_g, W m^{-1} °C^{-1}:

for $25 \leq T \leq 70°C$

from Shankland (1990)

$$k_{g,S} = 11.518 \times (1 + 8.2827\times10^{-3}\,T) / 1000 \quad \text{(III-54)}$$

from Tanaka et al. (1991)

$$k_{g,T} = [\, b_0 + b_1\times P/1000 + b_2\times(P/1000)^2 + b_3\times(P/1000)^3 \,] / 1000 \quad \text{(III-55)}$$

where

$$b_0 = -13.39 + 8.7293\times10^{-2}\,TK \qquad \text{(III-56)}$$

$$b_1 = 114.571 - 0.715448\times TK + 1.12416\times10^{-3}\,TK^2 \qquad \text{(III-57)}$$

$$b_2 = -36.1873 + 0.244739\times TK - 4.12885\times10^{-4}\,TK^2 \qquad \text{(III-58)}$$

$$b_3 = 111.45 - 0.649243\times TK + 9.50136\times10^{-4}\,TK^2 \qquad \text{(III-59)}$$

$$k_g = (k_{g,S} + k_{g,T})/2 \qquad \text{(III-60)}$$

III.2.3 Comparison with data

Comparison of property predictions with tabulation data is shown in Tables III-4.

Table III-1 List of 24 Fluids

Fluid No. in computer code	Name	Chemical Formula
ISUB = 1	Water	H_2O
ISUB = 2	CFC-11	CCl_3F
ISUB = 3	CFC-12	CCl_2F_2
ISUB = 4	CFC-13	$CClF_3$
ISUB = 5	HCFC-21	$CHCl_2F$
ISUB = 6	HCFC-22	$CHClF_2$
ISUB = 7	CFC-113	$C_2Cl_3F_3$
ISUB = 8	CFC-114	$C_2Cl_2F_4$
ISUB = 9	CFC-115	C_2ClF_5
ISUB = 10	Carbon Dioxide	CO_2
ISUB = 11	Benzene	C_6H_6
ISUB = 12	Ammonia	NH_3
ISUB = 13	Methanol	CH_4O
ISUB = 14	Isopropanol	C_3H_8O
ISUB = 15	Acetone	C_3H_6O
ISUB = 16	Ethanol	C_2H_6O
ISUB = 17	Hydrazine	N_2H_4
ISUB = 18	Oxygen	O_2
ISUB = 19	HFC-152a	$C_2H_4F_2$
ISUB = 20	HFC-134a	CH_2FCF_3
ISUB = 21	Nitrogen	N_2
ISUB = 22	HCFC-123	$CHCl_2CF_3$
ISUB = 23	HCFC-142b	$C_2H_3ClF_2$
ISUB = 24	C318	C_4F_8 (CYCLIC)

Table III-2 List of Subprograms

Subprogram names	Predicted Properties
CFC-12 Subprogram	v_g, ρ_f, h_f, h_g, μ_f, P_{sat} and T_{sat}
HCFC-22 Subprogram	v_f, v_L, ρ_f, ρ_L, h_f, h_L, Cp_f, Cp_g, Cp_L, ρ_f, ρ_g, ρ_L, k_f, k_g, k_L, λ and σ
HCFC-123 Subprogram	v_f, v_g, ρ_f, ρ_g, h_f, h_g, Cp_f, Cp_g, μ_f, μ_g, λ, k_f, k_g, P_{sat}, T_{sat} and σ
HFC-134a Subprogram	v_f, v_g, ρ_f, ρ_g, h_f, h_g, Cp_f, Cp_g, μ_f, μ_g, λ, k_f, k_g, P_{sat}, T_{sat} and σ
Water Subprogram	v_f, v_g, v_L, ρ_f, ρ_g, ρ_L, h_f, h_g, h_L, Cp_f, Cp_L, μ_f, μ_g, μ_L, k_f, k_L, Pr_f, Pr_g, Pr_L, λ, P_{sat}, T_{sat} and σ

Table III-3 Comparison of HCFC-123 special code and general code against McLinden et al.'s tabulation data.

	RMS error (%)	
	McLinden et al. (1989)	
	UO special code	UO general code
T_{sat}	0.12	0.38
P_{sat}	0.53	3.6
ρ_f	0.14	3.17
ρ_g	0.6	4.21
λ	0.10	1.38
μ_f	-	-
Cp_f	0.1	6.71
Cp_g	0.25	5.95
σ	0.9	3.35

Table III-4 Comparisons of HFC-134a special code against four different tabulation sources for temperature range from -30 to 80°C.

	RMS error (%)			
	McLinden et al. (1989)	Piao et al. (1991)	HOECHST (1989)	Diller et al. (1991)
T_{sat}	0.010 0.006*	0.028 0.006*	0.012 0.012*	-
P_{sat}	0.24 0.08*	0.37 0.11*	0.32 0.16*	-
ρ_f	0.26 0.31*	0.39 0.47*	0.35 0.41*	-
ρ_g	0.29 0.13*	0.24 0.20*	0.38 0.43*	-
h_f	0.77 0.24*	-	-	-
λ	0.17 0.17*	0.23 0.22*	0.60 0.55*	-
μ_f	-	-	-	3.13†
σ	0.92 0.77*	-	-	-

* Temperature range is from 15 to 70°C (59 - 158°F).
† Temperature range is from -22 to 46°C (-7 - 115°F).

APPENDIX IV

TABULATION OF CHF DATA

This Appendix contains seven tables which list the CHF data measured from UO, MR-7A and MR-1A loops:

Table IV-1 CHF data for HFC-134a from UO loop

Table IV-2 CHF data for HCFC-123 from UO loop

Table IV-3 CHF data for CFC-12 from UO loop

Table IV-4 CHF data for CFC-11 from UO loop

Table IV-5 CHF data for HCFC-22 from UO loop

Table IV-6 CHF data for HCFC-22 from MR-7A loop

Table IV-7 CHF data for HCFC-22 from MR-7A loop

Table IV-8 CHF data for water from MR-1A loop

where No.: data number

D: tube inner diameter (m)

L: heated length (m)

P: pressure at CHF location (kPa)

G: mass flux (kg m^{-2} s^{-1})

Xc: critical quality

HI: inlet subcooling enthalpy (kJ kg^{-1})

CHF: critical heat flux (kW m^{-2})

Table IV-1 CHF data for HFC-134a from UO loop

No.	D	L	P	G	Xc	HI	CHF
1	0.0042	1.001	1125.0	1383	0.456	24.340	140.4
2	0.0042	1.001	1127.9	1383	0.461	20.660	136.1
3	0.0042	1.001	1127.9	1383	0.465	15.320	129.3
4	0.0042	1.001	1127.9	1383	0.469	9.046	121.0
5	0.0042	1.001	1127.9	1381	0.478	2.422	113.3
6	0.0042	0.785	1127.9	1384	0.417	26.110	170.9
7	0.0042	0.785	1127.9	1384	0.430	20.510	164.3
8	0.0042	0.785	1127.9	1384	0.441	14.870	157.2
9	0.0042	0.785	1127.9	1383	0.450	8.896	148.4
10	0.0042	0.785	1127.9	1384	0.460	2.573	139.7
11	0.0042	0.996	1127.9	1841	0.354	30.340	167.8
12	0.0042	0.996	1127.9	1842	0.359	27.280	163.7
13	0.0042	0.996	1127.9	1840	0.370	20.510	153.7
14	0.0042	0.996	1127.9	1843	0.379	15.920	147.8
15	0.0042	0.996	1127.9	1842	0.385	9.646	137.3
16	0.0042	0.996	1127.9	1841	0.392	3.328	127.0
17	0.0042	0.781	1127.9	1845	0.313	29.910	197.3
18	0.0042	0.781	1127.9	1843	0.324	25.520	190.6
19	0.0042	0.781	1127.9	1844	0.338	17.550	176.4
20	0.0042	0.781	1127.9	1843	0.348	13.090	169.1
21	0.0042	0.781	1127.9	1844	0.358	7.695	159.8
22	0.0042	0.781	1127.9	1843	0.366	3.781	153.1
23	0.0042	0.996	1127.9	2304	0.285	30.920	185.1
24	0.0042	0.996	1127.9	2305	0.298	25.960	178.1

Table IV-1 (Continued)

No.	D	L	P	G	Xc	HI	CHF
25	0.0042	0.996	1127.9	2304	0.310	21.250	170.9
26	0.0042	0.996	1127.9	2307	0.322	15.170	160.9
27	0.0042	0.996	1127.9	2302	0.333	8.596	149.0
28	0.0042	0.996	1127.9	2303	0.340	3.479	139.5
29	0.0042	0.781	1127.9	2302	0.229	33.820	217.2
30	0.0042	0.781	1127.9	2303	0.254	26.110	205.4
31	0.0042	0.781	1127.9	2306	0.271	20.070	195.3
32	0.0042	0.781	1127.9	2306	0.284	15.020	186.4
33	0.0042	0.781	1127.9	2304	0.299	8.596	173.6
34	0.0042	0.781	1127.9	2304	0.312	3.026	162.8
35	0.0042	0.996	1127.9	2762	0.225	32.660	199.0
36	0.0042	0.996	1127.9	2768	0.240	27.720	191.8
37	0.0042	0.996	1127.9	2765	0.256	21.990	182.3
38	0.0042	0.996	1127.9	2766	0.271	15.320	170.2
39	0.0042	0.996	1127.9	2769	0.289	7.846	156.5
40	0.0042	0.996	1127.9	2764	0.299	3.328	147.9
41	0.0042	0.781	1127.9	2766	0.177	31.500	221.7
42	0.0042	0.781	1127.9	2768	0.202	23.900	208.5
43	0.0042	0.781	1127.9	2765	0.228	16.810	197.1
44	0.0042	0.781	1127.9	2762	0.243	12.490	189.7
45	0.0042	0.781	1127.9	2771	0.259	6.042	175.7
46	0.0042	0.996	1127.9	3227	0.176	32.370	205.3
47	0.0042	0.996	1127.9	3228	0.206	24.640	194.8
48	0.0042	0.996	1127.9	3227	0.222	19.630	186.5

Table IV-1 (Continued)

No.	D	L	P	G	Xc	HI	CHF
49	0.0042	0.996	1127.9	3225	0.234	15.470	179.0
50	0.0042	0.996	1127.9	3225	0.240	11.890	169.7
51	0.0042	0.781	1127.9	3227	0.137	32.080	233.4
52	0.0042	0.781	1127.9	3228	0.150	28.010	224.5
53	0.0042	0.781	1127.9	3230	0.170	21.400	210.2
54	0.0042	0.781	1127.9	3231	0.203	13.090	196.7
55	0.0042	0.781	1127.9	3226	0.224	7.545	186.7
56	0.0042	0.996	1127.9	3688	0.144	31.650	211.7
57	0.0042	0.996	1127.9	3691	0.157	27.570	203.9
58	0.0042	0.996	1127.9	3684	0.183	21.100	194.9
59	0.0042	0.996	1130.8	3688	0.208	14.580	184.8
60	0.0042	0.996	1127.9	3689	0.223	9.945	176.3
61	0.0042	0.781	1127.9	3685	0.107	32.810	246.5
62	0.0042	0.781	1127.9	3692	0.124	27.130	232.0
63	0.0042	0.781	1127.9	3688	0.142	21.400	217.4
64	0.0042	0.781	1127.9	3683	0.165	14.870	202.9
65	0.0042	0.781	1127.9	3684	0.197	7.245	190.5
66	0.0042	0.996	1660.1	1831	0.290	40.210	155.9
67	0.0042	0.996	1660.1	1829	0.299	35.290	148.7
68	0.0042	0.996	1660.1	1830	0.311	28.830	139.6
69	0.0042	0.996	1660.1	1824	0.320	22.320	129.1
70	0.0042	0.996	1660.1	1828	0.326	16.370	119.6
71	0.0042	0.996	1660.1	1827	0.343	8.962	109.8
72	0.0042	0.996	1660.1	1828	0.346	4.586	102.2

Table IV-1 (Continued)

No.	D	L	P	G	Xc	HI	CHF
73	0.0042	1.000	1660.1	1830	0.291	38.270	151.9
74	0.0042	1.000	1664.1	1829	0.301	31.250	141.0
75	0.0042	1.000	1660.1	1828	0.317	24.450	132.1
76	0.0042	1.000	1660.1	1825	0.333	16.220	120.5
77	0.0042	1.000	1660.1	1829	0.339	9.584	109.5
78	0.0042	0.785	1660.1	1831	0.247	40.950	184.9
79	0.0042	0.785	1660.1	1828	0.256	35.890	175.4
80	0.0042	0.785	1660.1	1826	0.273	28.830	163.9
81	0.0042	0.785	1660.1	1828	0.288	21.870	152.1
82	0.0042	0.785	1660.1	1828	0.304	15.450	141.9
83	0.0042	0.996	1660.1	2285	0.234	36.330	166.4
84	0.0042	0.996	1660.1	2280	0.255	28.530	154.5
85	0.0042	0.996	1660.1	2282	0.268	22.170	143.7
86	0.0042	0.996	1660.1	2283	0.282	16.220	134.2
87	0.0042	0.996	1660.1	2289	0.291	10.980	124.9
88	0.0042	1.000	1660.1	2289	0.249	29.730	155.3
89	0.0042	1.000	1660.1	2287	0.264	22.630	143.1
90	0.0042	1.000	1664.1	2287	0.279	16.530	133.6
91	0.0042	1.000	1660.1	2282	0.298	9.894	123.8
92	0.0042	0.785	1660.1	2288	0.180	40.360	200.8
93	0.0042	0.785	1660.1	2287	0.197	33.790	187.6
94	0.0042	0.785	1660.1	2287	0.213	28.380	178.0
95	0.0042	0.785	1660.1	2285	0.227	22.470	165.8
96	0.0042	0.785	1660.1	2287	0.244	16.370	154.8

Table IV-1 (Continued)

No.	D	L	P	G	Xc	HI	CHF
97	0.0042	0.996	1660.1	2743	0.185	36.330	179.9
98	0.0042	0.996	1660.1	2744	0.203	28.680	165.3
99	0.0042	0.996	1660.1	2744	0.224	21.110	152.0
100	0.0042	0.996	1660.1	2740	0.236	17.290	145.4
101	0.0042	0.996	1660.1	2747	0.252	12.060	137.2
102	0.0042	0.785	1660.1	2743	0.133	41.100	219.1
103	0.0042	0.785	1660.1	2745	0.147	34.990	204.3
104	0.0042	0.785	1660.1	2744	0.169	27.770	188.7
105	0.0042	0.785	1660.1	2741	0.183	22.470	176.6
106	0.0042	0.785	1660.1	2739	0.203	15.910	162.5
107	0.0042	0.996	1660.1	3201	0.139	41.690	206.2
108	0.0042	0.996	1660.1	3200	0.148	35.890	191.0
109	0.0042	0.996	1660.1	3201	0.168	29.130	177.9
110	0.0042	0.996	1660.1	3198	0.184	22.930	164.3
111	0.0042	0.996	1660.1	3201	0.201	17.750	154.7
112	0.0042	0.785	1660.1	3196	0.106	40.950	238.3
113	0.0042	0.785	1660.1	3198	0.120	34.540	219.4
114	0.0042	0.785	1660.1	3200	0.134	28.080	200.8
115	0.0042	0.785	1660.1	3198	0.153	21.560	183.8
116	0.0042	0.785	1660.1	3199	0.172	15.450	169.2
117	0.0042	0.996	1660.1	3656	0.117	40.950	221.0
118	0.0042	0.996	1660.1	3659	0.122	37.080	209.2
119	0.0042	0.996	1660.1	3661	0.135	30.790	191.7
120	0.0042	0.996	1660.1	3657	0.149	25.660	179.3

Table IV-1 (Continued)

No.	D	L	P	G	Xc	HI	CHF
121	0.0042	0.996	1660.1	3651	0.163	21.410	170.2
122	0.0042	0.785	1660.1	3657	0.086	39.760	253.6
123	0.0042	0.785	1660.1	3657	0.098	34.690	237.0
124	0.0042	0.785	1660.1	3655	0.113	28.230	215.1
125	0.0042	0.785	1660.1	3656	0.124	22.930	197.0
126	0.0042	0.785	1660.1	3658	0.136	18.970	186.1
127	0.0042	1.001	1660.1	1370	0.377	34.240	125.1
128	0.0042	1.001	1660.1	1371	0.384	27.930	117.4
129	0.0042	1.001	1660.1	1368	0.399	20.800	110.0
130	0.0042	1.001	1660.1	1372	0.395	16.830	103.8
131	0.0042	1.001	1660.1	1369	0.397	10.510	95.0
132	0.0042	1.001	1660.1	1368	0.390	4.429	84.8
133	0.0042	0.785	1660.1	1370	0.347	34.540	152.5
134	0.0042	0.785	1660.1	1372	0.362	27.770	144.0
135	0.0042	0.785	1660.1	1371	0.373	21.560	135.4
136	0.0042	0.785	1660.1	1372	0.381	16.060	127.4
137	0.0042	0.785	1660.1	1369	0.395	9.584	118.8
138	0.0042	0.785	1660.1	1373	0.396	5.057	111.2

Table IV-2 CHF data for HCFC-123 from UO loop

No.	D	L	P	G	Xc	HI	CHF
1	0.0042	1.001	987.4	1450	0.425	30.320	128.2
2	0.0042	1.001	983.2	1450	0.440	23.130	120.2
3	0.0042	1.001	977.0	1448	0.450	17.600	113.7
4	0.0042	1.001	977.0	1446	0.456	14.360	109.9
5	0.0042	1.001	979.1	1450	0.453	9.720	102.5
6	0.0042	1.001	983.2	1449	0.459	6.571	98.6
7	0.0042	0.785	981.2	1448	0.396	33.250	162.0
8	0.0042	0.785	981.2	1446	0.409	28.490	155.7
9	0.0042	0.785	981.2	1451	0.415	23.700	148.4
10	0.0042	0.785	972.9	1446	0.423	17.480	138.1
11	0.0042	0.785	972.9	1449	0.427	13.550	131.7
12	0.0042	0.785	977.0	1453	0.434	8.203	123.3
13	0.0042	1.001	983.2	1932	0.333	29.750	146.1
14	0.0042	1.001	975.0	1931	0.353	22.890	137.3
15	0.0042	1.001	977.0	1924	0.363	17.950	129.5
16	0.0042	1.001	981.2	1931	0.361	12.980	119.3
17	0.0042	1.001	983.2	1936	0.363	9.722	113.4
18	0.0042	0.785	979.1	1933	0.300	30.530	177.6
19	0.0042	0.785	977.0	1932	0.321	24.270	168.3
20	0.0042	0.785	979.1	1930	0.326	20.830	160.8
21	0.0042	0.785	981.2	1929	0.337	15.990	151.7
22	0.0042	0.785	981.2	1928	0.347	10.190	139.9
23	0.0042	1.001	979.1	2414	0.261	30.760	162.0
24	0.0042	1.001	981.2	2416	0.276	25.640	154.0

Table IV-2 (Continued)

No.	D	L	P	G	Xc	HI	CHF
25	0.0042	1.001	981.2	2410	0.296	20.260	146.5
26	0.0042	1.001	981 2	2413	0.310	15.180	138.2
27	0.0042	1.001	983.2	2419	0.315	10.070	127.2
28	0.0042	0.785	977.0	2415	0.214	34.600	199.9
29	0.0042	0.785	981.2	2417	0.236	29.520	192.2
30	0.0042	0.785	979.1	2413	0.250	24.500	181.9
31	0.0042	0.785	979.1	2417	0.262	20.480	173.8
32	0.0042	0.785	977.0	2418	0.276	16.560	167.0
33	0.0042	1.001	977.0	2897	0.227	29.280	176.9
34	0.0042	1.001	979.1	2901	0.244	24.270	168.4
35	0.0042	1.001	981.2	2898	0.254	21.060	162.3
36	0.0042	1.001	985.3	2899	0.271	16.110	153.5
37	0.0042	1.001	983.2	2897	0.278	11.470	142.4
38	0.0042	0.785	979.1	2898	0.153	34.830	210.3
39	0.0042	0.785	977.0	2894	0.174	29.730	200.8
40	0.0042	0.785	983.2	2898	0.197	24.390	191.7
41	0.0042	0.785	977.0	2898	0.215	20.250	184.5
42	0.0042	0.785	977.0	2898	0.228	16.680	177.1
43	0.0042	1.001	979.1	3379	0.156	34.490	192.6
44	0.0042	1.001	979.1	3381	0.181	29.170	184.9
45	0.0042	1.001	979.1	3383	0.207	23.580	177.2
46	0.0042	1.001	979.1	3382	0.221	20.480	172.2
47	0.0042	1.001	979.1	3387	0.235	16.680	165.3
48	0.0042	0.785	979.1	3379	0.100	39.650	237.0

Table IV-2 (Continued)

No.	D	L	P	G	Xc	HI	CHF
49	0.0042	0.785	975.0	3380	0.119	34.250	223.1
50	0.0042	0.785	979.1	3382	0.133	30.080	212.3
51	0.0042	0.785	977.0	3374	0.147	25.980	201.5
52	0.0042	0.785	981.2	3378	0.165	21.640	192.6
53	0.0042	1.001	981.2	3863	0.118	34.380	200.2
54	0.0042	1.001	979.1	3861	0.135	30.310	192.5
55	0.0042	1.001	979.1	3861	0.180	22.780	184.8
56	0.0042	1.001	970.9	3860	0.201	18.750	179.6
57	0.0042	0.785	979.1	3865	0.073	39.540	252.6
58	0.0042	0.785	977.0	3865	0.089	34.820	238.4
59	0.0042	0.785	977.0	3863	0.100	30.640	224.2
60	0.0042	0.785	975.0	3865	0.116	25.980	210.9

Table IV-3 CHF data for CFC-12 from UO loop

No.	D	L	P	G	Xc	HI	CHF
1	0.0042	1.001	1061.2	1530	0.477	17.820	124.9
2	0.0042	1.001	1061.2	1531	0.481	13.400	118.8
3	0.0042	1.001	1061.2	1531	0.480	9.731	112.5
4	0.0042	1.001	1061.2	1529	0.489	5.209	107.1
5	0.0042	1.001	1061.2	1534	0.494	2.156	103.5
6	0.0042	0.785	1061.2	1529	0.444	18.110	151.2
7	0.0042	0.785	1061.2	1533	0.452	13.500	144.1
8	0.0042	0.785	1061.2	1530	0.461	8.832	136.8
9	0.0042	0.785	1061.2	1531	0.467	6.119	132.7
10	0.0042	0.785	1061.2	1527	0.474	2.770	127.4
11	0.0042	0.998	1061.2	2045	0.375	18.400	141.2
12	0.0042	0.998	1058.7	2038	0.387	14.090	134.5
13	0.0042	0.998	1061.2	2039	0.394	9.432	126.5
14	0.0042	0.998	1061.2	2036	0.401	5.513	119.7
15	0.0042	0.998	1061.2	2035	0.408	1.132	112.4
16	0.0042	0.998	1061.2	2553	0.316	18.400	156.1
17	0.0042	0.998	1061.2	2557	0.326	14.780	150.1
18	0.0042	0.998	1061.2	2556	0.336	10.030	140.8
19	0.0042	0.998	1061.2	2559	0.346	6.119	133.7
20	0.0042	0.998	1061.2	2557	0.353	2.668	126.8
21	0.0042	0.998	1061.2	3057	0.262	18.400	165.3
22	0.0042	0.998	1061.2	3068	0.273	14.880	159.0
23	0.0042	0.998	1061.2	3066	0.285	10.930	150.8
24	0.0042	0.998	1061.2	3060	0.298	6.422	141.2

Table IV-3 (Continued)

No.	D	L	P	G	Xc	HI	CHF
25	0.0042	0.998	1058.7	3058	0.315	1.336	131.7
26	0.0042	0.998	1061.2	3583	0.225	17.620	173.3
27	0.0042	0.998	1061.2	3584	0.239	14.090	166.5
28	0.0042	0.998	1061.2	3579	0.254	9.931	157.6
29	0.0042	0.998	1061.2	3582	0.263	6.422	148.9
30	0.0042	0.998	1061.2	4103	0.190	17.620	179.5
31	0.0042	0.998	1061.2	4076	0.211	13.700	172.5
32	0.0042	0.998	1061.2	4082	0.222	10.630	165.7
33	0.0042	0.998	1061.2	4084	0.237	6.724	157.1
34	0.0042	0.781	1063.8	2044	0.351	16.940	167.7
35	0.0042	0.781	1061.2	2039	0.358	14.490	163.0
36	0.0042	0.781	1063.8	2037	0.367	10.130	154.1
37	0.0042	0.781	1061.2	2037	0.377	5.715	145.5
38	0.0042	0.781	1063.8	2044	0.385	2.157	139.0
39	0.0042	0.781	1061.2	2552	0.281	18.590	184.9
40	0.0042	0.781	1061.2	2551	0.296	13.900	175.3
41	0.0042	0.781	1061.2	2550	0.308	9.132	163.9
42	0.0042	0.781	1061.2	2557	0.314	6.321	157.4
43	0.0042	0.781	1061.2	2546	0.331	1.542	148.0
44	0.0042	0.781	1061.2	3054	0.223	18.300	190.5
45	0.0042	0.781	1061.2	3061	0.240	14.390	183.4
46	0.0042	0.781	1061.2	3060	0.256	9.731	172.4
47	0.0042	0.781	1063.8	3059	0.268	5.919	163.1
48	0.0042	0.781	1063.8	3049	0.282	2.362	154.8

Table IV-3 (Continued)

No.	D	L	P	G	Xc	HI	CHF
49	0.0042	0.781	1061.2	3571	0.163	22.560	207.0
50	0.0042	0.781	1061.2	3571	0.179	18.500	197.0
51	0.0042	0.781	1061.2	3574	0.202	13.600	187.3
52	0.0042	0.781	1061.2	3564	0.222	9.132	177.7
53	0.0042	0.781	1061.2	3574	0.233	6.119	170.0
54	0.0042	0.781	1061.2	4100	0.134	22.080	214.9
55	0.0042	0.781	1061.2	4083	0.147	18.690	204.0
56	0.0042	0.781	1061.2	4076	0.167	14.290	193.2
57	0.0042	0.781	1061.2	4080	0.189	9.532	183.0
58	0.0042	0.781	1063.8	4080	0.205	6.323	176.2
59	0.0042	1.001	1579.8	1534	0.396	20.430	104.4
60	0.0042	1.001	1579.8	1536	0.396	15.670	96.8
61	0.0042	1.001	1579.8	1537	0.393	11.260	89.2
62	0.0042	1.001	1579.8	1537	0.390	7.170	82.0
63	0.0042	1.001	1579.8	1535	0.387	2.656	74.3
64	0.0042	0.785	1579.8	1535	0.375	22.980	133.5
65	0.0042	0.785	1579.8	1538	0.381	18.990	127.0
66	0.0042	0.785	1579.8	1536	0.385	15.670	120.9
67	0.0042	0.785	1579.8	1536	0.394	10.940	113.3
68	0.0042	0.785	1579.8	1534	0.395	7.617	106.6
69	0.0042	0.785	1579.8	1536	0.394	3.742	98.5
70	0.0042	0.998	1579.8	2045	0.323	22.980	127.4
71	0.0042	0.998	1579.8	2046	0.329	20.320	123.1
72	0.0042	0.998	1583.2	2041	0.335	15.150	113.1

Table IV-3 (Continued)

No.	D	L	P	G	Xc	HI	CHF
73	0.0042	0.998	1579.8	2040	0.330	11.470	104.1
74	0.0042	0.998	1579.8	2043	0.326	6.712	93.1
75	0.0042	0.996	1579.8	2049	0.309	28.210	135.9
76	0.0042	0.996	1579.8	2051	0.324	21.960	126.0
77	0.0042	0.996	1579.8	2047	0.336	15.670	115.2
78	0.0042	0.996	1579.8	2049	0.339	13.580	111.6
79	0.0042	0.996	1579.8	2049	0.348	10.620	107.2
80	0.0042	0.996	1579.8	2051	0.342	8.437	101.3
81	0.0042	0.996	1579.8	2048	0.341	6.365	96.4
82	0.0042	0.998	1579.8	2559	0.251	23.690	139.7
83	0.0042	0.998	1579.8	2559	0.265	19.810	133.3
84	0.0042	0.998	1579.8	2553	0.283	15.050	125.8
85	0.0042	0.998	1579.8	2559	0.292	11.570	119.2
86	0.0042	0.998	1579.8	2559	0.295	7.833	110.1
87	0.0042	0.998	1579.8	3069	0.199	23.890	149.1
88	0.0042	0.998	1579.8	3062	0.211	19.910	140.6
89	0.0042	0.998	1579.8	3081	0.231	14.630	131.4
90	0.0042	0.998	1579.8	3060	0.252	10.090	123.5
91	0.0042	0.998	1579.8	3076	0.259	7.725	119.2
92	0.0042	0.998	1579.8	3576	0.154	28.210	171.2
93	0.0042	0.998	1579.8	3582	0.171	22.980	158.9
94	0.0042	0.998	1579.8	3595	0.180	19.910	151.8
95	0.0042	0.998	1579.8	3578	0.195	15.460	140.7
96	0.0042	0.998	1579.8	3589	0.206	12.100	132.9

Table IV-3 (Continued)

No.	D	L	P	G	Xc	HI	CHF
97	0.0042	0.998	1579.8	4092	0.131	28.310	185.2
98	0.0042	0.998	1579.8	4078	0.141	24.490	173.2
99	0.0042	0.998	1579.8	4074	0.154	20.220	160.7
100	0.0042	0.998	1579.8	4099	0.167	15.990	149.6
101	0.0042	0.998	1579.8	4103	0.177	12.310	138.7
102	0.0042	0.781	1579.8	2040	0.269	27.210	157.3
103	0.0042	0.781	1579.8	2043	0.280	23.380	150.5
104	0.0042	0.781	1579.8	2047	0.293	19.300	143.6
105	0.0042	0.781	1579.8	2043	0.308	15.460	137.4
106	0.0042	0.781	1579.8	2044	0.322	10.940	129.3
107	0.0042	0.781	1579.8	2050	0.326	7.617	121.8
108	0.0042	0.781	1579.8	2561	0.202	27.710	173.4
109	0.0042	0.781	1579.8	2554	0.213	23.990	164.3
110	0.0042	0.781	1579.8	2556	0.221	20.630	156.1
111	0.0042	0.781	1576.4	2556	0.238	15.770	145.9
112	0.0042	0.781	1579.8	2556	0.257	11.150	137.4
113	0.0042	0.781	1579.8	2565	0.271	6.942	128.9
114	0.0042	0.781	1579.8	3073	0.152	28.610	188.6
115	0.0042	0.781	1579.8	3069	0.164	24.390	176.6
116	0.0042	0.781	1579.8	3074	0.177	20.630	167.5
117	0.0042	0.781	1579.8	3071	0.191	15.880	154.3
118	0.0042	0.781	1579.8	3075	0.208	11.150	142.7
119	0.0042	0.781	1579.8	3588	0.123	28.010	201.8
120	0.0042	0.781	1579.8	3583	0.137	23.280	186.1

Table IV-3 (Continued)

No.	D	L	P	G	Xc	HI	CHF
121	0.0042	0.781	1579.8	3576	0.151	19.400	174.5
122	0.0042	0.781	1579.8	3589	0.163	15.570	163.2
123	0.0042	0.781	1579.8	3587	0.175	11.790	151.7
124	0.0042	0.781	1579.8	4108	0.115	23.280	199.8
125	0.0042	0.781	1579.8	4101	0.125	19.910	187.4
126	0.0042	0.781	1579.8	4099	0.136	16.510	175.0
127	0.0042	0.781	1579.8	4094	0.154	11.470	158.3

Table IV-4 CHF data for CFC-11 from UO loop

No.	D	L	P	G	Xc	HI	CHF
1	0.00438	1.000	1649.1	1048	0.417	41.130	105.9
2	0.00438	1.000	1652.1	1045	0.468	22.030	90.8
3	0.00438	1.000	1652.1	1046	0.490	12.270	82.8
4	0.00438	1.000	1652.1	2153	0.252	11.720	100.5
5	0.00438	1.000	1652.1	2164	0.193	33.010	134.2
6	0.00438	1.000	1652.1	2165	0.170	43.410	152.4
7	0.00438	1.000	1133.6	1045	0.575	10.560	102.5

Table IV-5 CHF data for HCFC-22 from UO loop

No.	D	L	P	G	Xc	HI	CHF
1	0.0042	0.785	1340.1	1501	0.451	23.360	203.5
2	0.0042	0.785	1340.1	1502	0.459	17.220	194.0
3	0.0042	0.785	1340.1	1502	0.465	12.540	186.6
4	0.0042	0.785	1340.1	1502	0.470	8.010	179.0
5	0.0042	0.785	1340.1	1500	0.482	1.571	170.3
6	0.0042	1.001	1340.1	1504	0.479	23.120	167.0
7	0.0042	1.001	1340.1	1499	0.482	18.320	159.8
8	0.0042	1.001	1340.1	1502	0.488	12.540	152.6
9	0.0042	1.001	1340.1	1501	0.493	8.137	146.9
10	0.0042	1.001	1340.1	1501	0.497	3.392	140.5
11	0.0042	1.000	1340.1	2010	0.395	20.970	188.2
12	0.0042	1.000	1343.4	2013	0.395	18.450	182.9
13	0.0042	1.000	1340.1	2007	0.403	13.160	174.4
14	0.0042	1.000	1343.4	2007	0.410	7.250	164.4
15	0.0042	1.000	1340.1	2000	0.418	2.093	156.1
16	0.0042	1.000	1343.4	2515	0.324	20.500	202.0
17	0.0042	1.000	1340.1	2509	0.332	18.200	199.1
18	0.0042	1.000	1340.1	2508	0.339	14.150	191.6
19	0.0042	1.000	1340.1	2503	0.351	7.755	179.9
20	0.0042	1.000	1340.1	2503	0.359	2.613	169.9
21	0.0042	1.000	1340.1	3008	0.273	21.210	216.0
22	0.0042	1.000	1340.1	2995	0.281	18.320	210.4
23	0.0042	1.000	1340.1	3002	0.294	13.040	201.2
24	0.0042	1.000	1340.1	2999	0.305	9.150	194.8

Table IV-5 (Continued)

No.	D	L	P	G	Xc	HI	CHF
25	0.0042	1.000	1340.1	2992	0.318	3.132	182.5
26	0.0042	1.000	1340.1	4002	0.199	22.290	238.3
27	0.0042	1.000	1340.1	3995	0.210	18.920	231.6
28	0.0042	1.000	1340.1	3991	0.228	12.660	218.4
29	0.0042	1.000	1340.1	3991	0.239	8.770	210.1
30	0.0042	1.000	1340.1	4002	0.258	3.132	200.1
31	0.0042	1.000	1343.4	3502	0.233	21.820	228.1
32	0.0042	1.000	1336.7	3505	0.241	18.910	223.2
33	0.0042	1.000	1343.4	3512	0.254	13.910	213.0
34	0.0042	1.000	1340.1	3506	0.268	8.770	202.4
35	0.0042	1.000	1340.1	3492	0.289	1.441	188.5
36	0.0042	0.499	1340.1	2003	0.286	18.560	286.4
37	0.0042	0.499	1340.1	2006	0.304	12.660	274.8
38	0.0042	0.499	1340.1	2000	0.315	8.644	265.2
39	0.0042	0.499	1340.1	1995	0.329	3.780	254.7
40	0.0042	0.499	1340.1	2512	0.217	18.320	295.1
41	0.0042	0.499	1340.1	2506	0.237	12.660	283.0
42	0.0042	0.499	1340.1	2498	0.255	7.374	270.4
43	0.0042	0.499	1340.1	2490	0.272	2.353	258.7
44	0.0042	0.779	1340.1	2000	0.356	20.970	222.2
45	0.0042	0.779	1340.1	1995	0.360	18.560	217.3
46	0.0042	0.779	1340.1	2002	0.369	14.030	209.8
47	0.0042	0.779	1340.1	1998	0.383	6.864	196.5
48	0.0042	0.779	1340.1	1997	0.390	2.873	189.1

Table IV-5 (Continued)

No.	D	L	P	G	Xc	HI	CHF
49	0.0042	0.779	1340.1	2501	0.284	22.530	241.1
50	0.0042	0.779	1340.1	2500	0.294	18.440	233.3
51	0.0042	0.779	1340.1	2498	0.308	13.040	222.8
52	0.0042	0.779	1340.1	2500	0.318	8.770	214.6
53	0.0042	0.779	1340.1	2500	0.329	3.521	203.5
54	0.0042	0.779	1340.1	3002	0.229	23.000	252.9
55	0.0042	0.779	1340.1	2996	0.244	19.050	246.9
56	0.0042	0.779	1340.1	2997	0.254	14.150	234.6
57	0.0042	0.779	1343.4	2998	0.268	9.155	224.2
58	0.0042	0.779	1336.7	2995	0.284	3.001	210.5
59	0.0042	0.779	1340.1	3503	0.186	23.360	261.9
60	0.0042	0.779	1340.1	3501	0.201	19.170	254.1
61	0.0042	0.779	1340.1	3511	0.217	13.660	241.9
62	0.0042	0.779	1340.1	3505	0.235	8.010	229.7
63	0.0042	0.779	1343.4	3497	0.248	3.911	220.0
64	0.0042	0.779	1340.1	4003	0.151	23.840	269.3
65	0.0042	0.779	1340.1	3995	0.171	18.320	257.9
66	0.0042	0.779	1340.1	3998	0.189	13.410	247.7
67	0.0042	0.779	1343.4	4005	0.206	8.522	237.6
68	0.0042	0.779	1340.1	4003	0.224	3.132	225.9
69	0.0042	1.000	1960.7	2005	0.340	24.950	162.5
70	0.0042	1.000	1960.7	2026	0.341	19.700	153.5
71	0.0042	1.000	1960.7	1994	0.346	14.890	142.5
72	0.0042	1.000	1960.7	1995	0.348	8.731	130.4

Table IV-5 (Continued)

No.	D	L	P	G	Xc	HI	CHF
73	0.0042	1.000	1965.1	2001	0.350	3.558	120.2
74	0.0042	1.000	1960.7	2504	0.268	25.980	176.7
75	0.0042	1.000	1960.7	2502	0.283	20.370	167.7
76	0.0042	1.000	1960.7	2491	0.296	14.750	157.5
77	0.0042	1.000	1960.7	2502	0.302	9.008	145.7
78	0.0042	1.000	1960.7	2497	0.304	4.965	135.3
79	0.0042	1.000	1960.7	2974	0.204	30.210	192.2
80	0.0042	1.000	1960.7	3012	0.216	24.950	184.1
81	0.0042	1.000	1965.1	2990	0.234	20.640	177.7
82	0.0042	1.000	1960.7	3010	0.251	14.750	168.4
83	0.0042	1.000	1965.1	3002	0.266	9.152	157.6
84	0.0042	1.000	1960.7	2987	0.276	3.556	144.3
85	0.0042	1.000	1960.7	3502	0.173	25.850	192.8
86	0.0042	1.000	1965.1	3507	0.195	19.850	183.1
87	0.0042	1.000	1960.7	3502	0.215	14.620	175.4
88	0.0042	1.000	1960.7	3499	0.229	9.975	165.8
89	0.0042	1.000	1960.7	3495	0.240	5.807	156.7
90	0.0042	1.000	1960.7	3999	0.148	25.980	204.9
91	0.0042	1.000	1960.7	3992	0.168	19.440	189.5
92	0.0042	1.000	1965.1	4004	0.186	13.950	178.7
93	0.0042	1.000	1960.7	3976	0.216	7.204	168.9
94	0.0042	0.779	1960.7	2002	0.302	24.690	191.8
95	0.0042	0.779	1965.1	1990	0.316	19.980	183.8
96	0.0042	0.779	1960.7	1998	0.323	15.160	174.7

Table IV-5 (Continued)

No.	D	L	P	G	Xc	HI	CHF
97	0.0042	0.779	1965.1	1993	0.337	9.013	163.3
98	0.0042	0.779	1960.7	1992	0.340	4.121	151.5
99	0.0042	0.779	1960.7	2492	0.222	27.660	207.3
100	0.0042	0.779	1965.1	2506	0.227	24.440	200.2
101	0.0042	0.779	1960.7	2503	0.242	19.840	192.3
102	0.0042	0.779	1960.7	2495	0.258	14.350	181.8
103	0.0042	0.779	1960.7	2508	0.278	8.454	172.9
104	0.0042	0.779	1960.7	2509	0.286	4.965	165.6
105	0.0042	0.779	1960.7	2998	0.180	24.690	211.7
106	0.0042	0.779	1960.7	3009	0.191	20.230	201.3
107	0.0042	0.779	1960.7	2999	0.205	15.430	189.6
108	0.0042	0.779	1965.1	2998	0.224	9.980	179.1
109	0.0042	0.779	1960.7	2992	0.245	4.262	169.2
110	0.0042	0.779	1960.7	3490	0.150	24.690	224.7
111	0.0042	0.779	1960.7	3503	0.159	20.370	211.5
112	0.0042	0.779	1965.1	3495	0.174	15.300	198.2
113	0.0042	0.779	1965.1	3492	0.189	10.530	186.4
114	0.0042	0.779	1960.7	3491	0.205	5.807	175.9
115	0.0042	0.779	1960.7	3995	0.118	28.300	249.9
116	0.0042	0.779	1960.7	3991	0.126	24.820	237.6
117	0.0042	0.779	1960.7	4000	0.136	20.230	221.4
118	0.0042	0.779	1960.7	3996	0.152	14.750	205.2
119	0.0042	0.779	1960.7	3995	0.173	8.316	187.7
120	0.0042	0.785	1960.7	1501	0.387	24.950	169.4

Table IV-5 (Continued)

No.	D	L	P	G	Xc	HI	CHF
121	0.0042	0.785	1960.7	1499	0.389	19.840	159.8
122	0.0042	0.785	1960.7	1499	0.389	14.620	149.1
123	0.0042	0.785	1960.7	1502	0.393	8.593	138.5
124	0.0042	0.785	1960.7	1499	0.391	3.980	128.4
125	0.0042	1.001	1960.7	1497	0.398	25.980	136.9
126	0.0042	1.001	1960.7	1499	0.399	20.100	128.0
127	0.0042	1.001	1960.7	1499	0.397	15.160	119.7
128	0.0042	1.001	1960.7	1498	0.394	9.699	110.4
129	0.0042	1.001	1960.7	1497	0.392	3.132	99.4

Table IV-6 CHF data for HCFC-22 from MR-7A loop

No.	D	L	P	G	Xc	HI	CHF
1	0.00807	1.61	1339.8	984	0.477	22.947	129.9
2	0.00807	1.61	1333.1	959	0.537	22.449	138.5
3	0.00807	1.61	1336.5	948	0.547	18.143	133.8
4	0.00807	1.61	1339.8	934	0.574	12.632	130.9
5	0.00807	1.61	1336.5	922	0.589	7.482	126.2
6	0.00807	1.61	1343.2	936	0.584	4.163	123.1
7	0.00807	1.61	1339.8	1920	0.301	18.152	168.5
8	0.00807	1.61	1336.5	1891	0.323	12.378	161.5
9	0.00807	1.61	1333.1	1892	0.339	7.605	156.9
10	0.00807	1.61	1326.5	1868	0.353	2.737	149.3
11	0.00807	1.61	1343.2	2875	0.210	16.091	188.3
12	0.00807	1.61	1336.5	2920	0.217	12.254	182.2
13	0.00807	1.61	1336.5	2905	0.233	7.228	173.1
14	0.00807	1.61	1339.8	2921	0.245	3.517	168.0
15	0.00807	1.61	1336.5	3900	0.145	14.480	193.3
16	0.00807	1.61	1346.5	3905	0.150	13.018	190.2
17	0.00807	1.61	1339.8	3898	0.178	7.485	187.1
18	0.00807	1.61	1339.8	3910	0.191	4.161	182.3
19	0.00807	1.61	1336.5	5858	0.091	11.880	202.6
20	0.00807	1.61	1333.1	5857	0.113	7.097	195.0
21	0.00807	1.61	1333.1	5835	0.137	2.739	193.0
22	0.00807	1.15	1326.5	955	0.482	20.520	174.2
23	0.00807	1.15	1349.9	971	0.469	18.301	168.8
24	0.00807	1.15	1329.8	959	0.489	12.614	163.6

Table IV-6 (Continued)

No.	D	L	P	G	Xc	HI	CHF
25	0.00807	1.15	1343.2	970	0.493	8.123	158.6
26	0.00807	1.15	1336.5	936	0.519	3.644	153.2
27	0.00807	1.15	1346.5	1916	0.251	17.685	204.7
28	0.00807	1.15	1329.8	1941	0.264	12.366	197.6
29	0.00807	1.15	1336.5	1962	0.276	7.608	190.3
30	0.00807	1.15	1333.1	1943	0.289	3.772	183.4
31	0.00807	1.15	1333.1	2932	0.144	16.798	214.8
32	0.00807	1.15	1336.5	2877	0.165	12.874	208.9
33	0.00807	1.15	1339.8	2909	0.182	7.866	200.9
34	0.00807	1.15	1336.5	2902	0.200	3.902	195.5
35	0.00807	1.15	1343.2	3898	0.089	16.946	220.9
36	0.00807	1.15	1333.1	3909	0.104	12.868	211.8
37	0.00807	1.15	1339.8	3905	0.123	8.119	201.1
38	0.00807	1.15	1336.5	3904	0.135	3.515	183.6
39	0.00807	1.15	1336.5	5763	0.052	15.095	243.4
40	0.00807	1.15	1346.5	5862	0.062	12.521	239.0
41	0.00807	1.15	1333.1	5865	0.078	7.605	216.3
42	0.00807	1.15	1333.1	5853	0.094	3.901	206.6
43	0.00807	0.88	1343.2	956	0.405	21.650	200.8
44	0.00807	0.88	1349.9	995	0.401	17.937	198.6
45	0.00807	0.88	1333.1	1007	0.412	12.744	194.0
46	0.00807	0.88	1333.1	969	0.444	7.351	186.7
47	0.00807	0.88	1343.2	983	0.445	4.163	182.3
48	0.00807	0.88	1339.8	1966	0.175	22.591	238.4

Table IV-6 (Continued)

No.	D	L	P	G	Xc	HI	CHF
49	0.00807	0.88	1333.1	1968	0.191	17.891	230.0
50	0.00807	0.88	1343.2	1941	0.211	12.887	219.3
51	0.00807	0.88	1343.2	1940	0.227	8.123	210.3
52	0.00807	0.88	1333.1	1943	0.242	3.901	204.0
53	0.00807	0.67	1329.8	912	0.374	23.384	241.9
54	0.00807	0.67	1346.5	922	0.378	17.806	230.6
55	0.00807	0.67	1343.2	911	0.395	13.135	223.0
56	0.00807	0.67	1336.5	944	0.400	6.846	216.1
57	0.00807	0.67	1349.9	934	0.414	3.521	210.4
58	0.00807	0.67	1333.1	1936	0.139	21.139	263.5
59	0.00807	0.67	1336.5	1944	0.149	18.022	255.9
60	0.00807	0.67	1339.8	1919	0.169	13.129	244.5
61	0.00807	0.67	1339.8	1941	0.187	8.119	236.0
62	0.00807	0.67	1333.1	1964	0.203	3.385	228.0
63	0.00807	0.67	1326.5	2978	0.067	19.441	278.5
64	0.00807	0.67	1333.1	2939	0.074	17.770	270.3
65	0.00807	0.67	1333.1	2927	0.089	12.992	250.6
66	0.00807	0.67	1333.1	2933	0.108	7.732	233.2
67	0.00807	0.67	1333.1	2897	0.131	3.127	224.8
68	0.00807	0.67	1339.8	3863	0.033	18.152	276.8
69	0.00807	0.67	1336.5	3928	0.060	12.502	270.0
70	0.00807	0.67	1333.1	3905	0.074	7.858	243.2
71	0.00807	0.67	1336.5	3858	0.092	3.515	225.1
72	0.00807	0.67	1329.8	5815	0.019	16.668	350.2

Table IV-6 (Continued)

No.	D	L	P	G	Xc	HI	CHF
73	0.00807	0.67	1336.5	5864	0.034	12.254	319.0
74	0.00807	0.67	1336.5	5895	0.046	8.115	286.5
75	0.00807	0.67	1343.2	5917	0.059	3.905	251.8
76	0.00807	1.61	1346.5	954	0.502	20.823	128.3
77	0.00807	0.67	1333.1	3887	0.037	20.302	313.1
78	0.00807	0.67	1329.8	3863	0.045	17.761	296.9
79	0.00807	0.67	1333.1	3976	0.058	12.372	267.4
80	0.00807	1.61	1964.1	1002	0.389	24.416	105.7
81	0.00807	1.61	1964.1	1033	0.376	19.041	99.5
82	0.00807	1.61	1973.0	1019	0.393	14.642	95.7
83	0.00807	1.61	1968.5	1001	0.404	8.345	88.2
84	0.00807	1.61	1968.5	962	0.430	2.606	82.7
85	0.00807	1.61	1946.4	2004	0.225	23.848	147.2
86	0.00807	1.61	1950.8	2020	0.234	18.614	138.5
87	0.00807	1.61	1959.6	1990	0.256	13.538	132.0
88	0.00807	1.61	1950.8	1980	0.272	7.777	123.1
89	0.00807	1.61	1950.8	1949	0.285	2.603	113.4
90	0.00807	1.61	1955.2	2979	0.120	23.612	157.2
91	0.00807	1.61	1950.8	3009	0.134	18.747	148.7
92	0.00807	1.61	1955.2	3035	0.149	13.938	140.1
93	0.00807	1.61	1968.5	3028	0.173	8.622	133.7
94	0.00807	1.61	1946.4	3018	0.205	2.037	127.1
95	0.00807	1.61	1964.1	3978	0.080	23.767	179.7
96	0.00807	1.61	1950.8	4024	0.091	19.144	167.5

Table IV-6 (Continued)

No.	D	L	P	G	Xc	HI	CHF
97	0.00807	1.61	1959.6	4004	0.109	13.674	152.7
98	0.00807	1.61	1959.6	4006	0.130	8.199	141.5
99	0.00807	1.61	1950.8	4024	0.164	2.179	138.2
100	0.00807	1.61	1959.6	6006	0.054	23.884	242.8
101	0.00807	1.61	1964.1	6018	0.069	19.173	224.6
102	0.00807	1.61	1964.1	6017	0.089	13.816	207.2
103	0.00807	1.61	1964.1	5995	0.112	8.756	194.6
104	0.00807	1.61	1964.1	6003	0.142	3.171	187.5
105	0.00807	1.15	1942.0	1027	0.370	24.094	146.2
106	0.00807	1.15	1950.8	1011	0.383	19.012	138.3
107	0.00807	1.15	1955.2	995	0.396	13.396	129.8
108	0.00807	1.15	1946.4	1000	0.408	7.358	123.2
109	0.00807	1.15	1950.8	1008	0.407	2.745	115.7
110	0.00807	1.15	1959.6	2005	0.176	24.403	181.0
111	0.00807	1.15	1964.1	2023	0.187	19.438	170.7
112	0.00807	1.15	1955.2	1994	0.209	14.073	161.9
113	0.00807	1.15	1959.6	2007	0.225	8.890	153.3
114	0.00807	1.15	1955.2	1990	0.257	2.321	145.9
115	0.00807	1.15	1950.8	3007	0.090	24.119	200.0
116	0.00807	1.15	1959.6	3008	0.106	18.899	185.5
117	0.00807	1.15	1964.1	3008	0.121	13.816	170.9
118	0.00807	1.15	1964.1	3004	0.141	8.203	157.4
119	0.00807	1.15	1959.6	3017	0.163	2.322	144.7
120	0.00807	1.15	1950.8	4033	0.124	2.886	155.2

Table IV-6 (Continued)

No.	D	L	P	G	Xc	HI	CHF
121	0.00807	1.15	1950.8	4010	0.103	8.192	169.1
122	0.00807	1.15	1955.2	3976	0.087	13.125	185.3
123	0.00807	1.15	1959.6	3995	0.070	18.899	207.6
124	0.00807	1.15	1955.2	3961	0.075	24.002	247.0
125	0.00807	1.15	1964.1	5960	0.035	24.027	307.2
126	0.00807	1.15	1950.8	5999	0.047	19.012	277.0
127	0.00807	1.15	1964.1	5996	0.065	13.951	251.2
128	0.00807	1.15	1964.1	5992	0.083	8.618	224.0
129	0.00807	1.15	1959.6	6034	0.112	2.322	206.3
130	0.00807	0.67	1946.4	1002	0.300	23.848	211.7
131	0.00807	0.67	1959.6	988	0.315	19.296	201.5
132	0.00807	0.67	1946.4	1040	0.320	12.977	194.8
133	0.00807	0.67	1964.1	1003	0.342	8.756	184.9
134	0.00807	0.67	1946.4	984	0.360	1.896	169.8
135	0.00807	0.67	1950.8	1956	0.111	23.600	239.8
136	0.00807	0.67	1950.8	2000	0.120	19.144	226.3
137	0.00807	0.67	1955.2	1992	0.139	13.802	211.2
138	0.00807	0.67	1959.6	2025	0.158	8.199	197.9
139	0.00807	0.67	1950.8	1968	0.188	2.179	184.5
140	0.00807	0.67	1959.6	3011	0.075	13.944	230.5
141	0.00807	0.67	1950.8	3008	0.093	8.330	205.7
142	0.00807	0.67	1964.1	2978	0.114	3.030	183.9
143	0.00807	0.67	1959.6	4009	0.019	24.274	327.9
144	0.00807	0.67	1959.6	3999	0.035	19.296	297.0

Table IV-6 (Continued)

No.	D	L	P	G	Xc	HI	CHF
145	0.00807	0.67	1964.1	4008	0.050	14.222	263.8
146	0.00807	0.67	1950.8	4010	0.069	8.192	227.3
147	0.00807	0.67	1946.4	4024	0.089	2.037	190.2
148	0.00807	0.67	1964.1	5992	0.013	19.041	380.2
149	0.00807	0.67	1955.2	5996	0.033	13.667	339.8
150	0.00807	0.67	1946.4	6032	0.054	7.773	291.4
151	0.00807	0.67	1964.1	6025	0.070	3.171	251.2
152	0.00807	1.61	1950.8	1002	0.386	23.860	104.5
153	0.00807	1.61	1946.4	1010	0.390	18.473	99.6
154	0.00807	1.61	1964.1	1017	0.391	13.681	94.0
155	0.00807	1.61	1955.2	1002	0.401	8.057	87.5
156	0.00807	1.61	1968.5	1007	0.409	2.889	82.8

Table IV-7 CHF data for HCFC-22 from MR-7A loop

No.	D	L	P	G	Xc	HI	CHF
1	0.00438	1.46	1345.1	4053	0.232	28.434	208.9
2	0.00438	1.46	1338.9	4084	0.243	23.480	201.2
3	0.00438	1.46	1342.2	4046	0.252	18.696	189.4
4	0.00438	1.46	1335.7	4044	0.263	13.885	180.4
5	0.00438	1.46	1318.6	4025	0.275	8.727	171.0
6	0.00438	1.46	1338.4	4018	0.278	6.527	165.0
7	0.00438	1.46	1337.1	4994	0.194	27.945	231.2
8	0.00438	1.46	1330.1	5028	0.207	23.013	223.0
9	0.00438	1.46	1341.5	4984	0.214	20.065	214.0
10	0.00438	1.46	1342.2	4944	0.232	14.206	201.9
11	0.00438	1.46	1339.9	4995	0.239	10.983	196.7
12	0.00438	1.46	1334.6	5000	0.260	5.045	188.0
13	0.00438	1.46	1341.3	6112	0.138	28.628	242.0
14	0.00438	1.46	1325.5	6023	0.176	21.208	234.4
15	0.00438	1.46	1330.1	6011	0.192	16.881	227.1
16	0.00438	1.46	1341.2	6033	0.208	12.022	218.0
17	0.00438	1.46	1340.7	5991	0.227	7.188	209.3
18	0.00438	1.46	1345.5	5945	0.239	4.265	203.5
19	0.00438	1.46	1342.2	7067	0.112	28.325	253.8
20	0.00438	1.46	1330.1	6968	0.130	24.658	248.1
21	0.00438	1.46	1329.3	7004	0.167	16.990	242.1
22	0.00438	1.46	1341.0	6992	0.186	12.756	236.9
23	0.00438	1.46	1317.9	6982	0.212	7.079	231.3
24	0.00438	1.46	1333.7	6978	0.233	2.768	226.7

Table IV-7 (Continued)

No.	D	L	P	G	Xc	HI	CHF
25	0.00438	1.46	1329.4	8076	0.095	27.591	268.9
26	0.00438	1.46	1339.6	7934	0.105	25.806	263.7
27	0.00438	1.46	1330.8	7958	0.138	18.795	256.4
28	0.00438	1.46	1329.5	8095	0.179	10.551	253.6
29	0.00438	1.46	1325.6	8098	0.199	6.347	249.4
30	0.00438	0.68	1345.2	3994	0.131	26.826	320.0
31	0.00438	0.68	1342.2	4010	0.146	21.684	305.0
32	0.00438	0.68	1330.1	3944	0.174	15.416	290.7
33	0.00438	0.68	1330.1	3987	0.195	8.530	273.0
34	0.00438	0.68	1330.1	4055	0.200	6.081	267.4
35	0.00438	0.68	1330.9	5026	0.082	25.950	328.2
36	0.00438	0.68	1342.9	4977	0.084	24.040	312.1
37	0.00438	0.68	1330.9	5005	0.106	18.597	299.8
38	0.00438	0.68	1332.8	4950	0.142	10.671	283.6
39	0.00438	0.68	1330.1	5029	0.170	3.848	271.9
40	0.00438	0.68	1330.1	5972	0.051	25.684	336.3
41	0.00438	0.68	1342.9	6030	0.061	22.322	322.2
42	0.00438	0.68	1330.1	6027	0.076	17.743	303.8
43	0.00438	0.68	1330.1	6001	0.109	10.558	287.2
44	0.00438	0.68	1331.2	6003	0.140	4.257	277.5
45	0.00438	0.68	1329.2	6970	0.060	17.981	322.9
46	0.00438	0.68	1339.8	6942	0.073	14.355	305.3
47	0.00438	0.68	1337.7	7071	0.096	8.844	293.4
48	0.00438	0.68	1344.0	7069	0.112	5.239	283.3

Table IV-7 (Continued)

No.	D	L	P	G	Xc	HI	CHF
49	0.00438	0.68	1349.0	7023	0.043	26.486	386.6
50	0.00438	0.68	1344.8	7000	0.052	23.158	365.5
51	0.00438	0.68	1342.2	8077	0.031	26.102	414.8
52	0.00438	0.68	1342.9	8030	0.038	23.682	395.8
53	0.00438	0.68	1344.5	7949	0.046	20.793	373.3
54	0.00438	0.68	1343.2	8015	0.063	14.994	338.1
55	0.00438	0.68	1340.4	7931	0.075	11.939	321.4
56	0.00438	0.68	1330.1	7963	0.108	4.486	300.3
57	0.00438	1.46	1935.6	4061	0.120	50.185	208.3
58	0.00438	1.46	1987.1	4015	0.123	49.470	204.4
59	0.00438	1.46	1958.7	4008	0.137	44.037	194.8
60	0.00438	1.46	1962.1	4080	0.146	38.127	184.6
61	0.00438	1.46	1986.4	3956	0.171	31.841	171.2
62	0.00438	1.46	1970.1	4042	0.198	23.185	161.4
63	0.00438	1.46	1932.1	3995	0.239	13.812	151.0
64	0.00438	1.46	1950.0	3975	0.259	7.353	139.8
65	0.00438	1.46	1974.3	5067	0.089	49.090	237.4
66	0.00438	1.46	1974.3	5060	0.098	44.182	223.5
67	0.00438	1.46	1963.4	5031	0.113	38.707	210.3
68	0.00438	1.46	1966.2	4961	0.140	30.154	191.2
69	0.00438	1.46	1958.5	5060	0.190	19.411	183.6
70	0.00438	1.46	1955.8	5091	0.218	13.361	178.0
71	0.00438	1.46	1961.3	4950	0.246	6.337	162.5
72	0.00438	1.46	1951.0	6089	0.071	49.581	275.2

Table IV-7 (Continued)

No.	D	L	P	G	Xc	HI	CHF
73	0.00438	1.46	1937.8	6049	0.080	45.971	263.2
74	0.00438	1.46	1965.7	5988	0.087	42.352	248.9
75	0.00438	1.46	1971.1	6059	0.103	36.593	236.5
76	0.00438	1.46	1973.2	5960	0.124	31.360	224.0
77	0.00438	1.46	1973.4	5958	0.174	21.108	212.1
78	0.00438	1.46	1986.4	6002	0.217	11.974	201.7
79	0.00438	1.46	1960.1	5989	0.237	6.910	193.2
80	0.00438	1.46	1968.6	7065	0.064	48.462	307.4
81	0.00438	1.46	1968.7	7020	0.072	45.047	293.5
82	0.00438	1.46	1953.0	7062	0.092	38.692	278.9
83	0.00438	1.46	1953.4	7005	0.108	33.026	259.1
84	0.00438	1.46	1962.1	6967	0.145	24.553	243.2
85	0.00438	1.46	1952.5	7015	0.199	13.846	232.2
86	0.00438	1.46	1952.0	6985	0.226	8.235	223.7
87	0.00438	1.46	1970.6	8021	0.057	46.952	333.4
88	0.00438	1.46	1962.1	8047	0.066	42.879	318.7
89	0.00438	1.46	1963.1	7952	0.076	39.147	301.4
90	0.00438	1.46	1962.1	8029	0.098	32.733	286.2
91	0.00438	1.46	1952.4	7960	0.133	24.662	268.1
92	0.00438	1.46	1950.6	7964	0.186	14.998	258.6
93	0.00438	0.68	1958.9	4059	0.061	48.717	378.5
94	0.00438	0.68	1947.8	4040	0.069	43.849	352.8
95	0.00438	0.68	1948.1	4029	0.077	39.990	335.1
96	0.00438	0.68	1945.3	4017	0.090	33.795	306.4

Table IV-7 (Continued)

No.	D	L	P	G	Xc	HI	CHF
97	0.00438	0.68	1946.2	4031	0.097	29.293	285.7
98	0.00438	0.68	1950.0	3922	0.126	22.619	263.4
99	0.00438	0.68	1942.7	4041	0.129	17.780	243.2
100	0.00438	0.68	1940.0	3959	0.154	11.207	221.2
101	0.00438	0.68	1937.8	3958	0.168	5.329	197.9
102	0.00438	0.68	1938.6	5001	0.040	47.291	428.9
103	0.00438	0.68	1950.0	4962	0.046	44.348	408.9
104	0.00438	0.68	1936.1	5014	0.049	40.105	383.8
105	0.00438	0.68	1933.1	4954	0.060	35.964	358.9
106	0.00438	0.68	1935.3	4947	0.067	31.598	332.6
107	0.00438	0.68	1962.1	4979	0.087	25.003	305.7
108	0.00438	0.68	1962.1	5027	0.096	19.768	277.9
109	0.00438	0.68	1961.4	5009	0.101	15.696	249.1
110	0.00438	0.68	1945.6	4977	0.127	7.784	217.7
111	0.00438	0.68	1945.9	5049	0.136	5.000	208.5
112	0.00438	0.68	1952.6	5979	0.020	47.984	489.7
113	0.00438	0.68	1950.2	6019	0.027	43.290	457.8
114	0.00438	0.68	1950.0	6000	0.036	38.706	426.0
115	0.00438	0.68	1950.0	5932	0.046	33.932	389.6
116	0.00438	0.68	1950.0	6046	0.056	27.757	352.3
117	0.00438	0.68	1962.1	6000	0.069	21.576	307.9
118	0.00438	0.68	1945.7	6042	0.094	13.163	266.5
119	0.00438	0.68	1945.5	6073	0.137	3.505	238.1
120	0.00438	0.68	1955.4	6986	0.016	47.550	559.7

Table IV-7 (Continued)

No.	D	L	P	G	Xc	HI	CHF
121	0.00438	0.68	1962.1	7041	0.020	43.251	521.8
122	0.00438	0.68	1950.0	6977	0.032	37.419	472.8
123	0.00438	0.68	1961.0	7005	0.043	30.892	419.6
124	0.00438	0.68	1959.1	7060	0.055	24.110	368.2
125	0.00438	0.68	1949.2	7044	0.076	16.699	319.4
126	0.00438	0.68	1944.6	6992	0.109	8.110	277.9
127	0.00438	0.68	1962.6	8056	0.003	47.496	619.3
128	0.00438	0.68	1950.0	7979	0.014	42.999	576.7
129	0.00438	0.68	1950.0	8049	0.025	36.697	522.0
130	0.00438	0.68	1950.0	8058	0.036	30.933	471.0
131	0.00438	0.68	1948.3	7951	0.048	25.627	420.7
132	0.00438	0.68	1946.1	7951	0.064	19.347	370.3
133	0.00438	0.68	1944.8	8003	0.087	11.648	319.7
134	0.00438	0.68	1960.0	7984	0.115	5.783	298.8

Table IV-8 CHF data for water from MR-1A loop

No.	D	L	P	G	Xc	HI	CHF
1	0.008	1.75	7039	2524	0.350	143.487	1932
2	0.008	1.75	7033	3864	0.236	145.433	2210
3	0.008	1.75	7049	5219	0.162	148.065	2337
4	0.008	1.75	6954	6489	0.120	151.372	2465
5	0.008	1.75	6968	7752	0.080	198.446	2830
6	0.008	1.75	6999	2587	0.348	117.115	1896
7	0.008	1.75	6998	3906	0.247	113.709	2165
8	0.008	1.75	7025	5296	0.180	110.688	2307
9	0.008	1.75	7013	7743	0.120	112.966	2599
10	0.008	1.75	6991	2514	0.378	30.409	1725
11	0.008	1.75	6994	3777	0.290	27.691	2003
12	0.008	1.75	7065	5147	0.229	31.221	2207
13	0.008	1.75	7001	6440	0.190	32.359	2341
14	0.008	1.75	6946	7640	0.172	26.547	2497
15	0.008	1.75	6849	7727	0.173	28.543	2561
16	0.008	1.75	6908	7745	0.166	34.735	2534
17	0.008	1.75	7043	2564	0.365	70.244	1815
18	0.008	1.75	7013	3892	0.266	67.049	2076
19	0.008	1.75	6979	5212	0.203	70.813	2245
20	0.008	1.75	6958	6577	0.159	76.715	2380
21	0.008	1.75	7039	7832	0.137	79.070	2554
22	0.008	1.75	6956	2587	0.299	313.375	2261
23	0.008	1.75	7028	3941	0.164	296.824	2448
24	0.008	1.75	6951	5187	0.106	284.188	2629

Table IV-8 (Continued)

No.	D	L	P	G	Xc	HI	CHF
25	0.008	1.75	7058	6314	0.067	314.077	2996
26	0.008	1.75	6956	7787	0.054	302.958	3422
27	0.008	1.75	7084	7673	0.028	455.367	4358
28	0.008	1.75	6996	2505	0.270	441.074	2426
29	0.008	1.75	7029	3677	0.165	384.163	2659
30	0.008	1.75	7014	5015	0.087	401.977	3051
31	0.008	1.75	6933	6404	0.049	401.838	3480
32	0.008	1.75	10088	2582	0.218	330.451	1816
33	0.008	1.75	9933	3953	0.108	327.108	2120
34	0.008	1.75	10064	5237	0.080	321.758	2553
35	0.008	1.75	10031	6423	0.069	324.517	3047
36	0.008	1.75	10043	7712	0.060	325.497	3564
37	0.008	1.75	10056	2401	0.267	208.893	1534
38	0.008	1.75	10036	3786	0.165	202.989	1813
39	0.008	1.75	9942	5053	0.119	201.708	2073
40	0.008	1.75	9971	6380	0.098	201.901	2411
41	0.008	1.75	10071	7806	0.085	211.746	2887
42	0.008	1.75	10039	2501	0.278	134.613	1427
43	0.008	1.75	10076	3867	0.181	131.422	1626
44	0.008	1.75	10059	5277	0.139	137.620	1928
45	0.008	1.75	9978	6350	0.132	138.911	2268
46	0.008	1.75	9995	7709	0.127	134.616	2658
47	0.008	1.75	10114	2551	0.289	81.798	1341
48	0.008	1.75	10056	3776	0.209	77.015	1517

Table IV-8 (Continued)

No.	D	L	P	G	Xc	HI	CHF
49	0.008	1.75	9997	5147	0.180	69.960	1803
50	0.008	1.75	10067	6544	0.169	74.523	2208
51	0.008	1.75	9971	2541	0.206	404.621	1962
52	0.008	1.75	10089	3820	0.100	406.339	2344
53	0.008	1.75	10085	5186	0.068	397.585	2882
54	0.008	1.75	10127	6464	0.052	389.759	3377
55	0.008	1.75	10121	7667	0.046	386.013	3903

APPENDIX V

PRESSURE DROP EQUATIONS FOR GAS-LIQUID FLOW

The derivation of the pressure drop equation for gas-liquid flow is mainly based on Butterworth's (1977) and Collier's (1981) work. The equations are derived based on the assumption of one-dimensional homogeneous flow.

Figure V-1 shows the force balance over a control volume adjacent to the tube wall, where P is the pressure, A_F the flow cross-sectional area, z the axial distance, τ_w the wall shear stress and s_p the perimeter of the control volume.

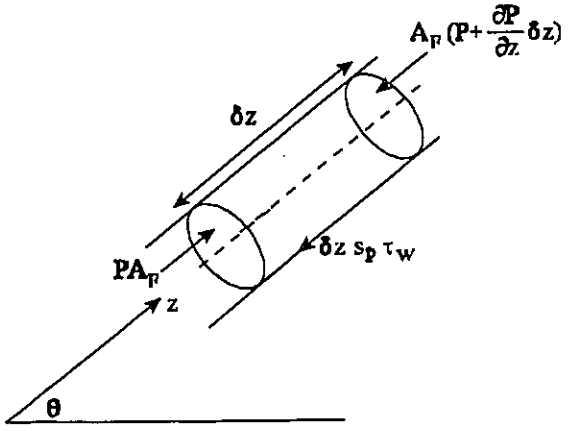

Figure V-1 Force balance on an element of the tube.

For single-phase flow

One-dimensional momentum equation

$$\int_A \left[P-\left(P+\frac{\partial P}{\partial z}\delta z\right)\right]dA_F = \int_{S_p} \tau_w \delta z ds + \int_{A_F} \frac{\partial}{\partial z}(GU_\infty)\delta z dA_F + \int_{A_F} \rho g \cdot \sin\theta \, \delta z dA_F \qquad \text{(V-1)}$$

(pressure force) (wall force) (momentum change force) (weight)

where G is the mass flux, U_∞ the flow velocity, ρ the fluid density and g the constant of the gravitational acceleration. From the one-dimensional assumption, the integration of Eq. (V-1) yields

$$\left[P-\left(P+\frac{\partial P}{\partial z}\delta z\right)\right]A_F = \tau_w \cdot s_p \cdot \delta z + \frac{d}{dz}(GU_\infty)\delta z \cdot A_F + \rho g \cdot \sin\theta \cdot \delta z \cdot A_F \qquad \text{(V-2a)}$$

or

$$-\frac{dP}{dz} = \frac{s_p}{A_F}\tau_w + G\frac{dU_\infty}{dz} + \rho g \cdot \sin\theta \qquad \text{(V-2b)}$$

One-dimensional energy balance

$$d(Pv) + du + d\left(\frac{1}{2}U_\infty^2\right) + d(g \cdot \sin\theta \cdot z) = dq - dW \qquad \text{(V-3)}$$

pressure energy	internal energy	kinetic energy	potential energy	heat input	external work

From thermodynamics,

$$du = dq + dLW - Pdv \qquad \text{(V-4)}$$

where the dLW is the loss of work. In present case, most of the loss of work is due to friction. Thus,

$$dLW = dW_f$$

where dW_f is the loss of work due to friction. Combining Eqs. (V-3) and (V-4), gives

$$vdP + U_\infty dU_\infty + g \cdot \sin\theta \, dz + dW_f = 0 \qquad \text{(V-5a)}$$

or

$$-\frac{dP}{dz} = \rho \frac{dW_f}{dz} + G\frac{dU_\infty}{dz} + \rho \sin\theta \cdot g \qquad \text{(V-5b)}$$

The total pressure gradient can be decomposed into

$$-\frac{dP}{dz} = -\frac{dP_f}{dz} - \frac{dP_a}{dz} - \frac{dP_g}{dz} \qquad \text{(V-6)}$$

where

$-(dP_f)/(dz)$	the frictional pressure gradient	(V-7a)
$-(dP_a)/(dz)$	the accelerational pressure gradient	(V-7b)
$-(dP_g)/(dz)$	the gravitational pressure gradient	(V-7c)

For two-phase flow

One-dimensional momentum equation

$$\int_{A_F}\left[P-\left(P+\frac{\partial P}{\partial z}\delta z\right)\right]dA_F = \int_{s_p}\tau_w \delta z\, ds + \int_{A_F}\frac{\partial}{\partial z}(G_f U_f + G_g U_g)\,\delta z\, dA_F + \int_{A_F}\rho g \cdot \sin\theta\, \delta z\, dA_F \qquad \text{(V-8)}$$

Simplifying this equation for one-dimensional flow, gives

$$-\frac{dP}{dz} = \frac{S_p}{A_F}\tau_w + \frac{d}{dz}[\alpha G_g U_g + (1-\alpha) G_f U_f] + g \cdot \sin\theta[\alpha \rho_g + (1-\alpha)\rho_f] \qquad \text{(V-9)}$$

where α is the void fraction and the subscripts "f" and "g" represent the saturated liquid phase and the saturated vapour phase, respectively. The mass flux and the flow velocity for each phase are calculated as follows:

$$G_f = \frac{\dot{m}(1-x)}{A_F(1-\alpha)} = \frac{G(1-x)}{1-\alpha} \qquad \text{(V-10a)}$$

$$G_g = \frac{Gx}{\alpha} \qquad \text{(V-10b)}$$

$$U_f = \frac{G_f}{\rho_f} \qquad \text{(V-11a)}$$

and

$$U_g = \frac{G_g}{\rho_g} \qquad \text{(V-11b)}$$

where $\dot{m}$ is the mass flow rate and x is the quality. Substituting Eqs. (V-10) and (V-11) into Eq. (V-9), gives

$$-\frac{dP}{dz} = \frac{S_p}{A_F}\tau_w + G^2 \frac{d}{dz}\left[\frac{x^2}{\alpha\rho_g} + \frac{(1-x)^2}{(1-\alpha)\rho_f}\right] + g \cdot \sin\theta[\alpha \rho_g + (1-\alpha)\rho_f] \qquad \text{(V-12)}$$

<u>One-dimensional energy equation</u>

Similar to Eq. (V-3)

$$d(Pv)_{2\phi} + du_{2\phi} + d\left(\frac{1}{2}U_{\infty}^2\right)_{2\phi} + d(g\cdot\sin\theta\cdot z)_{2\phi} = dq - dW \quad \text{(V-13)}$$

where

$$d(Pv)_{2\phi} = d[xPv_g + (1-x)Pv_f]$$

$$du_{2\phi} = dq + dW_f + Pd[xv_g + (1-x)v_f]$$

and

$$d\left(\frac{1}{2}U_{\infty}^2\right)_{2\phi} = d\left[\frac{1}{2}xU_g^2 + \frac{1}{2}(1-x)U_f^2\right]$$

The subscript "2ϕ" represents the two-phase mixture. After some rearrangement, Equation (V-13) becomes

$$-\frac{dP}{dz} = \rho_H\frac{dW_f}{dz} + \frac{1}{2}\rho_H G^2\left[\frac{x^3}{\alpha^2\rho_g^2}+\frac{(1-\alpha)^3}{(1-\alpha)^2\rho_f^2}\right] + \rho_H g\cdot\sin\theta \quad \text{(V-14)}$$

where

$$\frac{1}{\rho_H} = \frac{x}{\rho_g} + \frac{1-x}{\rho_f} \quad \text{(V-15)}$$

For homogeneous flow (no slip)

$$\frac{1}{\rho_H} = v_H \quad \text{(V-16)}$$

where the subscript "H" represents the homogeneous flow condition and

$$\alpha = \frac{1}{1+\frac{1-x}{x}\frac{\rho_g}{\rho_f}} \qquad \text{(V-17)}$$

Relation between the momentum and energy equations

For a single-phase flow, the respective terms in Eq. (V-2b), i.e. from the momentum equation, and Eq. (V-5b), i.e. from the energy equation, are identical. For a two-phase flow, the respective terms in Eq. (V-12), i.e. from the momentum equation, and Eq. (V-14), i.e. from the energy equation, are no longer identical except for the case of no slip between the phases (homogeneous flow). For a homogeneous flow condition, in a single-phase flow:

$$-\frac{dP_f}{dz} = \frac{s_p}{A_F}\tau_w = \rho\frac{dW_f}{dz} \qquad \text{(V-18)}$$

$$-\frac{dP_a}{dz} = G\frac{dU_\infty}{dz} = G^2\frac{dv}{dz} \qquad \text{(V-19)}$$

and

$$-\frac{dP_g}{dz} = \rho \sin\theta \cdot g \qquad \text{(V-20)}$$

and in a two-phase flow:

$$-\frac{dP_f}{dz} = \frac{s_p}{A_F}\tau_w = \rho_H\frac{dW_f}{dz} \qquad \text{(V-21)}$$

$$-\frac{dP_a}{dz} = G^2 \frac{d}{dz}\left[\frac{x^2}{\alpha\rho_g} + \frac{(1-x)^2}{(1-\alpha)\rho_f}\right] = \frac{1}{2}\rho_H G^2 \frac{d}{dz}\left[\frac{x^3}{\alpha^2\rho_g^2} + \frac{(1-x)^3}{(1-\alpha)^2\rho_f^2}\right] \tag{V-22}$$

and

$$-\frac{dP_g}{dz} = \rho_H g \cdot \sin\theta = g \cdot \sin\theta[\alpha\rho_g + (1-\alpha)\rho_f] \tag{V-23}$$

Substituting Eq. (V-17) into Eqs. (V-22) and (V-23), gives

$$G^2 \frac{d}{dz}\left[\frac{x^2}{\alpha\rho_g} + \frac{(1-x)^2}{(1-\alpha)\rho_f}\right] = \frac{1}{2}\rho_H G^2 \frac{d}{dz}\left[\frac{x^3}{\alpha^2\rho_g^2} + \frac{(1-x)^3}{(1-\alpha)^2\rho_f^2}\right] = G^2 \frac{dv_H}{dz} \tag{V-24}$$

and

$$\rho_H = [\alpha\rho_g + (1-\alpha)\rho_f] \tag{V-25}$$

Therefore,

$$-\frac{dP_a}{dz} = G^2 \frac{dv_H}{dz} \tag{V-26}$$

and

$$-\frac{dP_g}{dz} = \rho_H g \cdot \sin\theta \tag{V-27}$$

The pressure gradient due to friction depends on the correlation which is applicable to the homogeneous flow condition. From Collier (1981), for a single-phase flow, it is written as

$$-\frac{dP_f}{dz} = \frac{2f_{fo}G^2v_f}{D} \tag{V-28}$$

where D is the tube inner diameter and f_{fo} is the friction factor determined by the Blasius equation, i.e.,

$$f_{fo} = 0.079\left(\frac{GD}{\mu}\right)^{-1/4} \tag{V-29}$$

For a two-phase flow, the form similar to Eq. (V-28) is used

$$-\frac{dP_f}{dz} = \frac{2f_{TP}G^2v_f}{D}\left(1+x\frac{v_{fg}}{v_f}\right) \tag{V-30}$$

where D is the tube inner diameter and f_{TP} is determined by

$$f_{TP} = 0.079\left(\frac{GD}{\bar{\mu}}\right)^{-1/4} \tag{V-31}$$

where the $\bar{\mu}$ is the mean two-phase viscosity. The relation between $\bar{\mu}$ and the quality must satisfy the following limiting condition:

For x=0, $\bar{\mu}=\mu_f$

For x=1, $\bar{\mu}=\mu_g$

According to Collier, several possible forms of this relation are suggested by

(i) McAdams et al. (1942)

$$\frac{1}{\bar{\mu}} = \frac{x}{\mu_g} + \frac{1-x}{\mu_f} \tag{V-32}$$

(ii) Cicchitti et al. (1960)

$$\bar{\mu} = x\mu_g + (1-x)\mu_f \tag{V-33}$$

(iii) Dukler et al. (1964)

$$\bar{\mu} = \rho_H[xv_g\mu_g + (1-x)v_f\mu_f] \tag{V-34}$$

Because Eq. (V-32) is the most common definition of $\bar{\mu}$ according to Collier's comment, it is also chosen for the present work.